Phase I: Monitoring and Modeling Support for a Phosphorus/Eutrophication Model for Cayuga Lake

Final Phase 1 Report

December, 2014

This page intentionally left blank

Phase I: Monitoring and Modeling Support for a Phosphorus/Eutrophication Model for Cayuga Lake

Final Phase 1 Report
December, 2014

Prepared for

Cornell University

Prepared by

Upstate Freshwater Institute
Syracuse, NY

Department of Biological and Environmental Science
Cornell University
Ithaca, NY

Cornell Biological Field Station
Bridgeport, NY

Department of Ecology and Evolutionary Biology
Cornell University
Ithaca, NY

This page intentionally left blank

Table of Contents

Appendices Listing

This page intentionally left blank

List of Tables

List of Figures

Executive Summary

Introduction

This report documents progress in the study of phosphorus (P) and trophic state metics in Cayuga Lake, NY. The overarching goal of the study is to develop and test a water quality model for this lake that represents P-eutrophication dynamics. It is intended that this model will be capable of supporting a P Total Maximum Daily Load (TMDL) analysis for on the shallow southern end of the lake that receives 40% of the lake's total inflow, described as the "shelf". The model will also have predictive capabilities for inorganic (minerogenic) sediment, because these particles also influence metrics of trophic state, including P concentrations and water clarity.

The study has five technical elements: (1) monitoring of the five largest tributaries for forms of P, sediments, and related metrics, (2) monitoring of the lake for multiple forms of P, metrics of trophic state, sediment metrics, and selected biological communities, (3) setup and testing of a two-dimensional hydrothermal/transport model for the lake, (4) setup and testing of a watershed/landuse model to quantify the dependence of tributary constituent loading on landuse, and (5) development, testing, and application of a P-eutrophication water quality model for the lake that will be suitable to support a P TMDL. The study is being conducted in two phases, with the first phase including the first four of the above elements. This report documents the findings of the first phase, and considers how these influence development of the model in the second phase.

2013 Monitoring Program

The tributary and lake monitoring programs were conducted concurrently over the April through October interval of 2013. These were both temporally intensive and spatially extensive. Five tributaries were monitored, Fall Creek, Cayuga Inlet Creek, Six Mile Creek, Salmon Creek and Taughannock Creek (first four gaged for flow), that together represent 60% of the lake's watershed. There were two primary components of tributary monitoring (1) fixed frequency, bi-weekly collections, and (2) runoff event-based collections, to represent changes in concentration over the time course of the events.

Lake monitoring included: (1) the conduct of *in situ* measurements, (2) sampling for laboratory measurements of an array of water quality constituents to address the P-eutrophication and related sediment issues, (3) sampling and characterization of phytoplankton and zooplankton communities, and (4) the conduct of a spatially detailed dreissenid (quagga and zebra) mussel survey. Water quality monitoring was conducted at nine sites along the entire length of the lake, with two sites (No.'s 1 and 2) located on the shelf. Lake wide monitoring was conducted bi-weekly at all sites over the April-October interval. The frequency was increased to twice per

week in summer (June-September), at shallow sites 1 and 2, and at site 3, the nearest deep water ("pelagic") location.

Tributaries: Concentrations, P Bioavailability and Loads

The robust tributary data sets were analyzed, and together with flow rate (e.g., with units of m^3/d) information, were used to estimate constituent loading rates (e.g., with units of kg/d), that are necessary to drive mass balance type mechanistic models. The central element of this work was the development of loads that were calculated based on the bioavailability of each P form (ability of each form to support algal growth). Bioavailability bioassay experiments were conducted for three forms of P that sum to total P, soluble reactive P (SRP), soluble unreactive P (SUP), and particulate P (PP), for the major tributaries (Fall Creek, Cayuga Inlet Creek, Six Mile Creek and Salmon Creek) and two point sources. Tributary SRP, SUP, and PP were found to be completely, mostly, and less bioavailable, respectively. The estimated total bioavailable P load (BAP_L) for the study interval was only about 25% of the total P load, because the low bioavailability PP fraction dominated. Most of the BAP_L (> 70%) is received during high flow intervals. Point source contributions to the BAP_L are minor (~ 5%), reflecting the benefit of reductions from recent treatment upgrades. Salmon Creek represents a particularly potent source of P with a high BAP_L relative to its contribution to total inflow.

Reasonably strong empirical relationships between concentration and tributary flow (Q) were observed for forms of P, as well as a number of other constituents, that supported specification of concentrations on days without measurements for calculations of loading rates. The study period of 2013 had an above average flow, ranking 32nd in the 89 year record for Fall Creek, but the summer interval had particularly high flow ranking 6th highest of the record. Concentrations of particulate constituents increased dramatically in all of the tributaries during intervals of high Q; each of the tributaries demonstrated strong positive dependencies on Q for these constituents. The sediment delivered to Cayuga Lake was dominated by inorganic (minerogenic) material. Constituent loads were calculated at a time step of daily, to be consistent with the needs of the future mechanistic water quality model for the lake.

Cayuga Lake Watershed Modeling

The watershed model development for this project involved compiling the necessary meteorological, land cover, and land management data for the 860 square mile Cayuga Lake Watershed. Because there is interest in both particulate and soluble phosphorus, the decision was made to focus on the USDA Soil and Water Assessment Tool (SWAT), because it includes modules designed to simulate the necessary landscape phosphorus (P) transformations and in-stream P processes. The model has been set-up and tested for the major tributaries in the southern-end of the watershed. A primary focus has been the Fall Creek sub-watershed, because of the copious historical and on-going monitoring that provide data for calibrating and testing the model, and because it represents the largest sub-watershed area for Cayuga Lake. Additionally,

the model team is working with local Soil and Water Conservation Districts, Pro-Dairy, and the New York State Soil and Water Conservation Committee to develop a land management algorithm for Fall Creek and a strategy for extending it to the entire watershed. At this time, we have a preliminary land management algorithm that we are testing in collaboration with the aforementioned stakeholders and a preliminary model calibration. We will continue to refine these through early 2015. Currently there are two issues with the SWAT model that we need to correct: (1) the storm flow-to-base-flow ratio is too high and (2) the organic-to-inorganic phosphorus ratio is not agreeing with the UFI measurements. SWAT model files will be submitted as soon as these two issues are resolved.

Hydrothermal/Transport Submodel

A two-dimensional longitudinal – vertical hydrothermal/transport model (W2/T; the transport submodel of CE-QUAL-W2) was set up, tested, and preliminarily applied for Cayuga Lake. The model was supported by long-term monitoring of meteorological and hydrologic drivers and calibrated and validated using in-lake measurements made at multiple temporal and spatial scales over sixteen years. Measurements included (1) temperature profiles at multiple lake sites for ten years, (2) near-surface temperatures at one end of the lake for sixteen years, including irregular occurrences of upwelling events, (3) timing and magnitude of seiche activity (oscillations of stratified layers) for two years, and (4) transport of a conservative tracer. The model demonstrates excellent temporal stability, maintaining good performance in uninterrupted simulations over a period of fifteen years. Performance is better when modeling is supported by on-lake versus local land-based meteorological measurements.

The validated model has been applied through numeric tracer experiments, to evaluate various features of transport of interest to water quality issues for the lake, including (1) residence times of stream inputs within the entire lake and the shelf, (2) transport and fate of negatively buoyant (i.e., tending to plunge) streams, and (3) the extent of transport from the hypolimnion to the epilimnion. Multiple factors contribute to making W2/T an appropriate transport submodel for the P-eutrophication model for Cayuga Lake, including (1) the basin morphology and associated transport characteristics, (2) longitudinal differences in water quality metrics imparted from localized inputs, particularly extending from the southern end, and (3) the demonstrated performance of W2/T in representing transport in this lake across multiple time scales.

Limnology

A number of noteworthy limnological signatures were resolved through routine *in situ* instrumentation measurements, including (1) the development of strong thermal stratification in summer, (2) occurrences of seiche activity, (3) entry of turbid waters from the shelf area toward northern areas, (4) occurrences of deep chlorophyll maxima (DCM) in metalimnetic depths, and (5) abrupt changes on the shelf coupled to runoff events. Conditions on the shelf with respect to

optical metrics of water quality, including Secchi depth (SD, a measurement of clarity), were on average degraded relative to the deeper pelagic portions of the lake. These conditions were particularly acute following runoff events, primarily associated with inorganic (minerogenic) sediment received from the local streams. Differences between the pelagic sites for these metrics were generally minor, a recurring feature also observed for most of the laboratory measurements of collected samples. Spatial patterns for the upper waters for laboratory measurements for the nine sites were resolved on a time-averaged basis. A gradient in concentrations was observed for most parameters including multiple forms of P and metrics of sediments, with tributaries > site 1 (shelf, adjoining tributaries) > site 2 (shelf) > pelagic sites. Particularly noteworthy exceptions were chlorophyll *a* (Chl-*a*) and nitrate nitrogen (NO_3^-), for which no significant differences between the shelf and pelagic sites were observed. The New York State guidance value for the summer average concentration of total P (TP) of 20 µgP/L was exceeded at site 1 (shelf) and approached at site 2 (shelf).

Strong temporal variations were resolved for the shelf for most laboratory analytes that were linked to runoff events, during which the greatest differences with pelagic conditions prevailed. A key metric of the effects of minerogenic particles was demonstrated to be the projected area of minerogenic particles per unit volume (PAV_m). PAV_m is reported to be linearly related to contributions of minerogenic particles to PP, the minerogenic component of turbidity, the scattering and beam attenuation coefficients, and inversely related to SD. The vast majority of PAV_m delivered to the lake and found within the lake is clay mineral particles from the watershed. Increases in PAV_m on the shelf following runoff events, and lake-wide for the major events, were clearly resolved. The contributions of four particle size classes to PAV_m were represented in anticipation of the need for such an apportionment in model simulations of this attribute in the lake. The large contributions of these particles to PP on the shelf following runoff events and the low bioavailability of this P is not supportive of inclusion of such shelf observations in assessments of trophic state (e.g., state guidance value) status for that portion of the lake. A number of signatures were resolved for other metrics in pelagic waters that will be valuable to support testing of the water quality model for lake-wide conditions, including (1) depletions of soluble reactive P (SRP), dissolved silica (Si), and nitrate nitrogen (NO_3^-) in the upper waters over the spring to early summer interval, (2) increases in soluble unreactive P (SUP) in the upper waters in early summer, (3) mid-summer increases in particulate (PP) and particle organic carbon (POC) in the upper waters, and (4) increases in SRP in the near-bottom waters through early fall.

The DCM observed in the lake's metalimnion was not indicative of phytoplankton biomass maxima in those stratified layers. The relationship between the two common measures of phytoplankton biomass, POC and Chl-*a*, in the lake's upper waters was weak. POC was a better predictor of light scattering, SD, and PP than Chl-*a*. The long-term monitoring data associated with Cornell's Lake Source Cooling (LSC) facility was analyzed in an effort to identify trends. Higher TP concentrations and lower SD on the shelf compared to pelagic conditions, based on

summer average values, were recurring over the entire record (1998-2012). However, the lack of noteworthy differences in summer average Chl-*a* values between these areas was also recurring over the same period. Multiple statistical analyses were conducted on the three common trophic state metrics, TP, SD, Chl-*a*, to test for significant changes in the lake's upper waters. The only indication of a change was an increase in Chl-*a* in pelagic waters. However, given the indicated weakness of the trend and the inherent limitations in the metric, the change is not considered noteworthy. Significant increases in deep (hypolimnetic) water concentrations of SRP, and thereby total dissolved P (TDP) and TP, starting in 2004, as assessed by monitoring of the LSC discharge, have occurred.

The spring increase in phytoplankton (bloom) was dominated by the diatom group in 2013. The termination of this bloom was consistent with both limitation of this group by decreased Si concentrations and the timing of an increase in grazing zooplankton, patterns that are typical of north-temperate zone lakes in general. Cyanobacteria (previously blue-green algae) did not become sufficiently dense to form nuisance blooms or floating scums. Large *Daphnia*, a particularly efficient grazing zooplankton, capable of causing near-elimination of phytoplankton and other particles, and associated major increases in SD, were not present.

Quagga mussels were collected at all depths and in 96% of the samples collected in the extensive September-October survey of 2013. Zebra mussels were only collected at shallow depths (< 10 m), in 24% of the samples. Overall, dreissenid (includes quagga and zebra mussels) biomass decreased with depth in the lake from levels of 95 g/m^2 to less than 10 g/m^2 at depths deeper than 80 m. Application of literature-based and site specific P excretion rates to the lake wide biomass estimate support the hypothesis that mussel excretion has made a large contribution to the SRP increase in the hypolimnion. Although historic data are limited, the timing of the mussel expansion in the lake is consistent with that of the increase in hypolimnetic SRP after 2004.

Approach for Phase 2 Water Quality Modeling

The presentation and analyses of monitoring information for Cayuga Lake, particularly the detailed data set collected in 2013 as part of this study (Phase 1), have provided invaluable insights to guide Phase 2 of this study. In Phase 2 a mechanistic P-eutrophication model will be developed, tested and preliminarily applied to address the potential cultural eutrophication issue for the lake, with particular focus on the shelf. Extensive data analysis confirms that the P and sediment issues cannot be separated for this system.

The character of the conspicuous "disconnect" in the three common trophic state metrics (the concentration of TP, Chl-*a*, and Secchi depth) that has emerged in the limnological analyses established model attributes that will be necessary to adequately address these features. The disconnect refers to the lack of significant differences in Chl-*a* between the shelf and pelagic waters of the lake, despite clearly degraded TP (higher) and SD (lower) conditions on the shelf.

The disconnect has two primary elements (1) the greater contributions of minerogenic particles to TP and SD levels on the shelf from local tributary inputs, and (2) the absence of locally greater phytoplankton growth on the shelf despite higher concentrations of immediately bioavailable forms of P. The first element requires a robust treatment of minerogenic particles in the model. The second element requires attributes that appropriately represent the effects of (1) the short residence time of tributary inflows on the shelf, (2) the more limited availability of light on the shelf, particularly following runoff events, and (3) the diluting effect on local phytoplankton biomass concentrations from tributary inputs. Given that the Chl-*a* patterns for the shelf generally track lake-wide pelagic conditions, there are several nutrient and phytoplankton biomass signatures that were identified for pelagic waters that will be valuable in testing the P-eutrophication model for the entire lake.

Modeling activities in Phase 2 will embrace the principle of parsimony. Accordingly, there will be an effort to avoid overly complex components and submodels that can be accompanied by greater uncertainty and excessive computational demands. Robust temporal and spatial scales will be represented to address the primary signatures resolved in monitoring related to the project goals. Short-term patterns in response to runoff events, which are primary drivers of the shelf versus pelagic waters differences, need to be resolved, as well as the seasonality in phytoplankton growth manifested lake-wide, and the potential effects of year-to year differences in runoff. Spatial structure must resolve longitudinal differences on the shelf, between the shelf and pelagic waters, and lake-wide mixing and the effects of the thermal stratification regime. The two-dimensional model (W2/T) and the adopted segmentation scheme will provide a robust representation of these features. Drivers for the water quality model will include (a) local meteorological data, (2) hydrologic data for primary tributaries, and (3) loading rate estimates for multiple constituents, as described in this report.

A tentative listing of model state variables (n~30) has been presented that establishes that the water quality model to be developed and tested in Phase 2 will have robust predictive capabilities. The overall water quality model will be composed of several submodels, that include: (1) the two-dimensional hydrothermal/transport submodel, (2) a minerogenic particle submodel, (3) an optics submodel, (4) a phosphorus submodel, and (5) a phytoplankton growth/biomass submodel. Conceptual models depicting structural features are presented for each of the submodels in this report, which reflect insights and results of analyses derived from the Phase 1 work. However, the focus of the model remains P-eutrophication; specifically, the sediment sub-model is not being designed explicitly to support a sediment TMDL, which is outside the scope of this project.

Section 1. Background

1.1. Phosphorus, Cultural Eutrophication, Bioavailability of Phosphorus and Modeling

Cultural eutrophication remains a major contemporary water quality and ecological issue for lakes and reservoirs, despite advancements in the control of nutrient sources over the last four decades (Cooke et al. 2005). Control of phosphorus (P) is a primary management objective because it is the limiting nutrient in the vast majority of temperate inland waters (Hutchinson 1973, Sondergaard et al. 2007, Wetzel 2001). Accordingly, the behavior, or cycling, of this element has received substantial research attention (Wetzel 2001). P cycling is made complex by the large number of forms, processes, and transformations involved. Early studies and related models (Chapra 1997, Vollenweider 1976) to guide management often considered only the concentration of total P (TP) with respect to inputs (loads) and the in-lake pool of this critical nutrient. Partitioning of multiple forms of P became important in a management context as the differences in their potential to support primary production were recognized (DePinto et al. 1981, Reynolds 2006, Reynolds and Davies 2001, Sondergaard et al. 2007). Phosphorus that is available to support algal and cyanobacteria production is described as bioavailable (Auer et al. 1998, DePinto et al. 1981, Young et al. 1982), making critical the assessment of the fractions of each form of P that can support growth of primary producers and hence lead to eutrophication conditions.

Mechanistic mass balance P – phytoplankton (or eutrophication) models are widely used to guide management deliberations for systems with eutrophication issues, and are critical tools supporting P total maximum daily load (TMDL) analyses (Cooke et al. 2005). The "mechanistic" descriptor implicitly reflects the effort to utilize realistic process-based representations of lacustrine systems in a model structure. A broad range of model complexity (e.g., number of processes and interactions considered) has been adopted in contemporary modeling efforts (Arhonditsis and Brett 2004, Chapra 1997, Robson 2014). Most of these represent the patterns of the various operationally defined forms of P addressed in this study. Despite myriad differences in structural detail, these models generally share certain features, as they all accommodate: (1) external loading of multiple forms of P, (2) other environmental forcing conditions (e.g., light and temperature), (3) transport and mixing processes, and (4) the processes and associated kinetics that regulate P cycling, and phytoplankton growth and loss processes. Additionally, a model must represent important system-specific characteristics, including prominent features of the resident biological communities.

The phytoplankton community is a primary target for the simulation capabilities of mechanistic P-eutrophication models (Chapra 1997). Representative predictions of the concentration of phytoplankton biomass, and in some cases the community's composition, are goals of these modeling initiatives. Moreover the interplay between zooplankton and

phytoplankton dynamics (Wetzel 2001) may require representation of both communities for successful simulations. Accordingly, it is important to have contemporary robust characterizations of both the phytoplankton and zooplankton communities to guide related structural features of a system-specific model. Ultimately phytoplankton abundance is a primary environmental quality indicator. Different species of phytoplankton have different nutrient requirements, grow at different rates, are differently edible to the zooplankton that consume them, and end up in different places in the lake basin when they die and decompose (Reynolds 2006). Zooplankton species differ in how efficiently they consume phytoplankton, and in the taxa of phytoplankton they capture and ingest (Wetzel 2001). Water bodies with high densities of phytoplankton are turbid, affecting aesthetic quality, and decreasing light penetration with effects on the growth of rooted macrophytes, and the ability of fish to locate their prey. Cyanobacteria, a common component of the phytoplankton in phosphorus-enriched lakes, can cause nuisance conditions. *Daphnia*, a genus of cladoceran zooplankton, is a generalist, highly efficient filter-feeder with the capability of driving phytoplankton to very low densities, even when nutrient concentrations are high (Lampert et al. 1986). In contrast, herbivorous copepods are selective feeders that do not generally consume cyanobacteria and do not have a marked effect on phytoplankton densities. For these reasons, monitoring the abundance and taxonomic composition of both phytoplankton and zooplankton provides critical information for understanding the biological basis for phytoplankton response to nutrient enrichment in lakes, and for the broader impacts of plankton in the lake ecosystem.

Dense populations of the invasive dreissenid mussels have been demonstrated to have substantial water quality and ecological impacts associated with various aspects of their metabolism, including grazing, excretion and respiration (Higgins et al. 2010, Nalepa and Schloesser 2014). In a meta-analysis including several North American and European Lakes, mussel grazing of phytoplankton was associated with significant decreases in Chl-*a* and higher water clarity (Higgins et al. 2010). Zebra mussels, that prefer shallow rocky substrates, initially were dominant. These have been largely replaced by quagga mussels in many deep systems (Watkins et al. 2007, Nalepa et al. 2009), as they tolerate cold temperatures, soft substrates, and reduced abundance of food. Grazing by the large biomass of deep dwelling quagga mussels has been implicated in the disappearance of spring phytoplankton blooms in Lake Michigan in the early 2000's (Vanderploeg et al. 2010). The first detection of dreissenid mussels in Cayuga and Seneca Lakes was in 1991 (zebras) and 1994 (quaggas), closely following the Great Lakes expansion. By 2006, quagga mussels had largely replaced zebra mussels and had reached abundances at depths extending to 100 m (Watkins et al. 2012).

Partitioning external loads of P according to sources is fundamental information to support related rehabilitation initiatives, such as those guided by the TMDL analysis process (USEPA 1991). The bioavailability of P in external loads is increasingly incorporated in these modeling initiatives (Effler et al. 2002, Effler et al. 2012), an approach that has been embraced for the Cayuga Lake TMDL analysis (Prestigiacomo et al. 2015). Bioavailability bioassays are needed

to quantify the fractions of the various forms of P that are bioavailable in the important external sources to support estimates of the magnitudes of bioavailable P loads (Auer et al. 1998, Effler et al. 2012, Prestigiacomo et al. 2015). Accurate loading estimates also require: (1) an appropriate strategy for sampling the inputs (tributaries and point source inputs), and (2) application of appropriate calculation protocols (Defew et al. 2013). A focus on frequent sampling during runoff events is important, as a large portion of P loads carried by many streams annually occurs over relatively brief intervals of high flow (Longabucco and Rafferty 1998, Richards and Holloway 1987). The development of relationships between concentrations and stream flows (Q), or other drivers such as temperature, is a central feature in supporting load calculations (Raymond and Saiers 2010, Vogel et al. 2003), by providing a basis to specify concentrations for intervals not covered by measurements.

The estimates of external loads serve to support testing of both lake water quality and watershed models. Watershed models provide critical management information, particularly for systems such as Cayuga Lake where external loads are regulated primarily by non-point sources rather than point (e.g., discharges) sources. These tools, once validated, can support realistic projections of loading changes to be expected by various landuse management actions. Integration of these inputs to drive lake water quality projections provides an invaluable overall tool to support management deliberations related to potential improvements in lake quality.

The three common trophic state metrics are TP, the concentration of chlorophyll *a* (Chl-*a*; a surrogate of phytoplankton biomass), and Secchi disk depth (SD; Chapra 1997). Phosphorus – eutrophication models are expected to support predictions of each of these, as they may be specified for related water quality guidelines or standards. Moreover, consistent changes in all three parameters are generally assumed in response to management actions. However, inorganic (or minerogenic) particles can complicate relationships between the trophic state metrics because they, in addition to phytoplankton, have associated P and contribute to diminished SD (Effler and Peng 2014, Effler et al. 2014). Accordingly, the effects of minerogenic particles need to be included in P-eutrophication modeling initiatives where they influence importantly the TP and SD measurements. Otherwise, model predictions may not be reliable with respect to expectations in response to management actions. Indeed, systematic improvements in SD are widely expected in response to management actions directed at reductions in P loading and in-lake concentrations of P and phytoplankton biomass (Cooke et al. 2005).

1.2. Description of Cayuga Lake

Cayuga Lake (42º 41′ 30″ N; 76º 41′ 20″ W) is the fourth easternmost of the New York Finger Lakes (Figure 1-1), and has the second largest surface area (172 km^2) and volume (9.4 x 10^9 m^8) of this group of lakes. The mean and maximum depths are 55 m and 133 m, respectively. This long and narrow system has an aspect ratio (length along its major axis ÷ average width) of twenty-two (eleven, if maximum width is used), and is positioned along a mostly north-south axis that coincides with prominent wind directions (Figure 1-1). Cayuga

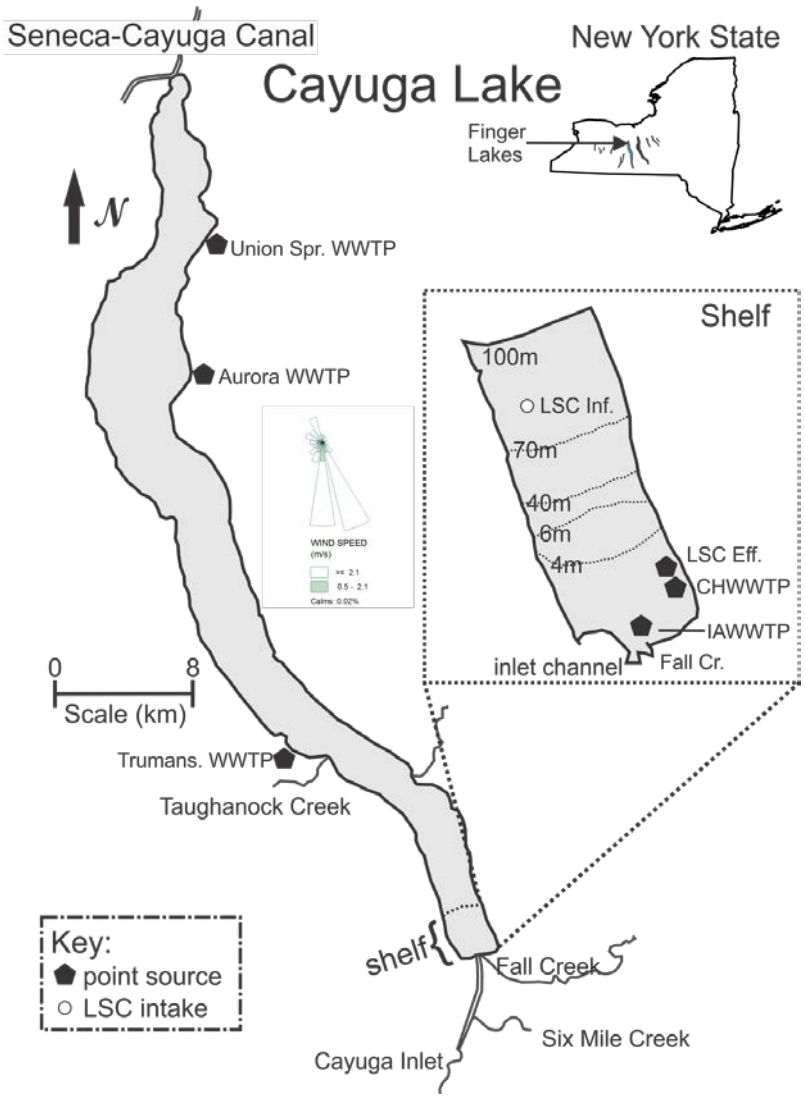

Figure 1-1. Cayuga Lake, position within New York, and the eleven Finger Lakes. Shown are five monitored tributaries, WWTPs and Lake Source Cooling (LSC) facility discharges. Four USGS gages, and the shelf portion of the lake at its southern end.

Lake has a warm monomictic stratification regime, stratifying strongly in summer through mid-fall, but only rarely developing complete ice cover (Oglesby 1978). Internal seiches (e.g.., lake-scale tilting of the metalimnion), internal waves (oscillations in stratified layers), and upwelling events occur in the lake in response to wind energy inputs, that are promoted by its elongated shape and the prevailing wind direction (Effler et al. 2010). The average retention time of the lake, calculated by dividing its volume by the total volumetric inflow rate (e.g., completely mixed assumption, Rueda et al. 2006), is nine years.

Nearly 40% of the total tributary inflow to the lake enters the southern end, specifically from Fall Creek, Cayuga Inlet, and Six Mile Creek (Table 1-1; Figure 1-1). Two other tributaries of noteworthy size enter the lake further north, Salmon Creek, that enters from the east, and Taughannock Creek that enters from the west (Figure 1-1). Thirty smaller streams, draining ~ 40% of the overall watershed, flow into the lake; the associated individual watersheds are small (< 3.5% of the total; Haith et al. 2012). Fall Creek, the largest of the tributaries, has the longest record of gaged flow (since 1925). Three other tributaries are gaged, Cayuga Inlet, Six Mile Creek and Salmon Creek. Agricultural landuse is particularly high in the Salmon Creek watershed (68%), but is also substantial in portions of the watershed with small tributaries and Fall Creek (Table 1-1). Effluent from two domestic wastewater treatment facilities (Ithaca Area WWTP (IAWWTP) and Cayuga Heights WWTP (CHWWTP)), serving the City of Ithaca and bordering suburbs, along with the discharge of spent cooling water from a "lake source cooling" (LSC) facility, also enter the southern end of the lake (Figure 1-1). The LSC facility withdraws cold water from the pelagic zone at a depth of 73 m to meet cooling demands for Cornell University (i.e., greater withdrawals in summer) and returns the spent cooling water to the shelf. Treatment targeting P removal has been upgraded for the two WWTPs over the last decade. In May 2006, IAWWTP, the largest of the WWTPs (Table 1-1), implemented micro-sand ballasted flocculation, that uses ionic polymer and ferric chloride for P removal. The CHWWTP as well as several smaller WWTPs that enter the lake further north (Figure 1-1) have chemical P treatment.

Cayuga Lake is a P-limited mesotrophic Lake (Effler et al. 2010, Oglesby 1978). The localized entry of such a large fraction of the tributary flow delivers locally high loads of various constituents to the lake's southern end. In particular, large quantities of phosphorus (see Section 3.6.1; Prestigiacomo et al. 2015), sediment (see Section 3.6.1.5 for TSS and Tn, Section 3.6.1.6 for PAV; Effler and Peng 2014), and dissolved organic carbon (DOC) and dissolved color (see Section 3.6.1.8; Effler et al. 2015a), are delivered to the southern end of the lake by these tributaries during runoff events. Conditions in the shallow southern end, designated the "shelf" (Figure 1-1; earlier demarcated by the 6 m contour of depth, now by the 10m contour of depth), have generally been considered degraded relative to the pelagic zone (Oglesby 1978, Effler et al. 2010, Effler et al. 2014). Monitoring since the late 1990s has established that two trophic states metrics, TP and SD, are significantly higher and lower, respectively, on the shelf compared with pelagic waters, and that Chl-*a* concentrations are not significantly different (Effler et al. 2010).

Table 1-1. Cayuga Lake tributaries stream flow, watershed description, land use, and 2013 sampling information

Tributary	Flow Information			Watershed		Land Use Percent[1]		
	USGS Gauge	Record	Mean Q (m^3/s)	Area (km^2)	%	A	F/B, R	U
Fall Creek	04234000	89y	6.08	330.9	17.7%	49%	40%	11%
Cayuga Inlet[2]	04233255	77y	2.70	240.8	12.9%	29%	56%	15%
Salmon Creek	0423401815	8y	3.60	233.8	12.5%	68%	25%	7%
Taughannock Creek[3]	-	-	3.39	173.0	9.3%	49%	40%	11%
Six Mile Creek	04233300	19y	2.07	134.1	7.2%	22%	63%	15%
Unmonitored Tributaries[4]	-	-	14.3	758.1	41%	62%	23%	15%
Total	**-**	**-**	**28.8**	**1870.7**	**100%**	**60%**	**26%**	**14%**

[1] A – agriculture, F/B – forest/brush, R – other rural, U – urban (from Haith et al. 2009);
[2] gauge moved in 2011;
[3] ungaged, flow estimates from VSA watershed model (Archibald et al. 2014);
[4] estimated from product of total gaged flow (sum) and ungaged: gaged watershed area ratio.

Summer (June-September) average concentrations of TP on the shelf have irregularly exceeded the sate guidance value of 20 µg/L, which has been identified as a water quality issue of concern. The New York State Department of Environmental Conservation has listed the southern end of Cayuga Lake (e.g., shelf) as an impaired segment with respect to P and sediment in *"The Final New York State 2012 Section 303(d) List of Impaired Waters Requiring a TMDL/Other Strategy"*.

1.3. Goals and Phasing for Phosphorus-Eutrophication Model Study for Cayuga Lake

The overarching goal of this study is to develop and test a water quality phosphorus/eutrophication model for Cayuga Lake. It is intended that this integrated model will be capable of supporting a phosphorus TMDL analysis for the shelf. This initiative recognizes the bioavailability concept for external P inputs and the potential importance of the phytoplankton, zooplankton, and mussel communities. Moreover, it is acknowledged that the lake model will also have comprehensive predictive capabilities for sediment (primarily minerogenic particles), because of its influence on both P and clarity levels in this lake (Effler et al. 2014, Effler and Peng 2014, Prestigiacomo et al. 2015), as well as potentially influencing phytoplankton production.

The overall Cayuga Lake study initiative has five technical elements:

1. tributary monitoring to support specification of dynamic loading conditions, the bioavailability of the external phosphorus inputs, and testing and application of the watershed/land use and lake phosphorus/eutrophication models,

2. lake monitoring for water quality variables and related biological communities,

3. setup and testing of a two-dimensional hydrothermal/transport model for the lake,

4. setup and testing of a watershed/land use model that will quantify the dependence of tributary loading on land use and meteorological drivers, and

5. development, testing and application of a phosphorus/eutrophication model for the lake.

This work is being conducted in a phased manner. Technical elements 1-4 are all part of Phase 1 of this two-phase project. The detailed scope and protocols agreed upon for the Phase 1 work were documented in the Quality Assurance Project Plan (QAPP) for "*Phase 1: Monitoring and Modeling Support for a Phosphorus/Eutrophication Model for Cayuga Lake"* (Upstate Freshwater Institute 2013). This report documents salient findings from the Phase 1 work. Specifically it presents and analyzes observations from the tributaries and lake, and describes the set-up and testing of a hydrothermal/transport model for the lake and model(s) for the watershed. A synthesis of the findings is presented in the context of structural needs of a lake water quality model, and desired modeling protocols, to meet the goals for a credible model system for Cayuga Lake.

This page intentionally left blank.

Section 2. Selective Review of Scope of Tributary and Lake Monitoring

2.1. Monitoring in 2013

An extensive monitoring program for the Cayuga Lake system was conducted in 2013 to support the development and testing of a phosphorus/eutrophication model. The scope of this program was ambitious with respect to: (1) the number and character of the parameters to be tracked, (2) the interdisciplinary character reflected in the parameter types, and (3) the temporal and spatial scales to be covered. The details of the study and monitoring program designs and the protocols adopted were comprehensively presented in a Quality Assurance Project Plan (QAPP), *"Phase 1 Monitoring and Modeling Support for a Phosphorus/Eutrophication Model for Cayuga Lake"* (Upstate Freshwater Institute 2013). The QAPP should be consulted to obtain more detailed information concerning project scope.

2.2. Watershed

The Cayuga Lake watershed is located in the Finger Lakes region of Central New York. It forms part of the Great Lakes Basin and its discharge via the lake outlet makes its way into Lake Ontario. The Cayuga Lake Watershed is a large watershed encompassing more than 223,000 hectares (ha) which are located in a total of 7 counties. These counties include Tompkins, Cortland, Cayuga, Seneca, Schuyler, Tioga, and Ontario. The location of the Cayuga Lake watershed in relation to these counties can be found in Figure 2-1.

A wide array of land uses are found within the watershed that include urban areas such as the City of Ithaca, rural areas dominated by agricultural land use, and natural landscapes such as forests and wetlands. A map of the land cover within the Cayuga Lake watershed can be found in Figure 2-2. Agricultural land use is of special importance in the Cayuga Lake watershed as it accounts for approximately 50% of the land cover and can be broken into two categories, cultivated crops and pasture land. Cultivated crops cover approximately 58,000 ha equaling 26% of the total watershed area. Figure 2-3 highlights the locations within the watershed where cultivated crops are the dominant land use. Similarly, pasture land accounts for 56,000 ha within the Cayuga Lake watershed which represents approximately 25% of the watershed area. Pasture lands within the watershed are highlighted in Figure 2-4. As can be seen in the figures, cultivated crops are more concentrated in the mid to northern sections of the watershed on both the east and west sides of the lake. Pasture lands, however, are evenly dispersed throughout the watershed with the only exception being the urbanized area at the southern end of Cayuga Lake where the City of Ithaca is located.

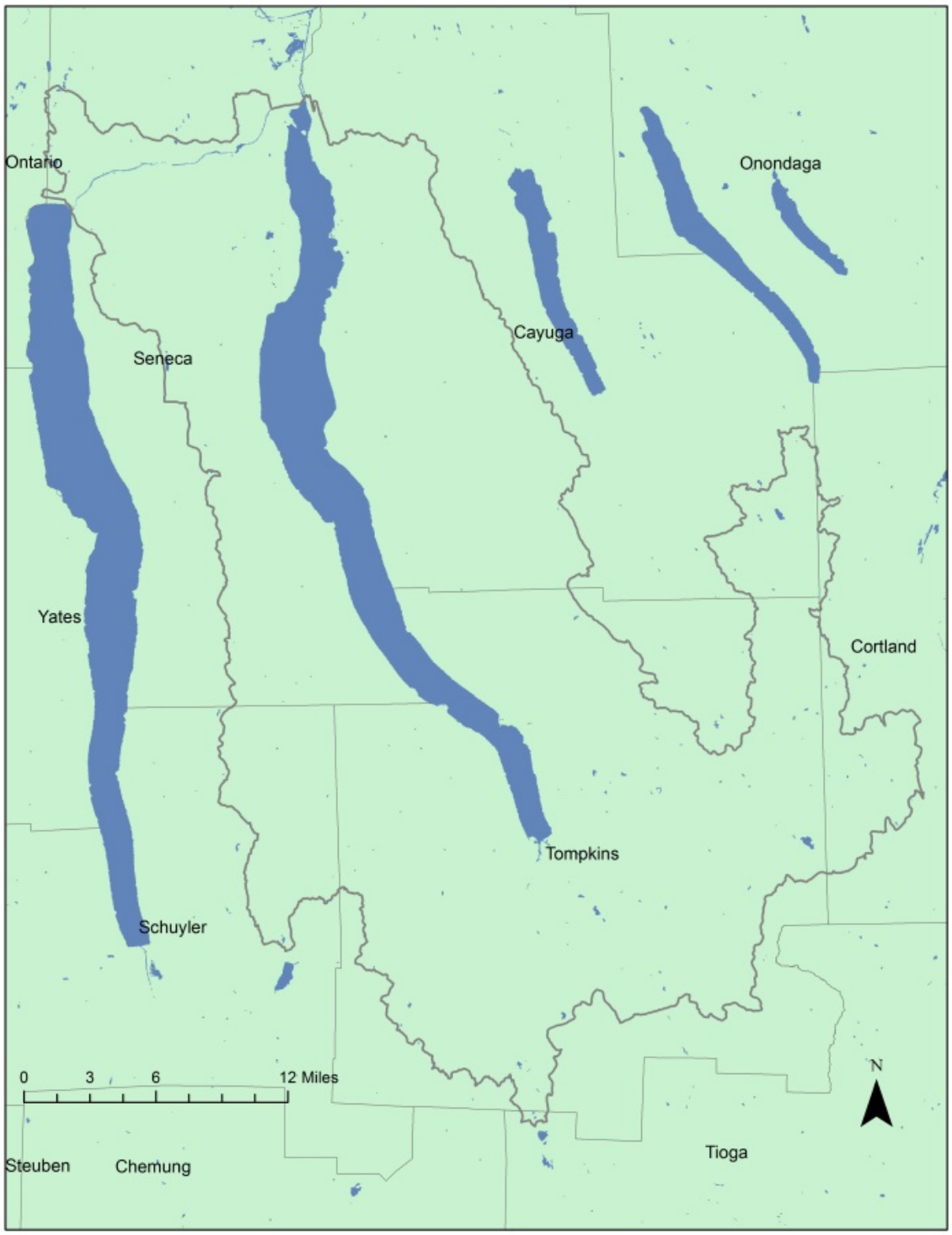

Figure 2-1. A map of the Cayuga Lake watershed with county boundaries.

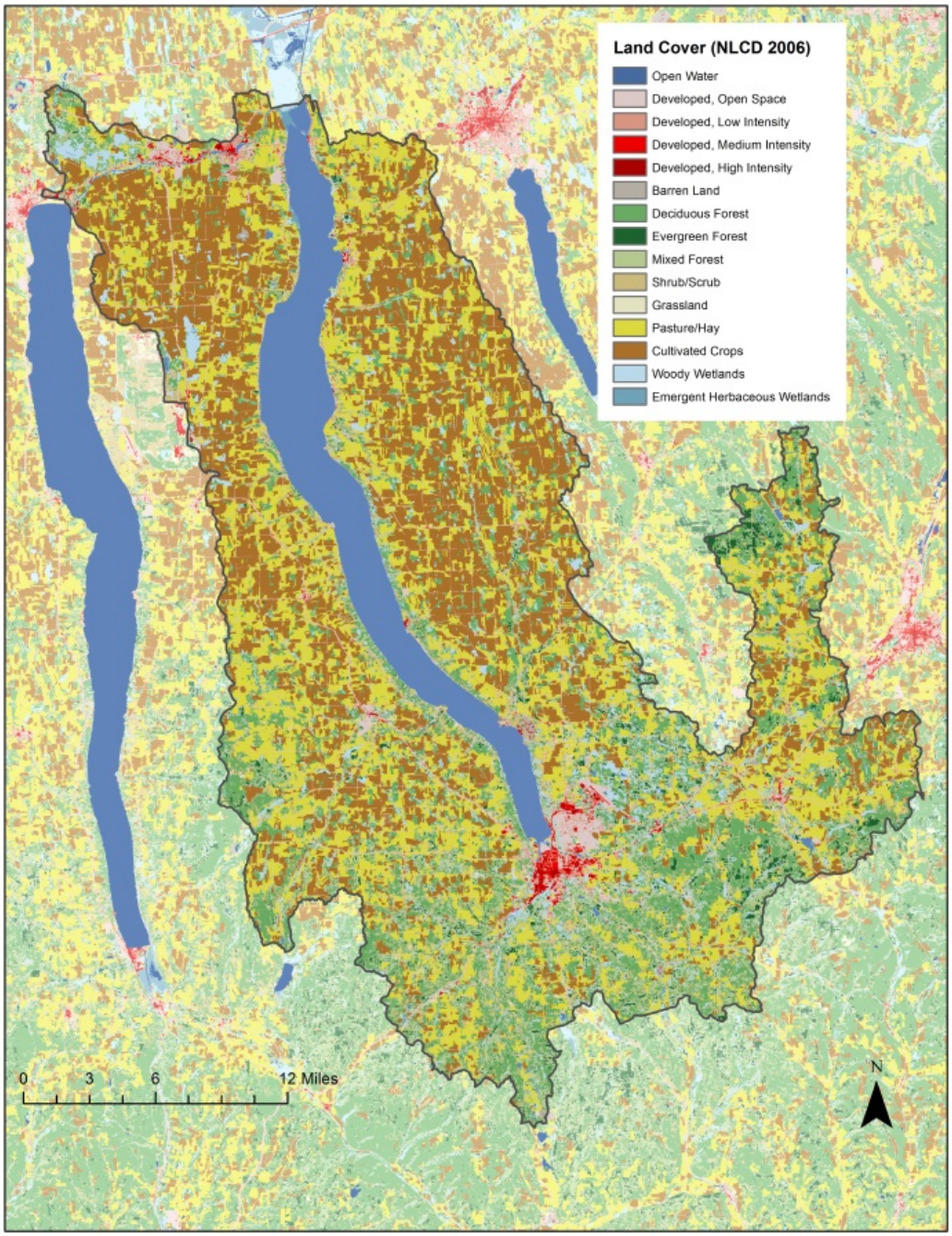

Figure 2-2 A map of the Cayuga Lake watershed with land use.

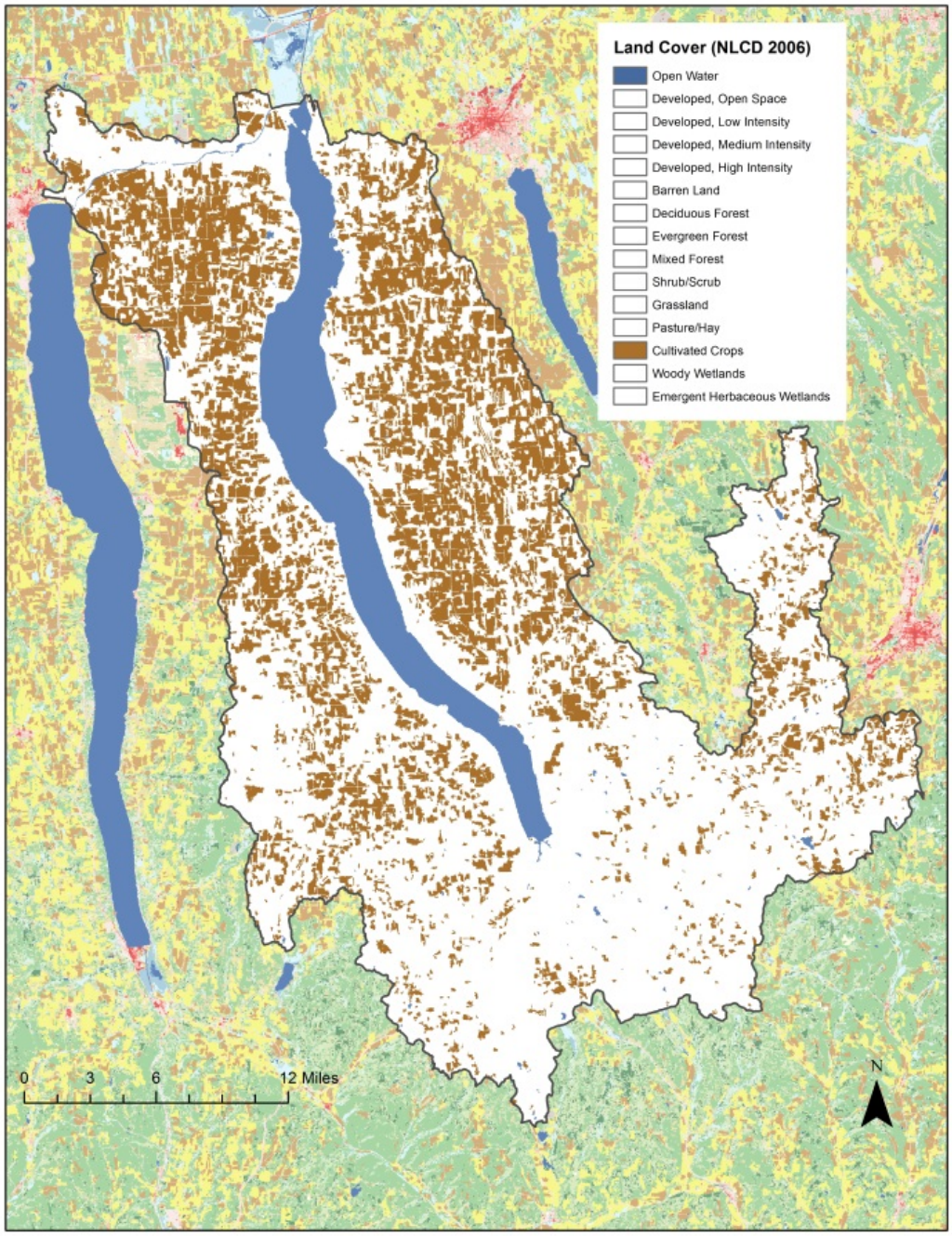

Figure 2-3. A map of the Cayuga Lake watershed with cultivated crop land use highlighted.

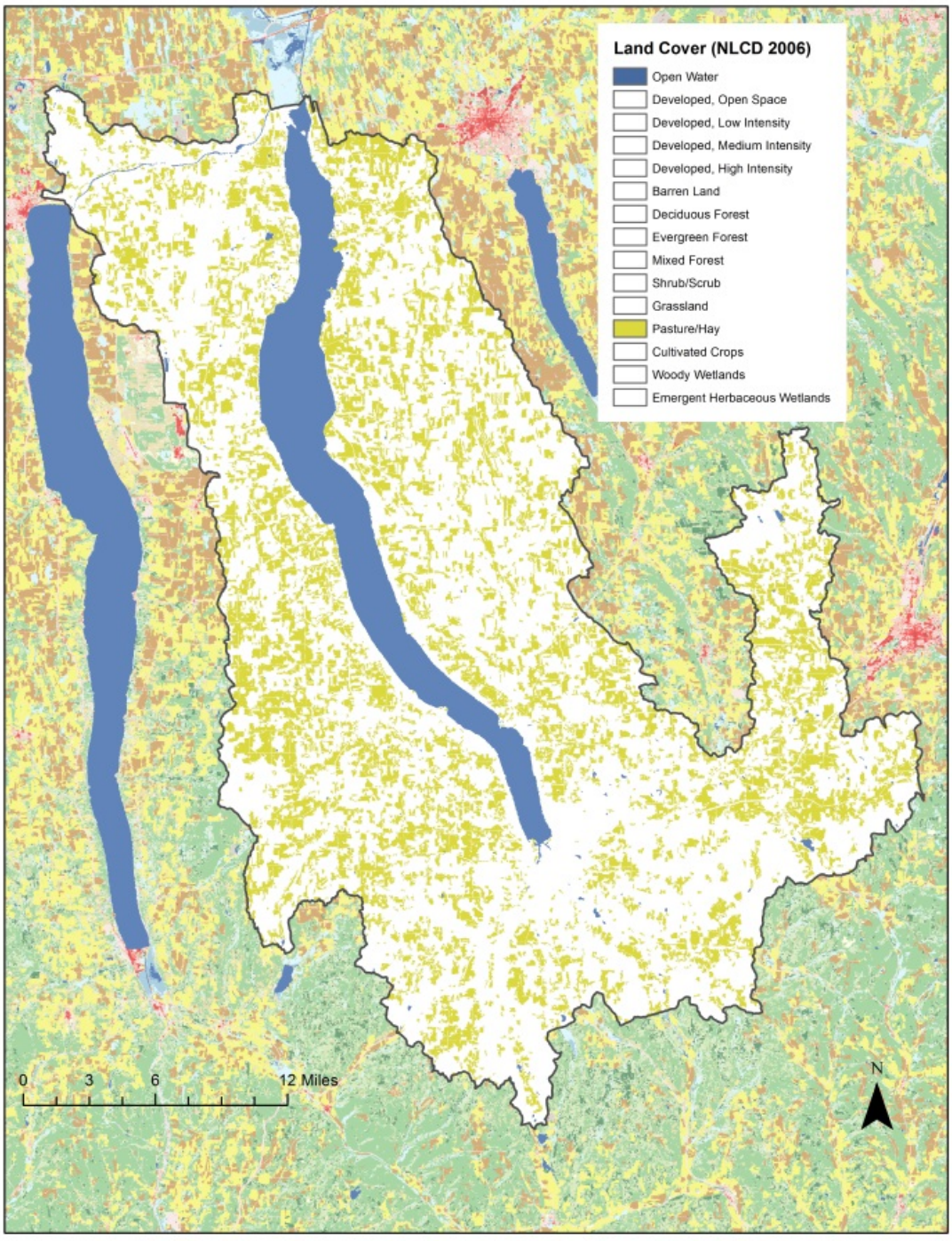

Figure 2-4. A map of the Cayuga Lake watershed with pasture/hay land use highlighted.

The larger Cayuga Lake watershed can be broken down into smaller subwatersheds. Many of the subwatersheds that contribute to the lake are small, but there are a few large subwatersheds which make the greatest contribution to the lake. These include, but are not limited to; Fall Creek, Six Mile Creek, Cayuga Inlet, Taughannock Creek and Salmon Creek. A map is provided in Figure 2-5 outlining the subwatersheds with the larger watersheds highlighted and labeled.

2.3. Tributaries

The five largest tributaries to the lake (Figure 2-6) were monitored in 2013; four of these tributaries were gaged by the USGS (Figure 2-6). The monitored tributaries are identified, and selected features presented in Table 1-1. There were four types of tributary sampling conducted during this Phase 1 project. Three were conducted at the mouths of the tributaries, fixed frequency (FF) sampling, runoff event (E) sampling, and bioavailability bioassay sampling. The fourth was upstream synoptic event (SE) surveys conducted on Salmon and Fall Creek during runoff events, to support watershed modeling. These samples were collected during two separate events: one in early April and one in late October – early November, for the mouth site and four upstream sites (Figure 2-6). For FF sampling Fall Creek, Cayuga Inlet, Salmon Creek, Six Mile Creek and Taughannock Creek were all monitored as close to the lake as conditions (e.g., accessibility, absence of backflow effects from the lake) allowed (Figure 2-6), at a frequency of once every two weeks (bi-weekly). The E sampling was conducted on Fall Creek, Cayuga Inlet, Salmon Creek, and Six Mile Creek for 11, 8, 10 and 8 wet weather events, respectively, during the March – November interval. This sampling was conducted through the use of automated sampling equipment. Sampling for the bioavailability bioassays was conducted at each of the four tributary mouth sites three times during the March – November interval in 2013. Samples for the bioassays were also collected on three occasions from IAWWTP and CHWWTP. The laboratory water quality parameters (specified in Table 2-1 for measured constituents and Table 2-2 for derived constituents) collected for FF, E and SE sampling are summarized on Table 2-3. Field measurements were made during for FF and SE samplings using a YSI hand held meter to obtain temperature (T), specific conductance (SC), and turbidity (Tn).

2.4. Lake

2.4.1. Field and Laboratory Water Quality Sampling

Two types of in-lake water quality sampling were conducted on Cayuga Lake in 2013 during the Phase 1 Project, lake-wide sampling and frequent south sampling. Lake-wide sampling was conducted twice per month (bi-weekly) April – October at lake sites 1-9 and one site I_L located near the mouth of the Cayuga Inlet channel (Figure 2-7). Frequent south sampling included sites 1-3 and I_L, only (Figure 2-7), and was conducted more frequently (twice per week) over the June – September interval. The metrics for lake water quality can be partitioned according to field measurements and laboratory measurements. The *in situ* water

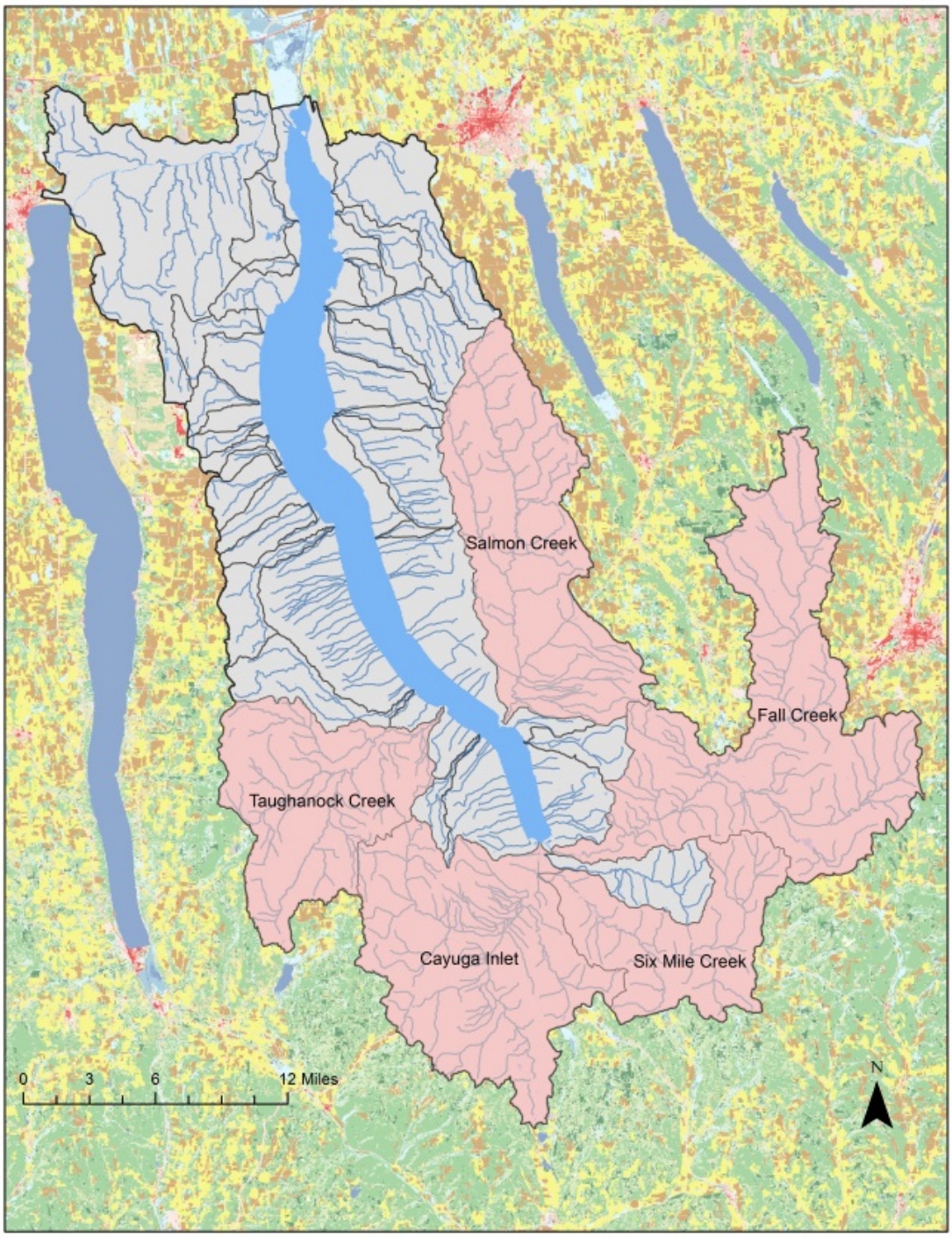

Figure 2-5 A map of the Cayuga Lake watershed with the larger southern subwatersheds highlighted in pink.

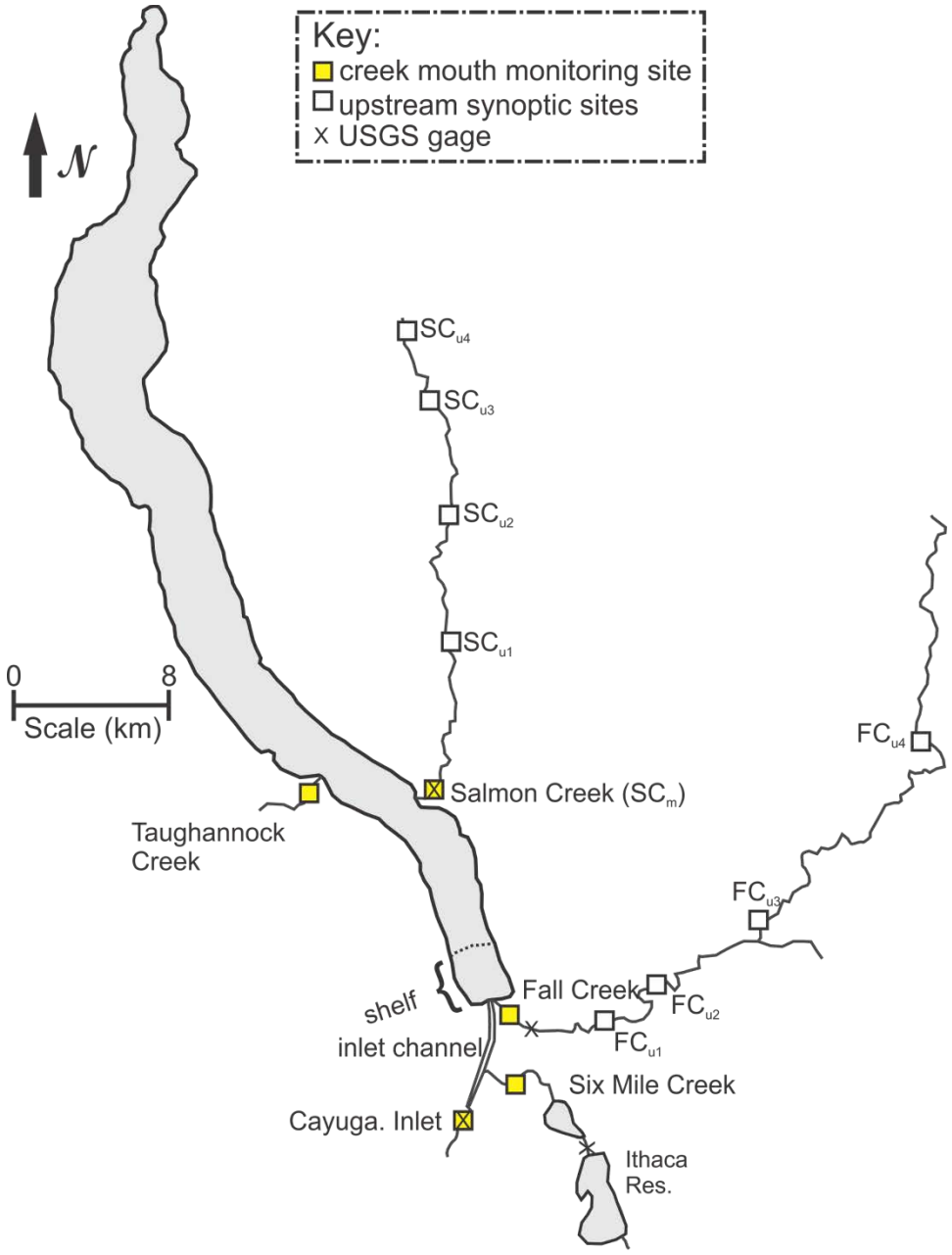

Figure 2-6. Cayuga Lake tributary monitoring sites for FF, E and SE sampling, in 2013.

Table 2-1. Listing, abbreviations and units of laboratory measured parameters.

No.	Pool	Analyte	Abbreviation	Unit
1	phosphorus	soluble reactive phosphorus	SRP	µgP/L
2		total phosphorus	TP	µgP/L
3		total dissolved phosphorus	TDP	µgP/L
4		total inorganic phosphorus	TIP	µgP/L
5	nitrogen	nitrate + nitrite	NO_X	µgN/L
6		ammonia	t-NH_3	µgN/L
7		total nitrogen	TN	µgN/L
8		total dissolved nitrogen	TDN	µgN/L
9	carbon	dissolved organic carbon	DOC	mgC/L
10		particulate organic carbon	POC	mgC/L
11	algal	chlorophyll *a*	Chl-*a*	µg/L
12		dissolved reactive silica	Si	mg SiO_2/L
13	particles	total suspended solids	TSS	mg/L
14		fixed suspended solids	FSS	mg/L
15		turbidity	Tn	NTU
16		beam attenuation at 660 nm	$\boldsymbol{c}_{660}$	1/m
17		projected area per unit volume, minerogenic particles (by SAX)	PAV_m	cm^2/L

Table 2-2. Listing, abbreviations, and units of parameters calculated from laboratory measured constituents.

No.	Pool	Analyte	Calculation	Abbreviation	Units
1	phosphorus	particulate phosphorus	= TP – TDP	PP	µgP/L
2		soluble unreactive phosphorus	=TDP – SRP	SUP	µgP/L
3	nitrogen	dissolve organic nitrogen	=TDN – (NO_X + t-NH_3)	DON	µgN/L
4		particulate nitrogen	=TN – TDN	PN	µgN/L
5	particles	volatile suspended solids	= TSS – FSS	VSS	mg/L

Table 2-3. Listing of laboratory measured parameter abbreviations and inclusion in monitoring for tributaries to Cayuga Lake in 2013.

Analyte		Tributary										
		Fall Creek			Cayuga Inlet		Salmon Creek		Six Mile Creek			Taughan-nock
		FF	E	SE	FF	E	FF	E	SE	FF	E	FF
phosphorus	TP	X	X	X	X	X	X	X	X	X	X	X
	TDP	X	X	X	X	X	X	X	X	X	X	X
	SRP	X	X	X	X	X	X	X	X	X	X	X
	TIP	X	X	--	X	X	X	X	--	X	X	X
nitrogen	NO_X	X	X	X	X	X	X	X	X	X	X	X
	t-NH_3	X	X	X	X	X	X	X	X	X	X	X
carbon	DOC	X	X	--	X	X	X	X	--	X	X	X
silica	Si	X	X	--	X	X	X	X	--	X	X	X
particles	TSS	X	X	X	X	X	X	X	X	X	X	X
	FSS	X	X	X	X	X	X	X	X	X	X	X
	Tn	X	X	X	X	X	X	X	X	X	X	X
	PAV_m	X	X	X	X	X	X	X	X	X	X	--

quality measurements, with the exception of Secchi disk depth, were conducted with a rapid profiling instrument. *In situ* water quality parameters measured on Cayuga Lake in 2013 for the two sampling regimes, their abbreviation, and locations and frequency of measurements are summarized on Table 2-4. Laboratory water quality parameters (defined in Table 2-1 for measured constituents and Table 2-2 for derived constituents) measured on Cayuga Lake in 2013 for the two sampling regimes, their abbreviation, and locations and frequency of measurements are summarized in Table 2-5.

2.4.2. Phytoplankton and Zooplankton Sampling

Phytoplankton and zooplankton sampling was conducted as part of the bi-weekly lake-wide program. For phytoplankton, samples were collected on Cayuga Lake in 2013 from the upper waters for 5 sites. Sites 3, 5 and 7 (Figure 2-7) were sampled as a composite of samples collected for the 0-10 m depth interval at 2.5 m increments. Sites 1 and 9 were sampled as a composite of 0 and 2.5 m samples because of their shallow depth. Lower water phytoplankton samples were collected at sites 3, 5 and 7 at a depth of 60 m. Two zooplankton tows were collected at sites 3, 5, and 7 (Figure 2-7); an epilimnion tow 0-10 m and a lower water tow 20-60 m. A zooplankton tow was collected at sites 1 and 9 over 0 and 2.5 m depth interval because of their shallow depth.

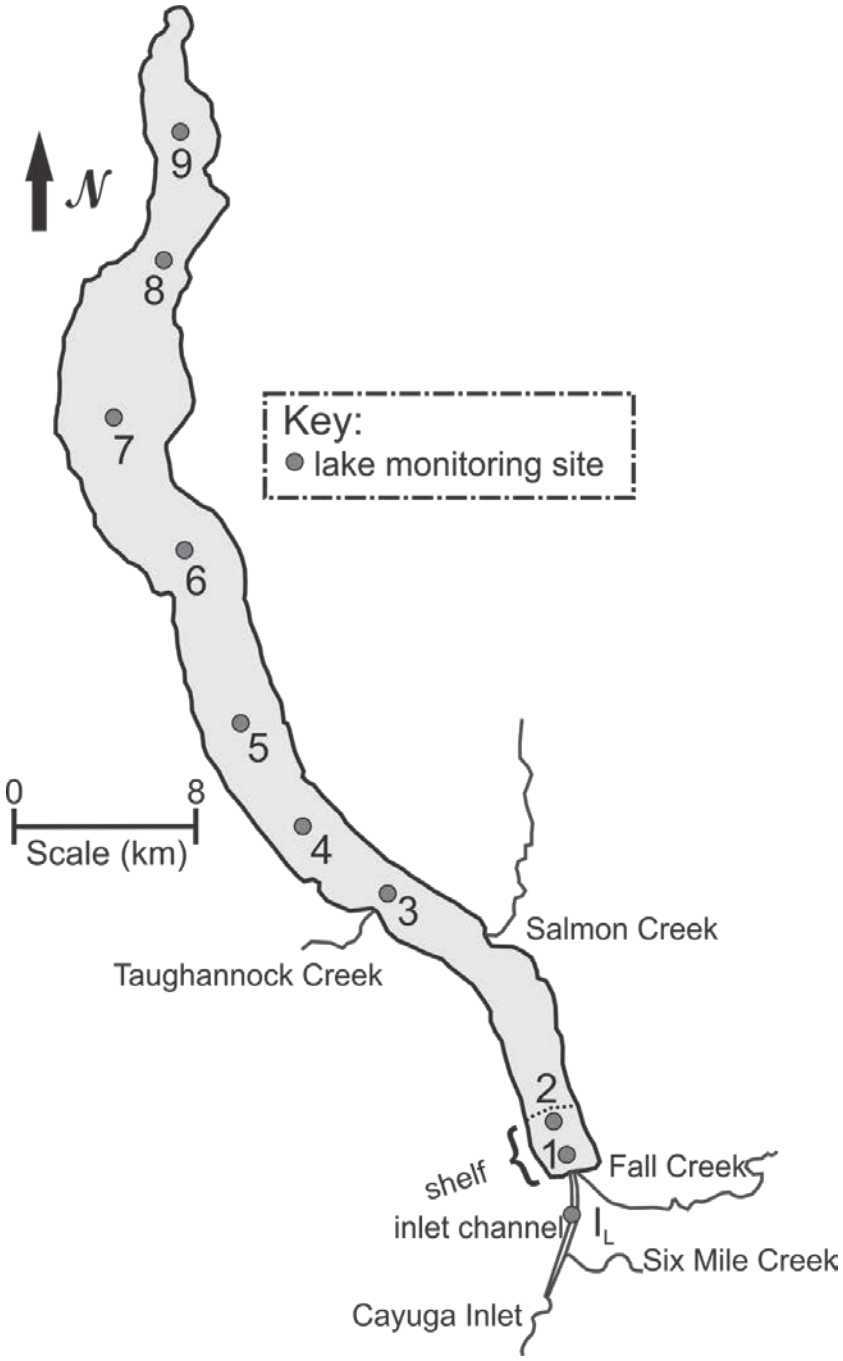

Figure 2-7. Monitoring sites in Cayuga Lake for 2013 program.

Table 2-4. Listing of field parameters, abbreviations and location and frequency of monitoring for two monitoring regimes, lake wide and frequent south, on Cayuga Lake in 2013.

No.	Analyte	Abbreviation	Lake Wide Sample (2/month; Apr. – Oct)		Frequent South Sampling 2/week summer (Jun-Sept.)	
			Sites	number samplings/site	Sites	number samplings/site
1	temperature	T	I_L and 1-9	16	I_L-3	40
2	specific conductance	SC	I_L and 1-9	16	I_L-3	40
3	field beam attenuation coefficient at 660 nm	c_{660_f}	I_L and 1-9	16	I_L-3	40
4	field turbidity	Tn_f	I_L and 1-9	16	I_L-3	40
5	field fluorometric chlorophyll *a*	Chl-*a*_f	I_L and 1-9	16	I_L-3	40
6	scalar photosynthetic solar radiation	E_0(PAR)	I_L and 1-9	16	I_L-3	40
7	Secchi disk	SD	I_L and 1-9	16	I_L-3	40

2.4.3. Dreissenid Mussel Sampling

A survey of dreissenid mussels (both zebra and quagga) was conducted for Cayuga Lake in 2013. The survey was conducted across 12 transects of the lake (Figure 2-8). These lateral transects consisted of a mid-lake site and 4 to 15 other sites (depending on the lake width) distributed evenly across the cross section of the lake at that transect. Phosphorus excretion experiments were conducted in the summer of 2014.

Table 2-5. Listing of laboratory measured parameter abbreviations and location and frequency of sampling for two sampling regimes, lake wide and frequent south, on Cayuga Lake in 2013.

Sampling Regime	Location and Depth	Analytes											
		Phosphorus		Nitrogen		Carbon		Algea		particles			
		TP, TDP, SRP	TIP	NO_X, t-NH_3	TN, TDN	DOC	POC	Chl-*a*	Si	TSS, FSS	Tn	c_{660}	PAV_m
Lake Wide Sampling (2/month; Apr-Oct.)	site	I_L-2, 9	I_L-2, 9	1-4, 6-9	1-3, 5, 7, 9	I_L-3, 7, 9	I_L-3, 7, 9	I_L-2, 9	1-4, 6-9	I_L-2, 9	1-3, 5, 7, 9	1-3, 5, 7, 9	1-3, 5, 7, 9
	depth (m)	0	0	0	0	0	0	0	0	0	0	0	0
	site	6-8	3-8	5	--	5	5	3-8	5	3-8	--	--	--
	depth (m)	0, 5, 10	0, 10	0, 5, 10, and 20-bottom every 20 m	--	0, 5, 10, and 20-bottom every 20 m	0, 5, 10, and 20-bottom every 20 m	0, 10	10, 20, 60, 100, 120	0, 10	--	--	--
	site	4	--	--	--	--	--	--	--	--	--	--	--
	depth (m)	0, 5, 10, 80, 100	--	--	--	--	--	--	--	--	--	--	--
	site	3, 5	--	--	--	--	--	--	--	--	--	--	--
	depth (m)	0, 5, 10, and 20-bottom every 20 m	--	--	--	--	--	--	--	--	--	--	--
Frequent South Sampling 2/week summer (Jun-Sept.)	site	I_L – 2	I_L – 2	--	--	--	I_L-2	I_L-2	--	I_L-2	I_L-2	I_L-2	I_L-2
	depth (m)	0	0	--	--	--	0	0	--	0	0	0	0
	site	3	3	--	--	3	3	3	--	3	3	3	3
	depth (m)	0, 5, 10, and 20-bottom every 20 m	0, 10	--	--	0	0, 10	0, 10	--	0, 10	0, 10	0, 10	

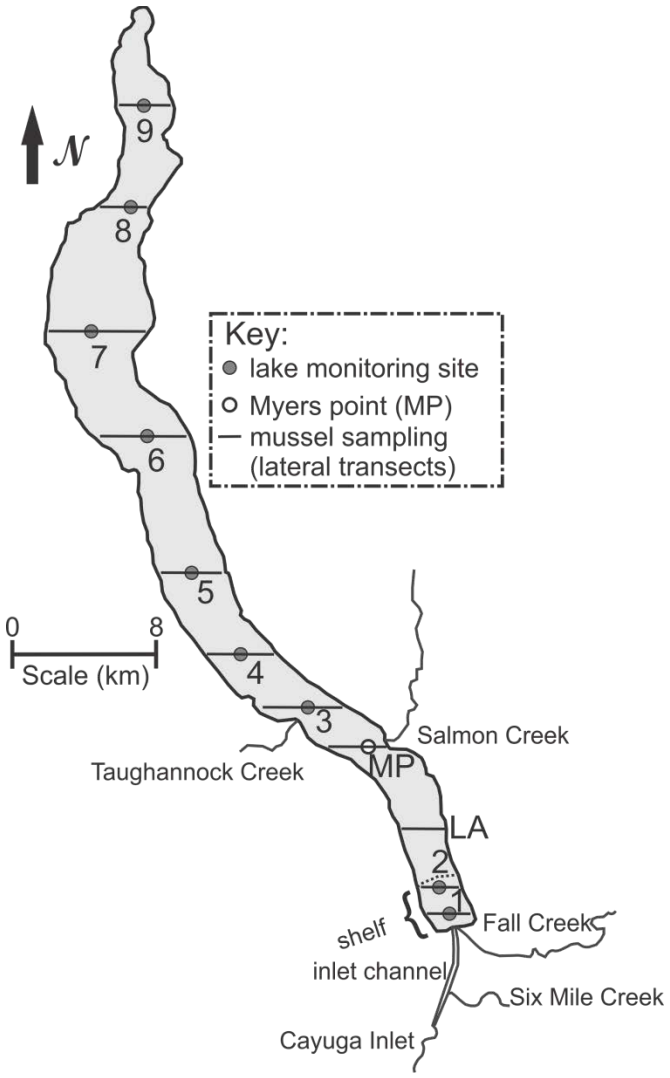

Figure 2-8. Monitoring transect locations for dreissenid mussel (both zebra and quagga) sampling in Cayuga Lake, 2013.

Section 3. Tributaries

3.1. Hydrology

3.1.1. Sources

A summary of the tributaries monitored in this study ranked according to watershed area is presented in Table 3-1. A map of the study system with sampling locations identified can be found in Figures 1-1 and 2-6.

Table 3-1. Tributary watershed areas, flow statistics, and volume delivered in 2013.

Tributary	USGS Gage No.	Total Watershed Area (km^2)	Percent of Total Watershed (%)	Annual Mean Flow (m^3/s)	April-October Mean Flow (m^3/s)	April-October Volume (m^3)[f]
Fall Creek	04234000	330.9	17.7	5.95	4.96	9.18×10^7 (22%)
Cayuga Inlet Creek	04233255	240.8	12.9	2.69	2.09	3.86×10^7 (9%)
Salmon Creek	0423401815 [a]	233.8	12.5	3.75	2.36	4.36×10^7 (10%)
Taughannock Creek	- [b]	173.0	9.3	3.11	2.59	4.80×10^7 (11%)
Sixmile Creek	04233300	134.1	7.2	2.09	1.61	2.97×10^7 (7%)
Ungaged Tributaries	- [c]	758.2	40.5	11.98	9.28	1.72×10^8 (41%)
Total Watershed	- [d]	1870.7[e]	100	29.56	22.89	4.24×10^8

[a] Jan. 1 through Feb. 11 flows were estimated from product of Fall Creek flow and Salmon Creek to Fall Creek watershed areas, similar to Eq. 3-1.
[b] estimated from product of Fall Creek flow and Taughannock Creek to Fall Creek watershed areas.
[c] estimated from the difference between total watershed flow and monitored flow
[d] estimated from product of gaged flow and ratio of total watershed area to gaged watershed area
[e] fraction volume delivered parenthetically
[f] does not includes the Seneca-Cayuga Canal

Fall Creek is largest tributary to Cayuga Lake and was the largest tributary monitored in 2013. Fall Creek has a watershed area of 330.9 km^2 which represents approximately 17.7 percent of the total Cayuga Lake watershed area (Haith et al. 2009). In addition to the four gaged tributaries (Table 3-1), Taughannock Creek was also monitored. Flows for Taughannock Creek were estimated using Fall Creek flows and the relationship between the Fall Creek and Taughannock Creek watershed areas (Eq. 3-1).

Eq. 3-1. $$Taughannock\ Creek\ Flow = Fall\ Creek\ Flow \cdot \frac{Taugh.Creek\ Area}{Fall\ Creek\ Area}$$

Estimates of total watershed flow were needed for subsequent analyses, as Cayuga Lake has numerous small, ungaged tributaries. Total watershed flows were estimated by the product of total gaged flow (Taughannock Creek included) and the ratio of total watershed area to gaged watershed area (Eq. 3-2).

Eq. 3-2. $$Total\ Watershed\ Flow = Gaged\ Flow \cdot \frac{Total\ Watershed\ Area}{Gaged\ Area}$$

USGS gaged daily flows were prorated by an adjustment factor to account for the portion of the watershed downstream (e.g., not monitored by gage) of the gaging station (Table 3-2). These final adjusted flows were used for all subsequent analyses and loading estimates. In most cases the adjustments were small (less than 8%), however the adjustment for Sixmile Creek was quite large (1.328) because the Sixmile Creek gage at Bethel Grove (04233300) only accounts for 75% of its total watershed area.

Table 3-2. Adjustment factors used to estimate total flows for each watershed.

Tributary	USGS Gage No.	Gaged Watershed Area (km^2)	Total Watershed Area (km^2)	Percent Watershed Gaged	Adjustment Factor
Fall Creek	04234000	326.3	330.9	98.6%	1.014
Cayuga Inlet Creek	04233255	224.6	240.8	93.3%	1.072
Salmon Creek	0423401815	227.1	233.8	97.2%	1.030
Sixmile Creek	04233300	101.0	134.1	75.3%	1.328

3.1.2. Flow Stratification

Daily flows for each monitored tributary were stratified into low and high flow regimes demarcated by the 2013 mean flow. Each tributary had its own specific flow stratification based on the mean flow for that tributary. Figure 3-1 shows the 2013 time series of flow for each monitored tributary and estimates of flow for the ungaged portion of the watershed. The largest flow source was the ungaged tributaries (2013 mean flow = 11.98 m^3/s) as the combined ungaged portion of the watershed was approximately 40.5 % of the total watershed area. Fall Creek had the largest individual mean flow in 2013 (5.95 m^3/s) and the other monitored tributaries had mean flows that generally ranked similarly to their watershed areas. The only exception was that Salmon Creek had the second highest mean flow (3.75 m^3/s) despite being the third largest monitored watershed (233.8 km^2).

.

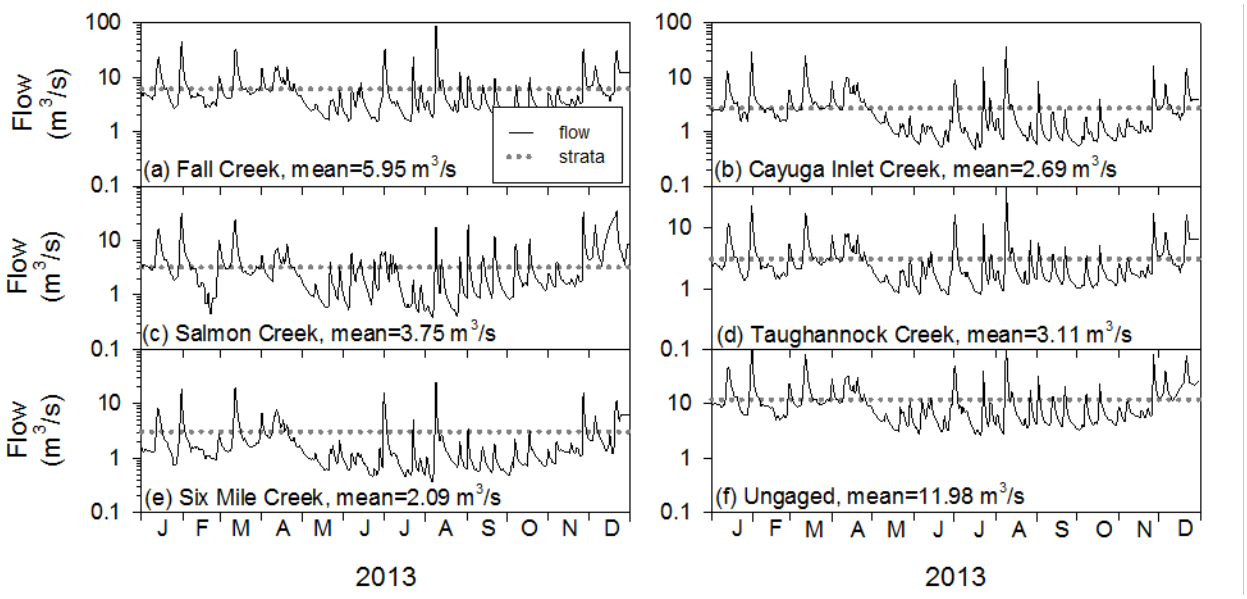

Figure 3-1. 2013 flow time series for monitored tributaries (line) with 2013 mean flow stratification (dotted) for: (a) Fall Creek, (b) Cayuga Inlet Creek, (c) Salmon Creek, (d) Taughannock Creek, (e) Sixmile Creek, and (f) total ungaged tributaries.

3.1.3. 2013 Flow Conditions

Using the long-term Fall Creek gage (89 year record) as a surrogate for Cayuga Lake watershed hydrology, the summer of 2013 was a relatively high flow period compared to previous years (Figure 3-2). This has important implications with regards to 2013 stream concentration observations and loading estimates (subsequently). The 2013 Fall Creek mean flow over the April–October interval (designated hereafter as A-O) was 4.96 m^3/s, 16% higher than the long-term (1925-2013) average (4.26 m^3/s). The 2013 A-O period flow ranked 32nd in the gage's 89 year history.

Over the 2013 June–September interval, Fall Creek mean flow was 5.03 m^3/s which was 2 times higher than the historic June–September interval average (2.32 m^3/s). The 2013 June–September interval flow was the 6th highest in the stream's 89 year record. Several large rain events impacted the southern Cayuga Lake watershed in the summer of 2013 which resulted in large flow events in Fall Creek (Figure 3-2) and other tributaries. Over the 2013 A-O interval for Fall Creek there were 24 events (defined as abrupt increases in flow with well-defined peaks) with 15 of them occurring between June and September. In particular, three large events (defined by peak flow) occurred on June 30, July 21, and the largest on August 8. The instantaneous peak flows for these events were 45.9, 35.0, and 113 m^3/s, respectively. Perhaps more importantly, these three events, despite only having combined 11 days duration, accounted for 22% of the A-O and 37% June–September volume delivered by Fall Creek to the lake. The

August 8 event was quite large, having a return interval of approximately 3.5 years according to a Log-Pearson Type III analysis. The June 30 and July 21 events had return intervals of 0.3 and 0.5 years, respectively. A list of all flow events for Fall Creek can be found in Appendix B1 and event sample counts and averages for all tributaries can be found in Appendix B2.

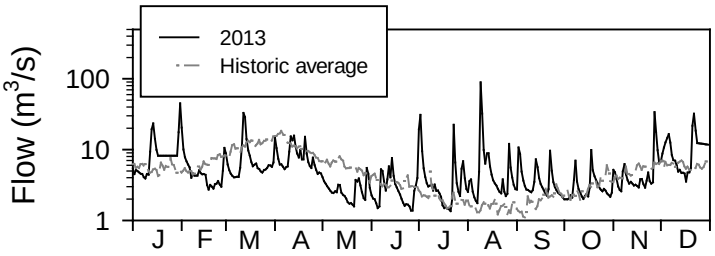

Figure 3-2. Flow conditions for Fall Creek for 2013 (black line) with historic daily average flows (gray line).

3.2. Monitoring

A review of the project background and objectives can be found in the QAPP (Upstate Freshwater Institute 2012).

3.2.1. Sampling Program

The tributaries were monitored for ten water quality constituents and three additional constituents were calculated from the original measurements. The complete list of the tributary parameters and acronyms can be found in Tables 2-1 and 2-2. The constituents sampled were: (1) TP, (2) TDP, (3) SRP, (4) Tn, (5) TSS, (6) FSS, (7) t-NH_3, (8) NO_X, (9) DOC, and (10) Si. The three calculated parameters were (1) PP (=TP-TDP), (2) SUP (=TDP-SRP), and (3) VSS (=TSS-FSS). To achieve the project objectives, the monitoring of these tributaries took two forms: biweekly and event-based monitoring. The 2013 monitoring program began in mid-March and concluded in early November. In total there were 19 biweekly sampling days. Samples during runoff events were collected from the gaged streams to: (1) characterize individual events, (2) identify differences in stream water quality at high versus low flow, (3) provide information to compare different tributaries at low and high flow, and (4) to improve each tributary's concentration-Q relationships to enhance the development of loading estimates. Figure 3-3 shows the flow time series for all monitored tributaries with the sampling dates presented.

Also, during two events, sample collections were completed at the mouths and at four additional upstream locations on Fall and Salmon Creeks (synoptic surveys). Each of these five locations were monitored six times during the course of the two events. The results of this monitoring were to be used in watershed modeling efforts and the results from the Fall and

Salmon Creek mouth sites were incorporated into the analyses in this report, including estimation of constituent loading. The results from these surveys, including temporal and spatial differences, are not specifically addressed further here, but graphical results can be found in Appendix B3.

3.2.2. Sampling According to Constituent Counts

Table 3-3 contains the number of samples collected for each constituent for each monitored tributary. As described in the QAPP (Upstate Freshwater Institute 2012), P and Tn were constituents of primary focus for this program and therefore were sampled with greater intensity than the secondary constituents (SS, t-NH_3, NO_X, DOC, and Si). The total number of samples collected satisfied all QAPP requirements.

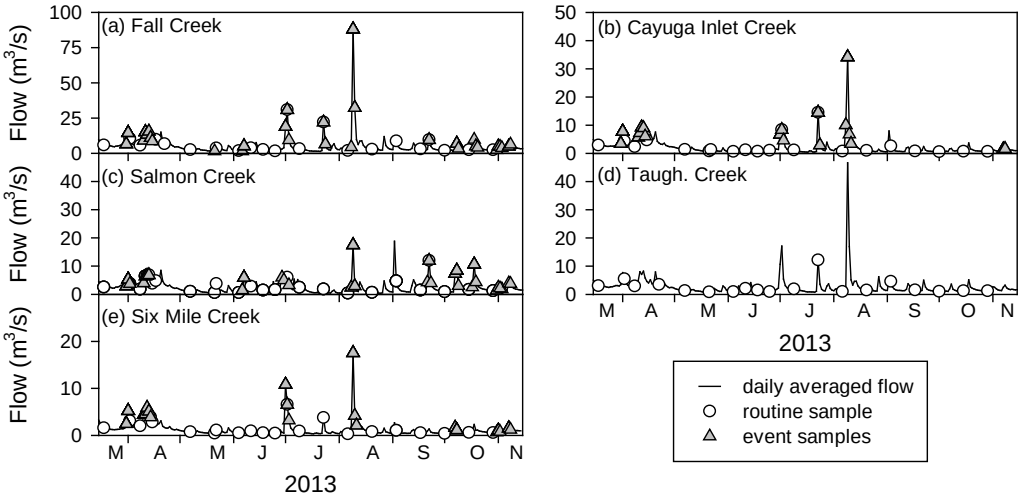

Figure 3-3. Flow time series and sampling coverage for monitored tributaries for biweekly and event samples for: (a) Fall Creek, (b) Cayuga Inlet Creek, (c) Salmon Creek, (d) Taughannock Creek, and (e) Sixmile Creek.

Table 3-3. Sample counts for primary and secondary constituents for monitored tributaries.

Tributary	Primary Constituents [a]						Secondary Constituents [b]						
	TP (µg/L)	PP (µg/L)	TDP (µg/L)	SRP (µg/L)	SUP (µg/L)	Tn[d] (NTU)	TSS (mg/L)	FSS (mg/L)	VSS (mg/L)	t-NH_3 (µg/L)	NO_X (µg/L)	DOC (mg/L)	Si (mg/L)
Fall Creek	97	96	97	88	87	93	63	63	63	66	62	57	57
Cayuga Inlet Creek	72	72	73	63	63	71	47	47	47	47	46	47	47
Salmon Creek	96	96	97	87	87	91	56	56	56	61	62	54	54
Taughannock Creek [c]	18	18	19	19	19	19	10	10	10	10	10	10	10
Sixmile Creek	79	79	80	70	70	78	46	46	46	49	50	48	47

[a] sampled biweekly and during events
[b] sampled monthly and during events
[c] sampled biweekly only
[d] see Appendix B-3

3.2.3. Temporal Coverage and Percent Inflow Monitored

The temporal coverage for both the primary and secondary constituents was robust, especially in comparison to a biweekly monitoring program (Table 3-4; see Taughannock Creek). Salmon and Fall Creeks were sampled with the greatest frequency with primary and secondary constituents being sampled on approximately 50 and 35 days, respectively (Table 3-4). Taughannock Creek had the lowest sampling frequency, as it was only monitored during the biweekly portion of the program (i.e., no event samples). During the A-O interval, for all four creeks for which event monitoring was conducted, a minimum of 17% (Cayuga Inlet Creek) of days were monitored for primary constituents and a minimum of 12% (Cayuga Inlet Creek and Sixmile Creek) of the days were monitored for secondary constituents.

Table 3-4. Number of sampling days with percent of study interval monitored (parenthetically) for Cayuga Lake tributaries.

Tributary	Primary Constituents [a]						Secondary Constituents [b]						
	TP (µg/L)	PP (µg/L)	TDP (µg/L)	SRP (µg/L)	SUP (µg/L)	Tn[d] (NTU)	TSS (mg/L)	FSS (mg/L)	VSS (mg/L)	t-NH_3 (µg/L)	NOx (µg/L)	DOC (mg/L)	Si (mg/L)
Fall Creek	48 (22%)	48 (22%)	50 (23%)	48 (22%)	48 (22%)	48 (22%)	35 (16%)	35 (16%)	35 (16%)	39 (18%)	39 (18%)	33 (15%)	33 (15%)
Cayuga Inlet Creek	36 (17%)	36 (17%)	38 (18%)	36 (17%)	36 (17%)	36 (17%)	25 (12%)	25 (12%)	25 (12%)	26 (12%)	26 (12%)	26 (12%)	26 (12%)
Salmon Creek	51 (24%)	53 (25%)	51 (24%)	51 (24%)	51 (24%)	50 (23%)	35 (16%)	35 (16%)	35 (16%)	40 (19%)	41 (19%)	34 (16%)	34 (16%)
Taughannock Creek [c]	18 (8%)	18 (8%)	19 (9%)	19 (9%)	19 (9%)	19 (9%)	10 (5%)	10 (5%)	10 (5%)	10 (5%)	10 (5%)	10 (5%)	10 (5%)
Sixmile Creek	40 (19%)	40 (19%)	41 (19%)	39 (18%)	39 (18%)	40 (19%)	26 (12%)	26 (12%)	26 (12%)	26 (12%)	27 (13%)	26 (12%)	26 (12%)

[a] sampled biweekly and during events
[b] sampled monthly and during events
[c] sampled biweekly only
[d] see Appendix B-3

Table 3-5 contains the percent of A-O inflow monitored for the primary and secondary constituents for each tributary. The combination of a biweekly and event based monitoring program enhanced the fraction of inflow monitored for each stream, as seen in the difference in flow coverage between the four gaged tributaries and Taughannock Creek. Approximately 42% and 35% of the inflow volume of the gaged streams was monitored for primary and secondary constituents, respectively. This represents comprehensive sampling coverage with respect to inflow volume.

Table 3-5. Percent of inflow monitored for Cayuga Lake tributaries, primary versus secondary constituents.

Tributary	Primary Constituents	Secondary Constituents
Fall Creek	44%	38%
Cayuga Inlet Creek	42%	37%
Salmon Creek	41%	33%
Taughannock Creek	15%	11%
Sixmile Creek	42%	32%

3.3. Constituent Concentrations

3.3.1. Field Triplicates Results as a Metric of Data Quality

Triplicate samples of water quality constituents were collected at the Salmon Creek mouth site (i.e., field triplicates) during the biweekly monitoring program. The precision of these field triplicates was used as a metric of data quality with high precision representing good quality. The statistic used to assess variability was the coefficient of variation (CV; %), defined as the standard deviation divided by the mean for each triplicate set (e.g., a low CV represents high precision). The distributions of the CVs for the primary and secondary constituents are presented in Figure 3-4. The precision of field triplicates was very good as average CVs for all constituents were less than 15% (median CVs were all less than 10%) and most CVs averaged less than 7%. The low CVs support the quality of the stream constituent concentration reported here and their integration into the loading estimates.

3.3.2. Time Series of Concentrations and Statistics

Detailed constituent statistics for all monitored tributaries can be found in Appendix B3. In general, constituent concentrations were lower during the spring of 2013 and increased during periods of higher flow during the summer months, as demonstrated for Fall Creek in Figure 3-5 (time series plots for other monitored tributaries can be found in Appendix B3). Particulate constituents increased dramatically during periods of high flow which was most conspicuous for the three largest events monitored in 2013: June 30, July 21, and August 8-9 (Figure 3-5b, d, and i). Time series of all constituents for Fall Creek over the August 5-12 interval which bounds the largest event are presented in Figure 3-6 (event constituent time series for all tributaries and monitored events are presented Appendix B3).

For the largest event monitored in 2013 (August 8-9) the maximum daily average TP and PP concentrations were 996 and 927 µg/L, respectively (Figure 3-6b). This represented 21 and 26-fold increases for TP and PP, respectively, from low flow conditions two days prior on August 6. Similar increases were observed for TP and PP during other monitored events. Increases of approximately 70-fold were observed for TSS (90% of which was FSS) and Tn for this event (Figure 3-6i and d).

Dissolved constituents were also generally lowest during periods of low flow and increased during runoff events, although the increases observed were less substantial than for particulate constituents. The lowest concentrations of SUP occurred mostly in April and October (Figure 3-5c), and there was substantially less variation in SUP concentration in the intervening months compared to SRP (Figure 3-5c), including during runoff events (Figure 3-6c). SRP concentrations were also lower (< 5 µg/L) in April and October, and higher in the summer months, but with abrupt increases to > 20 µg/L for the three major runoff events discussed previously (Figure 3-5c). During the August 8-9 event (Figure 3-6c), SRP and SUP increased 10 and 3-fold, respectively.

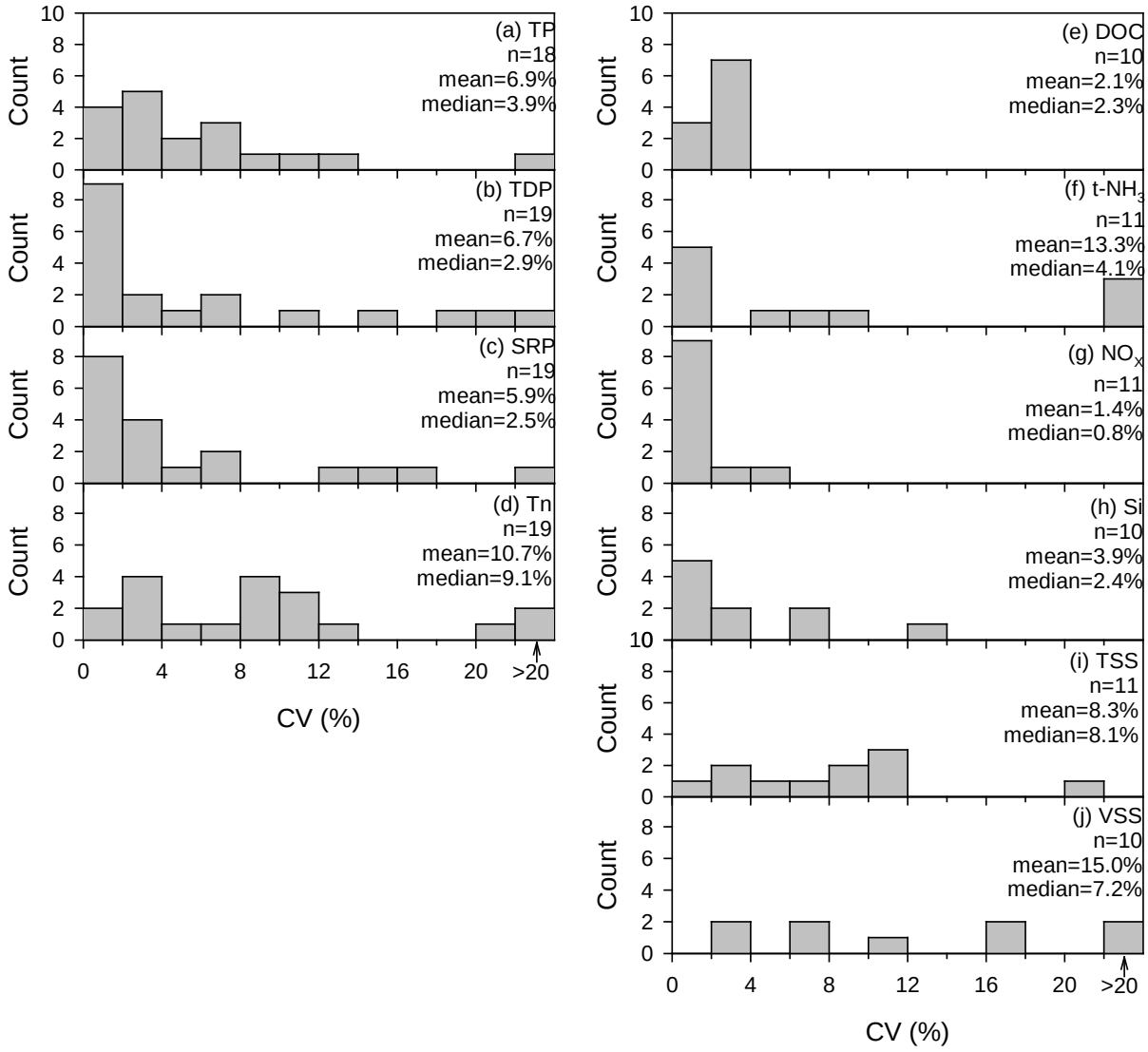

Figure 3-4. Distribution of coefficient of variations from Salmon Creek field triplicates for primary and secondary constituents: (a) TP, (b) TDP, (c) SRP, (d) Tn, (e) DOC, (f) t-NH_3, (g) NO_X, (h) Si, (i), TSS, and (j) VSS.

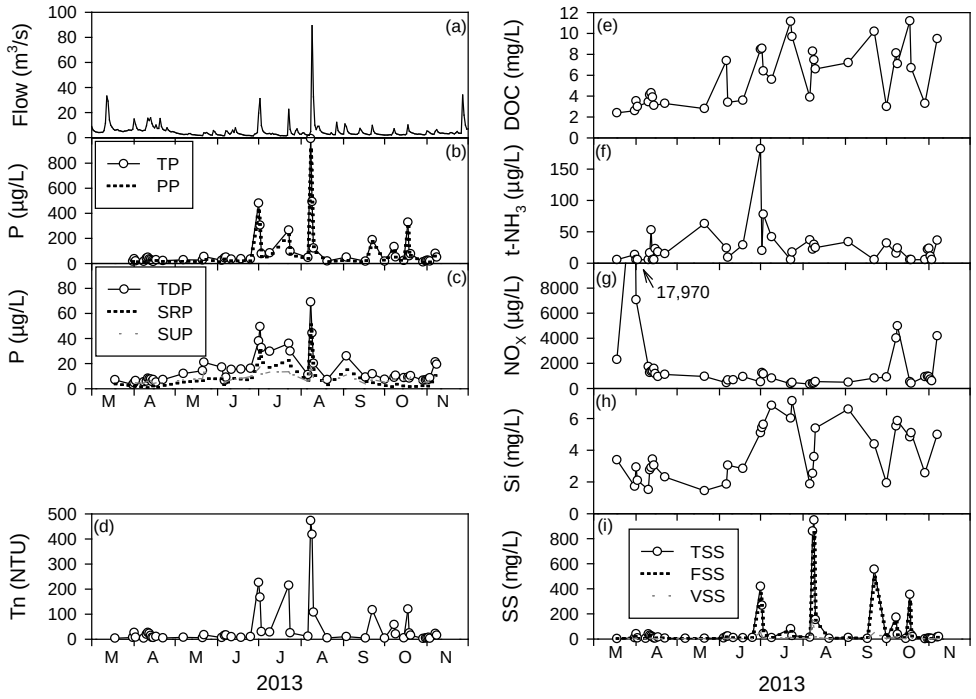

Figure 3-5. Time series of daily average concentrations for Fall Creek for: (a) flow, (b) TP and PP, (c) TDP, SRP, SUP, (d) Tn, (e) DOC, (f) t-NH_3, (g) NO_X, (h) Si, (i), TSS, FSS, and VSS.

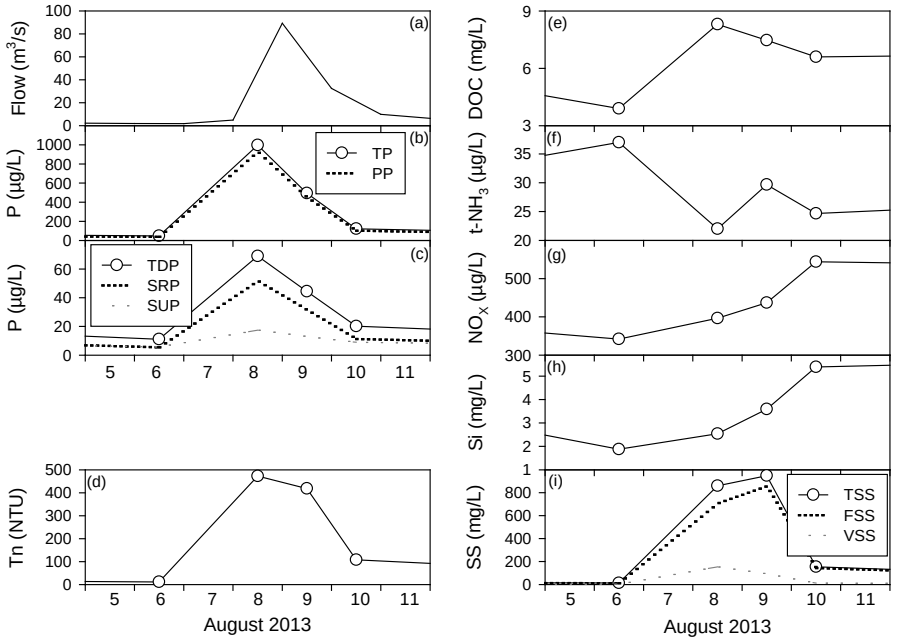

Figure 3-6. Time series of daily average concentrations for Fall Creek for the August 8-9 event: (a) flow, (b) TP and PP, (c) TDP, SRP, SUP, (d) Tn, (e) DOC, (f) t-NH_3, (g) NO_X, (h) Si, (i), TSS, FSS, and VSS.

With the exception of NO_X (Figure 3-5g), dissolved constituents showed patterns similar to SUP and SRP. DOC, t-NH_3, and Si concentrations were lowest in spring and fall and highest during the summer months (Figure 3-5e, f, and h). NO_X behaved differently than the other dissolved constituents as NO_X was observed to be highest in spring and fall and lower in the summer (Figure 3-5g). There was a very large spike in NO_X during a moderate runoff near the end of March during which the peak concentration was 17,790 µg/L. During the August 8-9 event NO_X and DOC increased slightly (Figure 3-6g and e; 2-3-fold), while the Si concentration increased from 1.9 mg/L to a peak of ~5 mg/L on August 10 (Figure 3-6h). t-NH_3 decreased during this event (41% decrease from August 6 to August 8; Figure 3-6f).

3.3.3. Concentrations: Tributary Low versus High Flow Concentrations

In general, constituent concentrations were low during periods of lower flow and increased during periods of higher flow as demonstrated for Fall Creek in Table 3-6 and in the form of box-whisker plots in Figure 3-7. Similar differences between low and high flow concentrations were observed for the other streams (Appendix B3).

Table 3-6. Low and high flow constituent averages for Fall Creek.

Constituents	Low Flow Average	High Flow Average	Percent Difference (%)
TP (µP/L)	37.3	126.8	+239
PP (µP/L)	25.9	109.6	+323
TDP (µP/L)	13.6	17.2	+26
SRP (µP/L)	6.4	9.8	+54
SUP (µP/L)	7.2	8.6	+19
Tn (NTU)	10.2	72.4	+612
TSS (mg/L)	10.4	141.6	+1,257
FSS (mg/L)	8.8	126.6	+1,341
VSS (mg/L)	1.6	15.0	+812
t-NH_3 (µgN/L)	23.4	26.6	+14
NO_X (µgN/L)	1,237	2,205	+78
DOC (mgC/L)	5.2	6.3	+23
Si (mg SiO2/L)	3.4	4.1	+21

In Fall Creek, mean TP increased 3.4-fold from low flow to high flow (Figure 3-7a). Similarly in the other streams, mean TP increased 3 to 5-fold from low to high flow with the largest increase between the flow regimes observed in Cayuga Inlet Creek (16.5-fold). For all tributaries the increase in TP between flow regimes was dominated by increases in PP as presented in Figure 3-8 which shows the relationship between the PP:TP ratio and flow for Fall Creek (Figure 3-8a) and other streams (Figure 3-8b). The relationship between PP:TP and flow

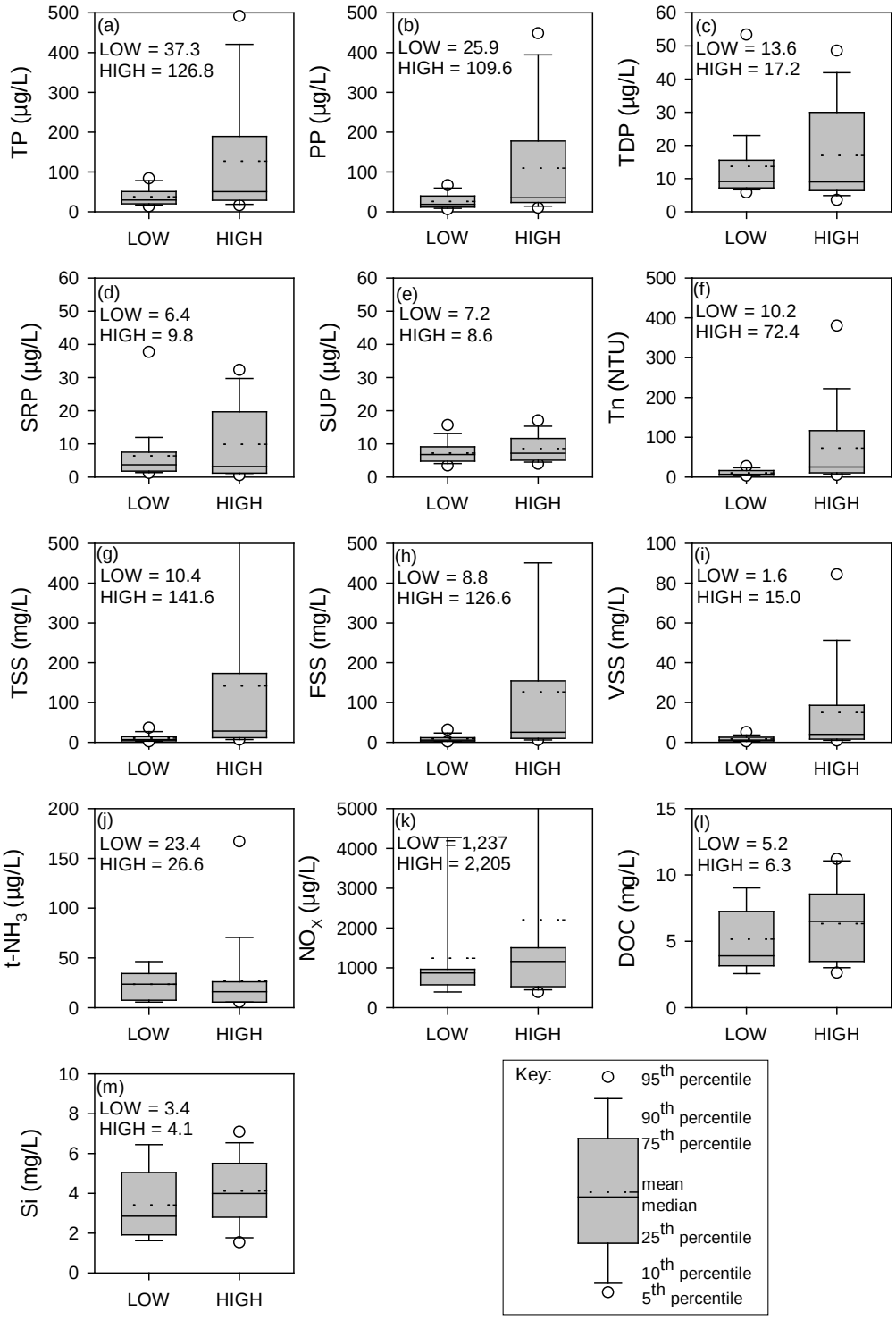

Figure 3-7. Box-whisker plots with key for Fall Creek for: (a) TP, (b) PP, (c) TDP, (d) SRP, (e) SUP, (f) Tn, (g) TSS, (h) FSS, (i) VSS, (j) t-NH_3, (k) NO_X, (l) DOC, and (m) Si. Low and High refer to constituent averages within the low and high strata, respectively (Table 3-6).

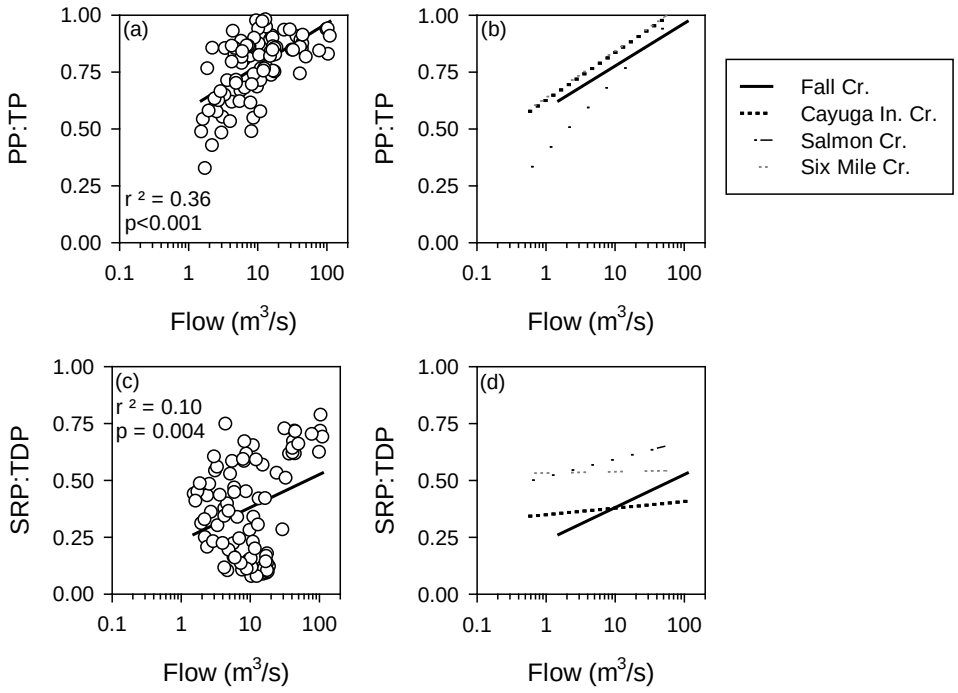

Figure 3-8. Phosphorus ratios versus flow for: (a) Fall Creek PP:TP, (b) PP:TP for all gaged tributaries, (c) Fall Creek SRP:TDP, and (d) SRP:TDP for all four gaged tributaries.

was positive and highly significant ($p < 0.001$) for all tributaries. Mean PP in Fall Creek increased more than 4-fold (Figure 3-7b) and increases in PP ranged 4 to 8-fold for the other streams, with a 24-fold increase observed in Cayuga Inlet Creek. Like PP, mean TSS and Tn increased dramatically from low to high flow (13.6 and 7-fold, respectively for Fall Creek; Figure 3-7g and f). Average TSS was observed to increase 6 to 20-fold from low to high flow in the other streams.

Dissolved constituents were also generally lower in the low flow stratum and increased in the high flow stratum, although the increases observed were less substantial than for particulate constituents. Mean SRP and SUP increased 54 and 19% from low to high flow in Fall Creek (Figure 3-7d and e). In the other tributaries, as with Fall Creek, SRP increases from low to high flow were more substantial than for SUP. Mean SRP in Sixmile Creek increased 36%, doubled in Salmon Creek, and increased 6-times in Taughannock Creek at high flow. Mean SUP increased between 19 and 100%. An increase (i.e., positive slope) was observed in the SRP:TDP ratio with increases in flow for all streams (Figure 3-8c and d). However, the relationship between SRP:TDP and flow was only significant in the case of Fall Creek ($p = 0.004$; Figure 3-8c).

All other streams had very shallow slopes and non-significant p values (all > 0.2). Fall Creek was an interesting case with regards to t-NH_3 in that Fall Creek was the only stream where mean t-NH_3 increased between low and high flow (+14%). For all other monitored steams, average t-NH_3 concentrations were lower in the high flow stratum. At high flow, mean NO_X increased 78% in Fall Creek (Figure 3-7k) compared to low flow and interestingly, mean NO_X increased only 10% in Salmon Creek from low to high flow. Mean NO_X in the remaining three streams nearly tripled during high flow compared to the low flow. In Fall Creek, DOC and Si concentrations (Figure 3-7l and m) demonstrated modest increases between the low and high strata (~ +20%). For DOC, the other monitored streams increased from low to high flow (20-100%), while increases in Si were mostly less than 20%. The only exception for Si was Taughannock Creek which increased 43% from low to high flow.

3.3.4. Concentrations: Comparisons of Tributaries at Low and High Flow

3.3.4.1. Low Flow Conditions

Under low flow conditions, Fall Creek had the highest average TP and PP concentrations, 37.3 and 25.9 µg/L, respectively (Figure 3-9a and c) of all monitored streams. Ranked second and third, respectively, Sixmile and Salmon Creek had a nearly equivalent low-flow TP concentration of approximately 28 µg/L (Figure 3-9a). Mean TP in Cayuga Inlet Creek was 13.4 µg/L which is approximately one-third of Fall Creek's concentration and Taughannock Creek had the lowest mean low flow TP concentration (11.3 µg/L). Variability in low-flow TP was substantially lower in Cayuga Inlet Creek and Taughannock Creek compared to than other streams. For all streams except Salmon Creek, low-flow TP was dominated by PP (Figure 3-10) with PP ranging from 50-68% of TP. Fall and Cayuga Inlet Creek had the highest PP:TP ratio at low-flow, 68 and 63%, respectively (Figure 3-10a and c). In contrast, in Salmon Creek PP was only 46% of TP (i.e., 54% of TP was TDP).

Salmon Creek's mean low-flow TDP and SRP concentration were the highest of all five monitored streams (Figure 3-9e and g). TDP and SRP concentrations were 18.3 µg/L and 12.7 µg/L, respectively. Approximately 59% of Salmon Creek's TDP was as SRP (Figure 3-10f). This was the second highest SRP:TDP ratio observed for all monitored tributaries and has important implications with regards to bioavailability (subsequently). Fall Creek had the second highest TDP concentration at low flow (13.6 µg/L) but unlike Salmon Creek, TDP in Fall Creek was dominated by SUP (7.2 µg/L) as the median SRP:TDP ratio was only 0.38. Sixmile Creek ranked third with regards to low-flow TDP (11.5 µg/L), 60% of which was in the form of SRP (highest SRP:TDP ratio at low-flow). Cayuga Inlet and Taughannock Creek both averaged approximately 5.0 µg/L of TDP which is substantially lower than the other tributaries. SRP:TDP ratios for these streams were also lower than the previous three streams, 36%, and 23%, for Cayuga Inlet Creek and Taughannock Creek, respectively (Figure 3-10d, and j).

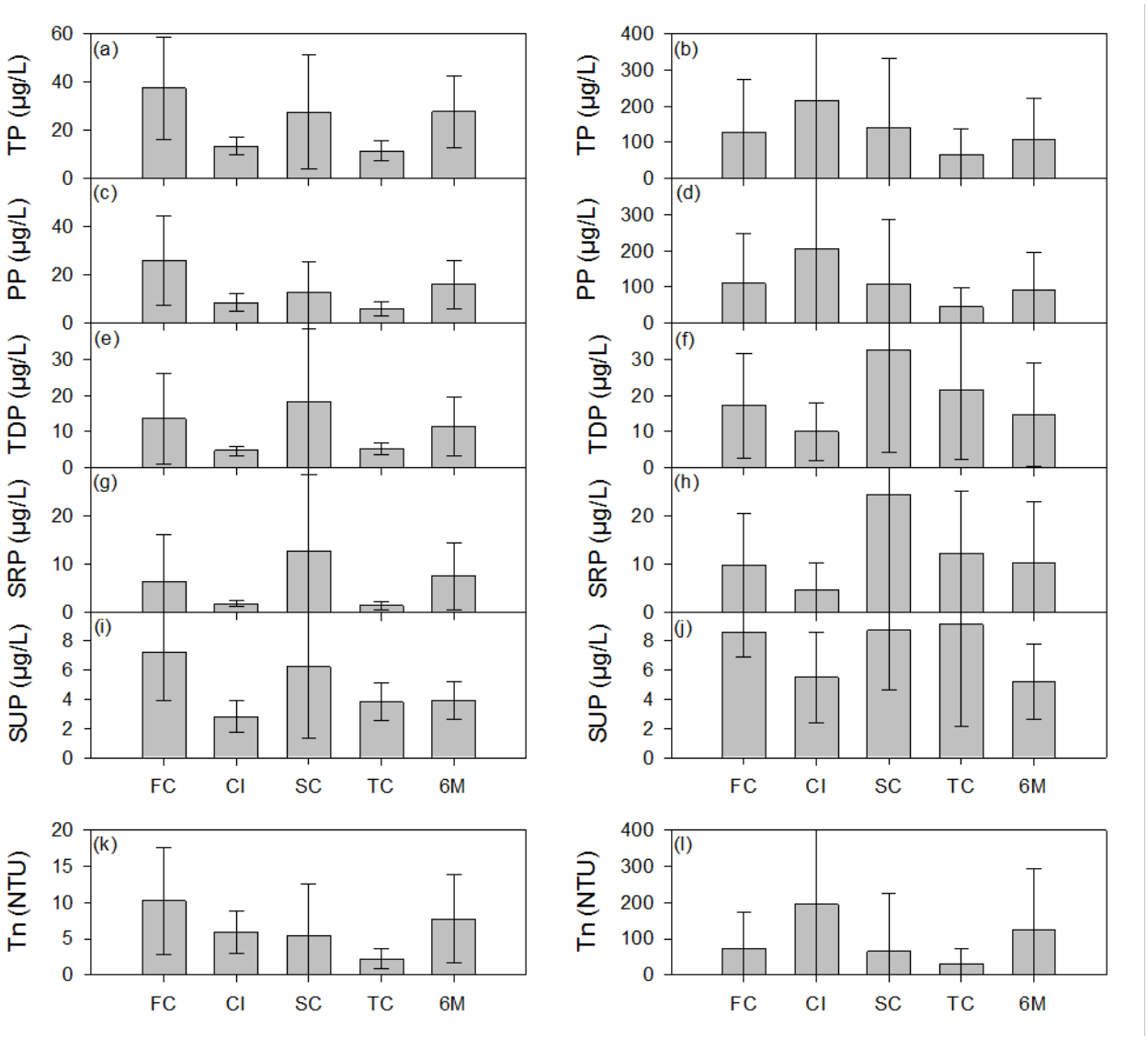

Figure 3-9. Grouped bar charts for all monitored tributaries depicting mean ± one standard deviation for: (a) TP at low flow, (b) TP at high flow, (c) PP at low flow, (d) PP at high flow, (e) TDP at low flow, (f) TDP at high flow, (g) SRP at low flow, (h) SRP at high flow, (i) SUP at low flow, (j) SUP at high flow, (k) Tn at low flow, and (l) Tn at high flow.

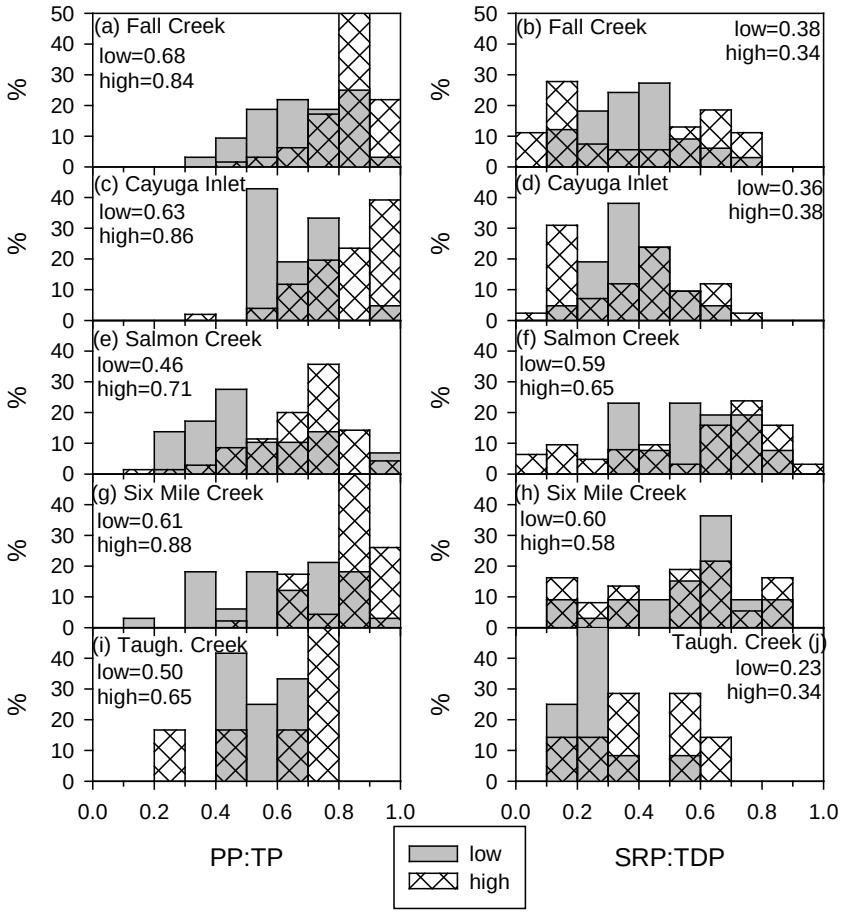

Figure 3-10. Phosphorus ratios for low and high flows for (a) PP:TP for Fall Creek, (b) SRP:TDP for Fall Creek, (c) PP:TP for Cayuga Inlet Creek, (d) SRP:TDP for Cayuga Inlet Creek, (e) PP:TP for Salmon Creek, (f) SRP:TDP for Salmon Creek, (g) PP:TP for Sixmile Creek, (h) SRP:TDP for Sixmile Creek, (i) PP:TP for Taughannock Creek, and (j) SRP:TDP for Taughannock Creek.

With regards to Tn (Figure 3-9k) and TSS (Figure 3-11i), Fall Creek had the highest low-flow average concentrations (10.2 NTU and 10 mg/L). Sixmile Creek had the second highest Tn (7.7 NTU) and TSS (5.8 mg/L) at low flow. The three other streams had mean Tn less than 6 NTU and TSS less than 6 mg/L at low-flow. For all cases, FSS concentrations dominated TSS at low flow (67-81%).

t-NH_3 concentrations were similar at all five tributary mouths, ranging from 19.1 to 28.4 µg/L (Figure 3-11c). NO_X was significantly higher than t-NH_3 in all streams (Figure 3-11e), especially for Salmon and Fall Creeks where NO_X concentrations were 55-200 times higher than t-NH_3 concentrations. Salmon Creek low-flow NO_X concentration was 4,593 µg/L (or 4.6 mg/L), and was 3.5 times higher than for the next highest stream, Fall Creek (1,237 µg/L). In both Salmon and Fall Creeks, NO_X was highly variable at low-flow. Cayuga Inlet and Sixmile Creek both had substantially lower NO_X, averaging less than 210 µg/L at low-flow.

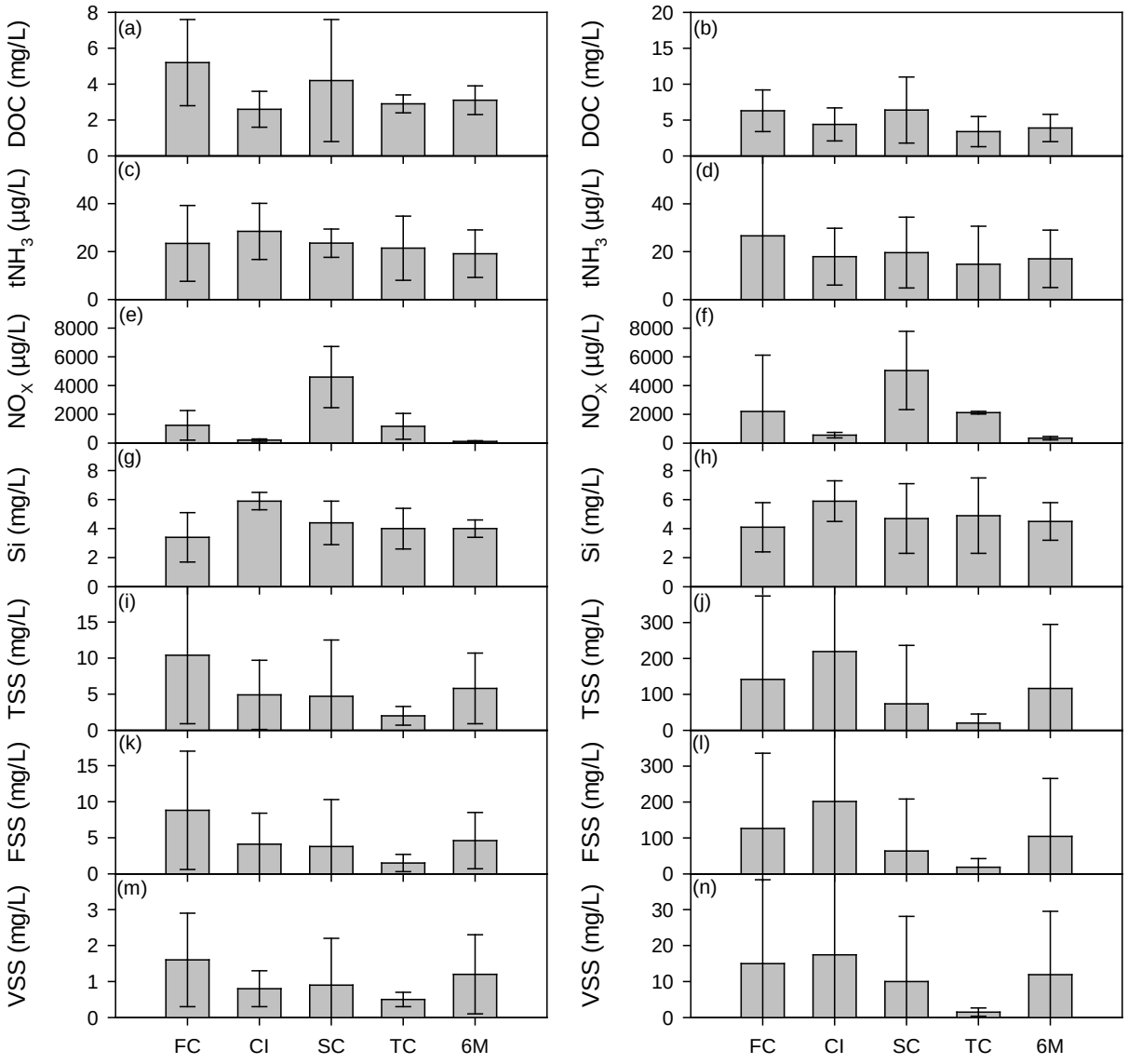

Figure 3-11. Grouped bar charts for all monitored tributaries depicting mean ± one standard deviation for: (a) DOC at low flow, (b) DOC at high flow, (c) t-NH_3 at low flow, (d) t-NH_3 at high flow, (e) NO_X at low flow, (f) NO_X at high flow, (g) Si at low flow, (h) Si at high flow, (i) TSS at low flow, (j) TSS at high flow, (k) FSS at low flow, (l) FSS at high flow, (m) VSS at low flow, and (n) VSS at high flow.

Concentrations of DOC and Si were generally similar between the five streams at low flow (Figure 3-11a and g). Fall Creek had the highest mean concentration of DOC at low flow (5.2 mg/L), but the range between streams was modest (2.8 to 5.2 mg/L). Mean Si concentrations were similar to DOC, ranging from 3.4 to 5.9 mg/L, with Cayuga Inlet Creek having the highest low-flow average.

3.3.4.2. High Flow Conditions

Taughannock Creek was not monitored during events and as a result only 7 samples were collected above its 2013 mean flow. Taughannock Creek high flow concentrations are presented in Figures 3-9 and 3-11 with the other tributaries, but because of the lack of event samples for Taughannock Creek, it will not be included in the "High Flow Conditions" discussion.

At high flow, the particulate constituents were generally much higher than at low flow. Cayuga Inlet Creek had the highest mean TP and mean PP at high flow (Figure 3-9b and d; 215.4 and 206.3 µg/L, respectively). For the other three streams with event samples, high-flow mean TP was greater than 100 µg/L. The order from highest to lowest mean high flow TP was: (1) Cayuga Inlet Creek, (2) Salmon Creek (139 µg/L), (3) Fall Creek (127 µg/L), and (4) Sixmile Creek (106 µg/L). For all streams, high flow TP was dominated by PP with PP representing between 65-88% of TP (Figure 3-10). The increase in the PP:TP ratio with increasing flow is consistent the results presented previously (Figure 3-8a and b) and likely reflects runoff induced erosion, increased stream resuspension and transport of particulates during high flow.

With regards to high flow TDP concentrations (Figure 3-9f), Salmon Creek was the highest of the five tributaries (32.4 µg/L), which was nearly 2 times higher than Fall Creek (17.2 µg/L). At high flow Sixmile Creek TDP averaged 14.7 µg/L and Cayuga Inlet Creek averaged 10 µg/L. Similar to low flow, Salmon Creek had the highest high-flow SRP concentration (Figure 3-9h; 24.4 µg/) and the highest SRP:TDP ratio at high flow (Figure 3-10f; 0.65). Sixmile Creek had the second highest high-flow SRP concentration and SRP:TDP ratio, 10.3 µg/L and 0.58, respectively. Fall Creek ranked third with regards to high-flow SRP concentration (9.8 µg/L) and Cayuga Inlet Creek had the lowest high-flow SRP only averaging 4.8 µg/L (Figure 3-9h). The SRP:TDP ratios for Fall Creek and Cayuga Inlet Creek were similar to each other and similar to their respective low-flow values (Figure 3-10b and d; ~ 35%). Salmon and Fall Creek had the highest high-flow SUP concentrations both averaging ~ 8.6 µg/L (Figure 3-9j).

At high flow, average FSS:TSS ratios were greater than 89% for all streams, which was an increase in the fraction when compared to low flow (67-81%). Mean Tn and TSS were highest in Cayuga Inlet Creek at high flow as presented in Figure 3-9l and Figure 3-11j, respectively. Cayuga Inlet, mean Tn was 194.2 NTU and mean TSS was 219.3 mg/L, 92% of which was FSS (201.9 mg/L). Fall Creek had the second highest TSS and FSS concentrations at high flow (141.6 and 126.6 mg/L, respectively). Sixmile Creek had the third highest TSS and FSS

concentrations at 116.5 and 104.6 mg/L (Figure 3-11j and l), respectively. Sixmile Creek had the second highest high flow Tn (Figure 3-9l; 124.9 NTU) behind only Cayuga Inlet Creek.

As with low flow, high flow mean t-NH_3 (Figure 3-11d) concentrations were similar for all tributaries ranging from 14.7 µg/L (Taughannock Creek) to 26.6 µg/L (Fall Creek). Fall Creek t-NH_3 was extremely variable. At high flow, mean NO_X (Figure 3-11f) was the highest in Salmon Creek (5,059 µg/L) which was more than twice that of Fall Creek (2,205 µg/L). Despite having no event samples, Taughannock Creek NO_X concentration (2,120 µg/L) at high flow was similar to Fall Creek. With regards to NO_X, Cayuga Inlet and Sixmile Creek were substantially lower than the other streams, 559 and 345 µg/L, respectively.

DOC and Si concentrations were generally similar between streams at high flow. Mean DOC (Figure 3-11b) was highest for Fall and Salmon Creeks at 6.4 and 6.3 mg/L, respectively. The difference between mean high-flow DOC for all other streams was small, ranging from 3.3 to 4.4 mg/L. High-flow Si concentration (Figure 3-11h) was highest in Cayuga Inlet (5.9 µg/L) and like, DOC, the range in Si for the other four streams was modest (4.1 to 5.0 mg/L).

3.3.5. Comparison with Other Sources, Previous Studies

During the course of the study, other data sources were investigated and compared with the 2013 data set. A brief description of the historic and contemporary data available and literature sources used for comparison is presented in Table 3-7. The data presented here was compared with other data sources by means of concentration-flow (Q) scatterplots. Fall Creek TP-Q scatterplots containing 2013 data and other contemporary data (2002-2013) are presented in Figure 3-12. As with TP-Q, the concentration-Q relationships for DOC, t-NH_3, NO_X, TSS, and Tn for the 2013 study and other sources compared favorably (Appendix B3). Noteworthy differences were observed between SRP-Q for different monitoring protocols (UFI and CSI, Bouldin) that appear to be analytical methodology based.

3.3.6. Hysteresis

Hysteresis refers to the differences in constituent concentrations at a given level of flow between the rising and falling limbs of a runoff event. This phenomenon is observed for particulates during runoff events with rising limb concentrations commonly being greater than falling limb concentrations at the same level of flow. For example, in Fall Creek during the June 30 event (Figure 3-13a), at 10 m^3/s on the rising limb the PP concentration was ~ 430 µg/L but it was 8-times less (55 µg/L) at 10 m^3/s on the falling limb. TSS and Tn behaved similarly to PP for this event on Fall Creek (Figure 3-13b and c). Interestingly in the case of dissolved constituents, TDP (Figure 3-13d) and NO_X (Figure 3-13e), the hysteresis effects were reversed; the concentrations were highest on the falling limb compared to the rising limb at a given level of flow. Similar patterns were observed for the other three tributaries during individual events (Appendix B3).

Table 3-7. Data sources investigated as part of the 2013 Cayuga Lake tributaries analysis.

Source	Tributaries	Time Interval	Relevant Parameters	References
Bouldin, D. R.	predominately Fall Creek	late 1970s-mid 1980s; 2001; 2008-2009	TDP, SRP, NO_X	Johnson et al. (1976a) Johnson et al. (1976b) Hergert et al. 1981
Likens, G. E.	multiple	early 1970s	P, N, others	Technical Report 81, Likens (1974a) Technical Report 82, Likens (1974b)
Community Science Institute (CSI)	Fall Creek, Cayuga Inlet, Salmon Creek, Taughannock Creek, Sixmile Creek	early 2000s-present	TP, SRP, t-NH_3, NO_X, TSS, Tn	
NYS Dept. of Environmental Conservation	Fall Creek, Cayuga Inlet, Sixmile Creek	2007	TP, DOC	
Upstate Freshwater Institute	Fall Creek, Cayuga Inlet Creek	2003-2006	TP, Tn	Effler et al. (2010)
Haith, D. A.	multiple	-	P, N	Haith et al. (2009)

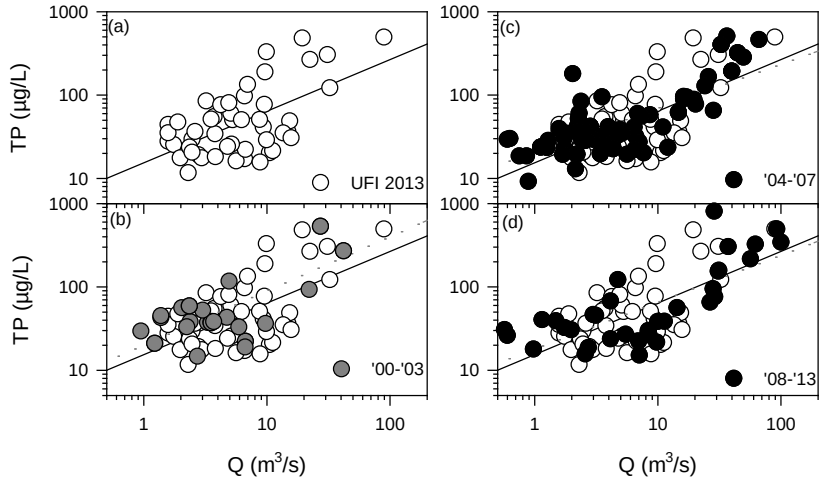

Figure 3-12. TP-Q scatterplots for: (a) 2013 Fall Creek data. 2013 Fall Creek TP-Q scatterplots with other contemporary data (CSI and UFI) presented for: (b) 2000-2003, (c) 2004-2007, and (d) 2008-2013.

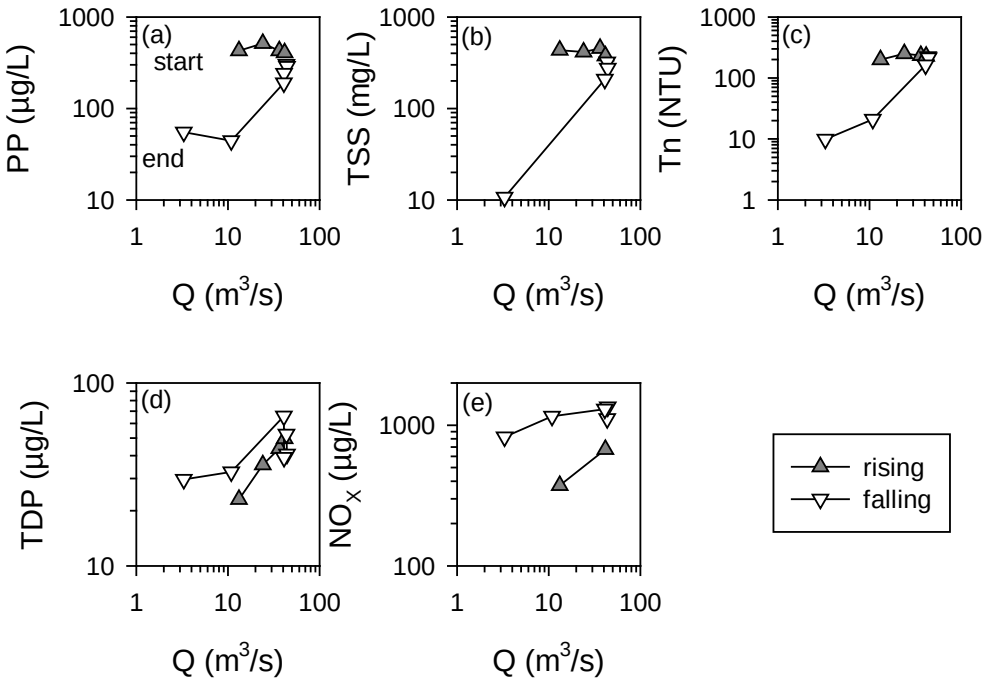

Figure 3-13. Concentration-Q plots for the June 30 event for Fall Creek for: (a) PP, (b) TSS, (c) Tn, (d) TDP, and (e) NO_X.

Certain constituents during the course of individual events showed hysteresis patterns but when comparing all rising limb samples with all falling limb samples in a concentration-Q format (Fall Creek; Figure 3-14), it was found that slopes between the rising limb concentration-Q and falling limb concentration-Q were not significantly different (Homogeneity-of-Slopes Model, Statistica 2003). Similar slope test results were found for Cayuga Inlet Creek and Salmon Creek, (Appendix B3). Sixmile Creek, however, demonstrated discrepant results compared to the previously mentioned streams. With regards to TP, SUP, TSS, FSS, and Tn, there were significantly ($p < 0.05$, Homogeneity-of-Slopes Model, Statistica 2003) different slopes between the rising and falling limb concentration-Q relationships (Appendix B3). The mechanisms driving these differences are currently unknown, but may be due to the influence of several upstream reservoirs on this stream.

3.4. Concentration-Driver Relationships

When characterizing in-stream water quality it is often necessary to develop relationships between environmental drivers and constituent concentrations. The primary drivers investigated in this analysis were stream flow and air temperature (as a surrogate of creek temperature). Also, turbidity-concentration relationships were developed to investigate potential future driver alternatives. The relationships between environmental drivers and concentration are important to: (1) assess stream concentrations at low-flow, (2) determine loading potential, (3) develop

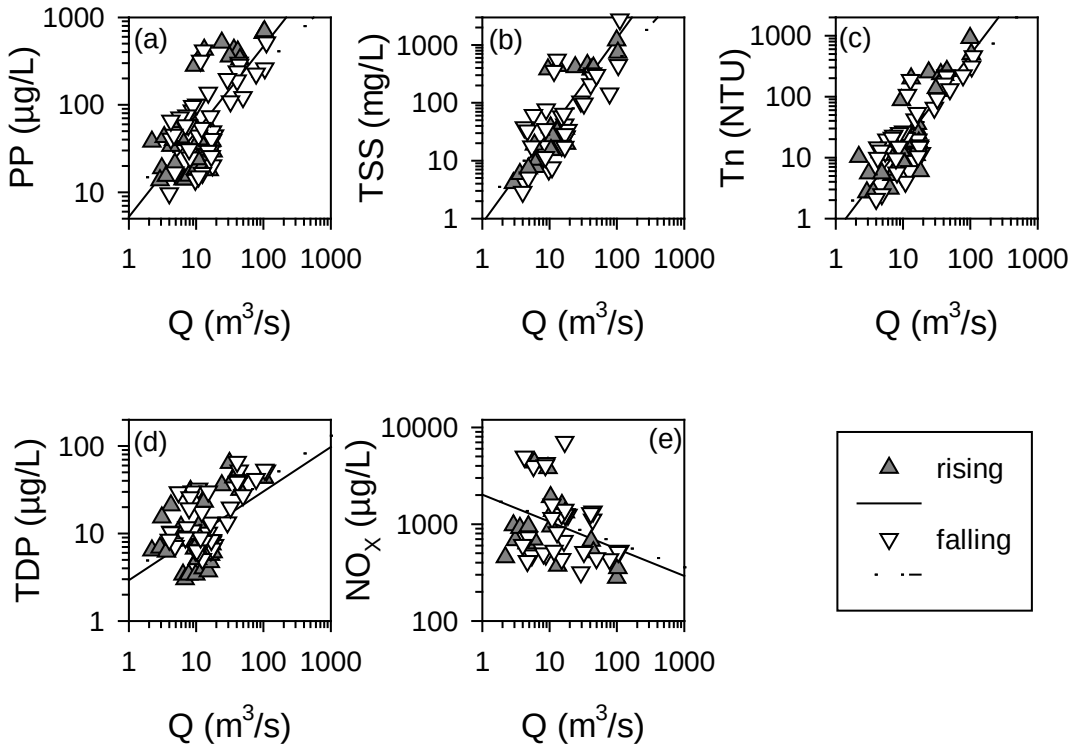

Figure 3-14. Concentration-Q plots for all events with rising and falling limb data identified, and associated linear least-squares regression fits, for Fall Creek for: (a) PP, (b) TSS, (c) Tn, (d) TDP, and (e) NO_X.

empirical models to estimate concentrations during periods when observations are not available, (4) assess seasonality, and (5) explore alternative drivers of concentrations (i.e., turbidity).

3.4.1. Stream Flow as a Driver of Concentration

3.4.1.1. Fall Creek

Relationships between stream flow (daily averaged) and constituent concentration (daily averaged) for Fall Creek are presented in Figure 3-15 in a log-transformed format. As expected, particulate-Q relationships (Figure 3-15a, c, j-m) were generally stronger (i.e., higher r^2), statistically significant ($p < 0.05$), and had larger slopes (i.e., loading potential) than dissolved constituents (Figure 3-15b, d-i). All concentration-Q statistics for Fall Creek and the other tributaries, including equations, r^2, p-values, and model mean square errors can be found in Appendix B4. Concentration-Q relationships for particulate forms of P were not particularly strong, but were statistically significant. Stream flow explained 35% of the variability in TP ($p < 0.001$; Figure 3-15a) and 39% of the variability in PP ($p < 0.001$; Figure 3-15c). Concentration-Q relationships for forms of SS and Tn (Figures 3-15j-m) were also statistically significant (all $p < 0.001$) and had $r^2 > 0.50$.

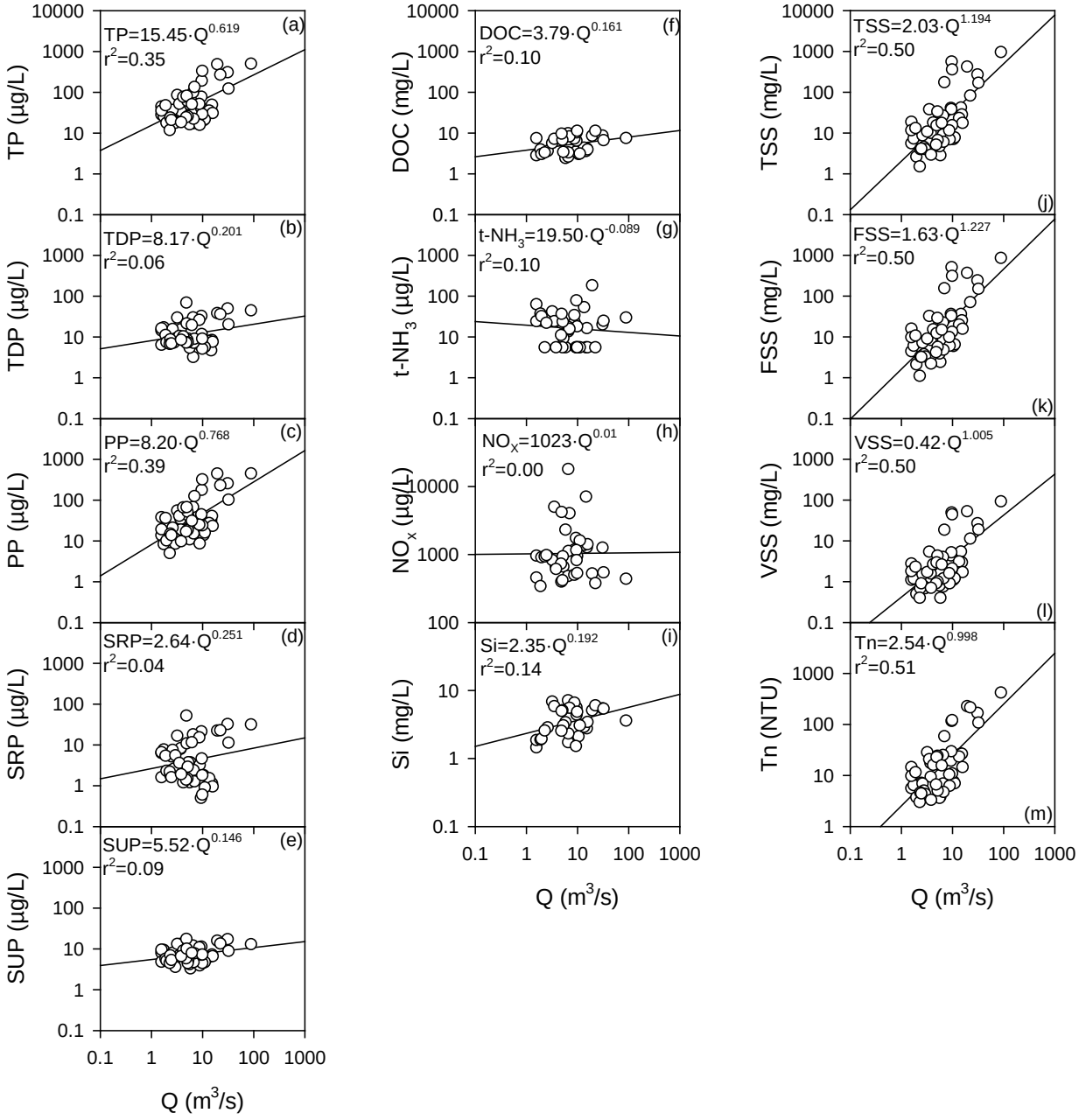

Figure 3-15. Concentration-Q plots for Fall Creek: (a) TP-Q, (b) TDP-Q, (c) PP-Q, (d) SRP-Q, (e) SUP-Q, (f) DOC-Q, (g) t-NH_3-Q, (h) NO_X-Q, (i) Si-Q, (j), TSS-Q, (k) FSS-Q, (l) VSS-Q, and (m) Tn-Q.

The dissolved constituent-Q relationships in Fall Creek were distinctly weaker than for the particulate constituents (Figure 3-15). The strongest relationship among the dissolved constituents was for Si-Q (r^2=0.14, p = 0.03; Figure 3-15i). The other dissolved constituents all had $r^2 \leq 0.1$. However, the concentration-Q relationship for SUP (Figure 3-15e) was also statistically significant (p = 0.04). The flow relationships for SRP (Figure 3-15d) and NO_X (Figure 3-15h) for Fall Creek were particularly weak ($r^2 < 0.04$) and neither was statistically significant (p = 0.19 and 0.96, respectively). The slope for the t-NH_3-Q relationship was negative (Figure 3-15g), indicating decreasing t-NH_3 concentrations with increasing flow.

3.4.1.1. Other Streams

Lines of the best-fit relationships for Fall Creek, Cayuga Inlet Creek, Salmon Creek, and Sixmile Creek are presented for concentration-Q relationships for all constituents in Figure 3-16 in log-transformed format. Detailed graphical relationships (with symbols) for Cayuga Inlet Creek, Salmon Creek, and Sixmile Creek can be found in Appendix B4. For all streams, the relationship between TP-Q and PP-Q were statistically significant ($p < 0.001$). The r^2 values of these relationships varied (0.35-0.62) between streams with Cayuga Inlet Creek being highest of the four streams with event samples. Sixmile Creek had the highest intercept for TP and PP (Figure 3-16a and c; 24.3 and 13.2 µg/L, respectively). With regards to PP-Q slope, Salmon Creek and Cayuga Inlet Creek were found to have the highest loading potential (slopes = 1.21 and 0.90, respectively). Fall Creek had the lowest PP loading potential among the four tributaries with event samples (slope = 0.77). The results for TP were similar for PP (Figure 3-16a).

Like PP, the concentration-Q relationships for Tn and SS forms were highly statistically significant ($p < 0.001$) for all streams (Figure 3-16j-m). Interestingly, Sixmile Creek had the highest intercept with regards to Tn (6.95 NTU) and all forms of SS; 5.21 mg/L, 4.12 mg/L, and 1.02 mg/L for TSS, FSS, and VSS, respectively. Loading potential for Tn and forms of SS were similar for the streams. The ranking of TSS slopes from order in highest to lowest was: (1) Salmon Creek (1.51), (2) Sixmile Creek (1.41), (3) Cayuga Inlet Creek (1.38), and (4) Fall Creek (1.19).

Dissolved P-Q relationships were substantially different between the four streams in terms of both intercepts and slopes (Figure 3-16b, d, and e). For SRP-Q, Salmon Creek had the highest intercept (5.27 µg/L) and slope (0.55) of all the monitored tributaries (Figure 3-16d) which have important ramifications with respect to P loading and bioavailability (see Section 3.6). The intercepts for Sixmile Creek and Fall Creek were also high (4.93 and 2.64 µg/L, respectively) and Fall Creek's SRP-Q slope was second highest (0.25). However, the loading potential of Sixmile Creek as represented by the slope was the lowest of all streams (0.03). With regards to SUP, Fall Creek had the highest intercept (Figure 3-16e; 5.52 µg/L) and Salmon Creek had the

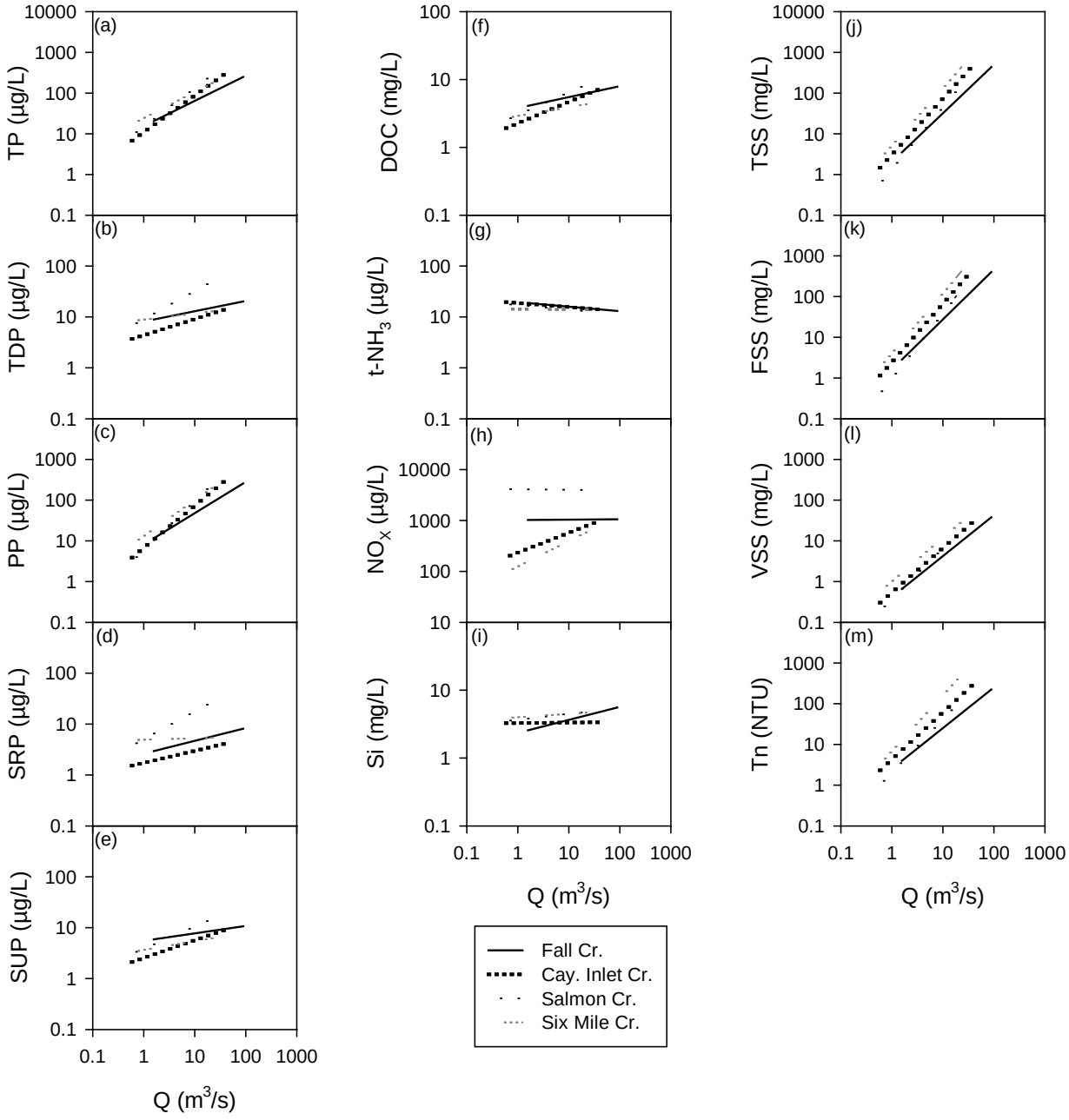

Figure 3-16. Concentration-Q plots (best-fit line only) for Fall Creek, Cayuga Inlet Creek, Salmon Creek, and Sixmile Creek for: (a) TP-Q, (b) TDP-Q, (c) PP-Q, (d) SRP-Q, (e) SUP-Q, (f) DOC-Q, (g) t-NH_3-Q, (h) NO_X-Q, (i) Si-Q, (j) TSS-Q, (k) FSS-Q, (l) VSS-Q, and (m) Tn-Q.

highest loading potential (slope = 0.44). Results for concentration-Q relationships for other dissolved constituents varied. t-NH_3-Q relationships were similar for all streams (Figure 3-16g) in terms of intercepts and negative slope. With regards to NO_X (Figure 3-16h), Salmon and Fall Creeks had the highest intercepts (4,113 and 1,023 µg/L, respectively). The loading potentials of the streams for NO_X were very different ranging from -0.01 (Fall Creek) to 0.50 (Sixmile Creek). DOC-Q intercepts were similar between all streams (Figure 3-16f), but the slopes were different ranging from 0.131 to 0.334. The DOC-Q relationships were only significant ($p < 0.005$) for Cayuga Inlet and Salmon Creek. The only statistically significant Si-Q relationship was for Fall Creek ($p = 0.03$; Figure 3-15i).

3.4.2. Air Temperature as a Driver of Concentration

Because flow was not a strong predictor for all constituents (especially dissolved constituents), the alternate driver, air temperature (T), was considered. Air T was considered instead of creek T because continuous, *in situ* measurements of T are currently not available for these streams. Figure 3-17 presents the relationship between air T and creek T for all five monitored streams. Air T was obtained from (Ithaca Game Farm Road Station) and creek T was measured during the biweekly portion and during some events with a hand-held YSI data sonde. The correlation between air and creek T was strong ($r > 0.92$) for all paired data justifying the use of air T as a surrogate of creek T.

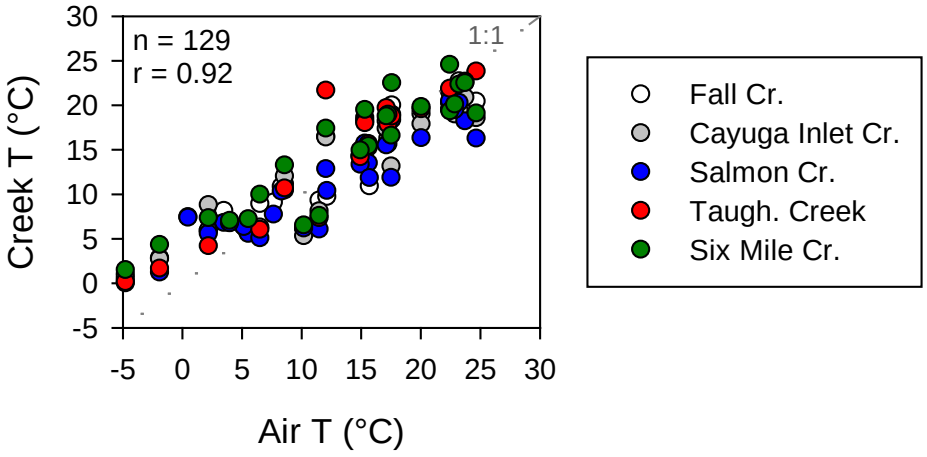

Figure 3-17. Air T versus creek T with correlation statistics for Fall Creek, Cayuga Inlet Creek, Salmon Creek, Taughannock Creek, and Sixmile Creek.

Particulate constituents were not strongly related to air T for Fall Creek (Figure 3-18a, c and j-m) as all had $r^2 < 0.2$. However, despite the weak correlations, PP, Tn and forms of SS for Fall Creek were significantly related to air T ($p < 0.02$). The relationships between air T and dissolved P were found to be positively correlated (e.g., concentration tended to be higher when warmer) and much stronger (Figure 3-18b, d-e) than the concentration-Q relationships. For

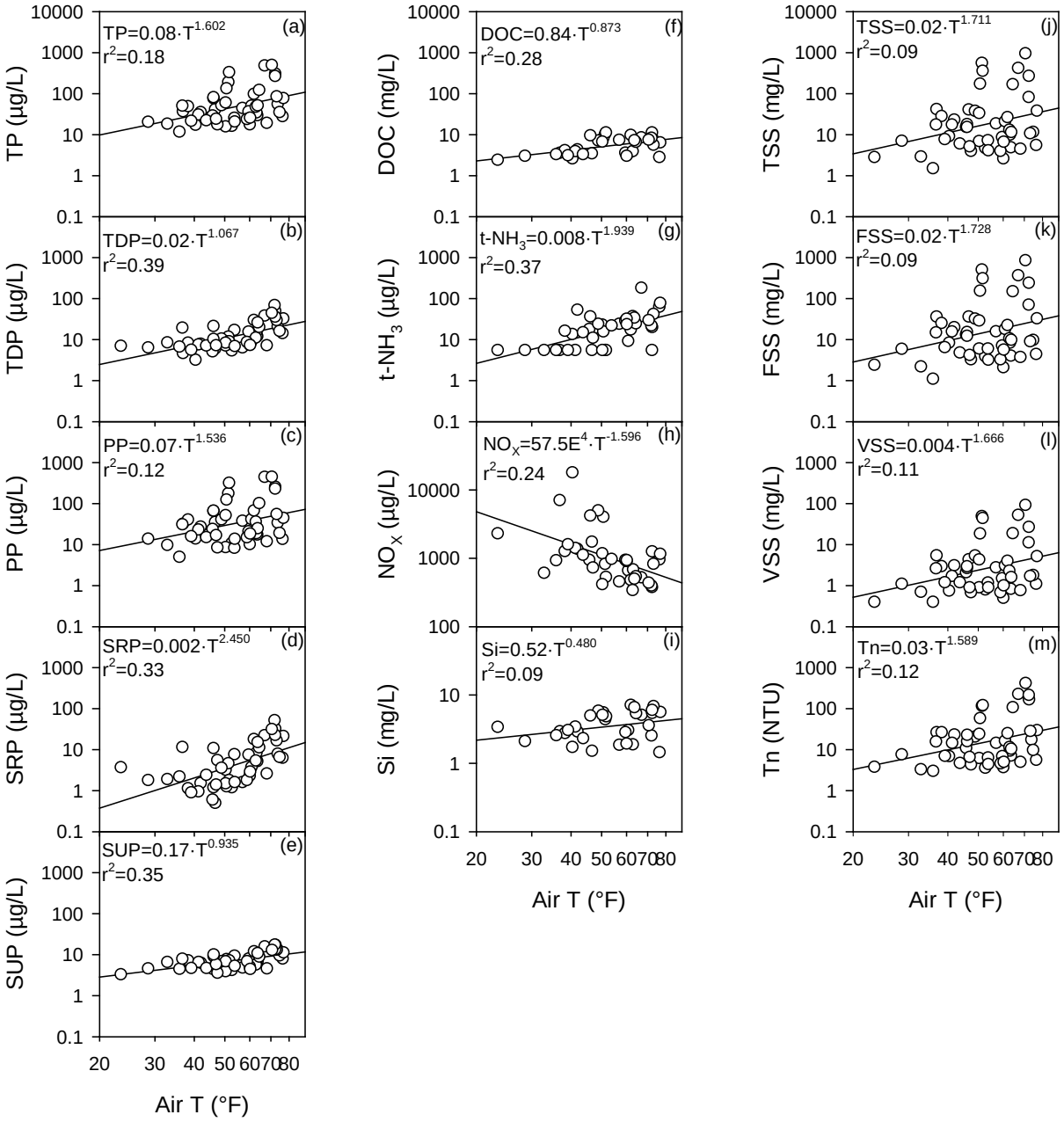

Figure 3-18. Concentration-Air T (°F) plots for Fall Creek: (a) TP-Air T, (b) TDP-Air T, (c) PP-Air T, (d) SRP-Air T, (e) SUP-Air T, (f) DOC-Air T, (g) t-NH_3-Air T, (h) NO_X-Air T, (i) Si-Air T, (j) TSS-Air T, (k) FSS-Air T, (l) VSS-Air T, and (m) Tn-Air T.

example in Fall Creek, the SRP-air T and SUP-air T relationships were statistically significant ($p < 0.001$) and had r^2-values of 0.33 and 0.35, respectively. The air T relationships for the other dissolved constituents were also positive. The only exception to this pattern was for NO_X (Figure 3-18h) which had higher concentrations during colder periods. Air T explained 37%, and 24% of the variability for t-NH_3, and NO_X (Figure 3-18g and h), respectively which was a large improvement compared to the concentration-Q relationships for these constituents. With regards to DOC and Si, the relationships with air T were slightly worse ($r^2 = 0.28$, and 0.09, respectively) than that with stream flow (Figure 3-18f and i).

The relationships between constituent concentrations and air T for the other streams displayed similar patterns to Fall Creek (Figure 3-19 and Appendix B4), including: (1) the relationships between particulates and air T were not especially strong, and unlike for Fall Creek, none were statistically significant, (2) the relationships between dissolved constituents and air T, generally, were as good or better (e.g., higher r^2, lower model p-values, and lower model error) than for flow, and (3) NO_X-air T relationships were negatively correlated. There were some observable differences in intercepts and slopes for some relationships, specifically with regards to SRP and NO_X (Figure 3-19d and h) attributable to background stream concentrations of these constituents.

The lack of strong relationships between the particulate and air T is most likely due to particulate concentration in streams being primarily driven by physical factors such as: (1) rainfall impact induced erosion, (2) overland flow transport to the streams, and (3) increased flow from runoff events and associated stream sediment erosion/resuspension and transport. For dissolved constituents, however the underlying mechanisms relating air (or creek) T to concentration remains unclear. The availability of inorganic phosphorus to plants is positively related to the activity of soil microbes that decompose organic matter (Pritchett and Fisher 1987) and the activity of soil microorganisms (bacteria and fungi) that decompose organic matter is temperature dependent with greatest microbial activity between 20° and 40° C (Brady and Weil 1996). Raymond and Saires (2010) found DOC export to be positively linked with temperature in Northeast forested watersheds, probably attributable to temperature effects on soil processes related to: (1) primary production, (2) soil respiration, (3) root exudation, and (4) dissolution of organic matter. In this study, stream DOC concentration was significantly related to air T in all cases (Appendix B4). Also, for all monitored streams (with the exception of Taughannock Creek), there was a significant positive ($p < 0.001$) relationship between stream DOC and SUP concentration as demonstrated in scatterplots in Figure 3-20 for Fall Creek and Cayuga Inlet Creek suggesting a possible common T mechanism regulating both DOC and dissolved P export in these watersheds.

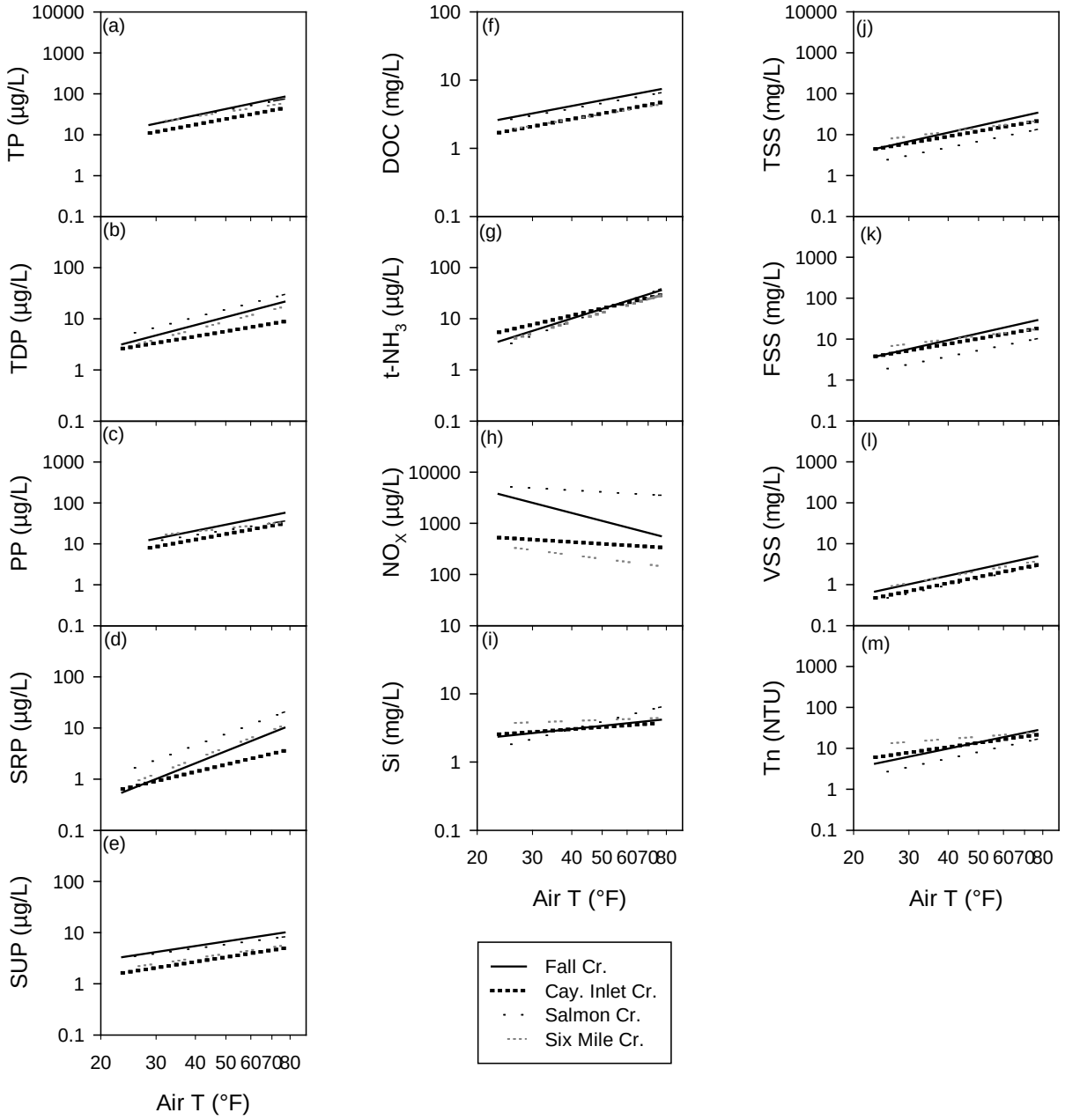

Figure 3-19. Concentration-Air T (°F) plots (best-fit line only) for Fall Creek, Cayuga Inlet Creek, Salmon Creek, and Sixmile Creek for: (a) TP-Air T, (b) TDP-Air T, (c) PP-Air T, (d) SRP-Air T, (e) SUP-Air T, (f) DOC-Air T, (g) t-NH_3-Air T, (h) NO_X-Air T, (i) Si-Air T, (j) TSS-Air T, (k) FSS-Air T, (l) VSS-Air T, and (m) Tn-Air T.

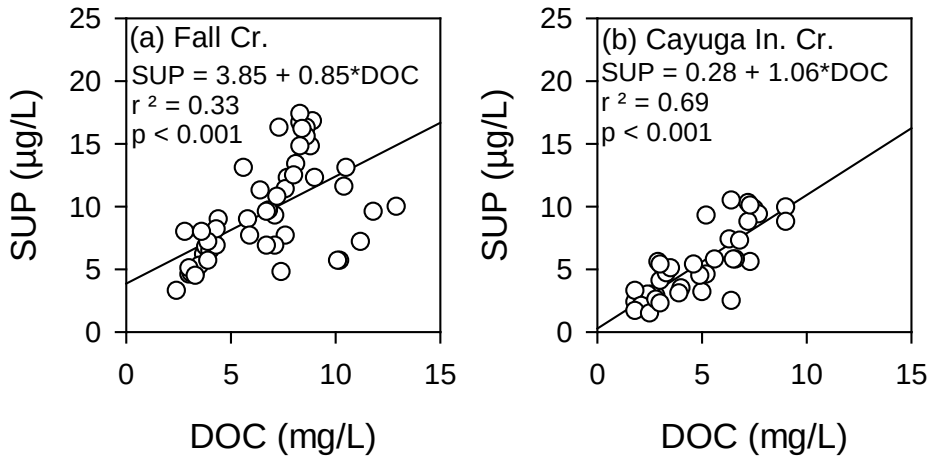

Figure 3-20. Relationship between stream DOC and stream SUP concentrations for: (a) Fall Creek and (b) Cayuga Inlet Creek.

3.4.3. Seasonality of Concentration-Flow Relationships

Because of the significant relationships between constituents and air T (especially the dissolved forms), the data from each stream were stratified into three seasons: (1) spring, March 1 – May 30, (2) summer, June 1 – September 30 (coincident with New York State regulators' application of summer for water quality standards), and (3) fall, October 1 – November 30. Post-stratification, the concentration-Q relationships for each constituent were re-evaluated. Substantial seasonal differences were indicated in all concentration-Q relationships for all constituents as presented for Fall Creek in Figure 3-21a-aj. The other four gaged streams showed similar patterns and can be found in Appendix B4. In most cases (except dissolved N), seasonal stratification resulted in improved model performance (r^2, mse, significance) compared to the non-stratified concentration-Q relationships (Appendix B4).

Stratification resulted in large improvements in phosphorus-Q relationships versus the overall, non-stratified relationships especially during the critical summer (June-September) period over which P targets are mandated for Cayuga Lake. For PP, the summer and fall r^2 (Figure 3-21c and d) were greater than 0.65, compared to the overall r^2 (Figure 3-21a) of 0.39. Similar improvements occurred with dissolved P. Summer and fall SUP (Figure 3-21 g and h) r^2 values were improved compared to overall (Figure 3-21e) and SRP spring and summer (Figure 3-21j and k) r^2 values were >0.4, compared to the r^2 = 0.04 overall (Figure 3-21i). Interestingly, the spring SRP-Q (Figure 3-21j) was particularly strong (r^2=0.57) and had a negative slope (i.e., dilution effect). Tn and TSS summer relationships (Figures 3-21o and s) were also strong (r^2 > 0.72) and were improvements compared to the overall relationships. Stratification did not improve concentration-Q relationships for t-NH_3 or NO_X (Figure 3-21u-x and Figure 3-21y-ab, respectively). Stratification improved concentration flow relationships for DOC and Si (Figure 3-21ac-af and Figure 3-21ag-aj, respectively). Each season had better fits for both of these

constituents compared to their respective overall concentration-Q relationships. The DOC r^2 in the fall (Figure 3-21af) was high (0.85) and the weakest relationship was in the summer (r^2 = 0.24; Figure 3-21ae). The Si r^2 values ranged from 0.25-0.38 (Figures 3-21ah-aj) which was much improved compared to overall Si-Q (r^2 = 0.15; Figure 3-21ag). Improved performance due to stratification in these cases is likely due to: (1) a good distribution of low and high flow samples within each stratum, and (2) indirect inclusion of an explanatory temperature effect. The generally poor performance of particulates (i. e., PP, Tn, and TSS) in the spring is likely due a lack of high flow samples within that period.

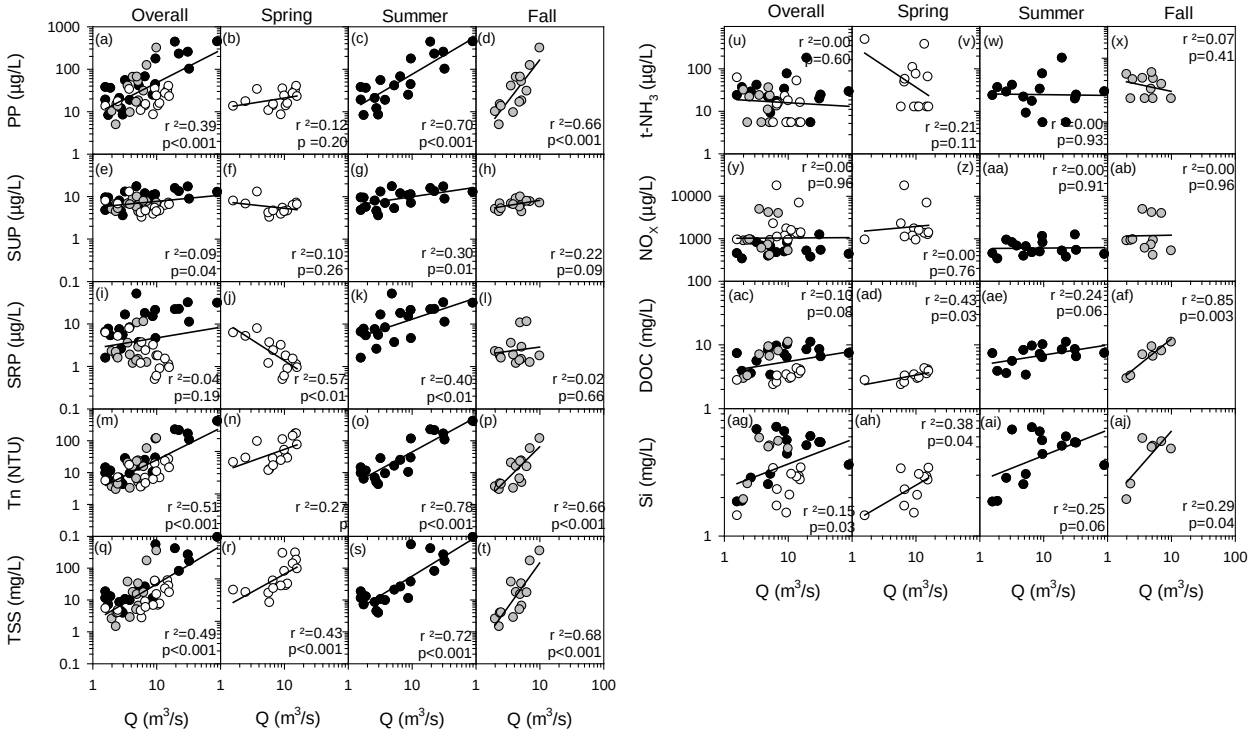

Figure 3-21. Fall Creek concentration-Q relationships for: (a) PP-Q overall with symbols for spring, summer, and fall identified, (b) PP-Q spring, (c) PP-Q summer, (d) PP-Q fall, (e) SUP-Q overall, (f) SUP-Q spring, (g) SUP-Q summer, (h) SUP-Q fall, (i) SRP-Q overall, (j) SRP-Q spring, (k) SRP-Q summer, (l) SRP-Q fall, (m) Tn-Q overall, (n) Tn-Q spring, (o) Tn-Q summer, (p) Tn-Q fall, (q) TSS-Q overall, (r) TSS-Q spring, (s) TSS-Q summer, (t) TSS-Q fall, (u) t-NH_3-Q overall, (v) t-NH_3-Q spring, (w) t-NH_3-Q summer, (x) t-NH_3-Q fall, (y) NO_X-Q overall, (z) NO_X-Q spring, (aa) NO_X-Q summer, (ab) NO_X-Q fall, (ac) DOC-Q overall, (ad) DOC-Q spring, (ae) DOC-Q summer, (af) DOC-Q fall, (ag) Si-Q overall, (ah) Si-Q spring, (ai) Si-Q summer, and (aj) Si-Q fall.

3.4.4. Turbidity-Concentration Relationships

The relationships between stream Tn and monitored constituents were considered for Fall Creek (Figure 3-22). Tn is an optical measurement of light scattering which is dominated by inorganic particles in these streams which is common to many other systems. Tn was observed to be a much better predictor of particulate constituents for Fall Creek than stream flow or air T. For example, PP-Tn for Fall Creek (Figure 3-22c) had r^2 and p-values of 0.93 and <0.001, respectively. Similarly, all the forms of SS all had r^2>0.92 and p<0.001 (Figures 3-22j-l). Surprisingly, the relationships between Tn and some dissolved constituents were also strong. For example SUP-Tn, DOC-Tn, Si-Tn were all statistically significant ($p < 0.001$) and had r^2 higher (0.47, 0.61, and 0.32, respectively) than for their respective stream flow or air T relationships. The SRP-Tn relationship (Figure 3-22d) was much stronger than for SRP-Q (Figure 3-15d). The relationships between dissolved nitrogen and Tn (Figures 3-22g and h) were not significant. The other streams demonstrated similar results to Fall Creek and are presented in Figure 3-23 and Appendix B4.

3.5. Methods of Load Estimation

The development of representative daily loading estimates requires: (1) an appropriate sampling strategy, (2) the development of relationships between concentrations and Q, or other potential drivers (Raymond and Saiers 2010; Vogel et al. 2003) to specify concentrations for intervals without measurements, and (3) application of appropriate calculation protocols (Defew et al. 2013, Johnes 2007, Dolan et al. 1981). The associated problems and challenges involved in loading analyses are well known because both constituent concentrations and flow rates are needed. The availability of continuous gauging (i.e., 15 minute, daily) of stream flow greatly improves the situation; however, for most constituents sampling frequency is much more limited because the costs and logistical problems of sampling and laboratory analyses are unrealistic. To compound the problem, a large portion of annual loads carried by many streams occurs over relatively brief intervals of high flow (Baker et al. 2014; Longabucco and Rafferty 1998; Richards and Holloway 1987). Improved loading estimates are generally supported by a stratified sampling design that combines fixed frequency (e.g., biweekly) and high flow or runoff event-based sampling (Yaksich and Verhoff 1983; Johnes 2007) that is enabled by implementation of automated sampling equipment (Baker et al. 2014, Longabucco and Rafferty 1998, Prestigiacomo et al. 2007). There are a number of different loading calculation approaches that have been developed to maximize the representativeness of daily loading estimates based on such data (Walker 1995).

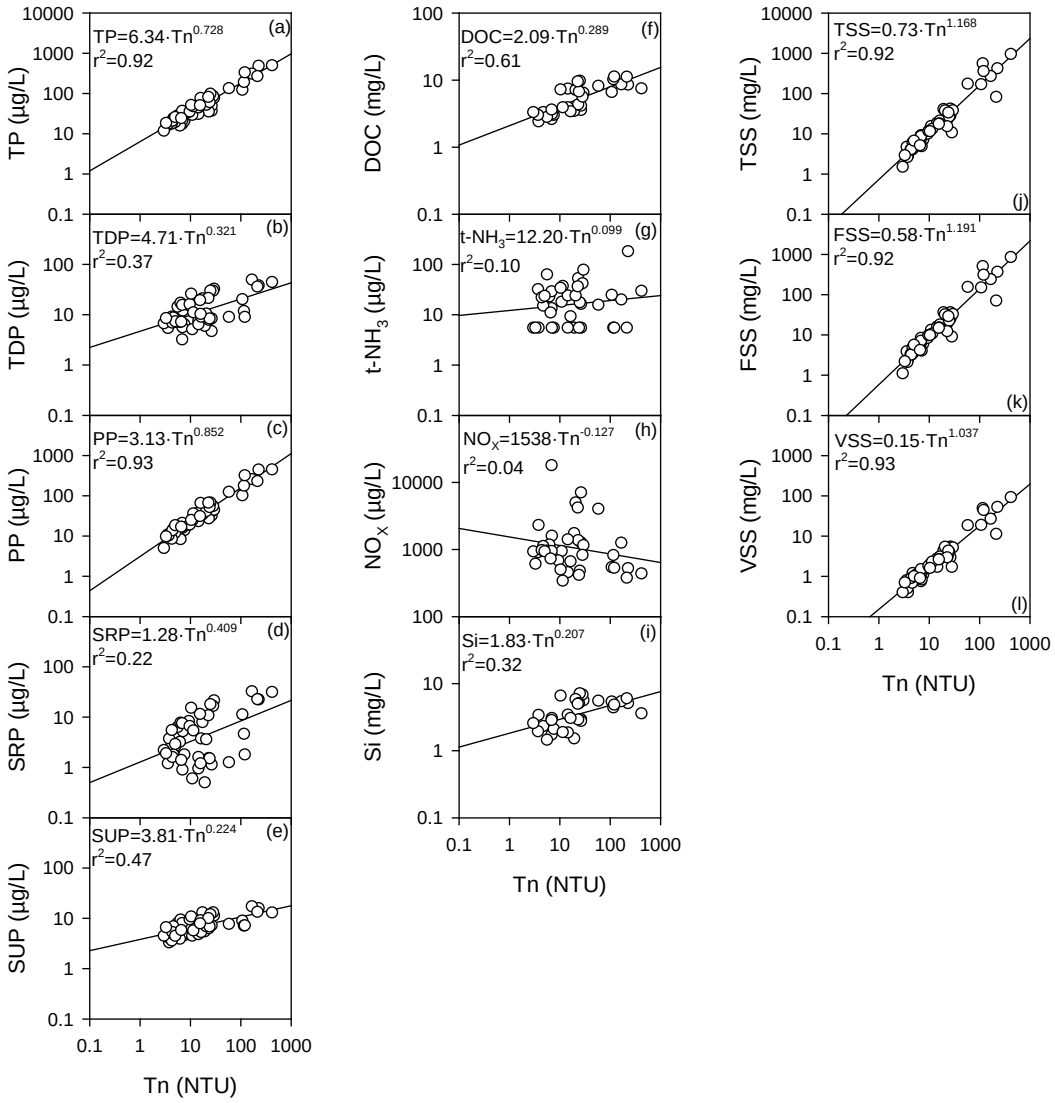

Figure 3-22. Concentration-Tn plots for Fall Creek: (a) TP-Tn, (b) TDP-Tn, (c) PP-Tn, (d) SRP-Tn, (e) SUP-Tn, (f) DOC-Tn, (g) t-NH_3-Tn, (h) NO_X-Tn, (i) Si-Tn, (j) TSS-Tn, (k) FSS-Tn, and (l) VSS-Tn.

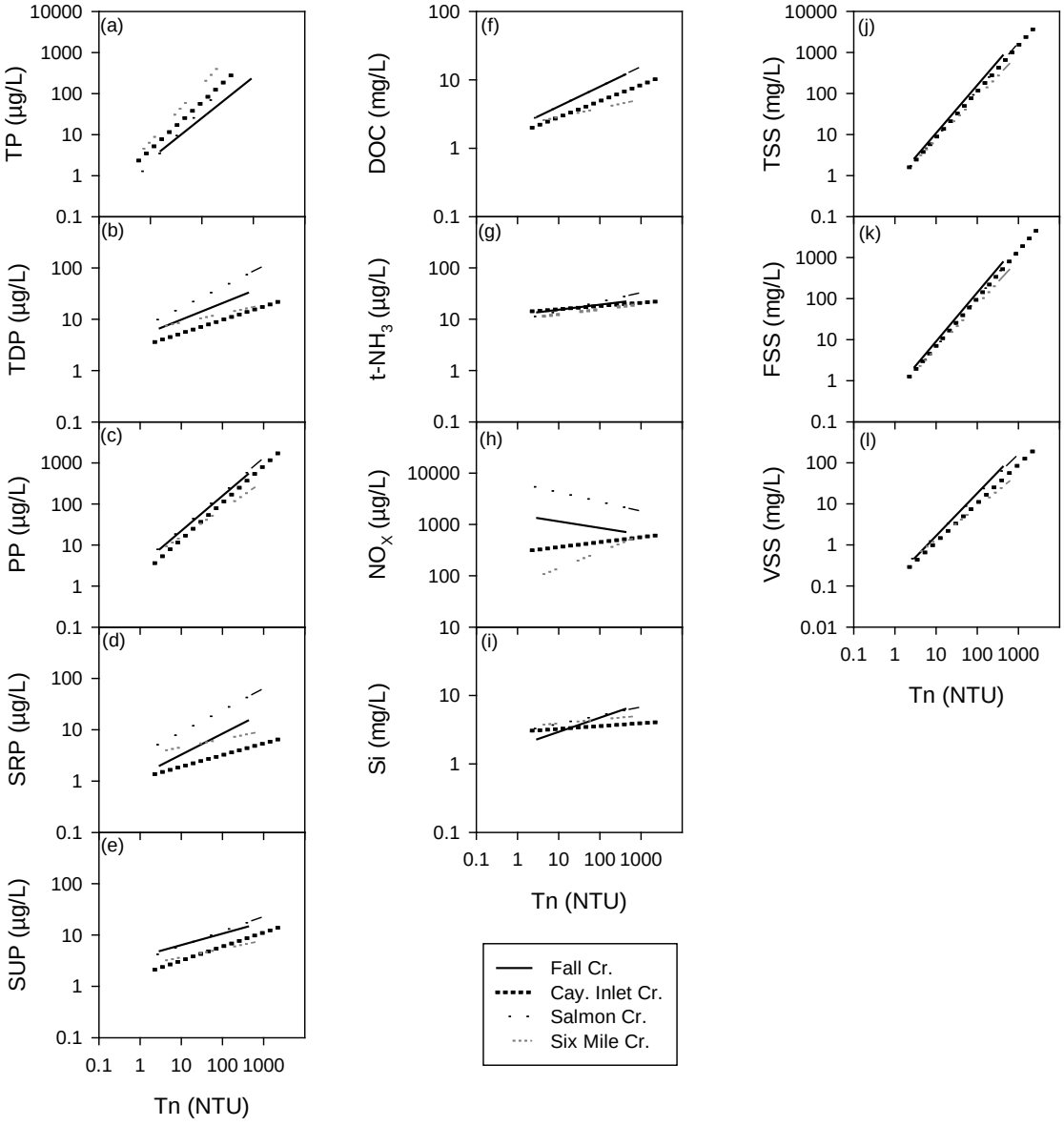

Figure 3-23. Concentration-Tn plots (best-fit line only) for Fall Creek, Cayuga Inlet Creek, Salmon Creek, and Sixmile Creek for: (a) TP-Tn, (b) TDP-Tn, (c) PP-Tn, (d) SRP-Tn, (e) SUP-Tn, (f) DOC-Tn, (g) t-NH_3-Tn, (h) NO_X-Tn, (i) Si-Tn, (j) TSS-Tn, (k) FSS-Tn, and (l) VSS-Tn.

3.5.1. Point Sources

Load estimates for major point sources were conducted for P only. The full suite of constituents monitored for tributaries were not available for these point source inputs. The three major point sources considered in this study were the: (1) Ithaca Area Wastewater Treatment Plant (IAWWTP), (2) Cayuga Heights Wastewater Treatment Plant (CHWWTP), and (3) Cornell University Lake Source Cooling Plant (LSC). Also, several other minor point sources were represented (Aurora WWTP, Union Springs Sewage Treatment Plant (STP), Trumansburg WWTP, and Interlaken STP). These smaller point sources were considered together as summed minor point sources. TP data from the Dryden STP and Freeville WWTPs were used to estimate their respective loads to Fall Creek's TP loading (TP_L) estimate (see Section 3.6.1.2).

Neither flow nor concentration in the point sources was strongly temporally variable, so monthly average loads (e.g., product of monthly average flow and monthly average concentrations) were calculated and summed to obtain A-O estimates. For a detailed analysis of the point source loads, including assumptions made about dissolved forms and bioavailability, see Prestigiacomo et al. (2015). Below is a link to a pdf of a draft manuscript currently submitted for review.

3.5.2. Tributaries

Constituent loads were calculated for the five monitored tributaries for the A-O interval of 2013. In addition, load estimates for the unmonitored small streams were estimated together as the product of the watershed area-weighted, flow-weighted concentrations obtained for the monitored tributaries and the estimated total Q for the minor streams (prorated from the gaged tributaries on an area basis) for the study period. Entire watershed estimates for the lake were made by summing the monitored and unmonitored load estimates. Loading rate (e.g., kg/d or $NTU \cdot m^3/d$ in the case of turbidity) was calculated as the product of the concentration (as daily averages) and the corresponding daily average flow rate for each source.

Phosphorus loads were calculated for the three forms of monitored P; PP (PP_L), SRP (SRP_L), and SUP (SUP_L). The sum of the three corresponds to the estimated TP load (TP_L) as presented in Prestigiacomo et al. (2015). A similar approach was used for suspended solids, as the sum of the load estimates for FSS (FSS_L) and VSS (VSS_L) was used to obtain the loading estimate for TSS (TSS_L). Loading estimates for t-NH_3, NO_X, DOC, Si and Tn were also calculated. Loads for the A-O period of interest were calculated as the summation of the rates for each day within that period.

More complex load estimation protocols were necessary for the tributaries than the point sources, due to the inherent complications of wide variations in both concentrations and Q. The continuous Q data from the four gaged tributaries, and estimates for Taughannock Creek (Eq. 3-1), were used in calculations of tributary loads. Empirical concentration-Q regression

Submitted to
JOURNAL OF THE AMERICAN WATER RESOURCES ASSOCIATION

APPORTIONMENT OF BIOAVAILABLE PHOSPHORUS LOADS ENTERING CAYUGA LAKE, NEW YORK[1]

Anthony R. Prestigiacomo, Steven W. Effler, David A. Matthews, Martin T. Auer, Benjamin E. Downer, Anika Kuczynski and M. Todd Walter

ABSTRACT: The integration of the phosphorus (P) bioavailability concept into a P loading analysis for Cayuga Lake, New York, is documented. Components of the analyses included the: (1) monitoring of particulate P (PP), soluble unreactive P (SUP), and soluble reactive P (SRP), supported by biweekly and runoff event-based sampling of the lake's four largest tributaries, (2) development of relationships between tributary P concentrations and flow, (3) algal bioavailability assays of PP, SUP, and SRP from primary tributaries and the three largest point sources, and (4) development of P loading estimates to apportion contributions according to individual nonpoint and point sources, and to represent the effects of interannual variations in tributary flows on P loads. Tributary SRP, SUP, and PP are demonstrated to be completely, mostly, and less bioavailable, respectively. Tributary specific differences in bioavailability are positively correlated with the percent agriculture landuse in the watersheds. Point source contributions to the total bioavailable P load (BAP_L) are minor (5%), reflecting the benefit of reductions from recent treatment upgrades. The BAP_L represented only about 26% of the total P load, because of the large contribution of the low bioavailable PP component. Most of BAP_L (> 70%) is received during high flow intervals. Large interannual variations in tributary flow and coupled BAP_L will tend to mask future responses to changes in individual inputs.

(KEY TERMS: environmental impacts; rivers/streams; point sources; lakes; nutrients; phosphorus; load estimates; bioavailability.)

INTRODUCTION

Despite advancements in wastewater treatment and control of nonpoint sources over the last thirty years, cultural eutrophication and its attendant water quality problems continue to be an issue for many lakes in the United States (Cooke *et al*., 2005). Reductions of phosphorus (P) inputs remain a primary management objective as it is the limiting nutrient in the vast majority of freshwater systems (Cooke *et al*., 2005). Partitioning external loads of P according to sources is fundamental information to support related rehabilitation initiatives, such as the total maximum daily load (TMDL) analysis process (U.S. EPA, 1991). Earlier initiatives often considered only total P (TP) with respect to concentration measurements, loading estimates, and mathematical models used to quantify cause (e.g., loads) and effect (e.g., lake concentrations; Chapra, 1997; Vollenweider, 1976).

Phosphorus exists in a wide array of chemical forms (Dodds, 2003), that differ substantially with respect to their availability to support primary production. Those forms that support algal production are termed bioavailable (Auer *et al*., 1998; DePinto *et al*., 1981; Young *et al*., 1982). It is valuable to consider bioavailability in the context of the three forms of P that are commonly measured in contemporary monitoring programs, that include TP, total dissolved P (TDP), and soluble reactive P (SRP). Two additional forms are calculated from these three as residuals: (1) particulate P (PP = TP – TDP), and (2) soluble

[1] *Respectively, Research Scientist (Prestigiacomo) and Research Engineers (Effler and Matthews), Upstate Freshwater Institute, P.O. Box 506, Syracuse, New York, 13214 (E-Mail/Tony@upstatefreshwater.org); Professor (Auer) and Graduate Students (Downer, Kuczynski), Department of Civil and Environmental Engineering, Michigan Technological University, Houghton, Michigan, 49931; Assoc. Professor, (Walter) School of Civil and Environmental Engineering, Hollister Hall, Cornell University, Ithaca, New York 14853.*

Click here to load phosphorus loading manuscript

relationships using daily averaged concentrations and flows were developed to support estimates of concentrations for times for which direct measurements were not available.

3.5.2.1. Load Estimation Methods: Multiple Protocols Investigated

Loading estimates can vary substantially depending on the calculation methods used (Walker 1995, Johnes 2007, Dolan et al. 1981). Because magnitudes of the estimates can be highly dependent upon calculation methodology, thirteen protocols (Table 3-8) were investigated as potential A-O load estimators for Fall Creek (for the three forms of P), to evaluate performance and represent the general level of uncertainty associated with the adoption of a particular approach. The thirteen adopted protocols can be partitioned into two groups: (1) those conducted with the FLUX32 software program (FLUX32 2013), and (2) those performed independently with empirical concentration-driver (i.e., flow or air T) relationships and temporally detailed driver information over the study period. Eleven of the thirteen methods were used to calculate P loads for the other gaged tributaries. The tabular results of each method, for each form of P for all tributaries can be found in Appendix B5.

The A-O estimates from the 13 methods are provided graphically for each of the three P forms; PP_L (Figure 3-24a) SUP_L (Figure 3-24b), and SRP_L (Figure 3-24c) for Fall Creek. Relatively good closure was obtained for the entire array of P loading estimates from all protocols (regression and non-regression); the coefficients of variation (CV) were 23%, 12%, and 18% for PP_L, SUP_L and SRP_L, respectively. It was determined that the non-regression methods (10-13) yielded systematically higher estimates than the regression methods, particularly for PP_L (Figure 3-24a) and SRP_L (Figure 3-24c). The regression methods were preferred because they: (1) utilize environmental driver information to explain some of the variability in observed concentration, and (2) can be used to provide daily load estimates from daily flows which are needed for input to the water quality model. Among the regression methods, the greatest uncertainty among the three P forms for Fall Creek was for PP_L. PP_L estimates ranged from ~ 7,600 to 11,300 kg. SRP_L estimates ranged from 850 to 1,200 kg and SUP_L were found to be the least variable, ranging only from 645 to 800 kg for the A-O study interval. Despite the range in estimates observed from the 9 regression protocols, convergence of the estimates for Fall Creek was still very good. CV values of 14%, 6%, and 15% were observed for PP_L, SUP_L, and SRP_L, respectively.

A-O estimates derived from most of these protocols were used in a comparative analysis only. Because of the daily load estimate requirements of the lake water quality model, only those methods that provided a daily time series of loading estimates were candidate approaches. The best candidate approaches were: (1) Protocol 1: concentration-Q regression stratified into low and high flow, (2) Protocol 6: concentration-Q regression stratified into three seasons, and (3) Protocol 9: multiple linear regression with flow and air T. The Fall Creek and total watershed P_L estimates (A-O) from each of these candidate approaches are presented in Table 3-9. These candidate approaches yielded precise results for Fall Creek and for the total watershed

Table 3-8. Loading estimate protocols adopted for forms of phosphorus (PP, SRP, SUP) for Cayuga Lake tributaries.

Protocol	Method Type	Stratification	Description	Reference
1.	FLUX32 Method 6 Interpolated	low/high flow	LN transformed Concentration (C) /flow (Q) regression using observed concentrations when available	FLUX32, 2013[a]
2.	FLUX32 Method 6	low/high flow	LN transformed C/Q regression (regression model only)	FLUX32, 2013
3.	FLUX32 Method 5	low/high flow	LN transformed C/Q regression with adjustments for flow wieghted concentrations	FLUX32, 2013
4.	FLUX32 Method 4	low/high flow	LN transformed C/Q regression with adjustments for variability between sampled and unsampled flows	FLUX32, 2013
5.	FLUX32 Method 6	baseflow/rising limb/falling limb	LN transformed C/Q regression stratified by flow regimes: (1) baseflow, (2) rising limb, or (3) falling limb	FLUX32, 2013
6.	FLUX32 Method 6	seasonal	LN transformed C/Q regression stratified by season: (1) spring (Mar. 1.-May 31), (2) summer (Jun. 1 – Sept. 30), or (3) fall (Oct. 1-Nov. 30)	FLUX32, 2013
7.[b]	Manual Regression on 15 minute flows	low/high flow	LN transformed C/Q regression using high frequency flow data (15 min.)	-
8.[b]	Manual Regression on 15 minute flow with event estimates	low/high flow	LN transformed C/Q regression using high frequency flow data (15 min.) and estimates of event loads	-
9.	Multiple Linear Regression with daily flow and air temperature	-	LN transformed C/Q regression with air temperature as a second independent driver	-
10.	FLUX32 Method 3	low/high flow	Ratio estimator similar to Beale's Ratio Estimator	FLUX32, 2013
11.	FLUX32 Method 2	low/high flow	Flow-wieghted Concenetration applied to daily flow record	FLUX32, 2013
12.	FLUX32 Method 1	low/high flow	Average load applied to daily flow record	FLUX32, 2013
13.	Monthly Averaged Concentrations	-	Concentrations averaged by month, monthly averages applied to each daily flow within each month	-

[a] see FLUX32 Software Manual for full description
[b] method used for Fall Creek only

estimates. The range in Fall Creek PP_L among the candidates was only 890 kg (11% of the average of the three candidates). Similar results were found for Fall Creek's SUP_L and SRP_L where the ranges in estimates were only 6% (42 kg) and 13% (116) of the candidates' average. The relatively small differences in the total watershed estimates were similar to Fall Creek (Table 3-9). The reasonable closure between all methods and the very good agreement between the candidate approaches supports the use of the best approach (subsequently) and provides a degree of assurance that the loading estimates obtained are representative for each stream and for the 2013 A-O interval as a whole.

3.5.2.2. Best Method for Load Estimation

The selected best method (Protocol 6; Table 3-8) was a log (natural) concentration-Q regression stratified into three seasons: (1) spring, March 1 – May 30, (2) summer, June 1 – September 30, and (3) fall, October 1 – November 30. This stratification resulted in a reasonably uniform distribution of data points within each season. This protocol provides loading rate estimates at the desired daily time step and uses direct estimates of loads for days of constituent

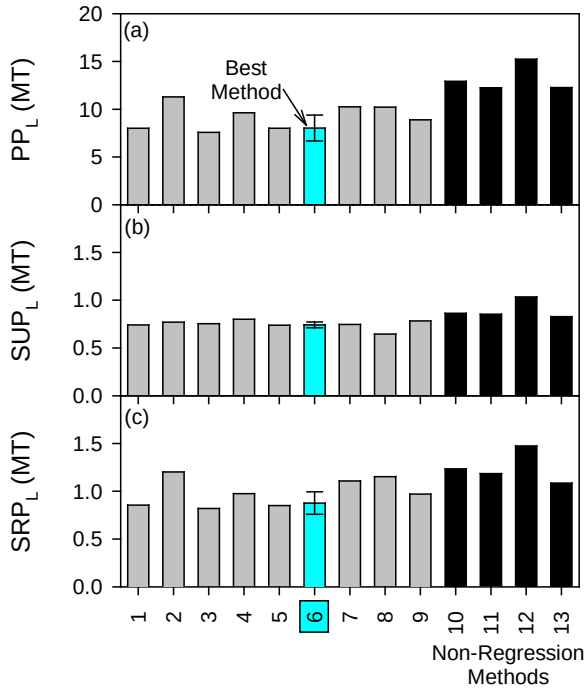

Figure 3-24. Estimates of tributary loads for Fall Creek for the A – O interval of 2013, according to multiple numbered calculation protocols (from Prestigiacomo et al. 2015): (a) PP_L, (b) SUP_L, and (c) SRP_L (see Tables 3-8, 3-9, and Appendix B5).

Table 3-9. April – October load estimates for selected candidate protocols for forms of P for Fall Creek and total watershed estimates (kg).

Protocol Number	2013 A-O Fall Creek Estimates			2013 Total Watershed Estimates		
	PP_L	SUP_L	SRP_L	PP_L	SUP_L	SRP_L
1	8,010	742	855	45,500	3,000	6,200
6	8,032	742	877	44,700	3,000	5,000
9	8,896	784	971	40,000	3,200	5,400

monitoring. Estimates for days intervening observations were based on the concentration-Q regression relationships and interpolated residuals (observed loads minus regression predicted loads). The daily load estimates between days were calculated as the sums of the regression estimates and interpolated residuals (FLUX32 2013). This method was selected over the other protocols because the : (1) output provided daily loading estimates required for the water quality model, (2) use of measured concentrations, (3) improved fit (r^2) between stratified concentration-Q relationships compared to overall concentration-Q relationships (Figure 3-21), (4) lower model mean square error (mse), and (5) better model performance as determined by comparisons between observed and predicted concentrations (lower root mean square error (RMSEs) and

median residuals. Comparisons of model fit, performance, and A-O load estimates for the three best approaches are provided in Table 3-10 (Performance statistics for other streams can be found in Appendix B5). Of interest was that Protocol 6 and Protocol 9 (multiple regression with flow and air T), generally performed better than Protocol 1 (stratification into low and high flow).

3.5.3. Data Outliers

Several data points were identified as outliers and were not included in concentration-Q analyses or in subsequent loading estimates. The outliers removed from analyses are summarized in Table 3-11. These daily averaged outliers were identified in the development of concentration-Q relationships and in the FLUX32 software. They were verified independently using standard residual analysis techniques to identify outliers and high leverage data (Cook's D, Studentized Residuals, and DEFITS; Neter et al. 1996). The most prominent case was for August 8 which was on the rising limb for the largest event monitored in 2013. Outliers were identified for all particulate constituents for Fall Creek, Cayuga Inlet Creek, and Salmon Creek (Aug. 9) during this event. The impact of including these data points on the A-O loads was striking as demonstrated for the case of PP_L in Cayuga Inlet Creek on August 8. The peak daily concentration for this case was 11,337 µg/L which was larger than any previously observed PP (or TP) measurement on record for this stream (Table 3-7). The A-O best estimate for PP_L for this stream (not including Aug. 8) was 9.3 MT. If the Aug. 8 outlier was included in the analysis, the PP_L for Aug. 8 alone would have been 10.6 MT! Given the good performance of the laboratory measurements for triplicate samples the identified outliers were attributable to unrepresentative samples. These samples were collected with automated equipment during major runoff events, when ambient conditions relative to representativeness of samples can be expected to be most challenging.

Table 3-10. Comparison of the best methods for daily loading estimates of the three forms of P for Fall Creek.

Constituent	Protocol	Method Type	Model Statistics			Model Performance	
			p-value	r^2	mse	RMSE[a] (µg/L)	median residual[b] (µg/L)
PP	1.	C/Q[c] 2 Flow Strat. Interp.	<0.001	0.41	0.74	87	-10.4
	6.	*C/Q Seasonal Strat.Interp.*	*<0.001*	*0.56*	*0.52*	*69*	*+0.7*
	9.	Multiple Linear Regression	<0.001	0.54	0.55	71	-10.9
SUP	1.	C/Q 2 Flow Strat. Interp.	0.09	0.06	0.17	3	-0.6
	6.	*C/Q Seasonal Strat.Interp.*	*<0.001*	*0.29*	*0.13*	*3*	*-0.2*
	9.	Multiple Linear Regression	<0.001	0.44	0.10	2	-0.3
SRP	1.	C/Q 2 Flow Strat. Interp.	0.19	0.03	1.28	10	-3.4
	6.	*C/Q Seasonal Strat.Interp.*	*<0.001*	*0.47*	*0.70*	*8*	*-1.0*
	9.	Multiple Linear Regression	<0.001	0.35	0.90	7	-2.5

[a] root mean square error defined as, RMSE = $\sqrt{\frac{\sum(OBS-PRED)^2}{n}}$

[b] median residual defined as the median of all observed concentration minus model concentrations

[c] C/Q = concentration-flow

Table 3-11. Summary of outliers removed from 2013 loading analysis.

Tributary	Date	Daily Average Concentration[1]					
		PP (µg/L)	FSS (mg/L)	VSS (mg/L)	Tn (NTU)	SRP (µg/L)	SUP (µg/L)
Fall Creek	Aug. 8	927.4 (927.4)	706.7 (706.7)	153.3 (153.3)	508 (508)	-	-
Cayuga Inlet Creek	Aug. 8	11,338 (12,640)	8,304 (8,712)	962 (968)	11,442 (12,368)	-	-
Salmon Creek	Apr. 10	-	-	-	-	0.5 (0.6)	6.6 (7.5)
	Aug. 9	919.5 (3,203)	725.2 (2,720)	89.1 (304)	957.9 (3,462)	-	-
	Oct. 17	322.5 (322.5)	138 (138)	27.9 (27.9)	135 (135)	-	-

[1] maximum observed concentration in parentheses

3.6. Load Estimates

3.6.1. April – October Best Estimates

Two flow strata were adopted to partition runoff event contributions (low versus high) for constituent loads (each constituent) for the gaged tributaries, demarcated by the 2013 mean Q. The Taughannock Creek loads were adjusted by a factor to compensate for the effect of no runoff event-based sampling (Table 3-12; Prestigiacomo et al. 2015). The adjustment factor for each constituent was determined from Eq. 3-3, where A-O $Load_g$ is the best estimate from gaged stream g based on all available data, A-O Biweekly $Load_g$ is the load estimate from gaged stream g based on the biweekly data set only. The adjustment factor for each constituent was calculated as the average of the A-O $Load_g$:A-O Biweekly $Load_g$ ratios from the four streams with event samples.

Eq. 3-3. $$Adjustment\ factor = \frac{\left(\sum_{g=4}^{n} \frac{A-O\ Load_g}{A-O\ Biweekly\ Load_g}\right)}{4}$$

Loading estimates for the unmonitored small streams were estimated together as the product of the watershed area-weighted, flow-weighted concentrations obtained for the five monitored tributaries and the estimated total flow for the minor streams (prorated from the gaged tributaries on an area basis) for the study period (Eq. 3-2).

3.6.1.1. Point Source Phosphorus and Bioavailability

A detailed review of the phosphorus bioavailability concept and description of the algal assay experiments applied to samples to determine the fraction bioavailable (fraction of P that can support algal growth, f_{BAP}) for PP, SUP, and SRP can be found in the attached manuscript (Prestigiacomo et al. 2015).

Table 3-12. Adjustment factors for Taughannock Creek loads.

Constituent	Adjustment Factor[1]
PP	1.97
SRP	1.27
SUP	1.14
FSS	3.14
VSS	4.13
Tn	3.46
DOC	1.43
Si	1.03
t-NH_3	1.38
NO_X	0.52

[1] final load estimate calculated as the product of the original estimate and adjustment factor

IAWWTP was the largest point source of TP_L. This source delivered ~ 730 kg to Cayuga Lake over the A-O period which was 52% of the total point source TP_L (1,415 kg; Figure 3-25a). The other point sources considered here, individually added substantially less TP_L than IAWWTP with contributions ranging from 190 kg (summed minor point sources) to ~ 300 kg (LSC).

The SRP in each of the three point discharges evaluated was found to be nearly completely available (f_{BAP} > 93%, Table 3-13). Dramatic differences in the bioavailability of PP were observed for the two largest WWTPs. Only ~ 1% in the IAWWTP effluent was bioavailable, compared to 25% for the CHWWTP discharge. The average f_{BAP} values were similar for SUP for these two WWTPs (63-73%). However, SUP from the LSC facility was found to be mostly unavailable (~ 8%). The bioavailabilities for the small WWTPs were specified, based on observations for facilities with similar types of treatment (e.g., Effler et al. 2002). The extent to which the estimated total bioavailable P loads (BAP_L's) were less than the TP_L estimates differed greatly among the discharges (Figure 3-25a and b). The greatest effect was for the IAWWTP where the BAP_L was 71% smaller than the TP_L. The smallest effect was for the LSC facility (25% lower), for which the completely bioavailable SRP fraction dominated. The overall BAP_L was only 46% of the TP_L (Figure 3-25b).

3.6.1.2. Tributary Phosphorus and Bioavailability

Fall Creek and Cayuga Inlet Creek each contributed ~ 9.6 MT of TP_L to Cayuga Lake (Figure 3-26a). Together, these two streams accounted for ~36% of the total TP_L (54.2 MT) to Cayuga Lake for the study period. The other three streams delivered ~ 12.1 MT of TP combined. The unmonitored watershed estimate of TP load was 21.4 MT. PP_L was the dominant form of P_L for the monitored streams over the 2013 A-O interval of (black bar segment; Figure 3-26a). PP_L:TP_L ratios ranged from 70-97% with an average of 83%. The SRP_L:TP_L ratio for all streams was 11.3%. SUP_L was the lowest contributor of TP_L: the average

Table 3-13. Phosphorus bioavailability results for inputs to Cayuga Lake.

		PP, f_{BAP}			SRP, f_{BAP}			SUP, f_{BAP}	
Tributary	n	average	CV	n	average	CV	n	average	CV
Fall Creek	3	10.6	60%	3	96.3	2%	3	92.7	7%
Cayuga Inlet Creek	3	5.7	64%	3	90.7	14%	3	59.7	24%
Salmon Creek	3	19.2	70%	3	98.5	0%	3	84.4	20%
Sixmile Creek	3	6.0	69%	3	95.3	6%	3	65.5	49%
CHWWTP	3	25.4	11%	3	98.5	1%	3	62.7	16%
IA WWTP	3	1.2	83%	3	93.1	1%	3	73.2	29%
LSC Effluent	2	-	-	2	98.1	2%	2	8.2	141%

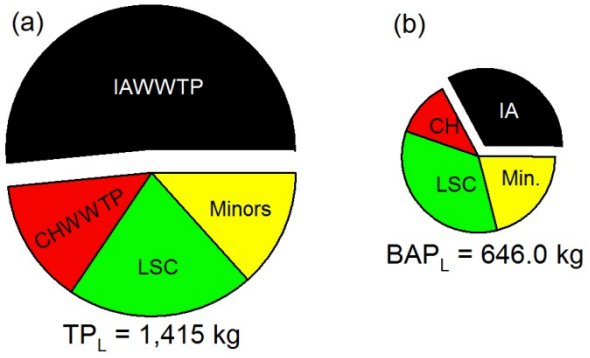

Figure 3-25. Apportionment of point source TP_L and BAP_L for the A-O interval 2013: (a) contributions of IAWWTP, CHWWTP, LSC, and four Small WWTPs (Minors) to point source TP loading (TP_L), and (b) contributions of the point sources to the bioavailable P Load (BAP_L; Table 3-14).

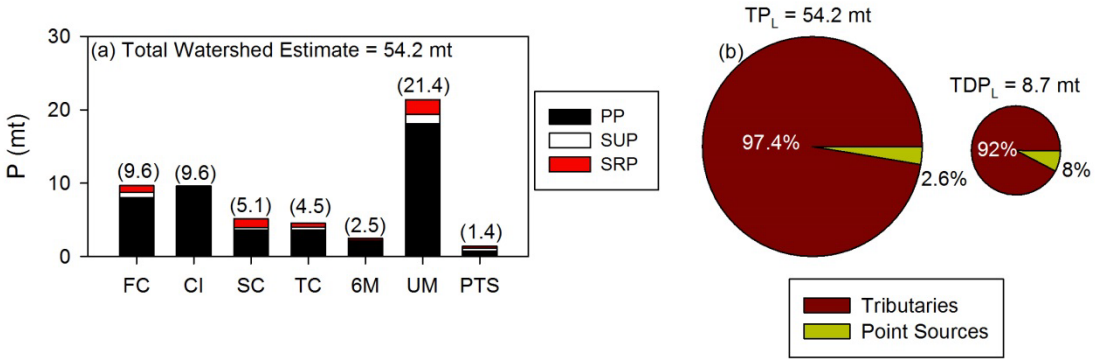

Figure 3-26. Estimated P loads to Cayuga Lake over the A-O interval of 2013: (a) TP_L, partitioned according to PP, SUP, and SRP, for monitored and unmonitored (UM) tributaries and point sources (PTS), and (b) overall TP_L and TDP_L partitioned according to tributaries and point sources.

SUP_L:TP_L ratio was only 6.1%. The tributaries (non-point sources) were the dominant sources of both TP_L and TDP_L (97.4% and 92%, respectively; Figure 3-26b).

The average f_{BAP} values and ranges for PP and SUP varied amongst the four assessed tributaries as presented in Table 3-13 and Figure 3-27. In all 4 cases, only a modest fraction of PP was bioavailable (Figure 3-27a). The ranking according to average f_{BAP} values for PP was Salmon Creek (19%) > Fall Creek (11%) > Sixmile Creek (6%) > Cayuga Inlet Creek (5.7%). Most of the SUP was available, and the same ranking amongst these tributaries prevailed (Figure 3-27b) with the exception that Fall Creek had the highest f_{BAP} for SUP (92.7%). The SRP fraction was essentially completely available in all cases. Wide temporal differences were observed for f_{BAP} for both PP and SUP in individual streams (Table 3-13) with PP f_{BAP} being the most variable (CV > 60%) and SRP f_{BAP} being least variable (maximum CV = 14%). An interesting finding in this study was that the average values of f_{BAP} for both PP ($r = 0.97$) and SUP ($r = 0.78$) were strongly correlated to the fraction of agricultural land use in the watersheds of the individual streams (Figure 3-27c). PP and SUP f_{BAP} estimates for Taughannock Creek and the unmonitored portion of the watershed were based Fall and Salmon Creek values, respectively, which was consistent with land use information (Haith et al. 2009). The progression of selected bioassays for PP (Figure 3-27d) is presented to contrast the features for Salmon Creek and Fall Creek for the July 22 sample. The time to reach plateau values for the PP experiments was about 10 d.

Loads of the bioavailable fractions of PP ($PP_{L/B}$), SUP ($SUP_{L/B}$), and SRP ($SRP_{L/B}$) were estimated for each of the monitored inputs by multiplying the loads for each of the three fractions by the respective average f_{BAP} values determined from the bioassays (Table 3-13). The overall load of bioavailable P (BAP_L) was calculated as the summation of the three fractions (= $PP_{L/B}$ + $SUP_{L/B}$ + $SRP_{L/B}$). Watershed yields of $PP_{L/B}$, $SUP_{L/B}$, and $SRP_{L/B}$ for the monitored tributaries were calculated by dividing those loads by the respective contributing watershed areas. The flow-weighted concentrations of the bioavailable P fractions were calculated for these tributaries by dividing the total loads by the total flow volume. The yields and flow-weighted concentrations serve as indicators of relative potencies of these sources of P. Phosphorus loading conditions for the three fractions are compared for the five monitored tributaries for the study interval in Figure 3-28. The PP_L levels for Cayuga Inlet Creek and Fall Creek were substantially greater than the other streams (9.3 and 8.0 MT, respectively; Figure 3-28a). However, the greater PP f_{BAP} for Salmon Creek (19.2%; Table 3-13) made its contribution nearly as large on a bioavailability basis ($PP_{L/B}$; Figure 3-28b), and the largest source on a bioavailability-yield basis (Figure 3-28c). The flow-weighted concentration of bioavailable PP was the highest for Salmon Creek (~ 16 µg/L); the next highest was for Cayuga Inlet (~ 14.6

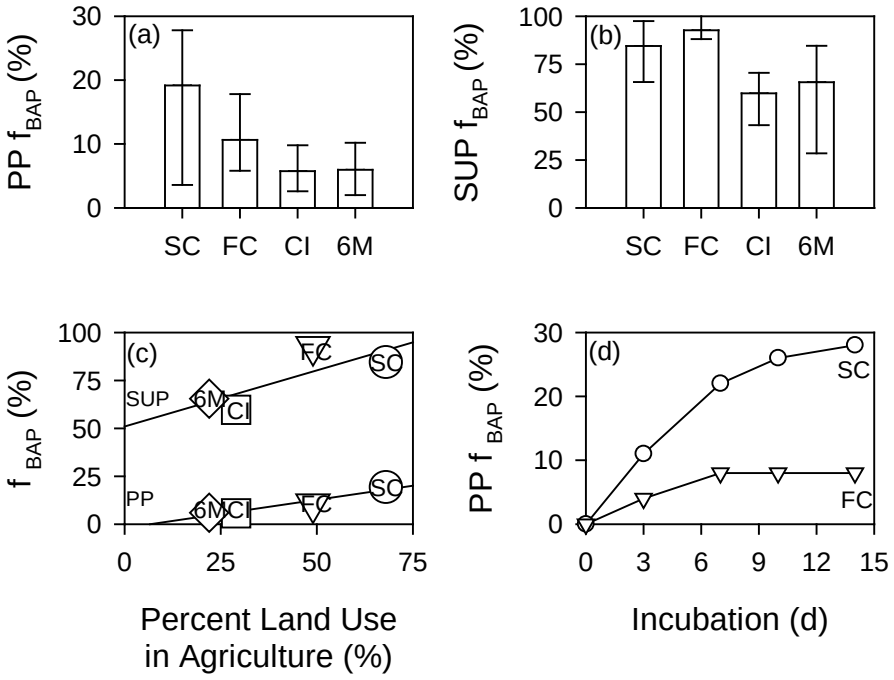

Figure 3-27. The fraction of forms of P that is bioavailable (f_{BAP}) for four gaged tributaries: (a) f_{BAP} for PP, averages with range bars, (b) f_{BAP} for SUP, averages with range bars, (c) evaluation of the dependencies of f_{BAP} for PP and SUP on percent agricultural land use in the watersheds, and (d) progression of bioavailability experiments for PP for two streams. SC-Salmon Creek, FC-Fall Creek, CI-Cayuga Inlet, and 6M-Sixmile Creek.

µg/L; Figure 3-28d) due to its high PP_L. The SUP_L's were the lowest of the three forms, including following adjustments for bioavailability (Figure 3-28e-h). Fall Creek had the greatest potency for this form of P (Figure 3-28g and h), with a flow-weighted concentration of ~ 7.5 µg/L. The largest SRP_L (≈ $SRP_{L/B}$) values were for Salmon Creek and Fall Creek (Figure 3-28i and j), that approached or exceeded the $PP_{L/B}$ levels for these streams. However, Salmon Creek stands out as the most potent SRP_L input, with the highest yield (~ 5 kg/km^2; Figure 3-28k) and flow-weighted concentration (~ 26.4 µg/L; Figure 3-28l). 90%, 65%, and 72% of $PP_{L/B}$ (Figure 3-28b), $SUP_{L/B}$ (Figure 3-28f), and $SRP_{L/B}$ (Figure 3-28i), respectively, were delivered during periods of high flow. The highest overall BAP_L estimates were from Fall (2.4 MT) and Salmon Creeks (2.1 MT; Figure 3-28n), but Salmon Creek was the most potent with respect to yield (9.2 kg/km^2; Figure 3-28o) and Q-weighted concentrations (49 µg/L; Figure 3-28p).

The paradigm based on earlier analyses, that SRP, SUP, and PP are completely, mostly, and less bioavailable, respectively (Auer et al. 1998, Reynolds 2006, Young et al. 1982), has

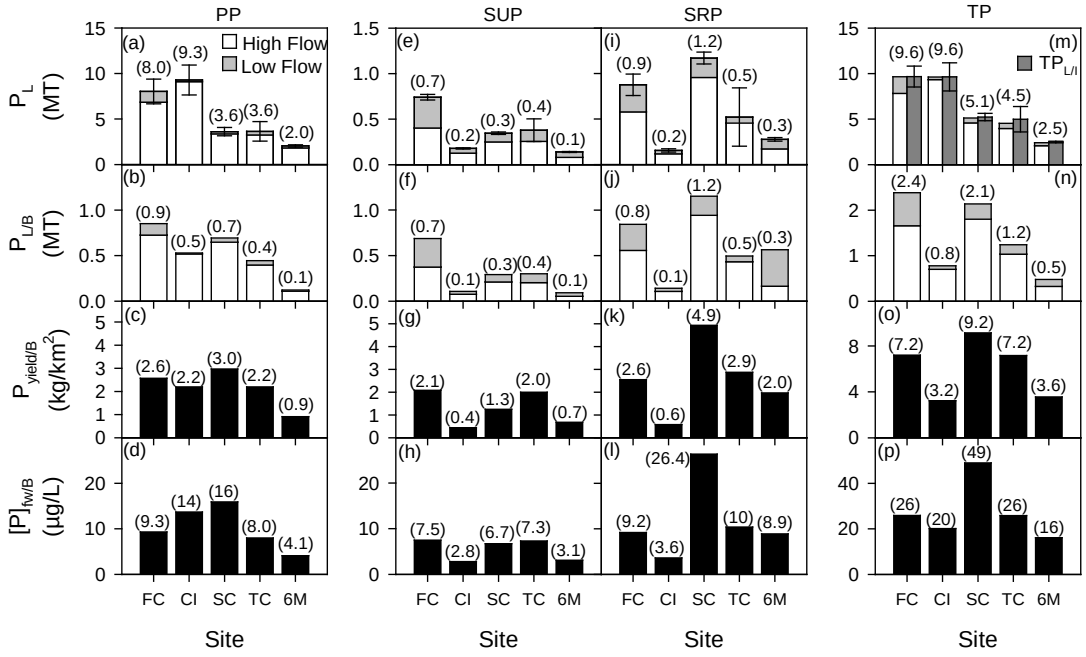

Figure 3-28. Estimated loads for forms of P for the A-O interval of 2013 for five monitored tributaries: (a) PP_L, (b) $PP_{L/B}$, (c) watershed yield of bioavailable PP, (d) flow-weighted concentration of bioavailable PP, (e) SUP_L, (f) $SUP_{L/B}$, (g) watershed yield of bioavailable SUP, (h) flow-weighted concentration of bioavailable SUP, (i) SRP_L, (j) $SRP_{L/B}$, (k) watershed yield of bioavailable SRP, and (l) flow-weighted concentration of bioavailable SRP, (m) TP_L and $TP_{L/I}$, (n) BAP_L, (o) watershed yield of BAP_L, and (p) flow-weighted concentration of BAP_L. Runoff event contributions indicated for (a) PP_L, (b) $PP_{L/B}$, (e) SUP_L, (f) $SUP_{L/B}$, (i) SRP_L, and (j) $SRP_{L/B}$, .(m) TP_L, and BAP_L. Vertical bars in these panels correspond to ± 95% confidence interval for the estimates. Values parenthetically.

generally been supported here for tributaries (Figure 3-27), though noteworthy structure with respect to sources and temporal variations were manifested. The precision observed for triplicate sample bioassays with the protocols adopted here for the three fractions (CV's for f_{BAP} of 6%, 4%, and 0% for PP, SUP, and SRP, respectively), conducted on the Maumee River (Ohio; Lambert et al. 2014), supports the spatial and temporal variability observed in this analysis. The substantial variations in the f_{BAP} for both PP (Figure 3-26a) and SUP (Figure 3-26b) apparently reflect dynamics in regulating features of composition in these streams in response to changes in drivers. Auer et al. (1998) reported wide differences in f_{BAP} for PP from two samplings of the West Branch of the Delaware River, New York. Our application of the f_{BAP} results, using the average of three observations uniformly to estimate $PP_{L/B}$ and $SUP_{L/B}$ for each of the characterized sources, is a reasonable approach that is consistent with the available information.

More temporally detailed assessments of f_{BAP} than conducted to date would be necessary to support the potential development of functionalities in which f_{BAP} values for individual sources would vary in response to a driver(s), which has yet to be identified. The f_{BAP} dependence on % agricultural landuse reported here (Figure 3-27c) is perhaps consistent with expectations, but has not been clearly resolved elsewhere (Ekholm and Krogerus 2003, Ellison and Brett 2006, Lyon et al. 2006). The wide differences in f_{BAP} for PP and SUP reported for tributaries of different systems (Auer et al. 1998, Effler et al. 2002; Ekholm and Krogerus 2003, Ellison and Brett 2006, Young et al. 1985) indicate system-specific bioassay experiments are necessary where the bioavailability concept is to be quantitatively implemented. These should at least address the PP and SUP factions.

The dominance of the contribution of PP_L to TP_L (84%; Figure 3-29a), combined with the generally low f_{BAP} of that fraction (Figure 3-26a), were primarily responsible for the large difference in TP_L and BAP_L; BAP_L was 77% (> 4-fold) smaller than TP_L (Figure 3-29b). Despite its low bioavailability, $PP_{L/B}$ was still the dominate form of BAP_L (44%; Figure 3-29b). The incomplete bioavailability of SUP was a much smaller effect, because of its lower contribution to TP_L and its greater availability. $SUP_{L/B}$ was 20% and $SRP_{L/B}$ was 37% of BAP_L, respectively. Moreover, implementation of the bioavailability concept has resulted in shifts in the relative contributions of various sources, with Salmon Creek being the most noteworthy case (Table 3-14). For example, Salmon Creek's hydrologic input was ~ 10% of the total for the study period, but its BAP_L contribution was > 15% making Salmon Creek the only case where percent contribution of BAP_L was greater than its flow contribution.

3.6.1.3. Credibility of TP_L Estimates

The load estimates for the three forms of P were used to estimate TP_L as described previously. In addition, TP loads for the study period for each stream were calculated independently using measured TP concentration data ($TP_{L/I}$) from the study period. Comparisons of TP_L and $TP_{L/I}$ (Table 3-15) were used to test the credibility of the component estimates (e.g., extent of closure). As a further test of TP_L credibility, a third set of TP loads was calculated for each stream using all available TP data including data from other sources ($TP_{L/A}$; UFI 2003-2006 and CSI 2002-2013; Table 3-7). For each stream, the additional data were used to define new TP-Q relationships and $TP_{L/I}$ and $TP_{L/A}$ estimates were calculated using Protocol 6 and compared to the 2013 TP_L estimates (Table 3-15). The results show that the three TP load estimates for each stream were very similar. With the exception of Taughannock Creek, the $TP_{L/I}$ and $TP_{L/A}$ estimates were within 2% of the TP_L. These results support both the underlying concentration data and the method used in P load estimation. The largest discrepancy between TP_L, $TP_{L/I}$, and $TP_{L/A}$ was for Taughannock Creek, but it was still modest (8-8.7%) relative to the larger uncertainty usually associated with load estimation (see Prestigiacomo et al. 2015 for a full description of P_L uncertainty analysis). Moreover this uncertainty is likely attributable to the fact that no event samples were collected on Taughannock Creek during the study period.

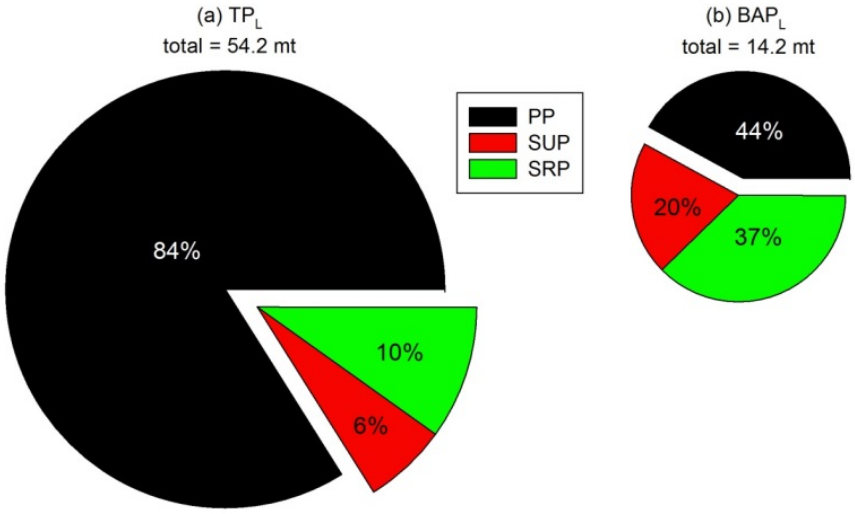

Figure 3-29. Pie-charts of contributions of sources of P to total loading for the A-O interval of 2013: (a) TP_L, and (b) BAP_L.

Table 3-14. Contributions of tributaries and point sources to phosphorus loads to Cayuga Lake according to forms and bioavailability.

	Percent Contribution (%)									
Source	**Q (%)**		**PP_L**	**SUP_L**	**SRP_L**	**TP_L**		**$PP_{L/B}$**	**$SUP_{L/B}$**	**$SRP_{L/B}$**	**BAP_L**
Fall Cr.	20.0		17.7	22.0	16.4	17.8		13.8	24.7	16.2	16.8
Cayuga In.	8.5		20.4	5.3	2.9	17.8		8.6	3.8	2.7	5.5
Salmon Cr.	10.0		7.9	10.3	21.9	9.5		11.2	10.5	22.1	15.1
Taugh. Cr.	10.6		8.0	11.3	9.8	8.4		6.2	12.6	9.6	8.7
Sixmile Cr.	6.5		4.5	4.2	5.2	4.5		2.0	3.3	5.1	3.4
Unmon. Tribs.	38.0		39.8	36.1	38.2	39.4		56.3	36.9	38.6	46.0
summed (%)	*93.6*		*98.4*	*89.1*	*9.4*	*97.4*		*98.0*	*91.9*	*94.3*	*95.4*
IAWWTP	1.1		1.1	6.9	0.7	1.3		0.1	6.1	0.7	1.5
CHWWTP	0.3		0.3	0.8	0.4	0.4		0.7	0.6	0.4	0.5
minor WWTP	0.1		0.2	1.4	0.9	0.3		0.9	1.2	0.9	1.0
LSC*	4.9		0.1	0.8	3.7	0.6		0.3	0.2	3.8	1.6
summed (%)	*6.4*		*1.6*	*10.9*	*5.6*	*2.6*		*2.0*	*8.1*	*5.7*	*4.6*
summed (%)	*100*		*100*	*100*	*100*	*100*		*100*	*100*	*100*	*100*

*input from hypolimnion.

Table 3-15. Comparison of TP_L, $TP_{L/I}$, and $TP_{L/A}$ estimates for all monitored streams (kg).

Tributary	n[1]	TP_L	n	$TP_{L/I}$	% Difference to TP_L	n	$TP_{L/A}$	% Difference to TP_L
Fall Creek	48	9,649	48	9,674	+0.3	179	9,669	+0.2
Cayuga Inlet Creek	36	9,619	36	9,636	+0.2	130	9,449	-1.8
Salmon Creek	51	5,129	51	5,232	+2.0	82	5,127	-0.0
Taughannock Creek	18	4,540	18	4,894	+8	46	4,936	+8.7
Sixmile Creek	40	2,459	40	2,478	+0.8	104	2,435	-1.0

[1] number of concentration measurements used to develop TP-Q relationships

3.6.1.4. Point Sources to Fall Creek

Fall Creek is an interesting case because two point sources, the Freeville WWTP and Dryden STP, discharge to Fall Creek (Dryden STP discharges to Fall Creek via Virgil Creek). These two point sources are relatively small with mean discharges of 0.52 and 0.25 MGD for Dryden STP and Freeville WWTP, respectively. The 2013 mean effluent TP concentrations for these point sources were 500 (Dryden) and 3,000 (Freeville) µg/L. The combined 2013 A-O load for these two point sources was estimated to be 567 kg. The best estimate of Fall Creek's total TP_L delivered during this interval was 9,649 kg. Therefore, despite their high effluent concentrations, the point sources contributed only approximately 6% of Fall Creek's TP_L. If the assumed point source TP_L has characteristics similar to CHWWTP, then approximately 136 kg is in the form of TDP. This TDP contribution would represent 8% of Fall Creek's TDP load (1,755 kg). This finding is noteworthy because it speaks to challenges in targeting sources for potential management to achieve P loading reductions for this stream.

3.6.1.5. Suspended Solids and Turbidity

FSS was the dominant form of TSS for the monitored streams over the A-O interval of 2013 (black bar segment; Figure 3-30a-c). FSS_L:TSS_L ratios ranged from 87-93%. Fall Creek and Cayuga Inlet Creek were the two largest sources of TSS for the study period, delivering 11.4 $\cdot 10^3$and 10.4$\cdot 10^3$MT, respectively (Figure 3-30a). Fall Creek and Cayuga Inlet Creek each accounted for ~ 21% of the total TSS load to Cayuga Lake (50.7$\cdot 10^3$ MT). The other three streams combined delivered ~ 8.3$\cdot 10^3$ MT. The unmonitored watershed estimate of TSS load was 20.5$\cdot 10^3$ MT. Cayuga Inlet Creek had the highest yield of TSS (43.4 MT/km^2; Figure 3-30b) and by far the largest flow-weighted concentration (271 mg/L; Figure 3-30c). Fall Creek ranked second in terms of yield and flow-weighted concentration (34.4 MT/km^2 and 124 mg/L, respectively). Sixmile Creek had the third largest yield and flow-weighted concentration (20.5 MT/km^2 and 93 mg/L), making this stream a relatively potent source of suspended solids relative to its watershed size (yield) and flow volume (flow-weighted concentration).

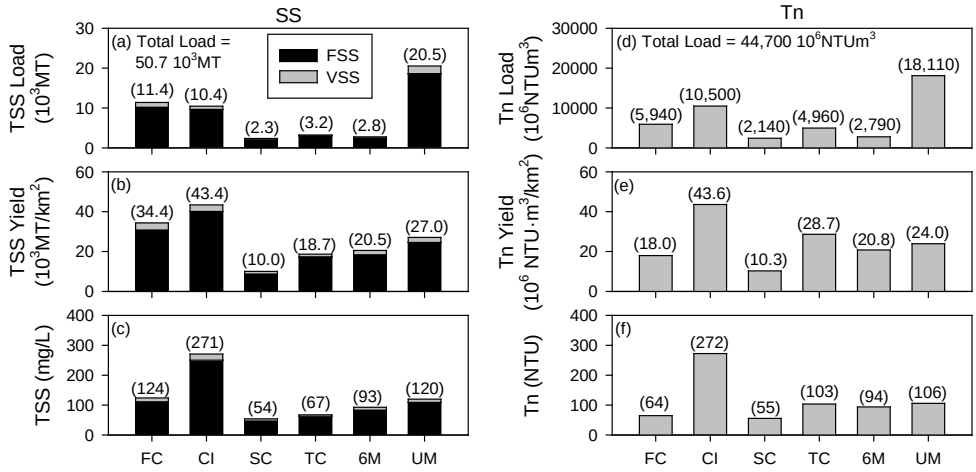

Figure 3-30. Features of A-O load estimates for monitored tributaries and unmonitored watershed for TSS and Tn: (a) TSS load, (b) TSS yield, (c) TSS flow-weighted concentration, (d) Tn load, (e) Tn yield, and (f) Tn flow-weighted concentration. Values parenthetically.

Tn loads (Figure 3-30d-f) followed patterns similar to TSS with the exception that Taughannock Creek ranked ahead of (third) Sixmile Creek in terms of load ($4{,}960 \cdot 10^6$ NTU·m^3; Figure 3-30d), yield ($28.7 \cdot 10^6$ NTU·m^3/km^2; Figure 3-30e) and flow-weighted concentration (103 NTU; Figure 3-30e). The unmonitored watershed estimate of Tn load was $18{,}110 \cdot 10^6$NTU·m^3.

3.6.1.6. Projected Area per Unit Volume Minerogenic Particles, PAV_m

PAV_m is a valuable metric for assessing the optical impacts associated with inorganic (minerogenic) particles in freshwater systems (for a full description see Section 5). PAV_m was determined for the same samples collected during the course of the biweekly and event monitoring for Fall, Cayuga Inlet, Salmon and Sixmile Creeks (Section 3.2). The measured PAV_m was partitioned according to the contributions of four size classes which will be used in the forthcoming water quality model (Figure 3-31). The size classes were: (1) < 2 µm, (2) 2 to 5.6 µm, (3) 5.6 to 11 µm, and (4) > 11 µm. The associated PAV_m contributions were identified as $PAV_{m/1}$, $PAV_{m/2}$, $PAV_{m/3}$, and $PAV_{m/4}$, respectively. Overall PAV_m demonstrates similar patterns to Tn and TSS. Thus, the relationships between PAV_m and Tn and TSS are very strong (r^2>0.9) and statistically significant (Figure 3-31a and b, respectively). PAV_m loads (units of m^2; $PAV_{m/L}$) were calculated in a manner similar to the other constituents (Section 3.5) and the patterns of the $PAV_{m/L}$ were similar to Tn_L and TSS_L.

Cayuga Inlet Creek was the largest single source of $PAV_{m/L}$ followed by Fall Creek and Sixmile Creek (Figure 3-31c). The contributions of the size classes to the overall $PAV_{m/L}$ were

34% for $PAV_{m/2}$, 29% for $PAV_{m/3}$, 27% for $PAV_{m/4}$, and 10% for $PAV_{m/1}$ (Figure 3-31e). The relative contributions of the four size classes differed somewhat between tributaries. For example, for Fall Creek $PAV_{m/3}$ was the largest contributor to Fall Creek's total PAV_m (Figure 3-31c and d). Whereas for Cayuga Inlet Creek and Sixmile Creek, $PAV_{m/2}$ was the largest fraction of total PAV_m (Figure 3-31c and d). Sixmile Creek was the only stream where $PAV_{m/1}$ was greater than $PAV_{m/4}$.

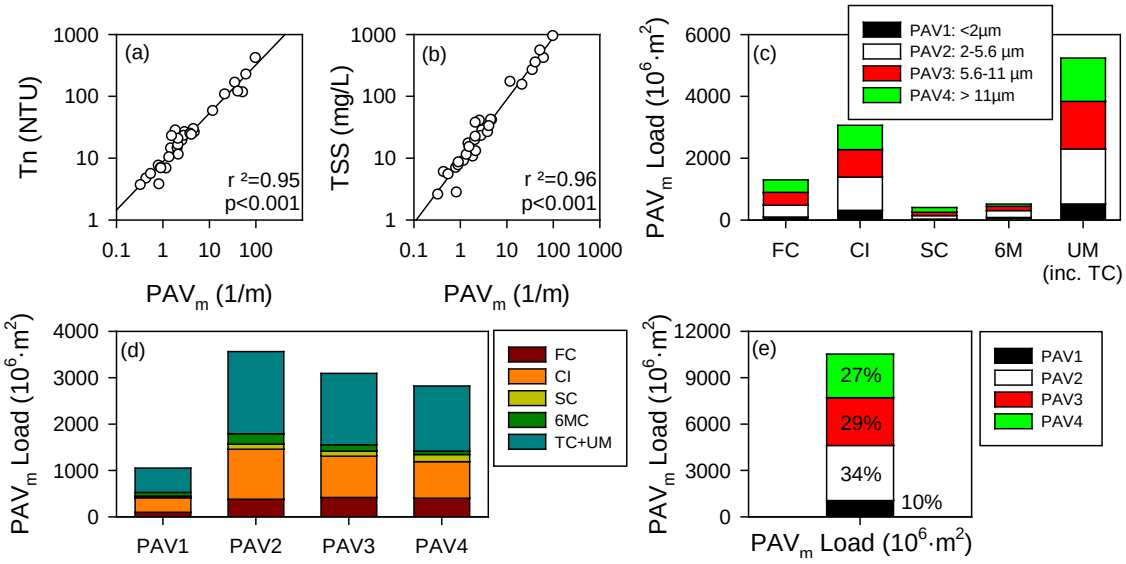

Figure 3-31. PAV_m relationships and loading estimates: (a) evaluation of the dependence of Tn on PAV_m in Fall Creek, (b) evaluation of the dependence of TSS on PAV_m in Fall Creek, (c) total watershed PAV_m loads for the A-O interval of 2013 according to tributary and the contribution of four size classes, (d) total watershed PAV_m loads for the A-O interval for four size classes, partitioned according to the contributions of various tributaries, and (e) the total watershed PAV_m load from all tributaries, according to the contribution of four size classes.

3.6.1.7. Dissolved Nitrogen

Fall Creek delivered 2.6 MT of t-NH_3 to Cayuga Lake over the study interval which was the dominant source on a percentage (25%; Figure 3-32a), yield (0.008 MT/km^2; Figure 3-32b), and flow-weighted concentration basis (29 µg/L; Figure 3-32c). Salmon and Taughannock Creeks' contribution to the total t-NH_3 load (10.4 MT) ranked second and third (1.1 and 1.0 MT, respectively). Sixmile Creek delivered considerably less t-NH_3 (0.56 MT). The unmonitored watershed estimate of t-NH_3 load was 4.2 MT. t-NH_3 yields (except Fall Creek) ranged from 0.003 (Cayuga Inlet Creek) to 0.006 (Taughannock Creek) MT/km^2. Salmon Creek had the second highest flow-weighted concentration (26 µg/L; Figure 3-32c) and the other monitored streams had similar flow-weighted concentrations, ranging between 19 and 21 µg/L. NO_X was the dominant form of dissolved N in the tributaries (Figure 3-32d) as the total watershed NO_X (744 MT) load was 70-times greater than the t-NH_3 load (10.4 MT) although the magnitudes of

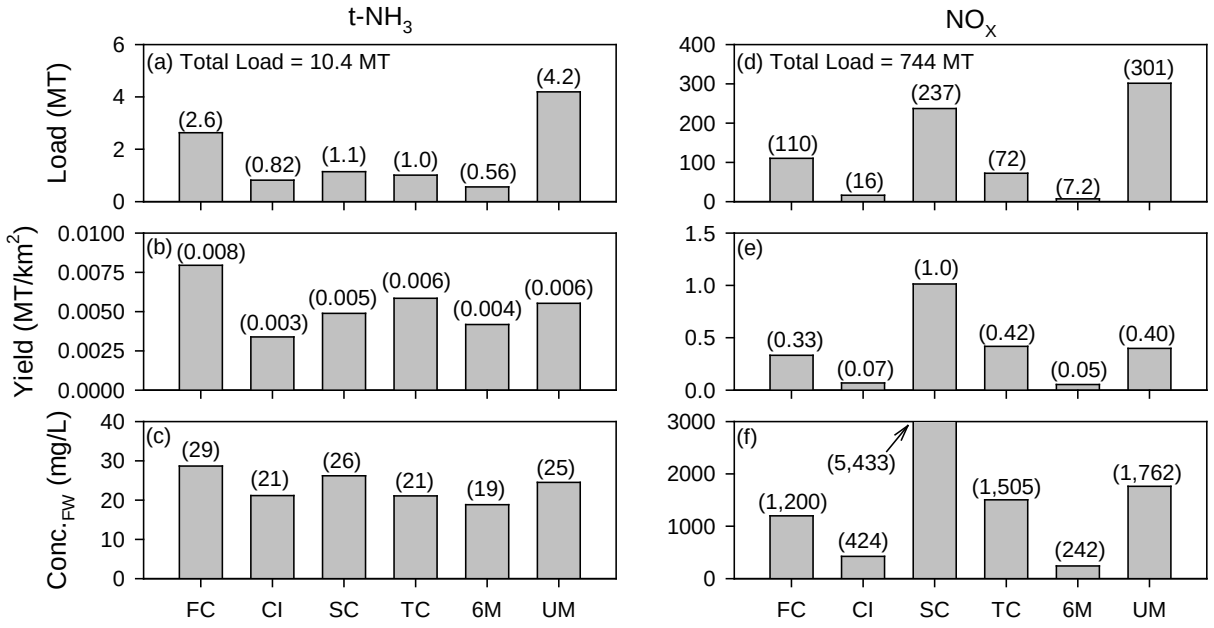

Figure 3-32. Features of A-O load estimates for monitored tributaries and unmonitored watershed for dissolved nitrogen, t-NH_3 and NO_X: (a) t-NH_3 load, (b) t-NH_3 yield, (c) t-NH_3 flow-weighted concentration, (d) NO_X load, (e) NO_X yield, and (f) NO_X flow-weighted concentration. Values parenthetically.

the NO_X load: t-NH_3 load ratio varied substantially by source. For example, the highest NO_X load: t-NH_3 load was for Salmon Creek (208) and the lowest was for Cayuga Inlet Creek (20).

Salmon Creek was the largest source of NO_X (237 MT; Figure 3-32d) and was more than double the next highest source, Fall Creek (110 MT). Taughannock Creek NO_X load was 72 MT and the contributions of Cayuga Inlet Creek and Sixmile Creek were much less than the other three streams (16 and 7.2 MT, respectively). The unmonitored watershed estimate of NO_X load was 301 MT. Because of its high NO_X load, Salmon Creek's yield (1.0 MT/km^2; Figure 3-32e) and flow-weighted concentration (5,433 µg/L; Figure 3-32f) were by far the largest of the monitored streams making it a very potent source of dissolved N. Taughannock Creek and Fall Creek ranked second and third with respect to NO_X yield and flow-weighted concentration (Figure 3-32e and Figure 3-32f) and were much higher than both Cayuga Inlet and Sixmile Creeks.

3.6.1.8. Dissolved Organic Carbon and Silica

Fall Creek was the dominant source of DOC to Cayuga Lake over the 2013 A-O interval (Figure 3-33a) followed by Salmon (227 MT) and Taughannock Creek (220 MT). The estimated load delivered by Fall Creek was 496 MT which was 2-5 times higher than the other monitored tributaries and represented ~ 25% of the total watershed estimate (1,989 MT). By comparison,

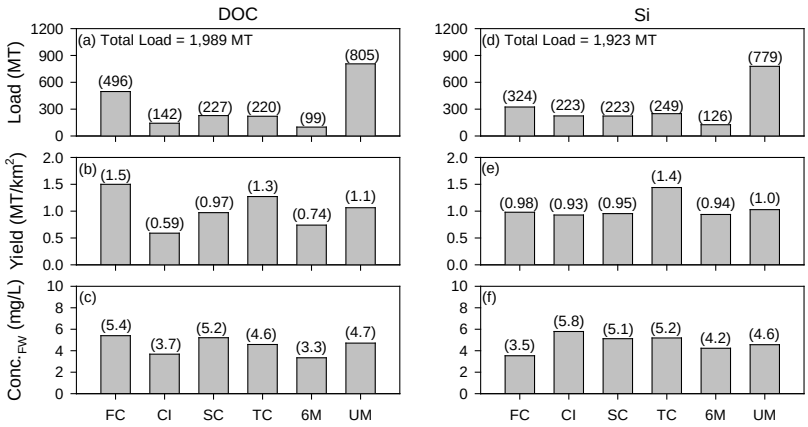

Figure 3-33. Features of A-O load estimates for monitored tributaries and unmonitored watershed for dissolved organic carbon and silica: (a) DOC load, (b) DOC yield, (c) DOC flow-weighted concentration, (d) Si load, (e) Si yield, and (f) Si flow-weighted concentration. Values parenthetically.

Cayuga Inlet Creek and Sixmile Creek had low DOC load estimates (142 and 99 MT, respectively). The unmonitored watershed estimate of DOC load was 805 MT. Fall Creek was also the largest yield (1.5 MT/km^2; Figure 3-33b) and had the highest flow-weighted concentration (5.4 mg/L; Figure 3-33c). Taughannock Creek had the second highest yield (1.3 MT/km^2) and third highest flow-weighted concentration (4.6 mg/L) behind Salmon Creek (5.2 mg/L).

Fall Creek was the largest source of Si (324 MT; Figure 3.31) and was the largest source on a percent basis (17% of total load; 1,923 MT). Taughannock Creek, Salmon Creek, and Cayuga Inlet Creek all had similar Si loads (223-249 MT; Figure 3-33d). Sixmile Creek delivered 126 MT of Si in 2013. The unmonitored watershed estimate of Si load was 779 MT. Taughannock Creek had the highest yield (1.4 MT/km^2; Figure 3-33e). Yields from the other monitored tributaries were similar, ranging from 0.93 to 0.98 MT/km^2 (Figure 3-33e). Ranking from highest to lowest of flow-weighted concentrations (Figure 3-33f) was: Cayuga Inlet Creek (5.8 mg/L), Taughannock Creek (5.2 mg/L), Salmon Creek (5.1 mg/L), Sixmile Creek (4.2 mg/L), and Fall Creek (3.5 mg/L).

3.6.1.9. Load Delivery at Low versus High Flow

As in many other systems, the tributaries to Cayuga Lake delivered the majority of their loads during brief intervals of high flow. This is due to: (1) most constituents demonstrated a positive dependence on flow and therefore had high concentrations at high flow (especially the particulates), and (2) loads are the product of concentration and flow, so that when flow is high loads will be high. Table 3-16 summarizes the high flow conditions for the five monitored streams in 2013. The number of high flow days varied slightly between streams, ranging from

Table 3-16. High flow conditions and load delivery during high flow over the A-O interval in 2013.

				Percent Delivered During High Flow (%)					
Tributary	**No. Days > Mean Q (d)**	**Percent High Flow Days (%)**	**Percent Flow Delivered (%)**	**PP_L**	**TSS_L**	**Tn_L**	**TDP_L**	**DOC_L**	**t-$NH_{3/L}$**
Fall Creek	39	18%	49%	85%	94%	91%	61%	55%	47%
Cayuga Inlet Creek	40	19%	57%	98%	99%	98%	73%	69%	49%
Salmon Creek	54	25%	60%	93%	97%	95%	80%	68%	58%
Taughannock Creek	42	20%	51%	89%	93%	95%	79%	52%	28%
Sixmile Creek	38	18%	52%	89%	96%	94%	61%	58%	47%

38-54 days during the 214 day study interval (18-25%). For all streams, a minimum of 49% of the flow volume over the study interval was delivered during these brief high flow intervals (range 49-60%).

In the case of Fall Creek, 85% of the A-O PP_L load was delivered during high flow. The percent of PP_L delivery was somewhat higher for the other streams (>89%; Table 3-16). Similarly, nearly all of TSS and Tn loads were delivered during high flow (> 91%; Table 3-16). Results for the dissolved parameters varied, however in almost all cases (with exception of t-$NH_{3/L}$), a majority of loads were delivered during high flow (Table 3-16), although the fractions delivered were substantially less than for the particulate constituents.

A closer look into the loading estimates shows that the majority of PP_L and BAP_L (as examples) were, in fact, delivered during 14 days during the three largest events in 2013; June 30-July 3, July 21-25, and August 8-12 (Table 3-17). The percent delivery varied between streams, but in the case of PP_L, a minimum of 44 % (Salmon Creek) and maximum of 94 % (Cayuga Inlet Creek) for the A-O total PP_L was delivered during those three events. The portion of BAP_L delivered was less than PP_L, due to the lower dependency of dissolved P on stream flow, however, in all cases with the exception of Salmon Creek (24%; Table 3-17), more than 50% of the total A-O 2013 BAP_L was delivered during the three largest events. The other particulate constituents showed results similar to PP_L and other dissolved constituents showed results similar to dissolved P_L. Because the brief intervals of high flow are so critical to overall load estimates, it is necessary have adequate sampling coverage at high flow to: (1) quantify high flow load conditions and (2) accurately quantify concentration-Q relationships in order to properly estimate high flow loads when observations are not available.

Table 3-17. High flow conditions and load delivery from the five monitored tributaries during the three largest events in 2013.

Tributary	PP_L			BAP_L		
	A–O Estimate (MT)	Event Total Load (MT)	Percent of Total A-O Load	A–O Estimate (MT)	Event Total Load (MT)	Percent of Total A-O Load
Fall Creek	8.0	5.8	73%	2.38	1.36	57%
Cayuga Inlet Creek	9.3	8.7	94%	0.78	0.63	81%
Salmon Creek	3.6	1.6	44%	2.4	0.57	24%
Taughannock Creek	3.6	2.8	78%	1.2	0.83	70%
Sixmile Creek	2.0	1.5	75%	0.48	0.25	52%

3.6.2. Interannual Variability in Loading Estimates

3.6.2.1. 2000-2012 April – October Best Estimates

The 2013 best estimate loads presented here are representative estimates given: (1) the closure of P estimates from the 13 protocols attempted for Fall Creek (Figure 3-24a-c, and Appendix B5), (2) the credibility of the TP_L estimates from the sum of P forms, $TP_{L/I}$, and $TP_{L/a}$ (Table 3-15), and (3) relatively low uncertainty associated with the P loads (Prestigiacomo et al. 2015). However, the 2013 loads are only representative for 2013 conditions (e.g., concentrations and flow). It is expected that the loads presented here vary substantially year-to-year (interannual) due to large interannual variations in stream flow. To estimate interannual variability in loading, the seasonal concentration-Q relationships developed for 2013 (for all constituents) were applied to the 13 A-O interval for the 2000-2012 period. The loading results for the 13 A-O intervals over the 2000-2012 period for all constituents can be found in Appendix B6. The discussion presented here is for BAP_L only.

BAP_L estimates from each stream, estimates for the unmonitored watershed, and total watershed estimates for the thirteen year period, with range bars (minimums and maximums) as the metric of variability in presented in Figure 3-34a. A wide range of runoff was represented in this analysis as the annual rankings of Fall Creek flows for the thirteen year period ranged from eighty-fifth to second (89 year record). The range in BAP_L over the 2000-2012 interval was, therefore, found to be quite large in some cases. For example, the 13y average BAP_L for Cayuga Inlet Creek was 2.3 MT with a range of 20.6 MT (Figure 3-34a). On a whole watershed basis, the range of BAP_L estimates was 83 MT (2.3 to 85.4 MT). This range in BAP_L estimates was 6, 39, and 128-times larger than the summed tributary load for 2013 (13.6 MT), the Salmon Creek load (2.14 MT) and the summed point source load for that year (0.65 MT; Figure 3-34b),

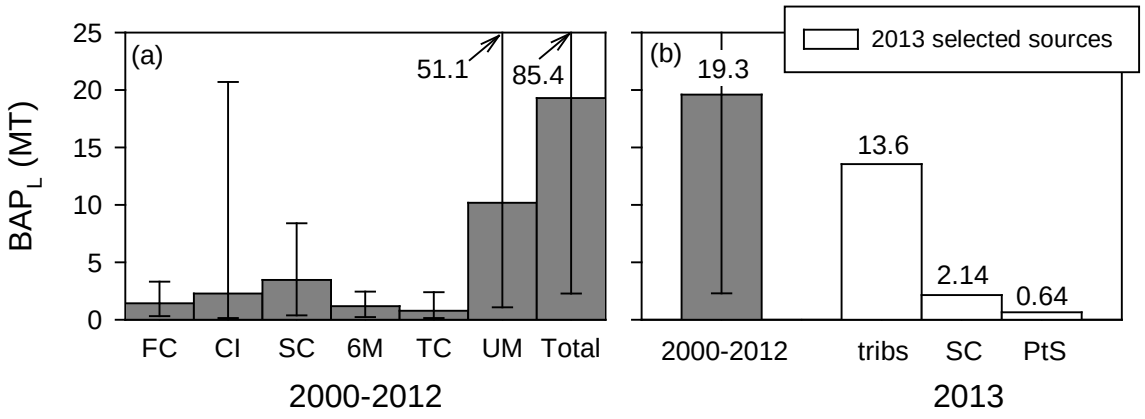

Figure 3-34. Average A-O BAP_L estimates for the 2000-2012 (13 y) period for: (a) monitored streams, unmonitored estimates (UM) , and total watershed estimates (Total), and (b) 2000-2012 average watershed BAP_L in relation to 2013 tributary BAP_L, 2013 Salmon Creek (SC) BAP_L, and 2013 point source (PtS) BAP_L. Bars represent minimum and maximum values over the 2000-2012 period.

respectively. The magnitudes of BAP_L from the individual sources presently are small relative to reasonable estimates of interannual variations in summed tributary BAP_L (Figure 3-34b). This interannual variability, driven by year-to-year differences in stream flow, will act to mask the effects of reductions from any individual input.

3.7. Summary

The summer of 2013 was a relatively high flow period compared to previous years. The 2013 A-O period flow ranked 32nd in the gage's 89 year history in terms of mean daily flow and the June-September interval was the 6th wettest on record. There were several large, well-defined runoff events with conditions that provided a good opportunity to investigate and analyze concentrations and loads from the tributaries to Cayuga Lake. The five largest tributaries were monitored for ten water quality constituents and three additional constituents were calculated from the original measurements. The monitoring program began in mid-March and concluded in early November and consisted of a biweekly and event monitoring program. The total number of samples collected satisfied all QAPP requirements. The temporal coverage for both the primary (forms of P and Tn) and secondary constituents was robust; approximately 42% and 35% of the inflow volume of the gaged streams was monitored for primary and secondary constituents, respectively. Data quality, defined by the precision of field triplicates, was very good supporting the use of stream concentration and loading estimates. Also, the 2013 data compared well with other contemporary data sources, further supporting the 2013 data set.

Concentrations of particulate constituents increased dramatically during periods of high flow which was most conspicuous for the three largest events (peak flows) monitored in 2013: June 30, July 21, and August 8-9. For example, Fall Creek mean TP increased 3.4-fold (on average from low flow to high flow. Similarly in the other streams, mean TP increased 3 to 5-fold from low to high flow with the largest difference between the flow regimes observed in Cayuga Inlet Creek (16.5-fold). Concentrations of dissolved constituents were also generally lowest during periods of low flow and increased during runoff events, although the increases observed were less substantial than for particulate constituents. For example, mean SRP and SUP increased 53 and 19% from low to high flow in Fall Creek.

Under low flow conditions, Fall Creek had the highest average TP and PP concentrations, 37.3 and 25.9 µg/L, respectively. For all streams, except Salmon Creek, low-flow TP was dominated by PP (50-68% of TP). Salmon Creek's mean low-flow TDP and SRP concentration were the highest of all five monitored streams, TDP and SRP concentrations were 18.3 µg/L and 12.7 µg/L, respectively. Approximately 59% of Salmon Creek's TDP was as SRP. NO_X concentration was much higher than t-NH_3 concentration in all streams, especially for Salmon and Fall Creeks where NO_X concentrations were 55-200 times higher than t-NH_3 concentrations. Salmon Creek low-flow NO_X concentration was 4,593 µg/L (or 4.6 mg/L), and was 3.5 times higher than for the next highest stream, Fall Creek (1,237 µg/L).

At high flow, the particulate constituents were generally much higher than at low flow. Cayuga Inlet Creek had the highest mean TP and mean PP at high flow (215.4 and 206.3 µg/L, respectively). With regards to high flow TDP concentrations, Salmon Creek was the highest of the five tributaries (32.4 µg/L), which was nearly 2 times higher than Fall Creek (17.2 µg/L). Similar to low flow, Salmon Creek had the highest high-flow SRP concentration. At high flow, average FSS was more than 89% of TSS for all streams, which was an increase in the fraction when compared to low flow (67-81%). Mean Tn and TSS were highest in Cayuga Inlet Creek at high flow. Cayuga Inlet, mean Tn was 194.2 NTU and mean TSS was 219.3 mg/L, 92% of which was FSS (201.9 mg/L). At high flow, mean NO_X was the highest in Salmon Creek (5,059 µg/L) which was more than twice that of Fall Creek (2,205 µg/L).

Particulate-Q relationships were generally stronger (i.e., higher r^2), statistically significant ($p < 0.05$), and had larger slopes (i.e., loading potential) than dissolved constituents although the significance and strengths of fit varied substantially between constituents and streams. Because flow was not a strong predictor for all constituents (especially the dissolved), the alternate driver, air temperature (T), was considered. Particulate constituents were generally not significantly or strongly related to air T. However, despite the weak correlations, PP, Tn and forms of SS for Fall Creek were significantly related to air T ($p < 0.02$). The relationships between air T and dissolved P were found to be positively correlated (e.g., concentration tended to be higher when warmer) and much stronger than the concentration-Q relationships. Based on the significant relationships between constituents and air T (especially the dissolved forms), the data from each stream was stratified into three seasons: (1) spring, March 1 – May 30, (2) summer, June 1 –

September 30 (coincident with New York State regulators' application of summer for water quality standards), and (3) fall, October 1 – November 30. After stratification, substantial seasonal differences were observed in all concentration-Q relationships for all constituents. In most cases (except dissolved N), seasonal stratification resulted in improved model performance (r^2, mse, significance) compared to the non-stratified concentration-Q relationships. Stratification resulted in large improvements in phosphorus-Q relationships versus the overall non-stratified relationships, especially during the summer (June-September) period.

Daily loads for each constituent were calculated for the five monitored tributaries, and estimated for the unmonitored portions of the watershed for the study interval. Phosphorus loads were also estimated for the largest point sources. Thirteen protocols were investigated as potential A-O load estimators for Fall Creek (for the three forms of P), to evaluate performance and represent the general level of uncertainty associated with the adoption of a particular approach. Relatively good closure was obtained for the entire array of loading estimate protocols (regression and non-regression); the coefficients of variation (CV) were less than 25% for all P forms. The good agreement between the methods investigated lends credence to the representativeness of the estimates from each stream and the 2013 A-O estimates as a whole. The regression methods were preferred because they: (1) utilize environmental driver information to explain variability in concentration, and (2) can be used to provide daily estimates which are needed for input to the future water quality model. The selected best method was a log (natural) concentration-Q regression stratified into three seasons. This method was selected over the other protocols because: (1) output provided daily loading estimates required for the water quality model, (2) use of measured concentrations, (3) improved fit (r^2) between stratified concentration-Q relationships compared to overall concentration-Q relationships, (4) lower model mean square error (mse), and (5) better model performance as determined by comparisons between observed and predicted concentrations (lower root mean square error (RMSEs) and median residuals).

PP was the dominant form of P for the monitored streams over the A-O interval of 2013. PP_L:TP_L ratios ranged from 70-97% with an average of 83%. The SRP_L:TP_L ratio for all streams was 11.3%. SUP_L was the least abundant form of P: the average SUP_L:TP_L ratio was only 6.1%. Cayuga Inlet Creek and Fall Creek were by far the two largest individual sources of TP_L for the study period (~9.6 MT). The tributaries (non-point sources) were the dominant sources of both TP_L and TDP_L (97.4% and 92%, respectively). The average f_{BAP} values and ranges for PP and SUP varied amongst the four assessed tributaries. In all 4 cases, only a modest fraction of PP was bioavailable. The ranking according to average f_{BAP} values for PP was Salmon Creek (19%) > Fall Creek (11%) > Sixmile Creek (6%) > Cayuga Inlet Creek (5.7%). Most of the SUP was available, and the same ranking amongst these tributaries prevailed with the exception that Fall Creek had the highest f_{BAP} for SUP (92.7%). The SRP fraction was essentially completely available in all cases. Wide temporal differences were observed for f_{BAP} for both PP and SUP in individual streams with f_{BAP} for PP being the most variable (average CV

> 60%) and f_{BAP} for SRP being least variable (maximum CV = 14%). An interesting finding in this study was that the average values of f_{BAP} for both PP and SUP were strongly, positively correlated to the fraction of agricultural land use in the watersheds of the individual streams. The paradigm based on earlier analyses, that SRP, SUP, and PP are completely, mostly, and less bioavailable, respectively has generally been supported here for tributaries, though noteworthy structure with respect to sources and temporal variations were manifested. The dominance of the contribution of PP_L to TP_L (84%), combined with the generally low f_{BAP} of that fraction, were primarily responsible for the large difference in TP_L and BAP_L; BAP_L was 77% (> 4-fold) smaller than TP_L. Moreover, implementation of the bioavailability concept has resulted in shifts in the relative contributions of various sources. For example, Salmon Creek's hydrologic input was ~ 10% of the total for the study period, but its BAP_L contribution was > 15% making Salmon Creek a potent source of BAP_L.

FSS was the dominant form of TSS for the monitored streams. FSS_L:TSS_L ratios ranged from 87-93%. Fall Creek and Cayuga Inlet Creek were the two largest sources of TSS for the study period, delivering $11.4 \cdot 10^3$ and $10.4 \cdot 10^3$MT, respectively. Cayuga Inlet Creek had the highest yield of TSS and by far the largest flow-weighted concentration. Sixmile Creek had the third largest yield and flow-weighted concentration, making this stream a relatively potent source of suspended solids relative to its watershed size (yield) and flow volume (flow-weighted concentration). NO_X was the dominant form of dissolved N in the tributaries as the total watershed NO_X load was 70-times greater than the t-NH_3 load. Fall Creek was the dominant source of DOC and Si to Cayuga Lake.

Similar to other lotic systems, the tributaries to Cayuga Lake delivered the majority of their loads during brief intervals of high flow because: (1) most constituents demonstrated a positive dependence on flow and therefore had high concentrations at high flow (especially the particulates), and (2) loads are the product of concentration and flow, so that when flow increases the loads will be higher. In addition, the interannual variability in loading was estimated to be quite large and dependent on annual flow conditions.

Section 4. Watershed Modeling

4.1. Model Selection

The selection of a model was the fundamental first step to this large scale modeling project. It is crucial that the model hydrology is representative of the region and that the model is responsive to the management scenarios of interest. In order to ensure that the optimal model was chosen for the Cayuga Lake Modeling Project an extensive evaluation of existing models was conducted and contextualized through input from the technical advisory committees and stakeholders.

It was determined that the Soil and Water Assessment Tool (SWAT) would be the tool best equipped to answer the questions posed. SWAT is a watershed-scale model frequently used in systems in which conservation and nutrient management are central to project goals. It uses process-based phosphorus cycling and is relatively flexible in the range of input data accepted (Veith et al. 2008, Nietsch et al. 2011). SWAT is also capable of evaluating both particulate and dissolved phosphorus as well as sediment movement within the landscape, conditions that are important to this project and will be discussed in further detail below. When choosing a model, it is also important to consider the relevant processes included in the model. Based on the complexity of phosphorus transport and the nature of the Cayuga Lake Watershed it was determined that in stream processes needed to be simulated. Unlike the General Watershed Loading Function (GWLF), SWAT considers many in-stream processes, such as biodegradation, deposition and accumulation.

It was also determined that the optimal application of SWAT in the Cayuga Lake Watershed is to apply the variable source area (SWAT-VSA) hydrology model developed by Easton et al. (2008). This method better represents the hydrology of areas with shallow soils and near surface restricting layers as can be found in central New York (Walter et al. 2000). SWAT-VSA is the most effective and accurate tool to model the Cayuga Lake Watershed and phosphorus and sediment transport within the watershed.

The primary compounds of interest in this study of the Cayuga Lake Watershed were identified by a number of important stakeholders; many of these compounds are outside the direct scope of the TMDL. Through conversations with experts in relevant fields and at public forums, it became clear that the focus of the project must be on phosphorus and sediment movement throughout the watershed. Phosphorus will be thoroughly evaluated in both its dissolved and particulate forms as particulate phosphorus makes up a large portion of phosphorus in the stream water and dissolved phosphorus is especially bioavailable (Bostrom et al. 1988). Dissolved phosphorus is also considered an important limiting nutrient in freshwater systems which in large quantities can lead to degraded water quality and eutrophication (Correll 1998). Similarly, sediments are to be included in the model because of their integral role in phosphorus transport and their impact on the perceived quality of the lake. Professor of

Geological Sciences, Daniel E. Karig has been consulted on the topic of sediment transport in the Cayuga Lake Watershed on numerous occasions. His expertise in this field is an invaluable resource to the modeling effort.

4.2. Input Data

As previously stated, SWAT is a quasi-physically-based, watershed-scale model that requires both spatial and tabular datasets to simulate chemical and sediment fluxes through surface and subsurface hydrology.

As mentioned, a number of spatial data are required by SWAT for proper model initialization. The first of these data obtained was a digital elevation model (DEM) from the US Geological Survey (USGS) National Elevation Data set (NED) (Gesch 2007, Gesch et al. 2002). These data have a resolution of 1 arc-second (approximately 30 meters) and are available throughout the watershed. Spatial and tabular representation of land cover was obtained from the National Land Cover Database published in 2006 (NLCD 2006) by the Multi-Resolution Land Characteristics Consortium (MRLC) (Fry et al. 2011). This data set is also at a resolution of approximately 30 meters and is uniformly available throughout the watershed. A spatial representation of soils throughout the watershed was obtained using TopoSWAT (Fuka et al. 2013). TopoSWAT is an automated ArcMap tool which combines the Digital Soil Map of the World developed by the Food and Agriculture Organization of the United Nations (FAO) in collaboration with The United Nations Educational, Scientific, and Cultural Organization (UNESCO; Fischer et al. 2008) with a soil wetness class to give a more accurate representation of soil type and its propensity to generate runoff.

Tabular data sets are also required by SWAT to best represent watershed conditions, these include meteorological and land management data. Accurate meteorological data are vital to optimal model performance; SWAT requires inputs for precipitation, minimum and maximum temperature, relative humidity, radiation, and wind speed. A number of meteorological data sources were selected to ensure the accuracy of input data. The Climate Forecast System Reanalysis (CFSR), a model generated dataset published by the National Center for Atmospheric Research (NCAR), is the primary source of meteorological data to be used in the Cayuga Lake Watershed Model because it is a continuous dataset available throughout the watershed (NCAR 2014). Where available, data were obtained from the Global Historical Climatology Network (GHCN), published by the National Oceanic and Atmospheric Administration (NOAA) through the National Climatic Data Center (NCDC) (Menne et al. 2012). These data are only available in the southern portion of the watershed and therefore are of limited utility to the modeling effort. Therefore, CFSR data are used for the majority of the model with GHCN data only being used to check accuracy of inputs.

The second data set crucial to the accuracy of the watershed model with respect to nutrient transport is data regarding land management in the area. Many types of agriculture are practiced

in the Cayuga Lake Watershed ranging from large scale Contained Animal Feeding Operations (CAFO's) to small scale dairy farms with pastured cows, to vegetable farms and vineyards. All of these farmers employ unique land management strategies and it is vital that the inputs to the model accurately reflect the diversity and spatial distribution of the various land management approaches. To ensure the accuracy of input data, a group of experts from a number of county Soil and Water Conservation Districts as well as various other organizations were consulted. These data will be discussed in further detail below.

4.3. Preliminary Hydrological Results

The watershed model has been tested, calibrated, and validated beginning with a number of larger subwatersheds in the southern end of Cayuga Lake, including Fall Creek, Six Mile Creek, and Salmon Creek. These watersheds were chosen for a number of reasons, the primary being the large amounts of historical data available in these subwatersheds, for model validation.

The USGS has a number of stream gages installed in the Cayuga Lake Watershed, primarily in the subwatersheds around the southern end of the lake. There is a gage near the outlet of Fall Creek (gage number 04234000); two are installed in Six Mile Creek; one near Brooktondale (gage number 04233286) and another near Bethel Grove (gage number 04233300). There is also a gage near the outlet of Salmon Creek (gage number 0423401815) and another near the mouth of the Inlet (gage number 04233500). These gages provide publicly available daily stream flow data over varying historical time frames (USGS, http://waterdata.usgs.gov/ny/nwis/rt).

Work is being done to model a number of subwatersheds in the southern portion of the lake and preliminary hydrological results for the Fall Creek Watershed will be presented here. Figure 4-1 displays the Fall Creek watershed with the location of the USGS stream gage denoted. Flow outputs from the model were compared to the flow measured at this gage (04234000) and the Nash-Sutcliffe model efficiency coefficient (NSE) was used to quantitatively evaluate the performance of the model (Nash and Sutcliffe 1970).

Preliminary model runs are conducted from 1990 to 2010, and evaluated over 15 years, 1995 to 2010, using a 5 year warm up period, 1990 to 1995. The results of this model initialization for the Fall Creek Watershed are presented in Figure 4-2. A visual evaluation of the two data sets indicates that the model is accurately capturing the timing of the peaks and valleys of the hydrograph. The output displayed in Figure 4-2 has an NSE of approximately 0.47, an acceptable value for preliminary model initialization.

4.4. Land Management Investigations

The Cayuga Lake Watershed is a watershed dominated by agriculture with approximately 50% of the land used for pasture or cultivated crops. Agricultural land use is frequently a significant contributor of nutrients, like phosphorus, to receiving water bodies (Correll 1998).

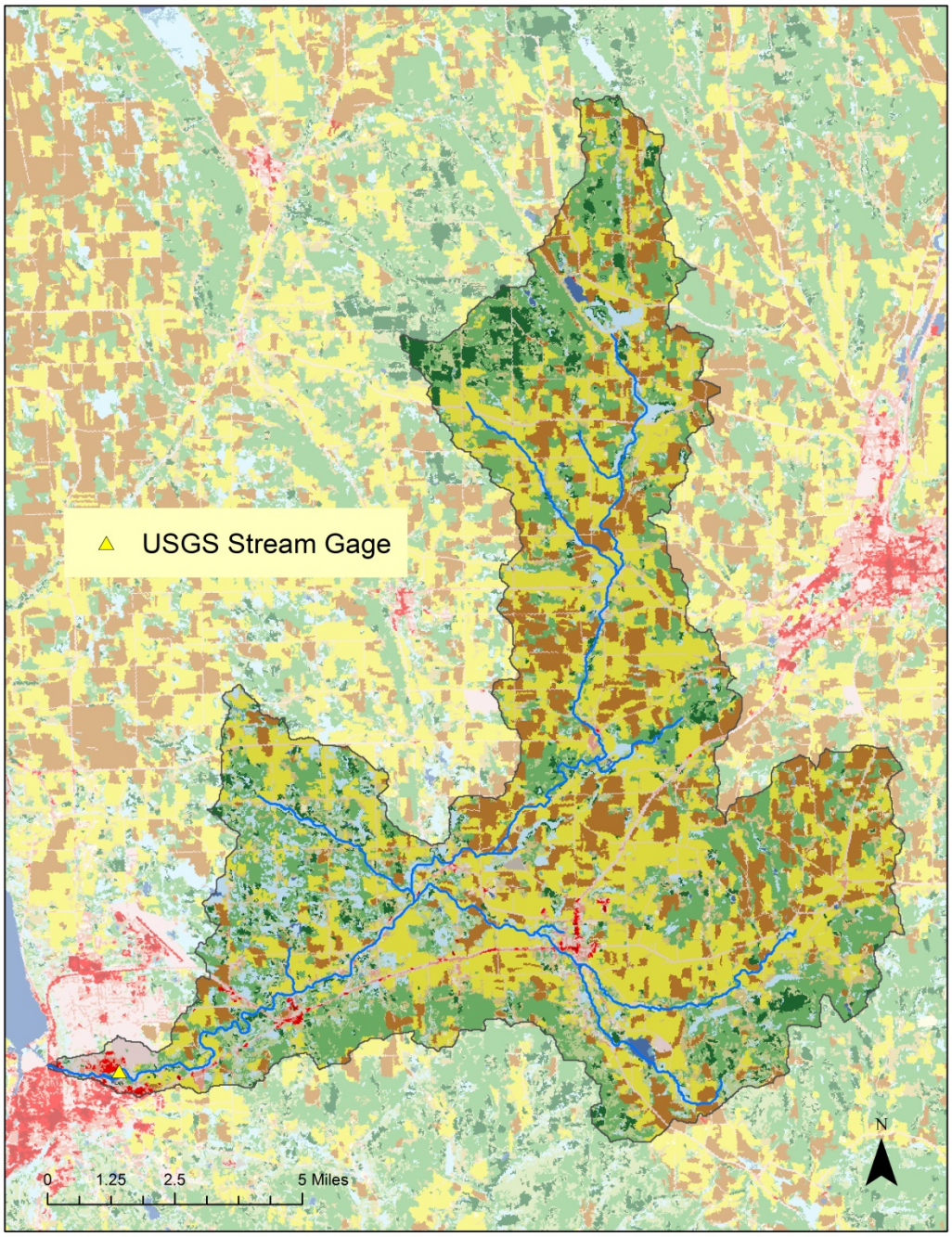

Figure 4-1. Fall Creek watershed with USGS stream flow gage denoted.

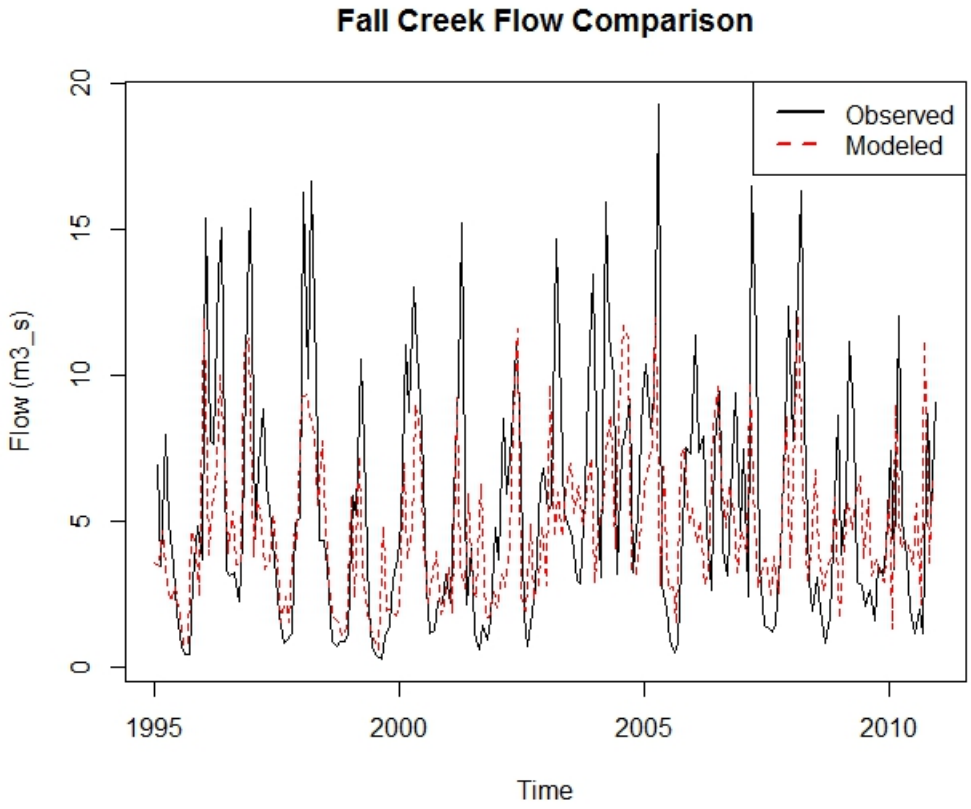

Figure 4-2. A comparison of USGS gage measured flow and model output flow. The solid black line indicates observed flow at the gage and the red dotted line denotes model outputs.

As a result, accurate land management inputs need to be provided to the model in order to be able to effectively predict nutrient fluxes within the watershed.

To ensure the accuracy of model inputs, as previously mentioned, a group of experts from a number of organizations were consulted on local land management practices. This group included Karl Czymmek, Aaron Ristow, Amanda Barber, Greg Albrecht, Jason Cuddeback, Gene Aarnio, Jon Negley, and Shawn Murphy. These individuals provided expert opinion when possible and conducted farm visits when necessary to ensure accurate characterization of land management practices. Their efforts were focused within the Fall Creek watershed but the data collected will be extended to other watersheds with similar land uses as appropriate and with their guidance. Table 4-1 summarizes the findings of the group which have been incorporated into the watershed model.

4.5. Preliminary Phosphorus Results

The wealth of data available in the southern tributaries applies not only to stream flow but also to phosphorus loads. A number of groups and organizations in the area regularly conduct water quality sampling which provides data for more precise validation of the watershed model. The Upstate Freshwater Institute (UFI) has conducted a thorough sampling campaign of the larger tributaries (http://energyandsustainability.fs.cornell.edu/util/clmp/laketribmonitoring.cfm), the Community Science Institute (CSI) also conducts water quality sampling in the southern portion of the Cayuga Lake Watershed (http://communityscience.org/database), and lastly, Dr. David Bouldin has a long record of water quality samples taken throughout Fall Creek 1972-1995 (http://ecommons.library.cornell.edu/handle/1813/8148).

Table 4-1. A summary of fertilization scheme for pasture/hay land use. Data were determined with the help of the previously mentioned group of advisees.

Fertilization Schedule Code	Land Use Code	Percent of Pasture/Hay Landuse	Application Timing	Average monthly Application Rate (kg/Ha)	Percent Incorporated
pasture 1	pasture/hay	15	year round	370	50%
pasture 2	pasture/hay	5	spring, summer, fall	370	50%
pasture 3	pasture/hay	2	spring, fall	148	0%
pasture 4	pasture/hay	10	spring, summer, fall	200	100%

As was the case with hydrological results, preliminary model output concerning phosphorus loads will be presented for the Fall Creek watershed. These results were obtained from a model run with the same time period of warm up and evaluation as the presented flow data. Figure 4-3 displays monthly phosphorus loads at the outlet of Fall Creek into Cayuga Lake. Two sites within the Fall Creek watershed were used to validate model output of phosphorus; both sites are monitored by CSI. Figure 4-4 presents a map of the Fall Creek watershed with monitoring locations highlighted. These two sites were selected from the numerous sites available due to the difference in contributing land area and stream flow that they represent. They Cayuga Street Bridge sampling location captures the majority of the watershed and closely characterizes the total load into the lake from this tributary. The Dryden Lake Outlet sampling point, however, represents a much smaller contributing area of land and provides valuable insight into the performance of the model on a smaller spatial scale. Sampling at these two sites began in 2002 and subsequent figures will display model output as well as measured data for the time frame in which sampling was conducted.

Total phosphorus loads at the Cayuga Street Bridge Sampling site are presented in Figure 4-5. This figure shows that the model is performing well at the watershed scale. Model output values fall within the range of values acquired from samples and appear to capture some peaks and trends in the data. Missed peaks could be attributed to undocumented land management changes or events. Figure 4-6 displays total phosphorus loads at the Dryden Lake Outlet sampling point. This figure shows that the model is likely over-predicting total phosphorus loads to the sampling point at the smaller scale. This is likely due to land management inputs and the difficulty in determining proper spatial distributions of land management strategies. At the larger scale, small discrepancies are smoothed out while at the smaller scale, minute inaccuracies are amplified in the output data.

An important and invaluable data set that was excluded from the current evaluation of model outputs was the UFI tributary monitoring dataset. The current preliminary model runs terminate in December of 2010 and UFI data collection began in 2013. While the current model time scale does not allow comparison of model outputs to these data, it will be incorporated into validation schemes as the time scale of the model run lengthens. This may provide additional improvements into model performance.

4.6. Continued Progress

While significant progress on the model has been made there is still work to be done. Currently, an effort is underway to refine internal hydrological parameters within the SWAT interface to more precisely represent the hydrology of the Finger Lakes region: right now we are over-setimating storm flow and underestimating baseflows. This problem is impacting our phosphorus load measurements. Another problem with our phosphorus estimates is that our organic-to-inorganic ratio is not agreeing with the UFI data from 2013. We are trying to determine if this is a problem in the model or in our parameters. Validation of model outputs of

sediments is also underway using CSI and Dr. David Bouldin's data sets. Lastly, a sensitivity analysis of the spatial distribution of land management strategies will be conducted to determine the extent to which this impacts model outputs. Once these tasks are completed, we will submit our model files.

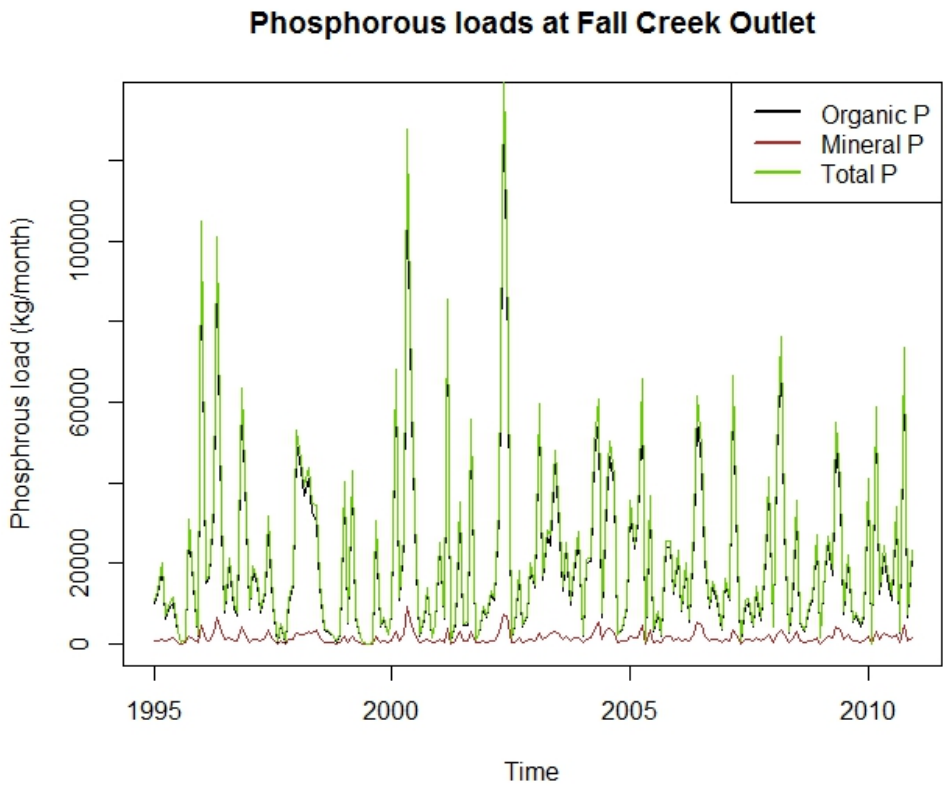

Figure 4-3. Model outputs of phosphorus loads from the Fall Creek watershed. As noted in the legend, the different colors denote different types of phosphorus.

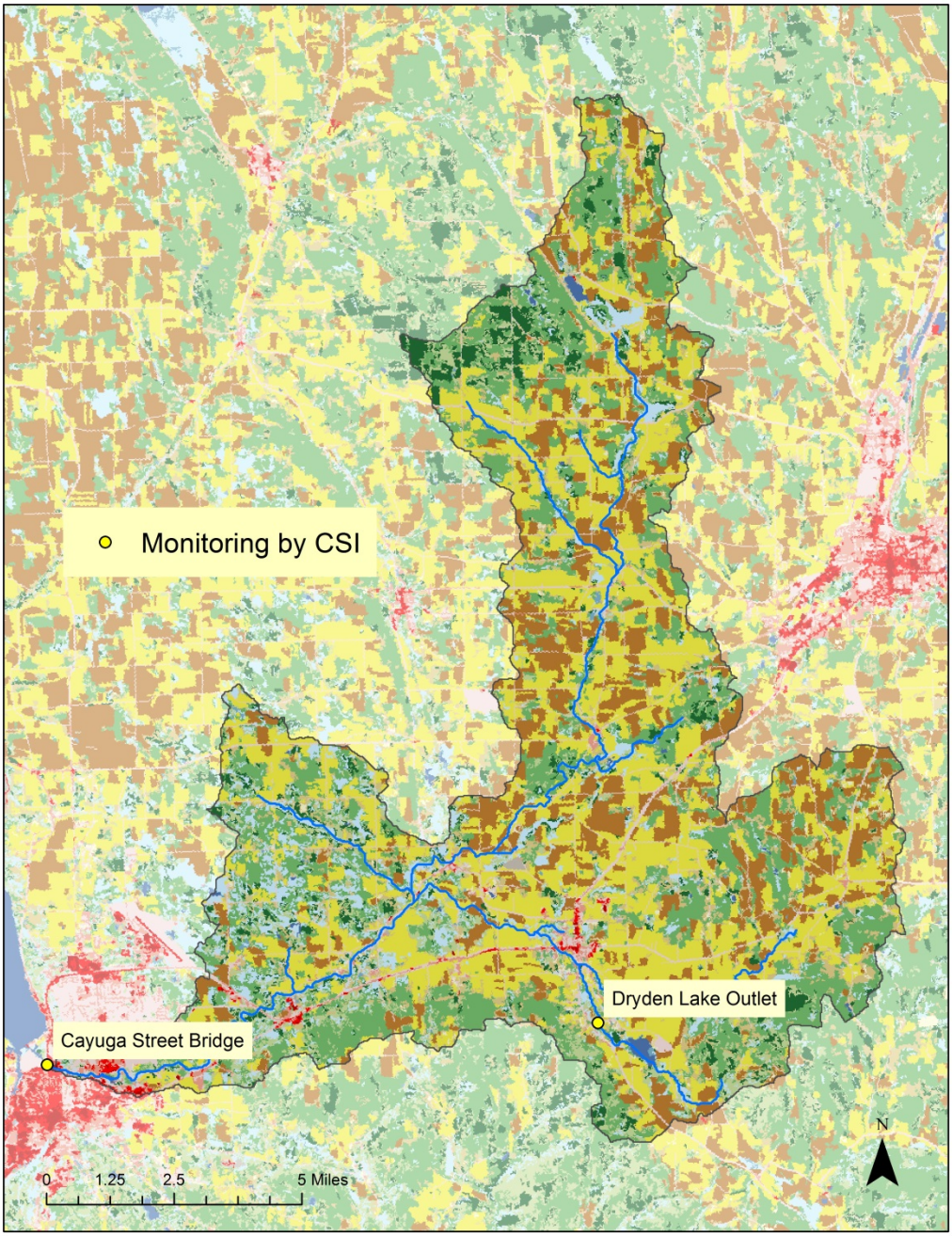

Figure 4-4. A map of the Fall Creek Watershed with CSI monitoring points of interest indicated.

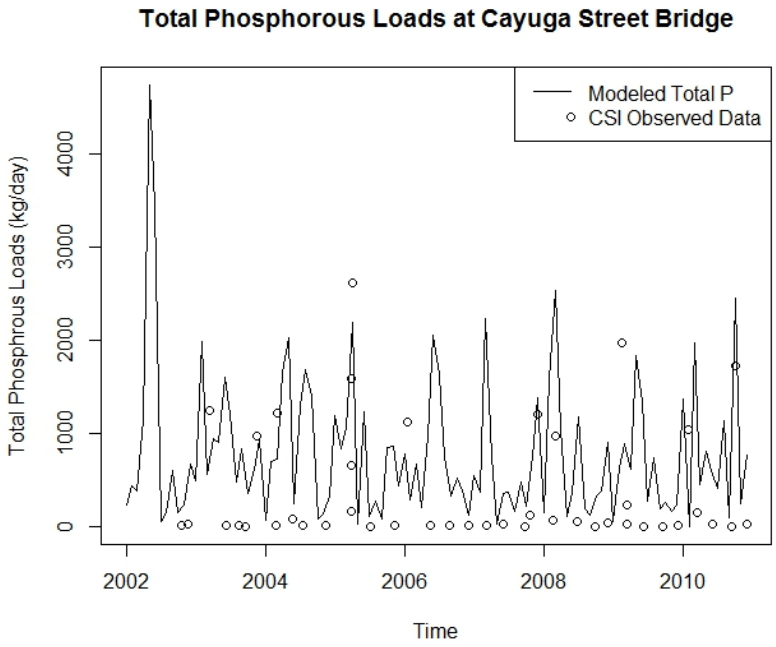

Figure 4-5. A comparison of total phosphorus loads at the Cayuga Street Bridge. The solid line indicates model output values while the circles show measured values of total phosphorus as sampled by CSI.

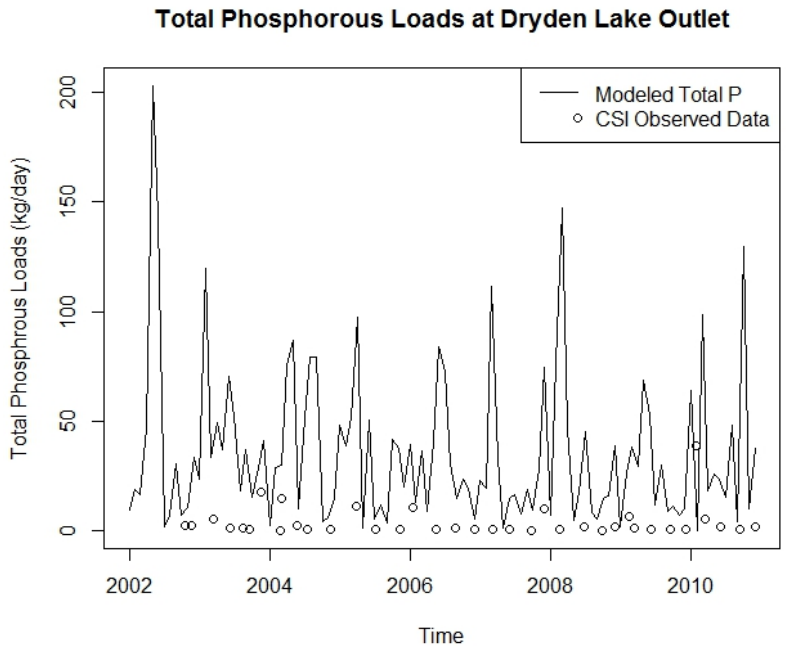

Figure 4-6. A comparison of total phosphorus loads at the Dryden Lake Outlet. The solid line indicates model output values while the circles show measured values of total phosphorus as sampled by CSI.

This page intentionally left blank.

Section 5. Cayuga Lake Limnology

5.1. Physical

5.1.1. Patterns from Rapid Profiling Instrumentation

5.1.1.1. Depth-Time Contours at Multiple Sites

Color contours of depth-time patterns are presented based on the bi-weekly longitudinal transects of *in situ* measurements made with rapid profiling instrumentation. The contours are presented for four parameters; temperature (T, °C), the beam attenuation coefficient ($\boldsymbol{c}_{660}$_f, 1/m), fluorometric chlorophyll *a* (Chl-*a*_f), and specific conductance (SC, µS/cm), that appears in a stacked format. Contours are presented in order for sites 1 through 8. The shallow northern site 9 is not considered in this format. Patterns for the pelagic sites are depicted first for the 0 to 30 m depth (0-20 m for site 8) interval, where most of the structure is manifested.

The shallow shelf sites (1 and 2) were generally not thermally stratified and demonstrated a seasonal heating cycle (Figures 5-1a and 5-2a). However, some temporal irregularities were evident, particularly at site 1 that was most closely positioned proximate to the tributaries. Cooler water intervals at this site in mid-August and September reflected the effects of tributary inputs with cooler water. These irregularities were less pronounce at site 2. However, together these patterns are indicative of the interplay between the shelf and the entering proximate tributaries. The T patterns for the pelagic sites (Figures 5-3a, 5-4a, 5-5a , 5-6a and 5-7a) portray a unifying seasonal stratification cycle for the lake; onset of stratification in May, with mostly progressive warming of the epilimnion into mid-July, and progressive cooling and deepening of the epilimnion starting in September. The epilimnion through summer was confined to depths ≤ 15 m. Differences among the pelagic sites were minor. Added temporal structure in the dynamics of the epilimnetic boundary was manifested for site 3 based on the more frequent monitoring in summer.

$\boldsymbol{c}_{660}$_f is strongly correlated with other optical metrics including turbidity and light scattering coefficient; these are all measures of particle content. Abrupt increases in $\boldsymbol{c}_{660}$_f occurred in early July and early August at site 1 (on the shelf, Figure 5-1b), in response to inputs from runoff events. High values also prevailed at this site in October. These signatures were attenuated at site 2 (Figure 5-2b). Some increases were observed in epilimnetic waters in July, August and September at site 3 (Figure 5-3b). However, the most distinct $\boldsymbol{c}_{660}$_f signatures at this site were abrupt increases in metalimnetic depths in early August and September, indicating the entry of turbid water as a plunging inflow (e.g., negatively buoyant density currents). Multiple increases in $\boldsymbol{c}_{660}$_f occurred in the epilimnion, that were generally manifested at all the pelagic sites (Figures 5-3b, 5-4b, 5-5b, 5-6b, 5-7b and 5-8b; note changes in color keys among these sites).

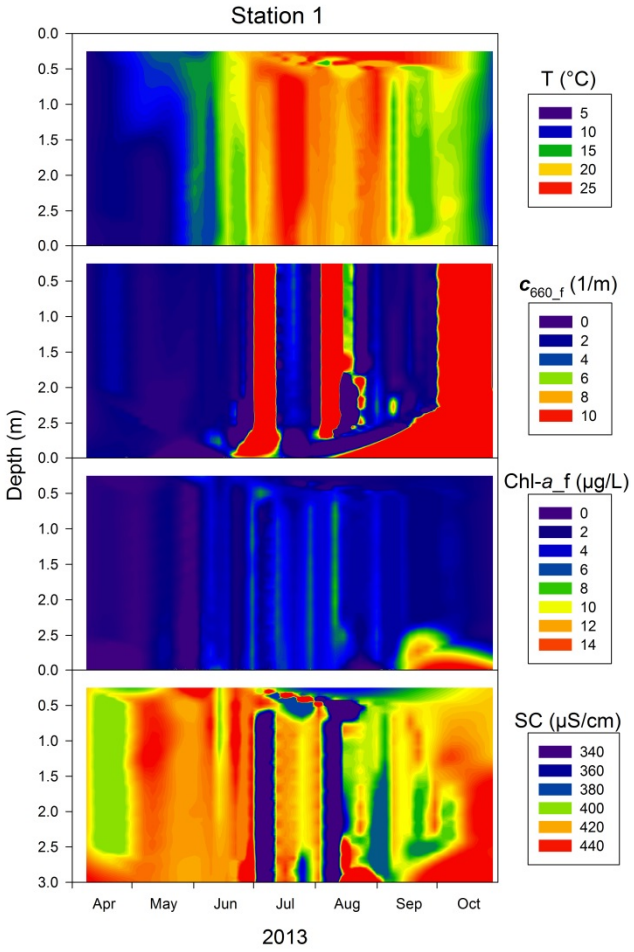

Figure 5-1. Color contours that describe the depth-time distribution of parameters in Cayuga Lake at site 1 in 2013. Based on field measurements with rapid profiling instrumentation: (a) temperature (T), (b) beam attenuation coefficient at 660 nm (c_{660}_f), (c) fluorometric chlorophyll *a* (Chl-*a*_f) and (d) specific conductance (SC).

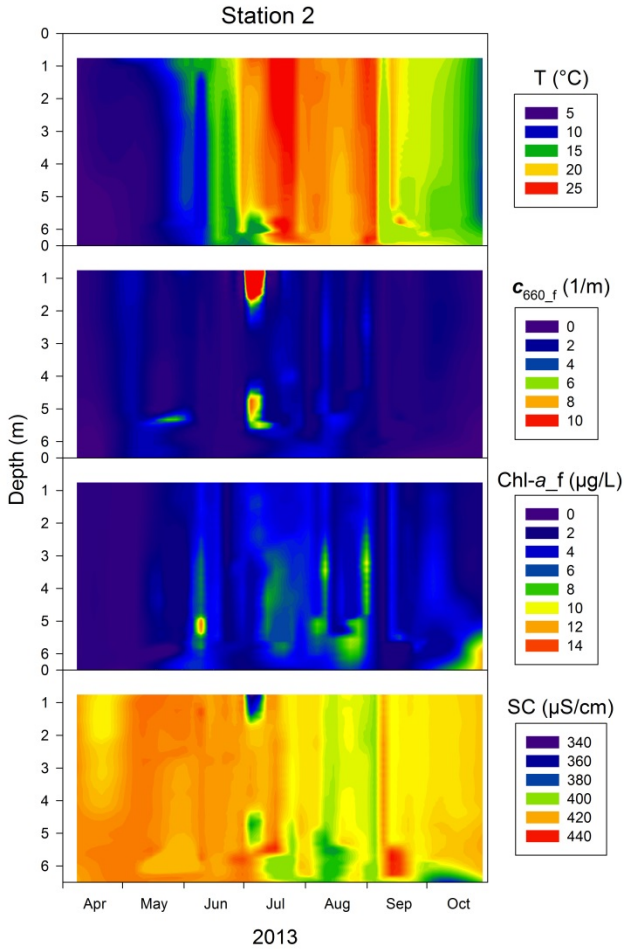

Figure 5-2. Color contours that describe the depth-time distribution of parameters in Cayuga Lake at site 2 in 2013. Based on field measurements with rapid profiling instrumentation: (a) temperature (T), (b) beam attenuation coefficient at 660 nm (c_{660}_f), (c) fluorometric chlorophyll *a* (Chl-*a*_f) and (d) specific conductance (SC).

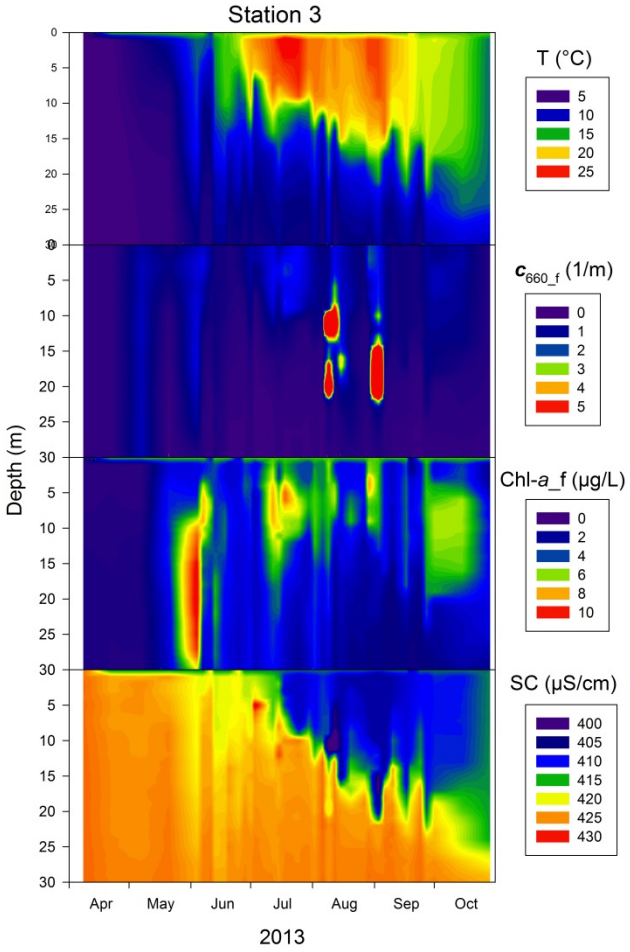

Figure 5-3. Color contours that describe the depth-time distribution of parameters in Cayuga Lake at site 3 in 2013. Based on field measurements with rapid profiling instrumentation: (a) temperature (T), (b) beam attenuation coefficient at 660 nm (c_{660}_f), (c) fluorometric chlorophyll *a* (Chl-*a*_f) and (d) specific conductance (SC).

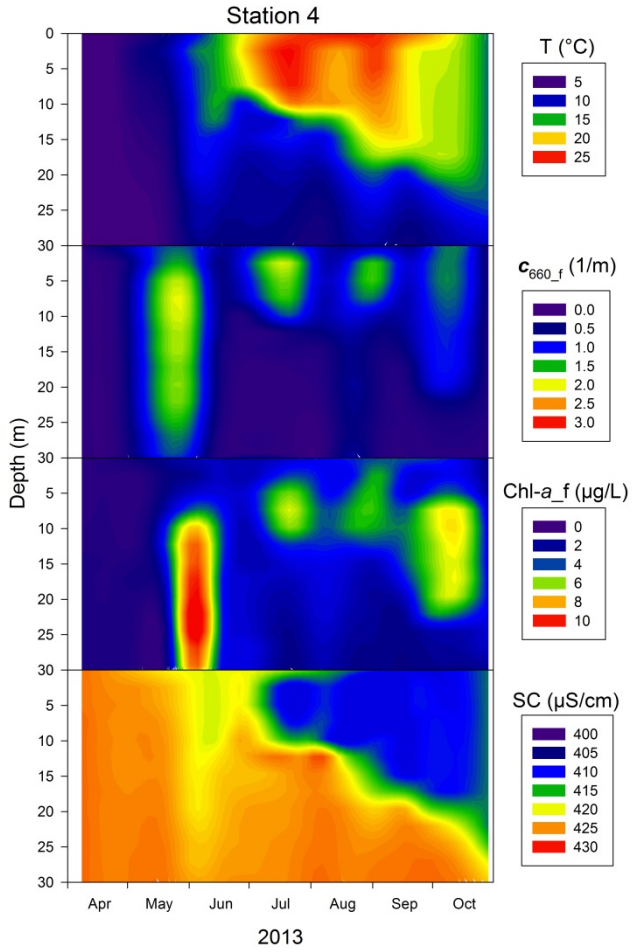

Figure 5-4. Color contours that describe the depth-time distribution of parameters in Cayuga Lake at site 4 in 2013. Based on field measurements with rapid profiling instrumentation: (a) temperature (T), (b) beam attenuation coefficient at 660 nm (c_{660}_f), (c) fluorometric chlorophyll *a* (Chl-*a*_f) and (d) specific conductance (SC).

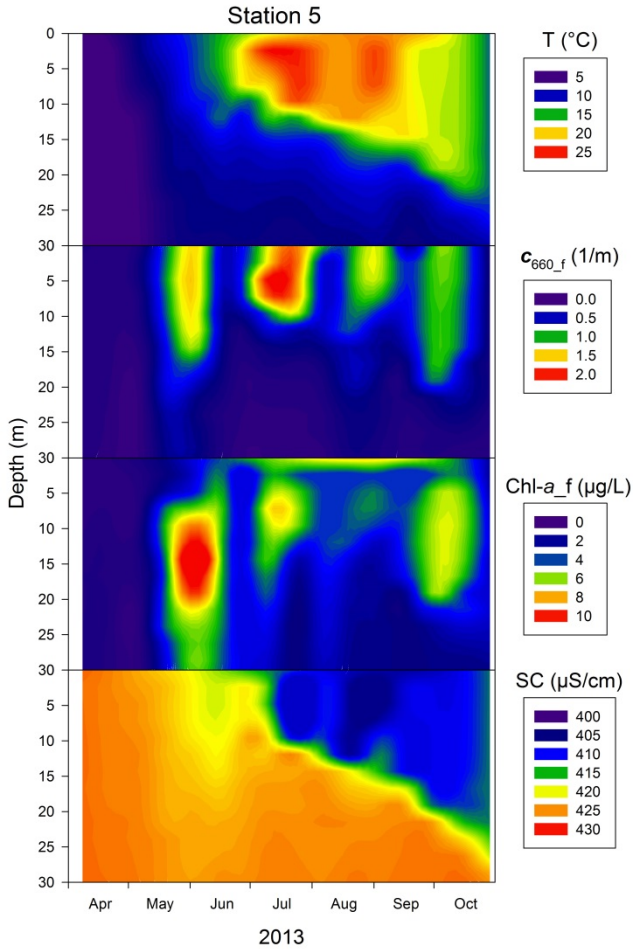

Figure 5-5. Color contours that describe the depth-time distribution of parameters in Cayuga Lake at site 5 in 2013. Based on field measurements with rapid profiling instrumentation: (a) temperature (T), (b) beam attenuation coefficient at 660 nm (c_{660}_f), (c) fluorometric chlorophyll *a* (Chl-*a*_f) and (d) specific conductance (SC).

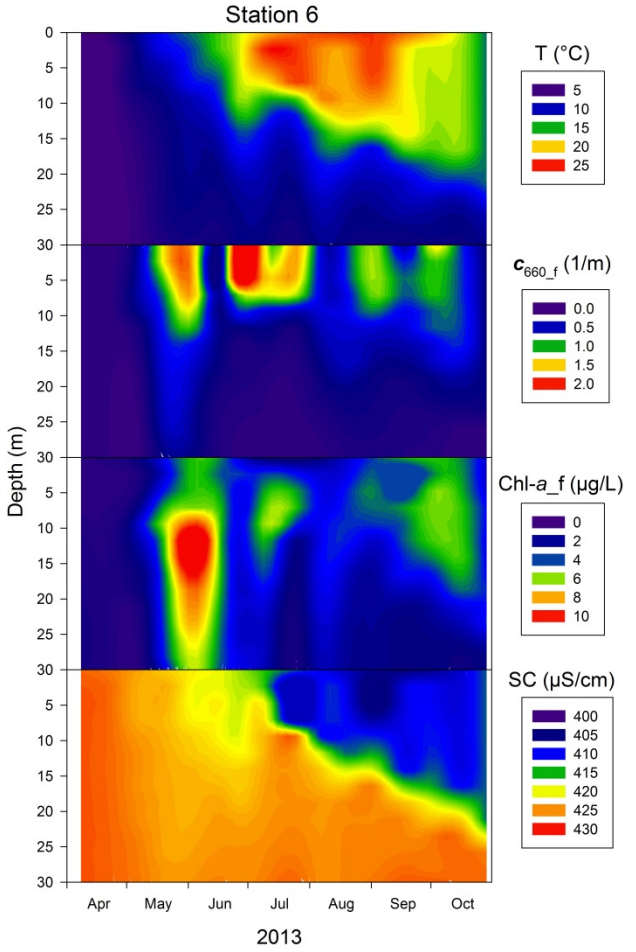

Figure 5-6. Color contours that describe the depth-time distribution of parameters in Cayuga Lake at site 6 in 2013. Based on field measurements with rapid profiling instrumentation: (a) temperature (T), (b) beam attenuation coefficient at 660 nm (c_{660}_f), (c) fluorometric chlorophyll *a* (Chl-*a*_f) and (d) specific conductance (SC).

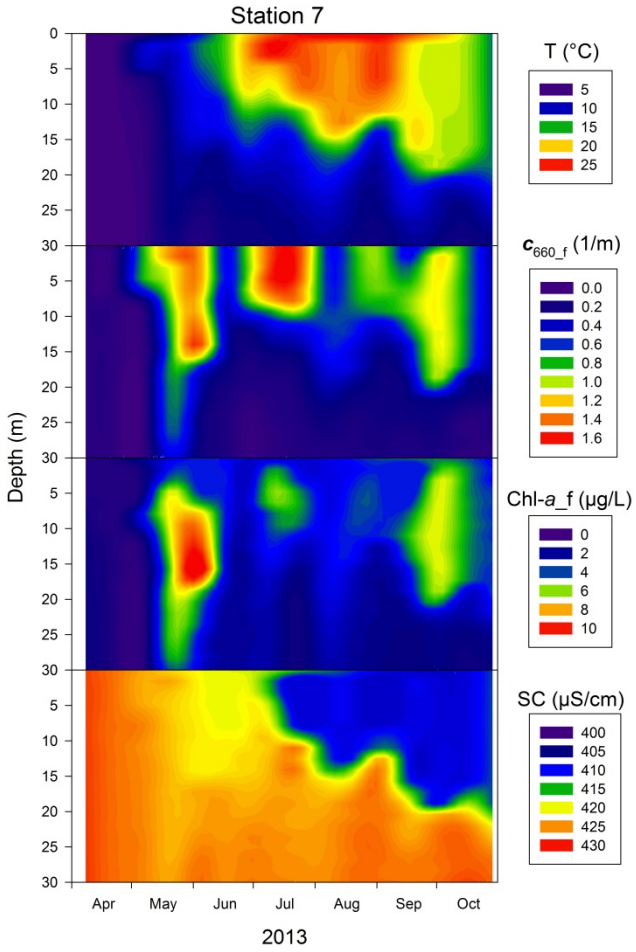

Figure 5-7. Color contours that describe the depth-time distribution of parameters in Cayuga Lake at site 7 in 2013. Based on field measurements with rapid profiling instrumentation: (a) temperature (T), (b) beam attenuation coefficient at 660 nm (c_{660}_f), (c) fluorometric chlorophyll *a* (Chl-*a*_f) and (d) specific conductance (SC).

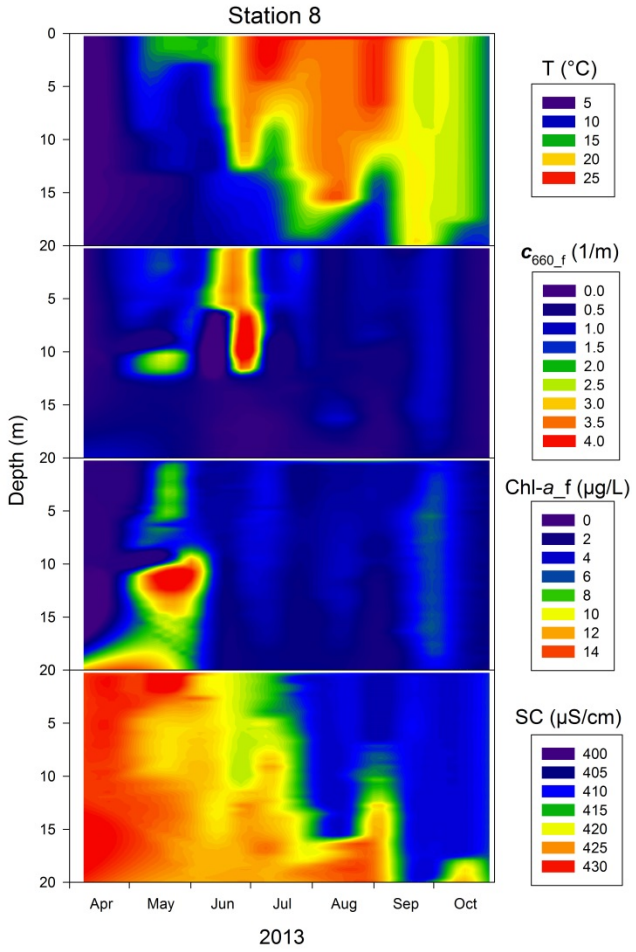

Figure 5-8. Color contours that describe the depth-time distribution of parameters in Cayuga Lake at site 8 in 2013. Based on field measurements with rapid profiling instrumentation: (a) temperature (T), (b) beam attenuation coefficient at 660 nm (c_{660}_f), (c) fluorometric chlorophyll *a* (Chl-*a*_f) and (d) specific conductance (SC).

The Chl-*a*_f patterns are considered primarily in the context of the occurrence of deep chlorophyll maxima (DCM); i.e., higher concentrations in stratified (metalimnetic) depths. Such structures need to be considered in the context of whether they depict increases in biomass or increases in the content of the Chl-*a* pigment within phytoplankton. In particular, the second of these alternatives is observed to occur in cases where light is relatively low, described as a photo-adaptation response. The most distinct DCM signature was observed in late May to early June when a substantial subsurface peak in Chl-*a*_f was observed at depths between 10 and 15 m at the pelagic sites (Figures 5-3c, 5-4c, 5-5c, 5-6c, 5-7c and 5-8c). Other increases in Chl-*a*_f were observed in the epilimnion.

SC serves as a passive tracer of inputs from the lake's tributaries. Decreases in tributary SC are observed with increases in stream flow (dilution effect). The relatively high runoff (stream flows) that prevailed during the study caused the SC of inputs to be often lower than the lake levels. The decrease observed in the lake's epilimnion, starting in June (Figures 5-3d, 5-4d, 5-5d, 5-6d, 5-7d and 5-8d), depicts the effects of the entry of the tributaries primarily into those upper waters. The dynamics on the shelf (Figures 5-1d and 5-2d) were more irregular with much greater variations (note different color scaling), supporting the position that the shelf serves as a transition between the entering tributaries and the lake's pelagic waters. The coincidence of the early July and early August high $\boldsymbol{c}_{660}$_f and low SC events was particularly striking at site 1 (Figure 5-1b and d). Vertical structure was observed on the shelf reflecting buoyancy effects in this transition area.

Color contours are presented for the entire water column at site 5 (Figure 5-9) where the depth approaches the maximum. In general the picture that emerges is that temporal structure is manifested primarily within the upper (e.g., ≤25 m) waters for these for parameters, with the exception of $\boldsymbol{c}_{660}$_f, for which near-bottom increases were observed in summer (Figure 5-9b). The near-bottom elevated $\boldsymbol{c}_{660}$_f levels are widely accepted as an indicator of a benthic nepheloid layer (BNL), a signature that is generally attributed to sediment resuspension (Gloor et al. 1994, Bloesch 1995).

5.1.1.2. Depth-Longitudinal Contours

Longitudinal patterns are presented for T, $\boldsymbol{c}_{660}$_f, Chl-*a*_f and SC for the upper 30 m of the lake, for four selected days of measurements in 2013 made along the axis of the lake (sites 1 through 9) with the rapid profiling instrumentation. These serve as coarse "snapshots" of longitudinal structure for these metrics. These have two imperfections. First, the substantial length between sites makes these representations approximate; e.g., the possibility of noteworthy structure being missed by the positioning of the nine sites cannot be discounted. Second, the time necessary to collect a complete set of measurements (5 to 8 hours) is not negligible compared to the period of internal waves (seiche activity; ~80 h see Section 6), that can have an effect of blurring (making somewhat less distinct) the signature. Note that the color scaling for magnitudes of the parameters has been changed amongst the days to aid resolution of structure.

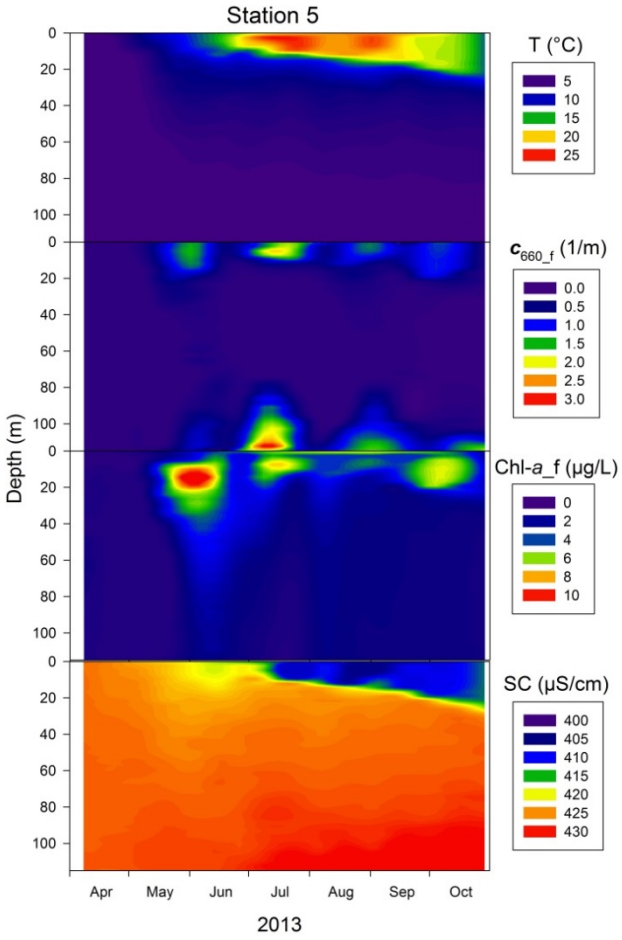

Figure 5-9. Color contours that describe the depth-time distribution of parameters in Cayuga Lake at site 5 for the whole water column in 2013. Based on field measurements with rapid profiling instrumentation: (a) temperature (T), (b) beam attenuation coefficient at 660 nm ($\boldsymbol{c}_{660}$_f), (c) fluorometric chlorophyll *a* (Chl-*a*_f) and (d) specific conductance (SC).

The longitudinal contours of April 22 (Figure 5-10) reflect spring turnover conditions. Structures were confined to small portions of the lake at it southern and northern ends, influenced by tributary inputs and sediment resuspension. Longitudinal structure was evident on June 4 (Figure 5-11). The epilimnion was tilted substantially, being much deeper in the southern part of the basin compared with the north (Figure 5-11a). This in turn influenced the longitudinal pattern of both $\boldsymbol{c}_{660}$_f (Figure 5-11b) and Chl-*a*_f (Figure 5-11c), causing the depths of elevated levels of both these metrics to also be deeper in the south relative to the northern portion of the lake. $\boldsymbol{c}_{660}$_f values were somewhat higher in the southern waters (Figure 5-11b); however, the DCM maximum was conspicuous throughout the pelagic waters, though the vertical details differed along the lake's axis (Figure 5-11c). The extent of tilt of the epilimnion was greatly diminished on August 6 (Figure 5-12a). The level of $\boldsymbol{c}_{660}$_f was somewhat higher in the southern portion of the lake (Figure 5-12b), with a structure consistent with a source(s) from the southern end (e.g., tributaries), though generally low values of $\boldsymbol{c}_{660}$_f prevailed throughout the lake. Chl-*a*_f levels were also somewhat higher in the south (Figure 5-12c). The somewhat lower SC, from reductions in tributary inputs (a dilution effect from increased flows in summer), was nearly uniformly distributed throughout the epilimnion (Figure 5-12d). The deeper boundary of the epilimnion by September 17 was nearly horizontal (Figure 5-13a). Levels of $\boldsymbol{c}_{660}$_f (Figure 5-13b) and Chl-*a*_f (Figure 5-13c) demonstrated only modest, but similar, longitudinal differences. The lower SC levels continued to be confined to, and track the dimensions of, the epilimnion (Figure 5-13d).

5.1.2. Selected Optical Characteristics

5.1.2.1. Spatial Patterns

Three optical metrics are considered here for the upper waters of Cayuga Lake, the beam attenuation coefficient (measured here at a wavelength of 660 nm; $\boldsymbol{c}_{660}$_f, 1/m), the diffuse attenuation coefficient for scalar photosynthetically active (400-700 nm) radiation (K_0(PAR), 1/m), and Secchi depth (SD, m). The beam attenuation coefficient ($\boldsymbol{c}_{660}$_f) is a reliable surrogate of the scattering coefficient (*b*) and turbidity (Tn; Kirk 2011). K_0(PAR) is important in specifying the light available at depth to support photosynthesis. SD is most closely related to the public's perception of water quality, on an optical basis (Effler 1985). To represent spatial patterns the average values are presented at each site for the entire study period (April - October) and the summer interval (June – September). Temporal variability is represented by a vertical bar that corresponds to one standard deviation.

A longitudinal gradient in $\boldsymbol{c}_{660}$_f extended from site 1 (on the shelf proximate to tributary inputs), where the highest levels were observed, to site 3 (Figure 5-14a). Differences among the pelagic sites were small, on average, as were the differences between the entire study period and the summer. An exception was the much higher entire study average compared with the summer average value for site 9. The averages for site 1 (~ 10 1/m) were approximately an order of magnitude greater than at pelagic sites (~ 1 1/m).

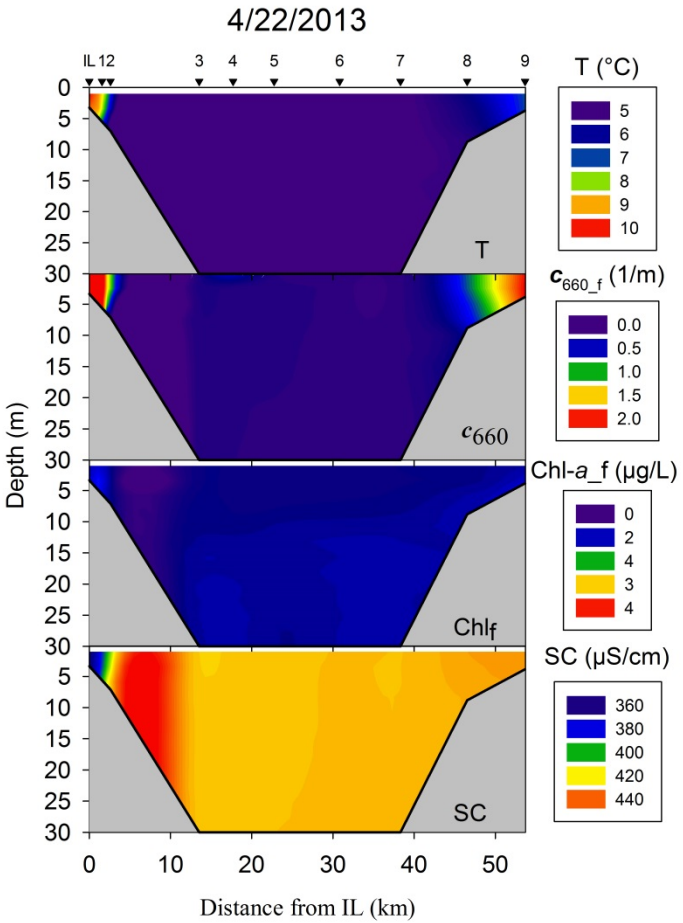

Figure 5-10. Depth-length contours of conditions in Cayuga Lake measured with rapid profiling instrumentation on April 22, 2013: (a) temperature (T), (b) beam attenuation coefficient (c_{660}_f), (c) fluorometric chlorophyll *a* (Chl-*a*_f) and (d) specific conductance (SC).

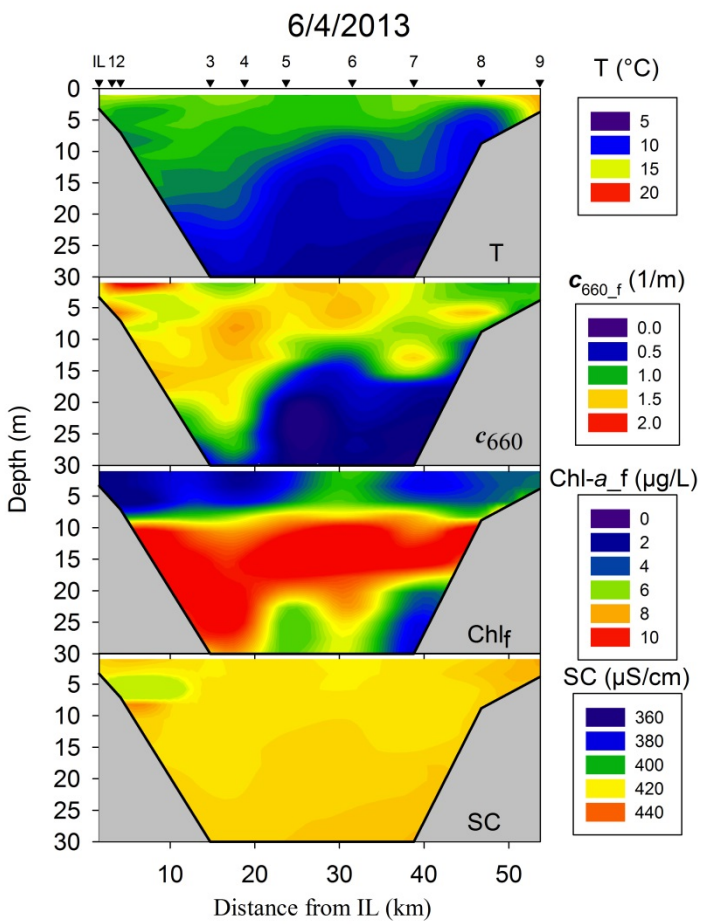

Figure 5-11. Depth-length contours of conditions in Cayuga Lake measured with rapid profiling instrumentation on June 4, 2013: (a) temperature (T), (b) beam attenuation coefficient (c_{660}_f), (c) fluorometric chlorophyll *a* (Chl-*a*_f) and (d) specific conductance (SC).

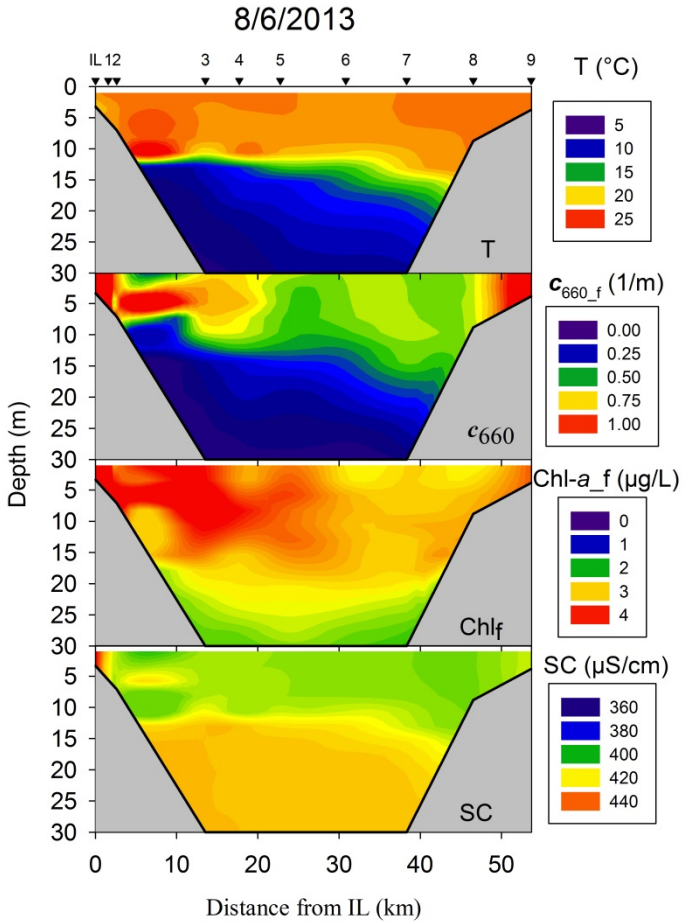

Figure 5-12. Depth-length contours of conditions in Cayuga Lake measured with rapid profiling instrumentation on August 6, 2013: (a) temperature (T), (b) beam attenuation coefficient (c_{660}_f), (c) fluorometric chlorophyll *a* (Chl-*a*_f) and (d) specific conductance (SC).

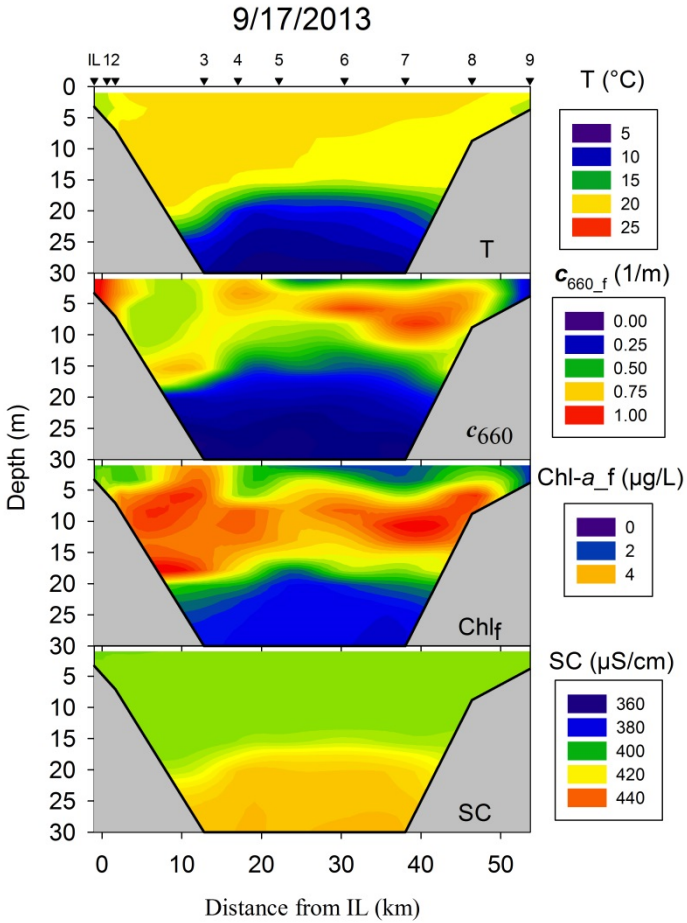

Figure 5-13. Depth-length contours of conditions in Cayuga Lake measured with rapid profiling instrumentation on September 17, 2013: (a) temperature (T), (b) beam attenuation coefficient (c_{660}_f), (c) fluorometric chlorophyll *a* (Chl-*a*_f) and (d) specific conductance (SC).

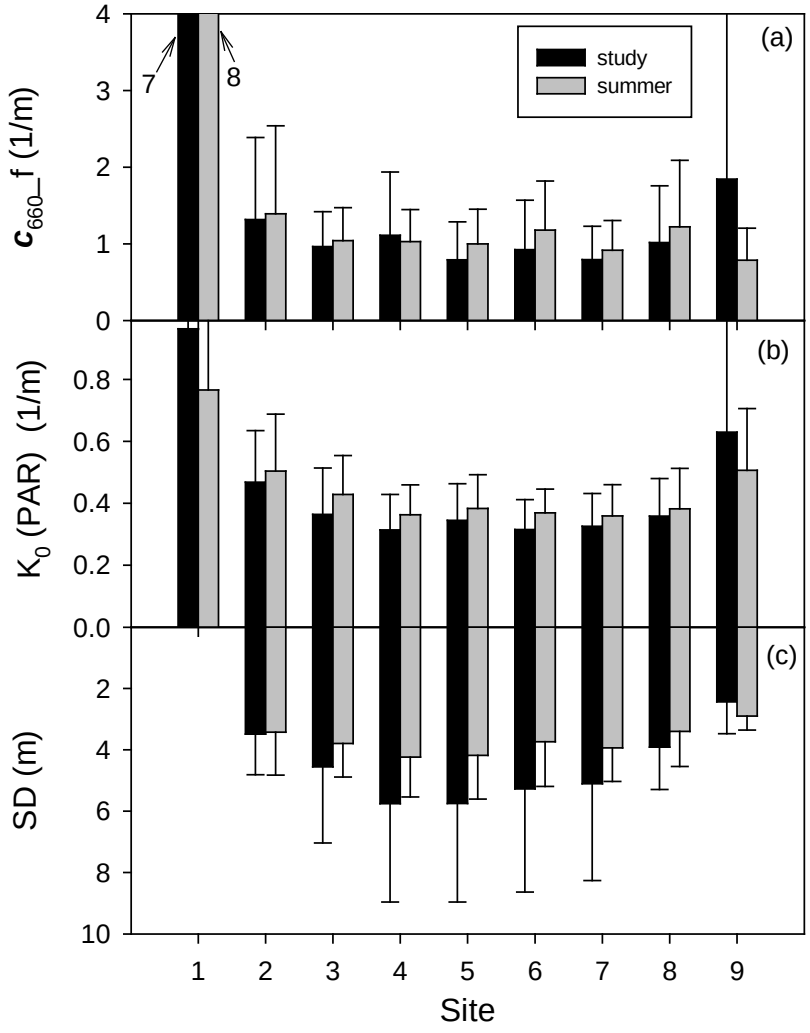

Figure 5-14. Spatial patterns for Cayuga Lake as average values at nine sites for two intervals in 2013, the entire study and summer (Jun-Sept.): (a) c_{660}_f, (b) K_0(PAR), and (c) SD. Temporal variability represented by on standard deviation bar.

Values of K_0(PAR) are most uncertain for site 1 because of its shallow depth. Spatial structure was manifested as decreases in K_0(PAR) extending from site 2 northward to site 4 (Figure 5-14b). This differs from a number of parameters for which pelagic uniformity extended further north instead starting from site 3. Higher values were observed for site 9. Average values were slightly higher for summer compared with the entire study except for site 9.

Site 1, usually, and site 2, occasionally (three times), were too shallow for representative SD observations (e.g., disk viewed on bottom). Accordingly, no site 1 data are presented. Quantitative comparisons of other sites with site 2 observations require deletions for those days (three) that the disk was viewed on the bottom at site 2. Well defined spatial differences emerge for SD based on average for the sites (Figure 5-14c). Average values increased from site 2 (even with adjustments for the three observations) to site 4, sites 4 and 5 were similar, and decreases from site 5 to 9 were observed. However, these trends based on average would likely be difficult to resolve in observations for most individual days, given the substantial temporal variations encountered. The distinctly higher average values at the pelagic sites based on the entire study period, versus the summer (Figure 5-14c), were largely associated with the especially high values encountered in spring (e.g., SD ~ 13 m), at the start of the monitoring.

5.1.2.2. Temporal Patterns

Temporal patterns are considered in the context of dynamics of stream flow, using Fall Creek conditions as the indicator. The Fall Creek hydrograph appears as the top panel of stacked time plots. Time plots are presented for two combinations of lake monitoring sites: (1) the first compares conditions on the shelf (sites 1 and 2) with the southernmost pelagic site (site 3), and (2) the second compares conditions at site 3 with other pelagic sites. The second of these also enables identification of added temporal structure that emerged from the more frequent monitoring at site 3.

Observations of K_0(PAR) converged at sites 2 and 3 on several occasions, and values at site 2 were higher, often by a wide margin on the other monitoring days (Figure 5-15b). Responsiveness to major runoff events (Figure 5-15a), particularly in early July and August, was depicted by coincident increases in K_0(PAR), particularly on the shelf at site 2, but also in pelagic waters at site 3. Differences between site 3 and the other pelagic sites (average of sites 4 – 8) were smaller by comparison (Figure 5-15c), and some additional temporal structure was manifested in more frequent site 3 observations (e.g., the abrupt increase K_0(PAR) in response to the early August event). Major variations were observed (~ 3-fold range) in K_0(PAR) on the shelf (Figure 5-15b) as well as in pelagic waters.

The depths of the epilimnion and the photic zone (1% light level) were compared to consider the potential for phytoplankton growth in stratified layers (i.e., deeper than the epilimnion). The photic zone depth is often assumed to coincide with the depth interval over which phytoplankton

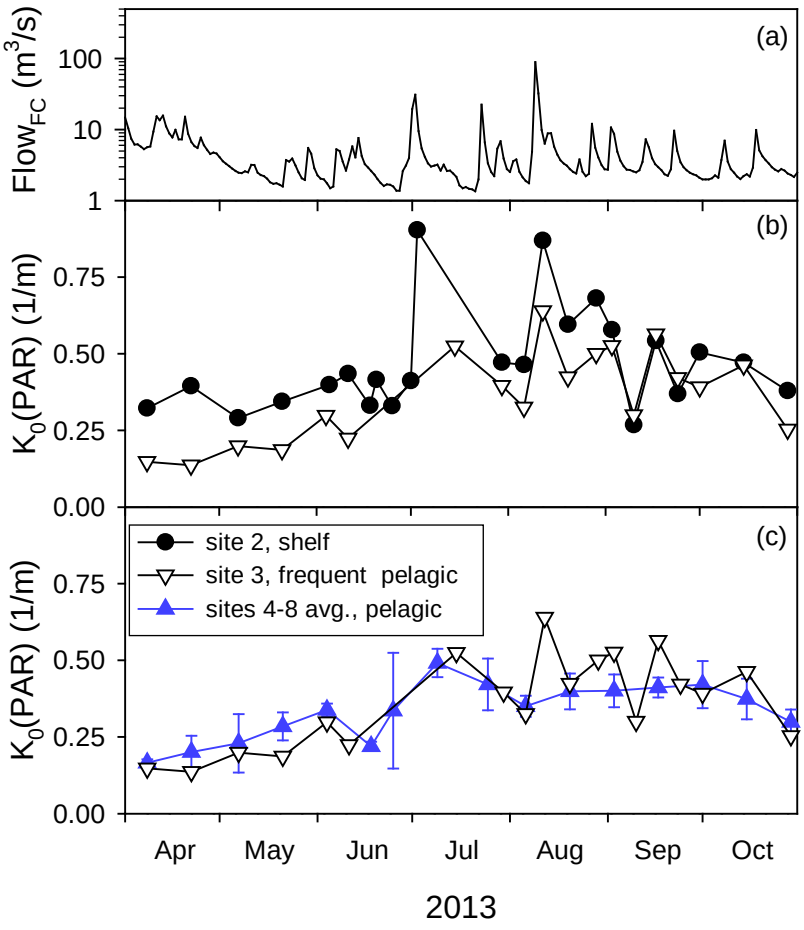

Figure 5-15. Temporal patterns for Cayuga Lake, 2013: (a) daily USGS flows in Fall Creek, (b) K_0 (PAR) at sites 2 and 3, the frequently sample pelagic site, and (c) K_0(PAR) at site 3 and the average of sites 4-8. Spatial variability represented range bars in (b) and one standard deviation bar in (c).

production exceeds respiration (Wetzel 2001); e.g., depth interval of potential phytoplankton growth. The dynamics of the photic zone depth, calculated from the dynamics of K_0(PAR), are presented for site 2 (Figure 5-16b), site 3 (Figure 5-16c) and site 5 (Figure 5-16d). The depth of the epilimnion was shallower than the photic zone for much of the mid-May (onset of stratification) to early July interval of the pelagic sites, but the epilimnion was generally deeper thereafter. Accordingly, there was some potential for phytoplankton growth below the epilimnion in the earlier (e.g., May) interval. However, the fraction of incident light reaching below the epilimnion during this interval was generally low (e.g., mostly < 10%).

The $\boldsymbol{c}_{660}$_f levels strongly diverged for site 2 and 3 (Figure 5-17b) following the major runoff events of early July and early August (Figure 5-17a). Site 2 values approached those for site 3 on only a few occasions, during relatively dry weather intervals. On other occasions site 2 values were shifted somewhat higher than site 3 observations. The change in scaling for the pelagic sites (Figure 5-17c) allows resolution of rather distinct temporal pattern with peaks in May, early June, mid- to late July, early August (site 3) and late August to early September (site 3). The July and early August peaks, at least in part, appear to reflect inputs from the major runoff events.

The greatest divergences in SD for sites 2 and 3 also occurred (Figure 5-18b) following the major runoff events of early July and early August (Figure 5-18a). Note that the SD y-axis is reversed from those of the other optical metrics, with higher values low on the scale. The greatest SD observations were observed early in the study in April, exceeding 12 m at site 3, the highest reported values we are aware of for the lake. Wide differences among the pelagic sites were observed in late April and early May (Figure 5-18c). The pelagic sites values converged thereafter for most of the study. SD values at site 2 converged with those at site 3 on only several occasions. More often SD values at site 2 were somewhat lower than at pelagic sites (Figure 5-18b). SD decreased through April and May at pelagic sites and increased in the first half of June (Figure 5-18c). Subsequently it decreased and remained between 3 and 4 m until September. A sharp increase in SD occurred at the end of the study period.

5.1.3. Minerogenic Particles

5.1.3.1. Spatial Patterns of PAV_m and Chemical Composition in 2013

The metric of minerogenic (inorganic) particle content used to represent their effects on both light scattering (i.e., turbidity and Secchi depth; Peng and Effler 2012, Effler and Peng 2014) and P concentration (Effler et al. 2014) is PAV_m, the projected area of minerogenic particles per unit volume of water. This abbreviation and a list of others related to PAV_m, that are introduced subsequently, are presented in Table 5-1. Average PAV_m levels are presented (Figure 5-19) for the six sites monitored (No.'s 1, 2, 3, 5, 7 and 9) along the lake's axis in 2013 for two time intervals, the monitored period (April-October) and summer (June-September). A logarithmic y-axis is used because of the wide variations in the observations, particularly on the shelf.

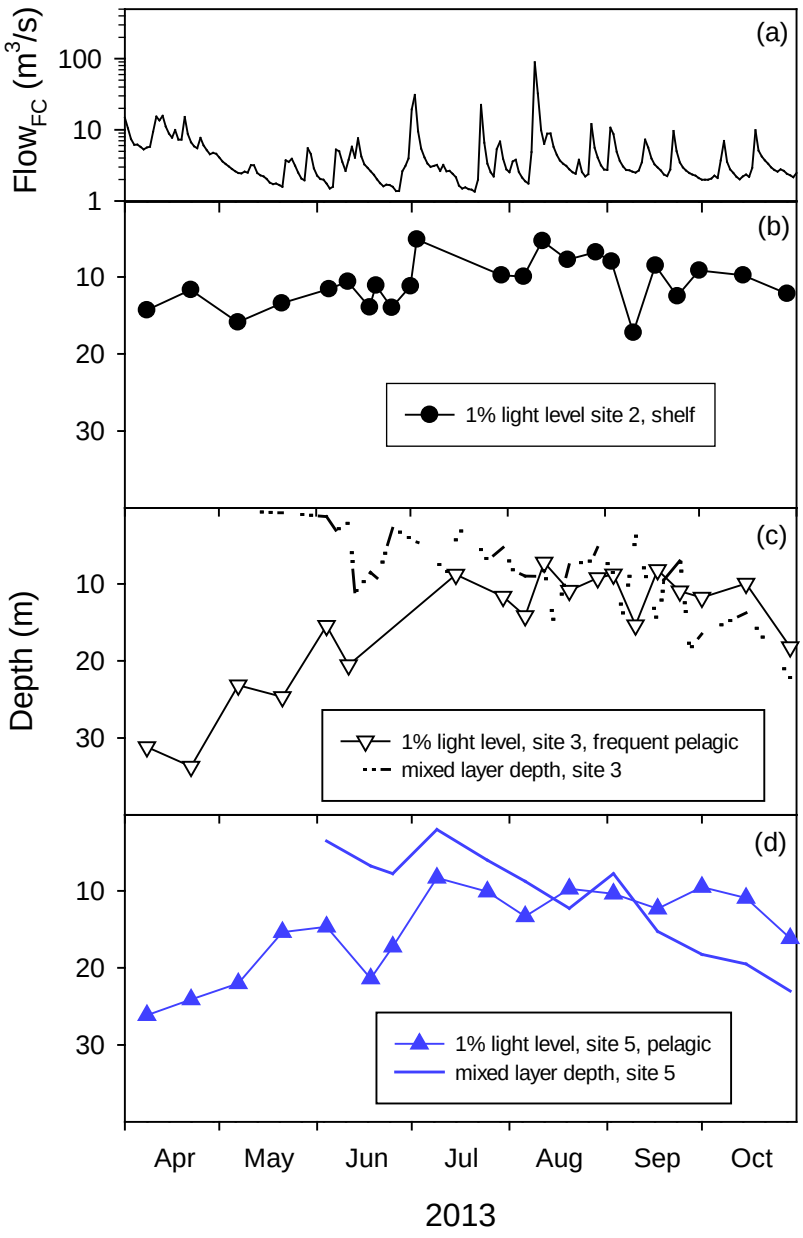

Figure 5-16. Temporal patterns for Cayuga Lake, 2013: (a) daily USGS flows in Fall Creek, (b) 1% light level at site 2 (c) 1% light level and mixed layer depth at site 3, the frequently sample pelagic site, and (d) 1% light level and mixed layer depth at site 5.

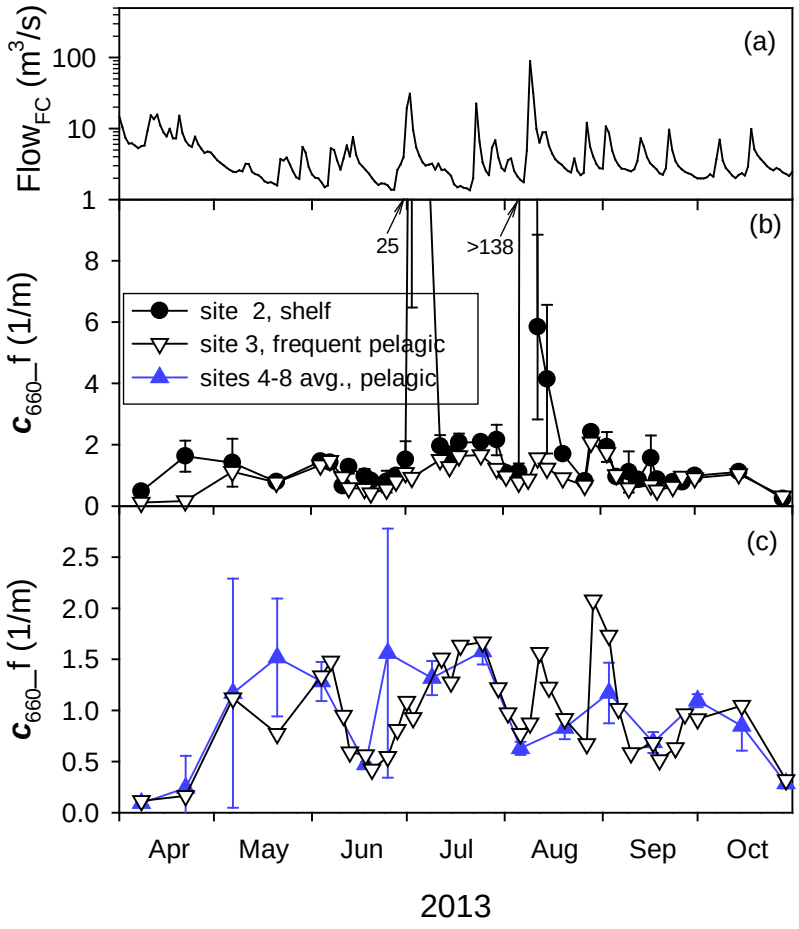

Figure 5-17. Temporal patterns for Cayuga Lake, 2013: (a) daily USGS flows in Fall Creek, (b) c_{660}_f at sites 2 and 3, the frequently sample pelagic site, and (c) c_{660}-f at site 3 and the average of sites 4-8. Spatial variability represented range bars in (b) and one standard deviation bar in (c).

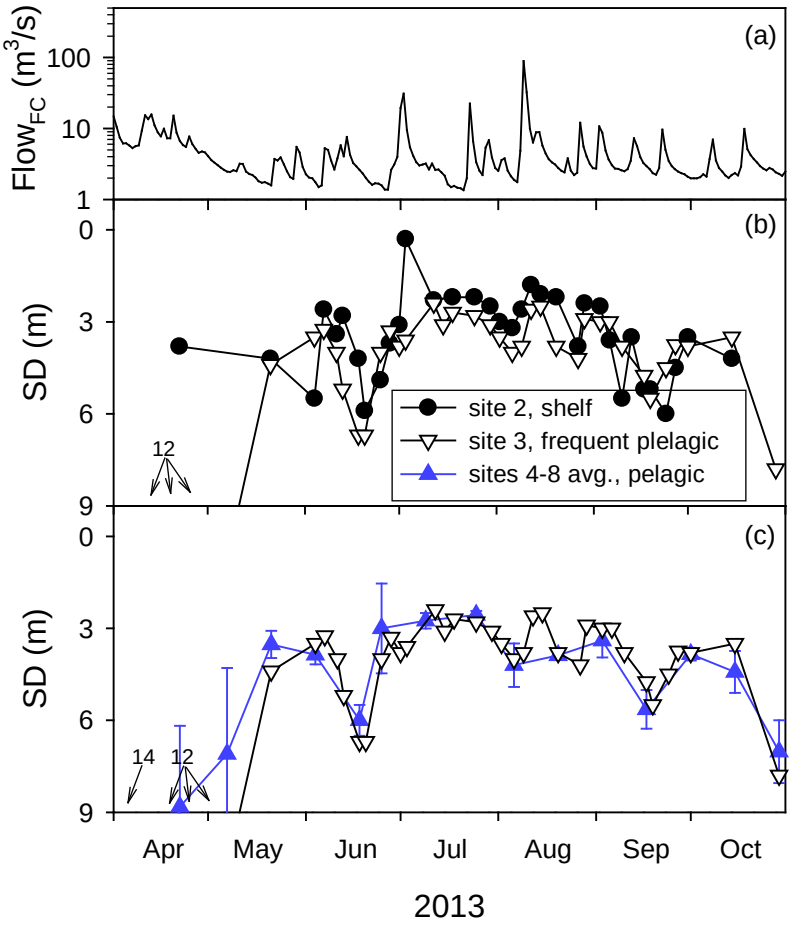

Figure 5-18. Temporal patterns for Cayuga Lake, 2013: (a) daily USGS flows in Fall Creek, (b) SD at sites 2 and 3, the frequently sample pelagic site, and (c) SD at site 3 and the average of sites 4-8. Spatial variability represented range bars in (b) and one standard deviation bar in (c).

Table 5-1. Listing of and abbreviations of optical parameter.

No.	Parameter	Abbreviation	Unit
1	particulate scattering coefficient	b_p	1/m
2	scattering coefficient of minerogenic particles	b_m	1/m
3	scattering coefficient of organic particles	b_o	1/m
4	total projected area of minerogenic particles per unit of volume of water	PAV_m	cm^2/L
5	particulate phosphorus associated with minerogenic particles	PP_m	µg/L
6	particulate phosphorus associated with organic particles	PP_o	µg/L

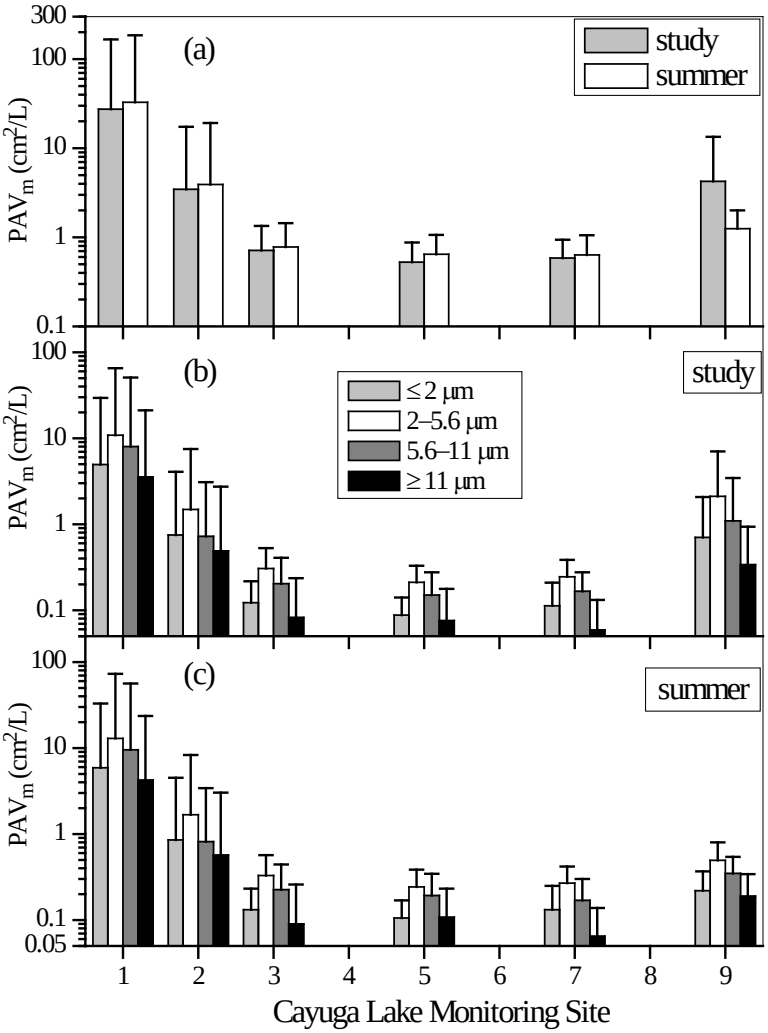

Figure 5-19. Spatial differences (six sites) in PAV_m and size classes of PAV_m for the upper waters of Cayuga Lake in 2013, as temporal averages: (a) PAV_m for the study period and for the summer, (b) PAV_m for four size classes for the study period, and (c) PAV_m for four size classes for the summer. Vertical bars are one standard deviation.

Temporal variability at each of the sites is represented by a vertical bar that corresponds to one standard deviation.

Longitudinal differences were manifested for PAV_m between the southern end of the lake, including between the shelf sites (sites 1 and 2), and pelagic site 3 (Figure 5-19a). Noteworthy longitudinal differences were not observed among the pelagic sites (3, 5 and 7). Higher levels relative to the pelagic sites were observed at the shallow site at the northern end (site 9). The study interval and summer averages were similar, except at site 9. Variations were greater at the shallower sites. The spatial differences, extending from the southern end, reflect the effects of tributary inputs, particularly during runoff events.

PAV_m was partitioned into the contributions of four different size classes, in anticipation of supporting related modeling needs. For example, this partitioning supports representation of different settling loss rates from the upper waters according to the size dependency described by Stokes Law. The four size classes are ≤ 2 µm, 2-5.6 µm, 5.6-11 µm, and >11 µm. The 2-5.6 µm size class made the greatest contribution to PAV_m, on average, throughout the lake (Figure 5-19b). The largest class, ≥ 11 µm, made progressively smaller contributions (on average) extending from the shelf (sites 1 and 2) through the pelagic sites (to site 7). This signature is consistent with the operation of the size sorting process of deposition, whereby larger particles are lost preferentially due to higher settling velocities. However, the relative contribution of the smallest particles (≤ 2 µm) also decreased from the shelf to pelagic sites (Figure 5-20b), a pattern that suggests the operation of particle aggregation, the combination of particles to form larger ones. The spatial patterns depicted by this presentation format were similar for the summer (Figure 5-19c) compared with the entire study period (Figure 5-19b).

Partitioning PAV_m according to chemistry classes (Peng and Effler 2007, Peng et al. 2009, Peng and Effler 2012) provides insights concerning the origins of the minerogenic particles. The contributions of four broad classes are considered, clay minerals, quartz, calcium-rich, and other. Clay minerals and quartz inherently have allocthonous (watershed) origins. The Ca-rich class is mostly calcium carbonate (calcite), that in hardwater lakes such as Cayuga Lake primarily is formed autochthonously through precipitation of calcite ($CaCO_3$; Effler and Peng 2014). Clay minerals dominated PAV_m at site 2 throughout the study period (Figure 5-20a), establishing its origins from watershed inputs. While clay minerals were also generally dominant through pelagic areas (Figure 5-20b), there was a noteworthy difference. Calcite made increased contributions through pelagic waters, in portions of July (Figure 5-20b). This timing appears to be somewhat earlier than observed previously for the lake; e.g., the phenomenon usually occurs in August (Effler and Peng 2014). This spatial difference (site 2 versus pelagic) is generally consistent with the lack of conspicuous signatures of other forms of autochthonous production (e.g., phytoplankton) on the shelf, despite the delivery of enriched inputs of nutrients from the local tributaries.

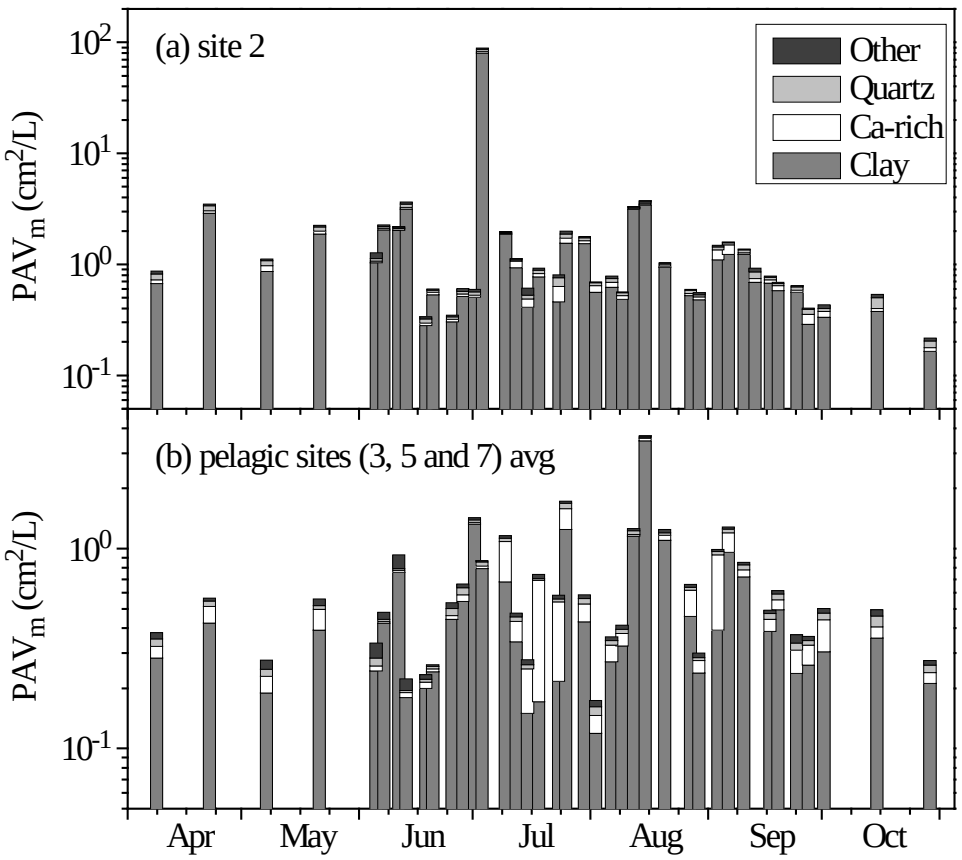

Figure 5-20. Temporal patterns of minerogenic particle chemistry for the upper waters of Cayuga Lake in 2013, according to four chemistry classes of PAV_m: (a) site 2, and (b) average of three pelagic sites (sites 3, 5, and 7).

5.1.3.2. Temporal Patterns of PAV_m in 2013

Given the dominance of clay minerals in regulating PAV_m in Cayuga Lake (Figure 5-20), and their watershed origins, times series of PAV_m in the lake over the study period (Figure 5-21) are presented in the context of the Fall Creek hydrograph over the same period (Figure 5-21a). Fall Creek is the single largest tributary and inflow dynamics in this stream are a good indicator of those for total inflow to the lake (Effler et al. 1989). Flow rates (Q) from this tributary were elevated for much of April and substantial runoff event peaks were observed in early and late July and early August (Figure 5-21a). A number of smaller events occurred.

PAV_m levels were often higher at site 1 (the most proximate site to the inputs from the southern tributaries) than at site 2, the other shelf site (Figure 5-21b). Major (one to two orders of magnitude) increases in PAV_m were resolved for these sites in response to the early July runoff event and the early August event (particularly for site 1). Additional positive responses were resolved in late July and early September. The general gradient effect from the southern tributary inputs was also observed though less continuously, in comparison with the temporal patterns of sites 2 and 3 (Figure 5-21c). PAV_m levels were distinctly lower at site 3 from early April until mid-June, when concentrations converged during a lower runoff interval. Site 2 levels were much higher soon after the early July runoff event. Less dramatic differences persisted for much of July (Figure 5-21c).

The temporal patterns converged for the three pelagic sites indicating spatial uniformity over this portion of the lake during the study. However, strong temporal variations were observed (Figure 5-21d) that demonstrated clear couplings to the timing of runoff events (Figure 5-21a). These responses were most clearly resolved from the more frequent site 3 observations. Lake-wide increases of about one order of magnitude were observed in response to the runoff events of early July, late July, early August, and early September (Figure 5-21d). Clearly, the upper waters of Cayuga Lake are highly responsive to sediment inputs. Accordingly, the dynamics of PAV_m and other related water quality attributes (e.g., light-scattering, turbidity, Secchi depth, and particulate P) are influenced by input received from runoff events. The timing and magnitude of these effects are driven by those same features of runoff events, that have generally a stochastic type variability.

A temporal analysis is presented here for a shorter time scale of a single month, August of 2013, that includes the single largest runoff event of the study period (peak flow on August 9). The minerogenic particle populations of the near surface waters were sampled on eight occasions over that month at sites 1, 2 and 3. Temporal patterns of PAV_m partitioned into four size classes are considered for each of these sites, and partitioned according to the four size classes (Figure 5-22) specifically PAV_m values associated with each of size classes and their contributions to total (summed) PAV_m are presented. The focus is on the effects of such events (Figure 5-22a). The goals include: (1) basic characterization, and (2) potential insights into processes influencing the observed dynamics.

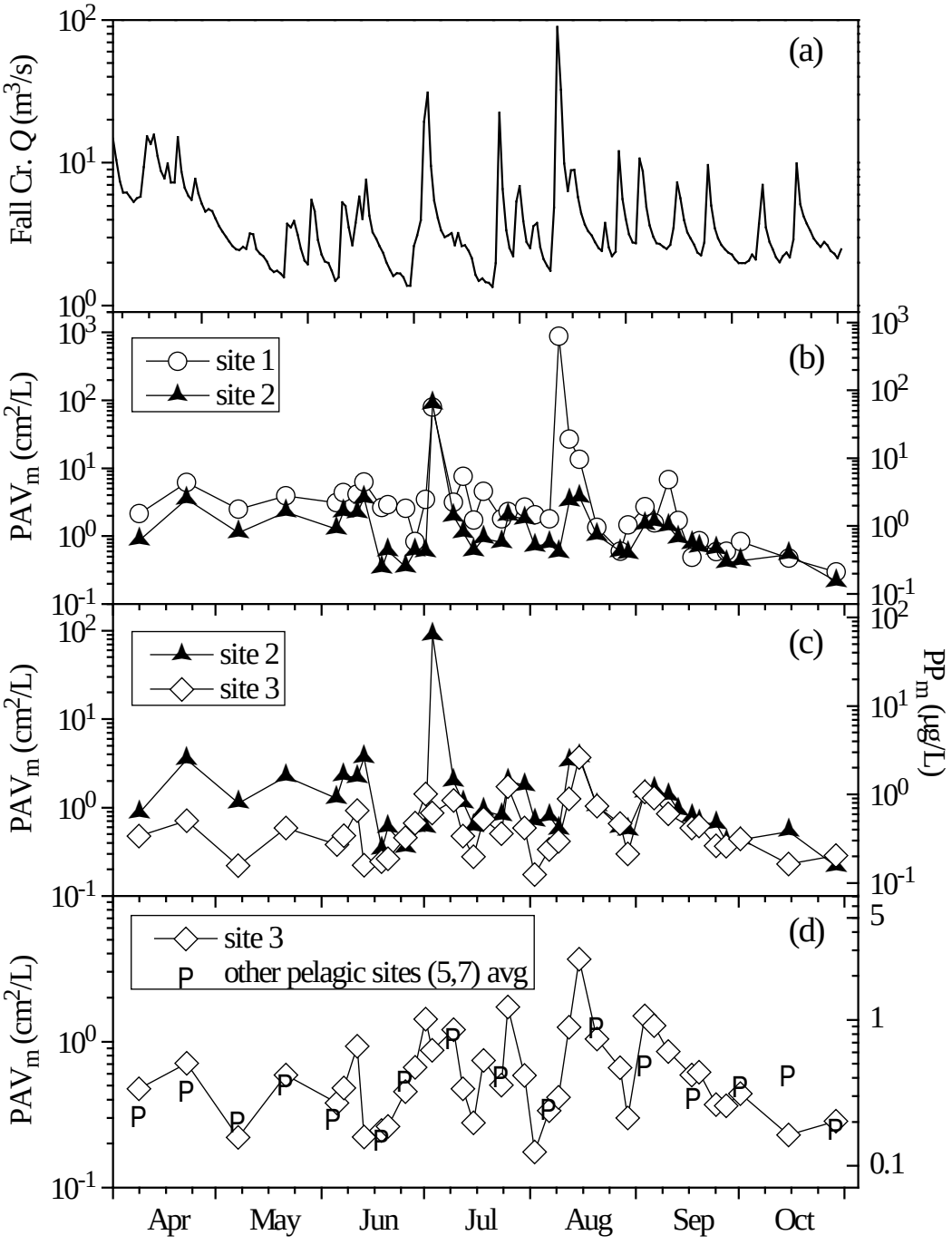

Figure 5-21. Time series for the April–October interval for the upper waters of Cayuga Lake in 2013: (a) daily average stream flow (Q) in Fall Creek, (b) PAVm at sites 1 and 2, (c) PAVm at sites 2 and 3, (d) PAVm at site 3, averages for sites 5 and 7 included for comparison. Y-axis on the right side in (b)–(d) indicates estimated levels of particulate phosphorus associated with minerogenic particles.

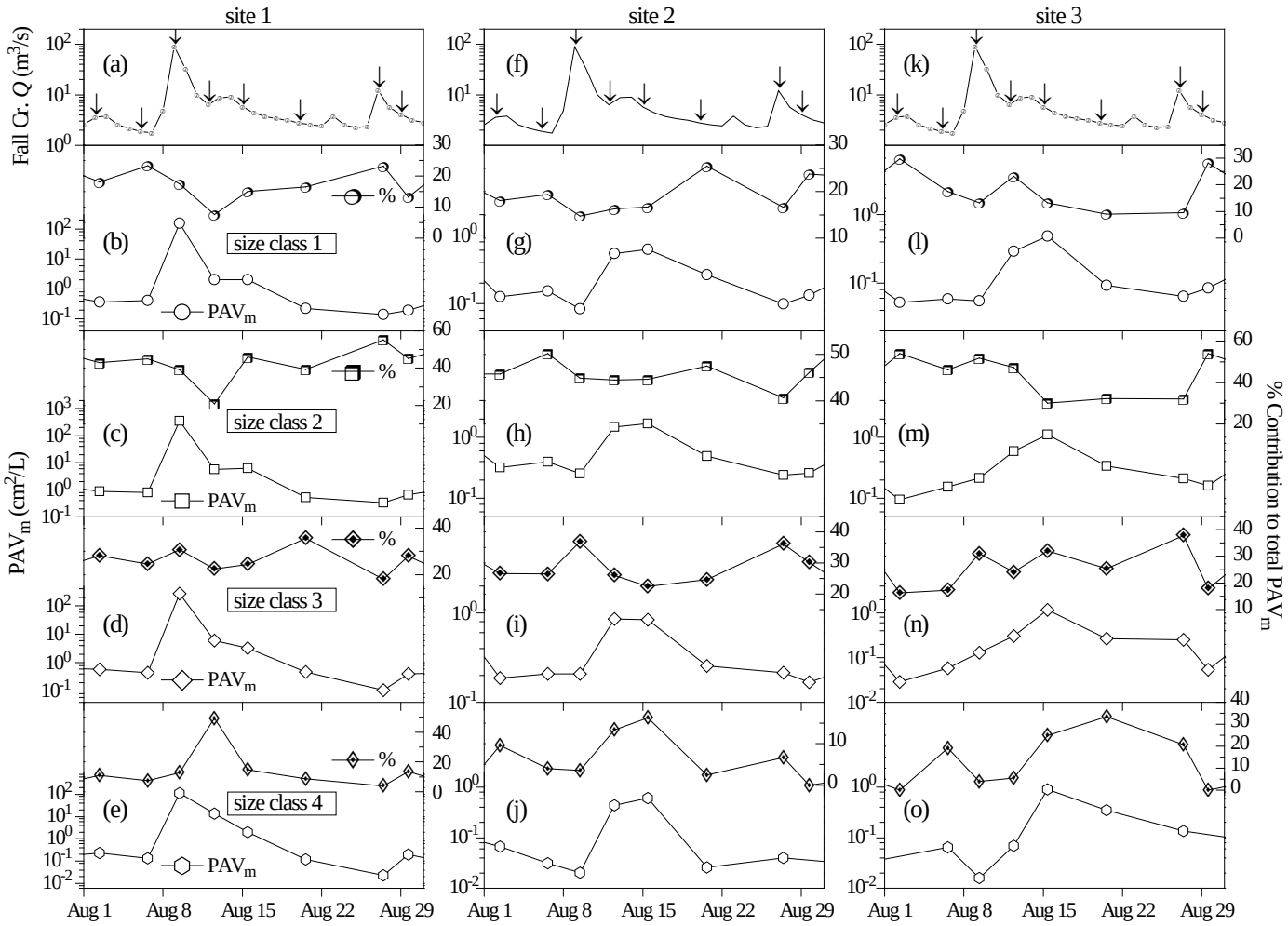

Figure 5-22. Time series for the upper waters of Cayuga Lake in 2013for the month of August in 2013, daily average stream flow (Q) in Fall Creek and PAVm for four size classes and their contributions to the total PAVm (Y-axis on the right), for three sites: (a) Fall Creek Q, (b)–(e) PAVm in size classes 1–4 and their relative contributions to total at site 1; (f)–(j) same as (a)–(e), but for site 2; and (k)–(o) for site 3.

The lowest PAV_m levels for each of the size classes at all the sites were observed before the event and twelve to eighteen days after the event, during low runoff intervals (Figure 5-22). The highest PAV_m values were observed at site 1 for all four of the size classes, proximate to the tributaries, the day of the runoff peak (Figure 5-22b-e). Increases at sites 2 and 3 were not observed until the next sampling, four days later (Figure 5-22g-j, l-o; August 13). Peak concentrations at site 3, that were two to three orders of magnitude lower than the peaks at site 1, were observed another two days later (Figure 5-22l-o; August 15). This temporal progression depicts a general movement of the particles delivered during the event by the tributaries through the shelf and subsequently pelagic waters. The three smallest of the four size classes all made noteworthy contributions at site 1, the day of the peak inflow and PAV_m, with the largest size class making only a minor contribution (Figure 5-22a-e). By the following sampling day (August 13) the apportionment of contributions from the four classes had shifted dramatically. The single largest contributor (~ 50%) instead was the largest class, with compensating decreases by the two smallest size classes (Figure 5-22b-e). This shift is consistent with the effects of the operation of particle aggregation processes, as there was no shift to increased relative contribution by this size class in the inputs delivered by the tributaries. The timing of this signature of aggregation is consistent with that of increased PAV_m, as increased particle concentrations are expected to lead to increased particle collisions that promote coagulation. Similar, though somewhat diminished, and delayed, aggregation signatures were observed for both site 2 (Figure 5-22g-j) and site 3 (Figure 5-22l-o). These patterns suggest that the decreases in PAV_m observed in the lake, following increases caused by runoff events, are not only driven by simple size-dependent deposition, but are also influenced by aggregation processes. Time series of percent contributions of the four size classes to PAV_m are presented in a cumulative format, extending progressively from the mouth of Fall Creek (Figure 5-23a), through the shelf sites (Figure 5-23c and d), to pelagic site 3 (Figure 5-23e). The most conspicuous changes in the distributions among the four size classes appear to have been linked to runoff events. These were coincident with the events at the stream mouth and nearly so at the nearby site 1 on the shelf. Responses were more delayed further off-shore at site 2, and even more so for pelagic site 3. The general decrease of the contribution of the largest size class (> 11 µm) from the stream to the lake is depicted, consistent with local size-dependent deposition losses. The strongest potential aggregation signature appears to be the mid-August increase in this size class at site 3 (Figure 5-23e), that followed the early August major runoff event.

5.1.3.3. Water Quality Implications of Minerogenic Particles: 1999-2006

Minerogenic particles have substantial water quality implications, and specifically for the P-eutrophication issue for Cayuga Lake. These particles influence optical metrics of water quality, including SD, Tn and $\boldsymbol{c}_{660}$_f (a surrogate metric of the light scattering coefficient, *b*). Moreover, P is commonly associated with these particles. Accordingly, these particles interfere with simplistic assumptions that SD measurements and concentrations of P are regulated entirely by

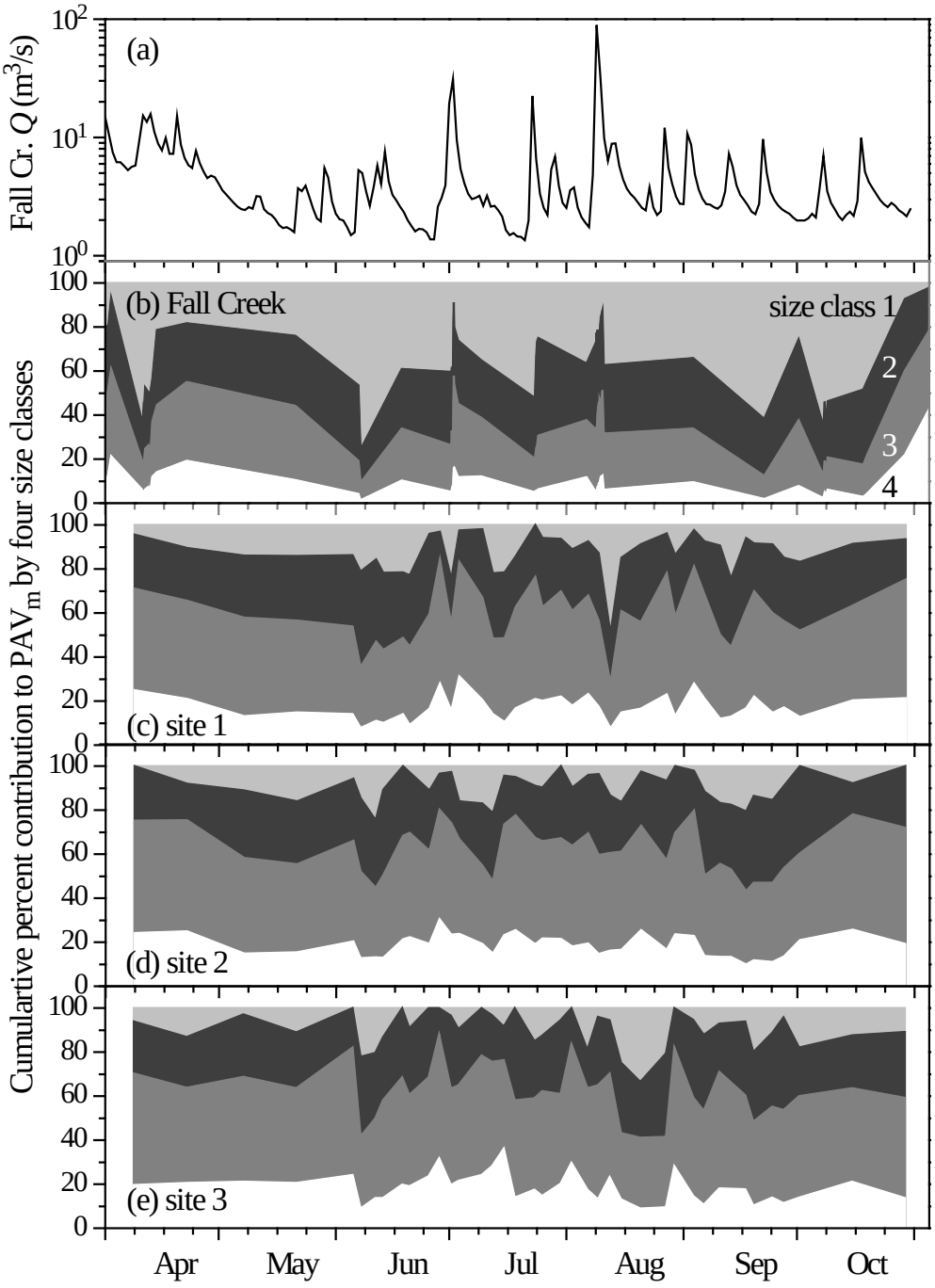

Figure 5-23. Time series for Fall Creek and the upper waters of Cayuga Lake in 2013: (a) Fall Creek daily average flow, (b) cumulative percent contributions to PAV_m by four size classes in Fall Creek, (c)–(e) cumulative percent contributions to PAV_m by four size classes in Cayuga Lake, sites 1, 2 and 3, respectively.

phytoplankton. The SAX technology has been applied previously for Cayuga Lake, based on sampling done as part of LSC monitoring over the 1998-2006 period, to characterize this minerogenic particle assemblage and evaluate their role with respect to SD and the TP pool. Particular focus has been directed at the contrasting characteristics of the shelf versus pelagic waters associated with the systematic difference in particle concentrations between these areas.

Two papers, prepared during this project, are included in this report that addressed these issues for Cayuga Lake. The first of these is a long-term study of minerogenic particles that documents the light scattering characteristics of these particles and their associated role in influencing water clarity. Below is a link to a pdf of the manuscript.

The second paper develops protocols to partition the contributions of bioseston and minerogenic particles to particulate P (PP) and turbidity (Tn). The systematically higher Tn and PP levels on the shelf over the 1998-2006 period, particularly following runoff-events, were demonstrated to be a result of elevated PAV_m associated with tributary inputs. The minerogenic component of PP (PP_m) was reported to represent on average 14% of PP in pelagic waters and 23% on the shelf. Below is a link to a pdf of the manuscript.

5.1.3.4. Water Quality Implications of Minerogenic Particles: 2013

The implications of PAV_m levels for contributions to the PP pool have been extended to the conditions of 2013, based on the stoichiometry developed for the lake by Effler et al. (2014); PP_m:PAV_m = 7.10 mg/m^2. The predicted estimates of PP_m (i.e., associated with minerogenic particles) are represented in the context of contributions to PP as the ratio PP_m:PP. Values of PP_m:PP were responsive to tributary inputs on the shelf and in pelagic waters (Figure 5-24). The effects were greatest on the shelf (Figure 5-24b and c) and diminished at pelagic site 3 (Figure 5-24d). The ratio was > 0.2 (i.e., PP_m was greater than 20% of PP) at site 1 for the samplings of April to mid-June (Figure 5-24b). Values of $\geq$ 0.7 were observed on five occasions at that site following runoff events (Figure 5-24a) in mid-May, mid-June, early July, early August, and early September. Two values were greater than 1.0, reflecting overestimates of PP_m for those occasions. These overestimates are not inconsistent with the level of uncertainty for the PP_m:PAV ratio reported by Effler et al. (2014) for individual estimate applications such as those. Better performance was reported on a summer average basis (Effler et al. 2014). A similar form of responsiveness to runoff events was observed further off-shore on the shelf at site 2 (Figure 5-24b), though ratio values were shifted somewhat lower compared with site 1.

This effect of increased minerogenic particle contributions to the PP pool of the lake, particularly after runoff events, extended out into pelagic waters, though the signature was diminished relative to the shelf (Figure 5-24d). The estimated PP_m:PP exceeded 0.15 on four occasions at site 3 in 2013, with timing features that appeared to be linked to runoff events. Some delay was evident relative to the shelf sites, consistent with the time necessary for particles to be transported from tributary inputs to pelagic locations. The diminished effects relative to

Limnol. Oceanogr., 59(2), 2014, 325–339

doi:10.4319/lo.2014.59.2.0325

Long-term study of minerogenic particle optics in Cayuga Lake, New York

Steven W. Effler and Feng Peng *

Upstate Freshwater Institute, Syracuse, New York

Abstract

The dynamics of light scattering by minerogenic particles in the upper waters of Cayuga Lake, New York, were characterized for the spring–autumn interval of 8 yr (1999–2006) at pelagic and nearshore sites with a scanning electron microscope interfaced with automated image and x-ray analyses (SAX). SAX results were used to estimate the minerogenic scattering coefficient (b_m) through Mie theory calculations. SAX–Mie supported a two-component model for particulate scattering (b_p) that included an organic component of scattering (b_o), estimated from a bio-optical model. The credibility of the b_m estimates and the two-component modeling approach was demonstrated through good closure of the modeling results with bulk values of b_p (estimated from measurements of the beam attenuation coefficient at 660 nm). The average of the ratio $b_p : (b_m + b_o)$ was 1.03 (average relative error 19.4%). Two minerogenic particle types were important in regulating the dynamics of b_m—clay minerals that increased in concentration in response to runoff events, and calcium carbonate precipitated mostly on small organic particles during short-term late-summer whiting events. b_m was attributed to particles in the size range of 1–10 μm. Variations in b_m dominated the overall variations in b_p and Secchi disk depth; differences in b_o explained well those observed in b_p during dry weather intervals of low b_m. Higher b_m values, mainly associated with clay mineral particles, were observed at the nearshore site as opposed to the pelagic location; there was a positive linkage between these levels and tributary flow rate.

Light scattering by particles, a fundamental process regulating radiative transfer in water (Kirk 2011), is important in determining apparent optical properties (AOPs, depend on geometry of the light field) of interest, including clarity (Preisendorfer 1986) and the remote sensing signal (Woźniak and Stramski 2004). The total scattering coefficient (b; m^{-1}), corresponding to the integration of the volume-scattering function over all directions (Kirk 2011), quantifies a central feature of the light-scattering regime. b is an inherent optical property, independent of the geometry of the light field. The magnitude and spectral features of the particulate component of scattering, b_p (which greatly exceeds that due to water), depend on multiple attributes of a particle population, including the number concentration (N), the particle size distribution (PSD), the composition of the individual particles and their shapes (Babin et al. 2003).

The particle populations of aquatic ecosystems are heterogeneous, varying in time and space and differing greatly among systems in response to an array of drivers (Stramski et al. 2004, 2007; Peng and Effler 2011). Protocols for resolving the various components of light scattering are needed to understand these differences and dynamics, and to identify their origins and drivers, objectives that are consistent with the reductionist approach advocated by Stramski and co-workers (Stramski et al. 2001, 2004, 2007). Inorganic, or minerogenic, particles are of particular interest in coastal and inland (so-called Case 2) waters because of their relatively greater contributions to b_p, compared with the open oceans (i.e., Case 1; Babin et al. 2003; Bowers and Binding 2006; Woźniak et al. 2010). Minerogenic particles have increasingly been reported to be important in influencing common optical metrics of water quality for inland waters, including Secchi depth (Z_{SD}; Swift et al. 2006; Peng and Effler 2011) and turbidity (Peng et al. 2009*b*; Peng and Effler 2010). These particles have three general origins: terrigenous (allochthonous) inputs (Kirk 1985; Peng et al. 2009*b*), re-suspension (Peng and Effler 2010), and autochthonous production (Weidemann et al. 1985).

The reductionist approach has recently been advanced (Peng et al. 2009*a*) through forward estimates of the minerogenic component(s) of b_p (i.e., b_m) for inland waters based on an individual particle analysis technique, scanning electron microscopy interfaced with automated image and x-ray analyses (SAX). SAX measures the light-scattering attributes of minerogenic particles (N, PSD, elemental x-ray composition, and shapes) that serve as inputs (exclusive of shape) to Mie theory calculations of the scattering efficiency factor ($Q_{bm,i}$) for the individual particles (Peng and Effler 2007). The estimates of b_m are made according to

$$b_m(\lambda) = \frac{1}{V}\sum_{i=1}^{N_m} Q_{bm,i}(m_i,\lambda,d_i)\mathrm{PA}_{m,i} \qquad (1)$$

where V is the sample volume, N_m is the number of minerogenic particles in a sampled volume of water, and $\mathrm{PA}_{m,i}$ is the projected area (m^2) of minerogenic particle i. $Q_{bm,i}$ depends on the complex refractive index (m_i, function of composition) and size (d_i) of the particle, and the wavelength of light (λ). This SAX–Mie approach supports further partitioning of b_m into contributions according to size and particularly composition (e.g., clay minerals, quartz, and calcite) of particles (Peng and Effler 2010, 2011).

Early research with the SAX–Mie approach had appropriately focused first on testing the credibility of the forward estimates of b_m for a range of particle assemblage conditions (*see* review of Peng and Effler 2012), before

* Corresponding author: fpeng@upstatefreshwater.org

Click here to load long-term minerogenic particle manuscript

Article

Partitioning the contributions of minerogenic particles and bioseston to particulate phosphorus and turbidity

Steven W. Effler, Anthony R. Prestigiacomo*, Feng Peng, Rakesh Gelda, and David A. Matthews
Upstate Freshwater Institute, PO Box 506, Syracuse, NY 13214
** Corresponding author email: tonyp@upstatefreshwater.org*

Received 19 August 2013; accepted 8 January 2014; published 17 April 2014

Abstract

Protocols to partition the contributions of bioseston and minerogenic particles to turbidity (T_n) and particulate phosphorus (PP), as described by summations of the 2 components, are developed, tested, and applied. The analysis is based on coincident observations of T_n, PP, chlorophyll *a* (Chl), and the summation of the projected areas of individual minerogenic particles per unit volume (PAV_m) for the wide variations encountered in time and between near-shore and pelagic sites over an 8-year study of Cayuga Lake, New York. PAVm was determined from an individual particle analysis technique, scanning electron microscopy interfaced with automated image, and X-ray analyses (SAX). The partitionings are based on a stoichiometric approach that adopts Chl and PAV_m as the metrics of bioseston and minerogenic particles, respectively, and estimates developed here for stoichiometric ratios that relate T_n and PP to these 2 components. The systematically higher T_n and PP levels at the near-shore site, particularly following runoff events, are demonstrated to be a result of elevated PAV_m associated with allochthonous inputs. A reasonably good match of the partitioned 2-component summations with bulk observations is reported. Application of the 2-component PP model establishes minerogenic particles made, on average, noteworthy (~10%) to substantial (≥20%) contributions to PP. The minerogenic particle component of PP was largely responsible for the greater summer average total phosphorus (TP) concentrations at the near-shore versus the pelagic site, the interannual variations in the differences between these sites, and exceedance of the TP water quality limit at the near-shore site. Minerogenic particles were the dominant component of T_n, a finding that is demonstrated to be consistent with optical theory, based on the much greater efficiency of side-scattering for minerogenic versus organic particles.

Key words: bioavailability, bioseston, minerogenic particles, particulate phosphorus, stoichiometry, turbidity

Introduction

Minerogenic (inorganic) particles play important ecologic and water quality roles in aquatic ecosystems by presenting reactive surfaces (O'Connor 1988, Hupfer et al. 1995), affecting the concentrations and stoichiometry of particulate constituents (Hecky et al. 1993, Effler et al. 2012), influencing metabolic activity (Phlips et al. 1995), contributing to net sedimentation (Bloesch 2004), and degrading optical water quality through the process of light scattering (Kirk 1985, Peng and Effler 2011). Sources of these particles to the water columns of lakes and reservoirs include allochthonous inputs from watersheds (Longabucco and Rafferty 1998), autochthonous production of oversaturated mineral phases (Yin and Johnson 1984, Homa and Chapra 2011), and sediment resuspended from bottom deposits (Bloesch 2004, Peng and Effler 2010). Water quality monitoring programs often do not include direct measurement of minerogenic particle assemblages, and those that do have primarily relied on gravimetric measurements: the mass remaining on a filter (per unit volume of sample) after exposure to a high temperature to burn off organic contributions. Such measurements have precision issues

DOI: 10.5268/IW-4.2.681

Inland Waters (2014) **4**, pp. 179-192

Click here to load a pdf of the partitioning of minerogenic particles manuscript

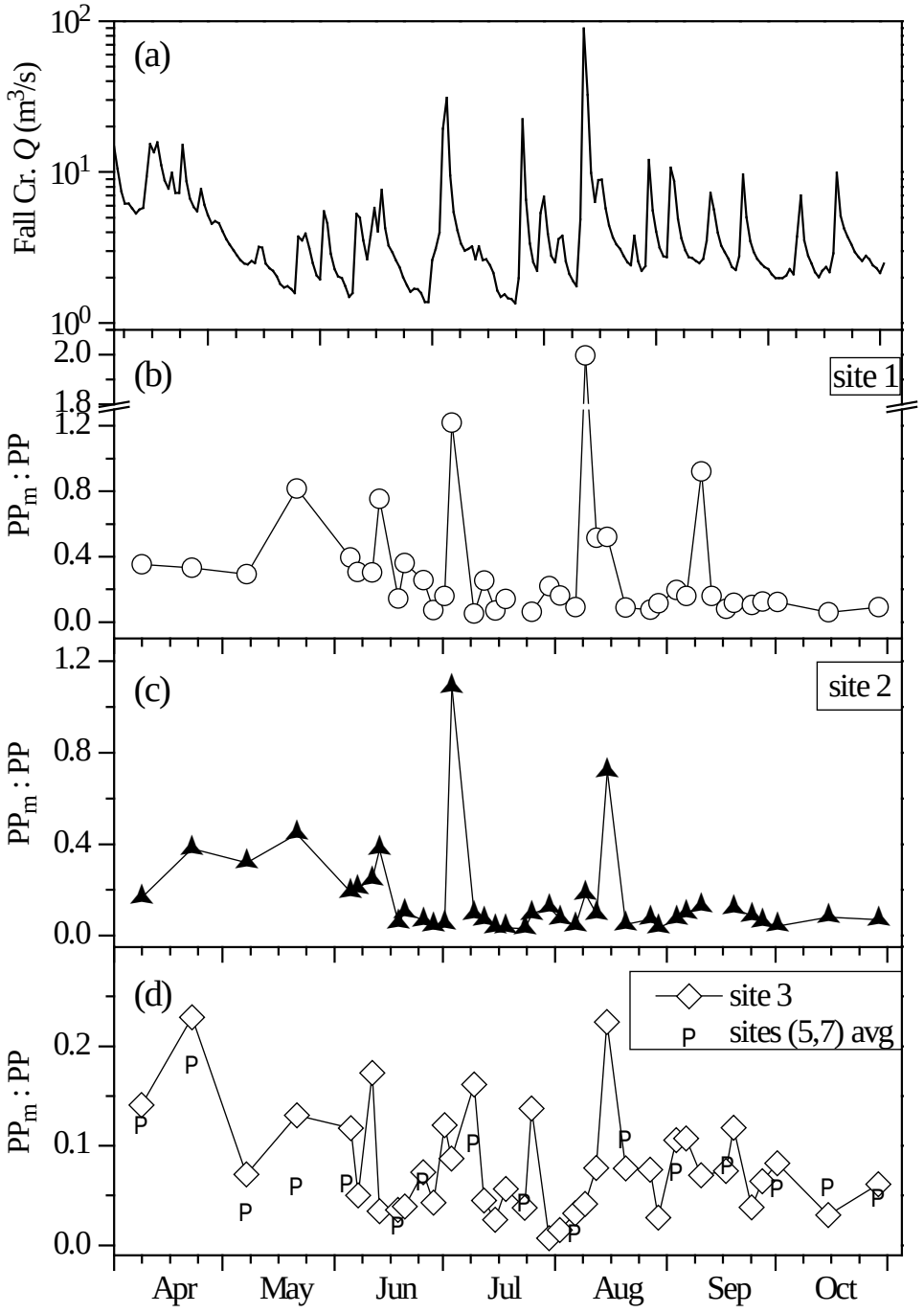

Figure 5-24. Time series for Apr–Oct interval of 2013: (a) daily average stream flow in Fall Creek, (b)–(d) PP_m : PP for sites 1–3, respectively; averages for sites 5 and 7 included in (d) for comparison.

the shelf sites probably reflects both the operation of dilution from mixing with epilimnetic waters and the loss of particles from deposition over the intervening time interval.

Distributions of PP_m:PP for the various sites monitored for PAV_m in 2013 are presented in a histogram format. The mean values were substantially greater than the medians on the shelf (Figure 5-25a and b), indicating strong deviations from normal populations, depicting the extreme effects of the major runoff events. These metrics converged more for the pelagic site (Figure 5-25c). Moreover, differences in the distributions for the various pelagic sites were minor (Figure 5-25c). The important and noteworthy contributions of PP_m to PP on the shelf and in pelagic waters, respectively, particularly after runoff events, supports the position that this contribution needs to be considered when addressing the TP pool and its use as a trophic state metric in this lake.

Effler et al. (2014) used the following two-component summation to partition the contributions of minerogenic particles and bioseston (phytoplankton and its organic particle retinue) to PP

Eq. 5-1. $$PP = PP_m + PP_o$$

where PP_o is the bioseston component of PP. This equation is parameterized using stoichiometric ratios; and adopting Chl-*a* and PAV_m as the independent variables, according to

Eq. 5-2. $$PP = (PP_o{:}Chl\text{-}a)\cdot Chl\text{-}a + (PP_m{:}PAV_m)\cdot PAV_m$$

where the best estimate for PP_o:Chl-*a* was reported to be 1.53.

This two component partitioning was applied to the observations for the summer of 2013 for sites 1, 2 and 3. The summer average TP values for these sites were 35.2, 18.9 and 13.3 µgP/L, respectively (Figure 5-26). The value for shelf site 1 exceeded the New York State guidance value of 20 µg/L. Though TDP levels were greater on the shelf (particularly for site 1) compared to the pelagic site, the differences in PP between these areas of the lake were larger. Similar Chl-*a* concentrations were observed for pelagic and shelf sites (subsequently described in detail, Section 5.2.2). The exceedances of the guidance value on the shelf are demonstrated to be attributable to the high PP_m levels on the shelf (Figure 5-26). This raises questions related to application of a TP guidance value on the shelf, as the intent of such a limit is to protect against cultural eutrophication driven degradation of water quality. Its implementation should be supported by TP being either entirely bioavailable or the bioavailable fraction at least remaining uniform throughout the lake. Neither of these conditions seemed to have prevailed in Cayuga Lake in 2013 (Figure 5-26), nor in other years (Effler et al. 2014). PP_m has been reported to have limited bioavailability elsewhere (DePinto et al. 1981, Young et al. 1985, Auer et al. 1998, Effler et al. 2002, Ekholm and Krogerus 2003). Site-specific assessments have now established this is also the case for the major Cayuga Lake tributaries (Prestigiacomo et al. 2015). These observations, together with the low bioavailability (3%) of PP for a shelf sample collected soon

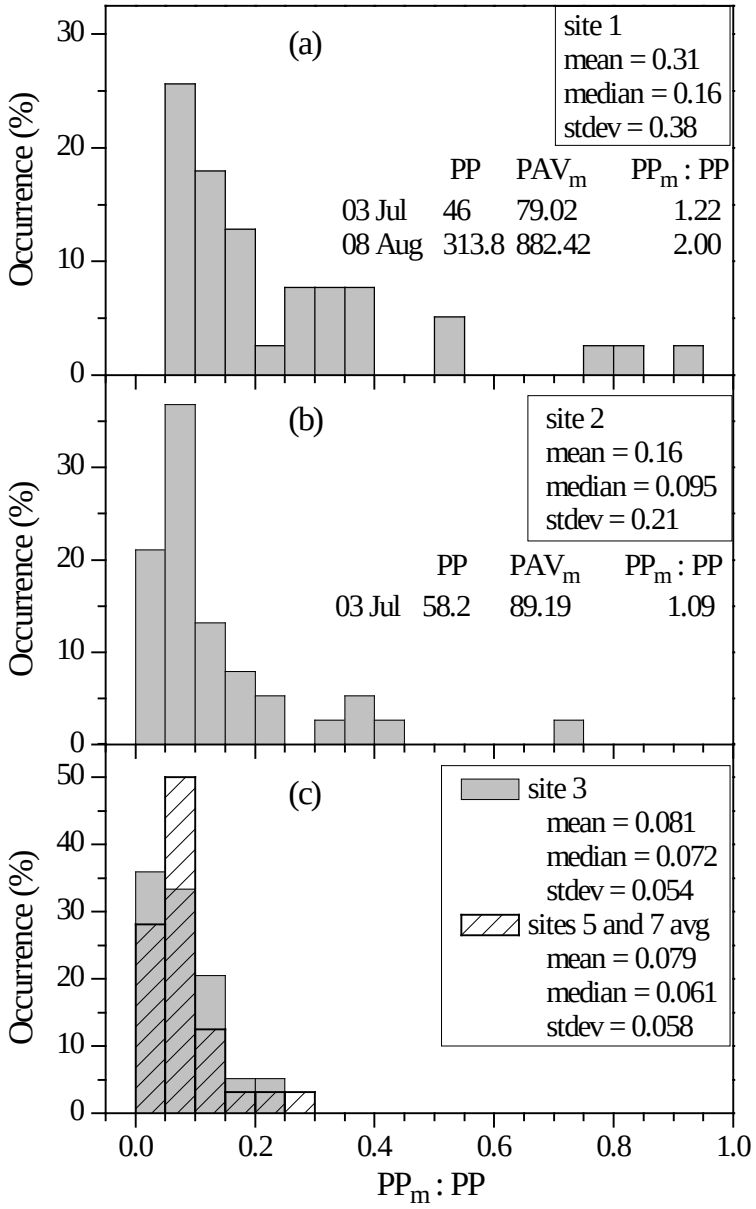

Figure 5-25. Distributions of PP_m : PP for the upper waters of Cayuga Lake in 2013: (a) site 1, (b) site 2, and (c) site 3, compared with sites 5 and 7. Statistics included, with values for days with PP_m : PP > 1.0 listed.

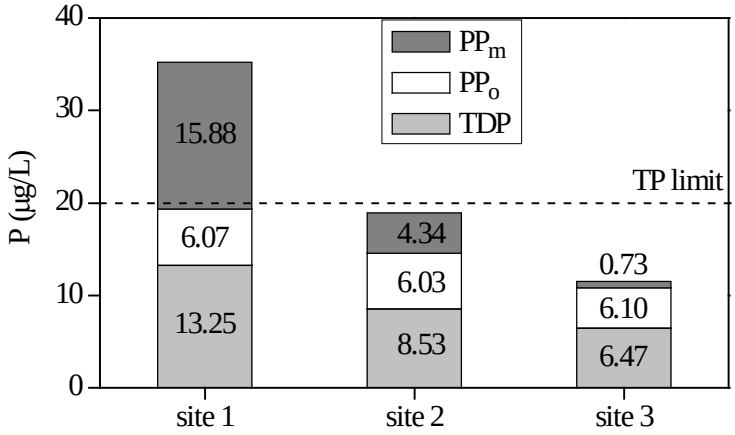

Figure 5-26. Comparisons of summer average TP concentration for the upper waters of Cayuga Lake in 2013 for three sites, partitioned according to contributions of TDP, PP_o and PP_m. TP limit of 20 µg/L included for reference.

after the early July event, establishes the elevated TP concentrations on the shelf following such events are essentially uncoupled from trophic state. Accordingly, such observations should not be integrated into assessments of this area relative to a TP guidance value (Prestigiacomo et al. 2015).

Minerogenic particles have increasingly been reported to be important in influencing common optical metrics of water quality in inland waters, including Secchi depth (Swift et al. 2006, Peng and Effler 2011, Effler and Peng 2014). The effects of these particles as well as organic particles on clarity are mediated by light scattering, as quantified by the light scattering coefficient for particles (b_p, 1/m; Davies-Colley et al. 2003, Effler and Peng 2014). Scattering coefficients considered here are for a wavelength of 660 nm, a commonly adopted reference wavelength (Effler and Peng 2014). A two-component partitioning of b_p has been adopted and successfully tested elsewhere (Peng et al. 2009), and specifically for Cayuga Lake (Effler and Peng 2014), according to

Eq. 5-3. $$b_p = b_m + b_o$$

where b_m is the scattering coefficient for minerogenic particles, and b_o is the scattering coefficient for organic particles. Values of b_m have been estimated by SAX characterizations of the light scattering attributes of minerogenic particles, that serve as inputs to Mie theory

calculations of scattering efficiency for individual particles, and support the estimates of b_m (Effler and Peng 2014). The value of b_m can also be calculated from PAV_m (as determined with SAX) according to

Eq. 5-4. $$b_m = PAV_m \cdot \langle Q_{b,m} \rangle$$

where $\langle Q_{b,m} \rangle$ is the average scattering efficiency factor. Values of $\langle Q_{b,m} \rangle$ have been found to be highly uniform within individual systems and even among different systems; the appropriate value for Cayuga Lake is 2.30 (Effler and Peng 2014).

The b_o component of scattering has been attributed to phytoplankton and their particulate retinue (e.g., bacteria, organic detritus). An empirical bio-optical model based on Chl-*a*, developed by Loisel and Morel (1998), was adopted to estimate b_o in Cayuga Lake by Effler and Peng (2014), and is used here to address the conditions of 2013.

Eq. 5-5. $$b_o = 0.347 \cdot \text{Chl-}a^{0.766} \cdot 0.97$$

The summation of the b_m and b_o estimates was found to close reasonably well with bulk measurements of b_p (Effler and Peng 2014). We have used paired observations of PAV_m and Chl-*a* here to evaluate the effects of minerogenic particles on b_p, and in turn on SD. The dependence of SD on b_p is specified by a system-specific empirical expression presented by Effler and Peng (2014)

Eq. 5-6. $$SD = 0.16 \cdot b_p + 0.004$$

The role of minerogenic particles in influencing b_p and SD is depicted by comparing their predicted distributions for cases that include and exclude the b_m component, for sites 1, 2, and 3. The estimates of b_o and their distributions were quite similar for the three sites (Figure 5-27) because of the similarities of the observed Chl-*a* levels. The estimates of b_p and their distributions were shifted higher by the inclusion of b_m. The effect increased moving from the pelagic site 3 (Figure 5-27c) onto the shelf (Figure 5-27a and b; site 2 first, followed by site 1) toward the tributary sources of allochthonous minerogenic particles. SD values for the case of exclusion of b_m were similar for the three sites (Figure 5-28) because of the uniformity of b_o (i.e., Chl-*a*). These values generally exceeded the depth of site 1 and often also the depth of site 2, but these conditions do not compromise the intent of the analysis to depict the general effects on clarity of b_m. Inverse patterns were predicted for SD compared with that for b_p (Figure 5-27 and 5-28), consistent with the relationship between SD and b_p (see Eq. 5-6). Values of SD and their distributions shifted lower by the inclusion of the effects of b_m. This effect was the least at the pelagic site, but became greater on the shelf, with the largest decreases in SD on the shelf (site 1), proximate to the tributaries.

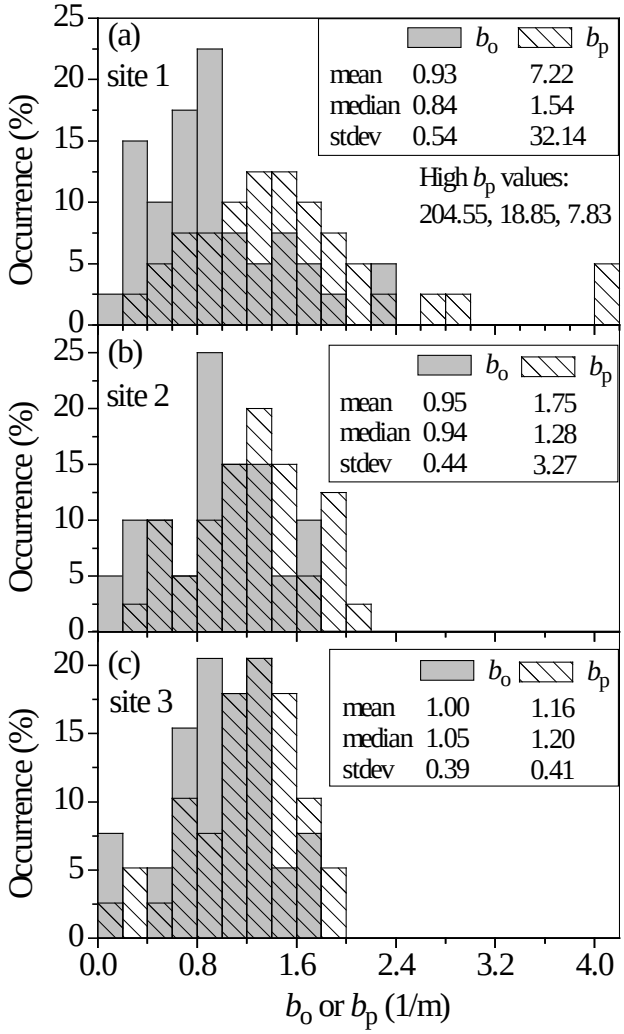

Figure 5-27. Predicted distributions of b_o and b_p (b_o + b_m) for the upper waters of Cayuga Lake in 2013 based on observations of Chl-*a* and PAV_m for 2013, with statistics: (a) site 1, (b) site 2, and (c) site 3.

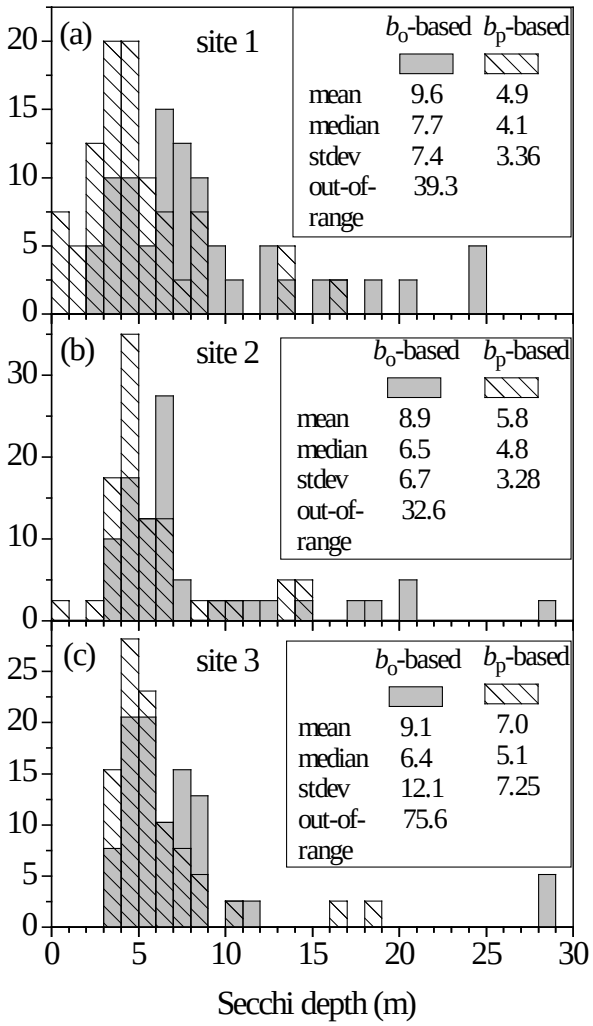

Figure 5-28. Predicted distributions of SD for two cases, b_p due to b_o only, and b_p due to b_o + b_m (b_p = b_o + b_m) for the upper waters of Cayuga Lake based on observations of Chl-*a* and PAV_m for 2013, with statistics: (a) site 1, (b) site 2, and (c) site 3.

Minerogenic particles have previously been demonstrated to play an important role in influencing overall particle optics in Cayuga Lake and related metrics of optical water quality, including SD (Effler and Peng 2014) and Tn (Effler et al. 2014). These particles, supplied primarily from the watershed, have a noteworthy impact on optical metrics of water quality for the pelagic portions of the lake and a major impact on the shelf because of large local inputs from the tributaries. This position is supported by recent system-specific contributions to the literature (Effler and Peng 2014, Effler et al. 2014) as well as the findings for the 2013 program of measurements and the related analyses conducted here.

5.1.3.5. The Relationship Between FSS and PAV_m

While FSS is an acknowledged metric of inorganic suspended solids, it has measurement quality issues at low concentrations that were manifested in the Cayuga Lake data set for pelagic sites (e.g., Figure 5-29a). PAV_m, in contrast, does not suffer from this problem, as these measurements have been demonstrated to be highly consistent with optical observations and pelagic sites (Effler and Peng 2014). No significant relationship was found between paired measurements of FSS and PAV_m at site 5 (Figure 5-29a). In sharp contrast, a linear relationship emerged for these two metrics for the higher FSS concentration range observed on the shelf at site 1 (Figure 5-29b). Accordingly, FSS may be included as a target state variable for the shelf for the interval following runoff events, but not for pelagic areas.

5.1.4. Summary

The use of rapid profiling instrumentation to make vertically detailed measurements of T, $\boldsymbol{c}_{660}$_f, Chl-*a*_f and SC, over time and along the lake's primary axis provided robust signatures of lake processes. Noteworthy signatures resolved from depth-time contour plots for multiple sites included: (1) abrupt changes in SC (decreases) and $\boldsymbol{c}_{660}$_f (increases) on the shelf from runoff events, (2) occurrences of metalimnetic deep chlorophyll maxima (DCM) at pelagic sites, (3) occurrences of interflow signatures at a pelagic site indicating the plunging of a tributary, and (4) summertime epilimnetic decreases in SC depicting entry of diluted tributary inflows associated with the elevated runoff. Signatures manifested in depth-length contours depicted tilting of lake layers from seiche activity, a DCM throughout pelagic waters on certain days, and sediment input (high $\boldsymbol{c}_{660}$_f) from the southern portion of the lake entering pelagic areas.

Patterns of the optical measurements of K_0(PAR), SD and $\boldsymbol{c}_{660}$_f were presented and analyzed. Conditions on the shelf for all three metrics were in general degraded relative to pelagic waters, while differences between pelagic sites were minor. The most degraded conditions on the shelf were observed following runoff events. Some potential for algae growth below the epilimnion (e.g., photic zone deeper) in early summer was indicated, but the potential effect (% of incident light reaching greater depths) is minor. The highest known SD values for Cayuga Lake (~13 m) were observed in the spring of 2013, throughout the pelagic region.

Minerogenic (inorganic) particles have been demonstrated to play important roles in the water quality issues for Cayuga Lake by increasing P concentrations and clarity decreasing, based on earlier (LSC; 1999 -2007) monitoring. A key metric has evolved from individual particle analyses, the projected area of minerogenic particles per unit volume (PAV_m). PAV_m levels were reported in a previous section to be highly correlated with FSS and Tn in the tributaries. PAV_m has been apportioned according to size classes (n = 4) to support water quality modeling for the lake, and according to chemistry (mineral) classes, to establish origins. Inherently terrigenous clay mineral particles dominate in the tributaries, on the shelf, and in pelagic waters. Internally produced (authochthous) calcite ($CaCO_3$) makes a noteworthy contribution, of limited duration (~2 weeks in July or August), at pelagic sites in most years. Most of the PAV_m is associated with particle sizes in the range of 1 to 11 µm. Major abrupt increases in PAV_m occur on the shelf in response to runoff event-driven inputs. While the signatures in pelagic waters are diminished, those responses of increase were clearly manifested in the summer of 2013 after the major runoff events. Relationships between PAV_m and associated P, and b_p and thereby SD (particulate light scattering coefficient), were applied in preliminary analyses to depict the roles of minerogenic particles in influencing these metrics. Minerogenic particles were found to be responsible for the exceedance of the TP guidance values at site1, and the approach to the limit at site 2, in 2013. Water clarity conditions would have been much greater on the shelf, and also event substantially better in pelagic waters, without the contribution of minerogenic particles (PAV_m) to the magnitude of light scattering.

5.2. Laboratory Analytes: Patterns

5.2.1. Data Quality

Analyses of triplicate near-surface samples, collected bi-weekly from site 5, were conducted to assess the representativeness of data considered in the following analyses. Performance is represented by the coefficient of variation (CV) for the analytical results. This metric of data quality includes the effects of both analytical precision and the representativeness of individual samples. The results for the various analytes are presented in tabular form (Table 5-2). The average CV was less than 10% for seven of the twelve analytes (Table 5-2). Low concentrations common to lacustrine waters contributed to the higher CVs for four of the other five analytes for which higher CVs were observed. For example, suspended solids analyses are known to be analytically challenging for most lakes because of low concentrations. The worst performance was for fixed suspended solids (FSS; average CV = 37.3%). Even though detection limit concentrations were often approached for SRP and t-NH_3, reasonably good performance was observed (15.1 and 14.2%, respectively). The performance for the suite of laboratory analytes was good overall. These levels of uncertainty are generally small relative to the temporal and spatial variations described subsequently as noteworthy, supporting the identified patterns as

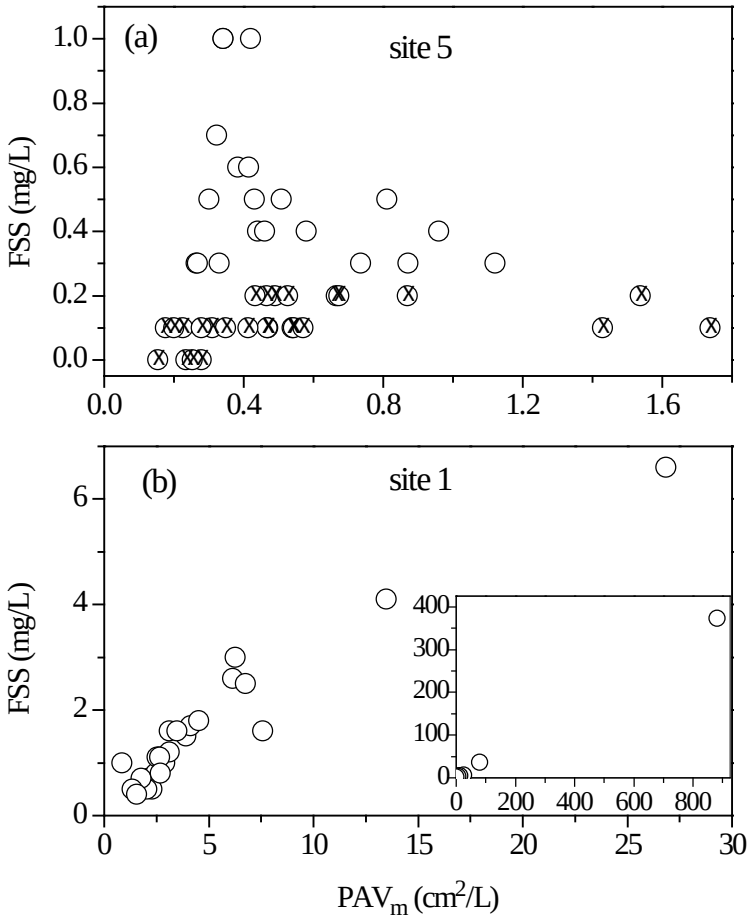

Figure 5-29. Scatter plots of FSS vs. PAV_m for the upper waters of Cayuga Lake in 2013: (a) site 5, uncertain FSS data are marked with '×', and (b) site 1, with inset showing the full data range.

Table 5-2. Performance of Cayuga Lake laboratory triplicates at site 5 for 0 m samples

No.	Analyte	Abbreviation	Number observations	CV (%)
1	dissolved organic carbon	DOC	16	3.8
2	particulate organic carbon	POC	16	13.0
3	chlorophyll *a*	Chl-*a*	16	5.6
4	nitrate + nitrite	NO_X	16	5.3
5	ammonia	t-NH_3	16	14.2
6	total nitrogen	TN	16	10.6
7	total dissolved nitrogen	TDN	11	7.2
8	total phosphorus	TP	16	5.0
9	total dissolved phosphorus	TDP	16	7.4
10	soluble reactive phosphorus	SRP	16	15.1
11	total suspended solids	TSS	16	11.4
12	fixed suspended solids	FSS	14	37.3
13	beam attenuation at 660 nm	c_{660}	16	5.7

real versus potentially manifestations of uncertain measurements.

5.2.2. Spatial Patterns

Spatial patterns are considered through comparisons of the average values for the nine lake sites for two time intervals, the entire study period and summer (as defined by regulators, June-September). Temporal variations are represented by vertical bars with a magnitude of one standard deviation. Flow–weighted (fw) concentrations for the summed four gaged tributaries (~40% of the total inflow), calculated by dividing the estimated total load (for these tributaries) by the total rate of inflow, are presented for the same two intervals (set of bars left of lake concentrations) to provide context for the lake concentrations.

The four measured forms of phosphorus (P) all demonstrated similar spatial patterns (on average, Figure 5-30a-d), with the highest concentrations observed proximate to the tributary inputs on the shelf and decreases at pelagic sites. Differences within the pelagic area (sites 3-8) were minor by comparison. Tributary fw concentrations were much higher than lake concentrations for each of the four forms of P (Figure 5-30a-d), demonstrating the lake acts as a major sink for the P inputs it receives. The tributary concentrations of TP, TDP and SRP were higher in summer compared with the whole study, driven largely by the high overall runoff (multiple large events) over that interval (see Section 3.3). Differences between the two intervals were smaller for these forms of P in the lake. Concentrations were most temporally variable on the shelf. The summer average TP concentrations at sites 1 and 2 exceeded and approached the

guidance value of 20 µg/L, respectively (Figure 5-30a). Concentrations at pelagic sites were decidedly lower. Soluble (e.g., filtrate of 0.45 µm filters) forms of P (TDP) represented roughly 50% of the P (Figure 5-30b). Concentrations of the completely bioavailable SRP were substantially lower than TDP (Figure 5-30c); summer average concentrations at pelagic sites ranged from 1.1 to 1.8. The much greater temporal variability for the entire study period compared to summer reflects the inclusion of the much higher concentrations that prevailed early during spring mixing. Note that TIP is, like SRP, an operationally defined form of P (Clesceri et al. 1998). Accordingly, the detailed composition(s) of the included constituents is somewhat uncertain. TIP represented somewhat less than 50% of TP at all the sites except site 1, where its contribution was greater (Figure 5-30a and d).

Two forms of P calculated as residuals of measured forms, SUP (= TDP – SRP) and PP (= TP – TDP), had some similar spatial features (Figure 5-31a and b) to those directly measured (Figure 5-30). However, the differences between the tributary and lake concentrations of SUP were the smallest of the forms considered (Figure 5-31a). Accordingly, the difference between the shelf and the pelagic sites was also the smallest. The differences between the tributaries and the lake for PP and those between the shelf and pelagic sites were much greater (Figure 5-31b). The higher concentrations for the summer interval reflected the greater inputs from the tributaries during that interval associated with runoff events.

The TP pool can be partitioned as the sum of SRP, SUP and PP. Average concentrations and percent contributions of these three forms of P are presented for sites 1, 2, 3 and the average of the other pelagic sites (4-8) in Table 5-3 for the summer. PP dominates the shelf sites (particularly site 1), while SUP made similar contributions at the pelagic sites. During the summer, SUP was on average ~3 fold greater at the pelagic sites than SRP (Table 5-3).

Silica (as SiO_2) is a key nutrient for diatoms that were prominent members of the phytoplankton community (subsequently, Section 5.4.1.3.1) during the 2013 study period. Concentrations of SiO_2 were several fold greater in the tributary inflow compared to lake levels (on average, Figure 5-32), indicating the lake acts as a major sink for this constituent. This is at least in part associated with uptake of this material by diatoms (incorporated into frustules, Wetzel 2001). Unlike the forms of P, a gradient was manifested in the average values for both time intervals that extended from the shelf northward throughout the pelagic zone. However, the decreasing trajectory within the pelagic zone was modest relative to temporal variations. Lake concentrations for the entire study were, on average, higher than summer levels at pelagic sites, and greater temporal variability was observed for that interval (Figure 5-32). These features reflect the effects of SiO_2 depletion during the spring phytoplankton growth when diatoms were a prominent component of that community.

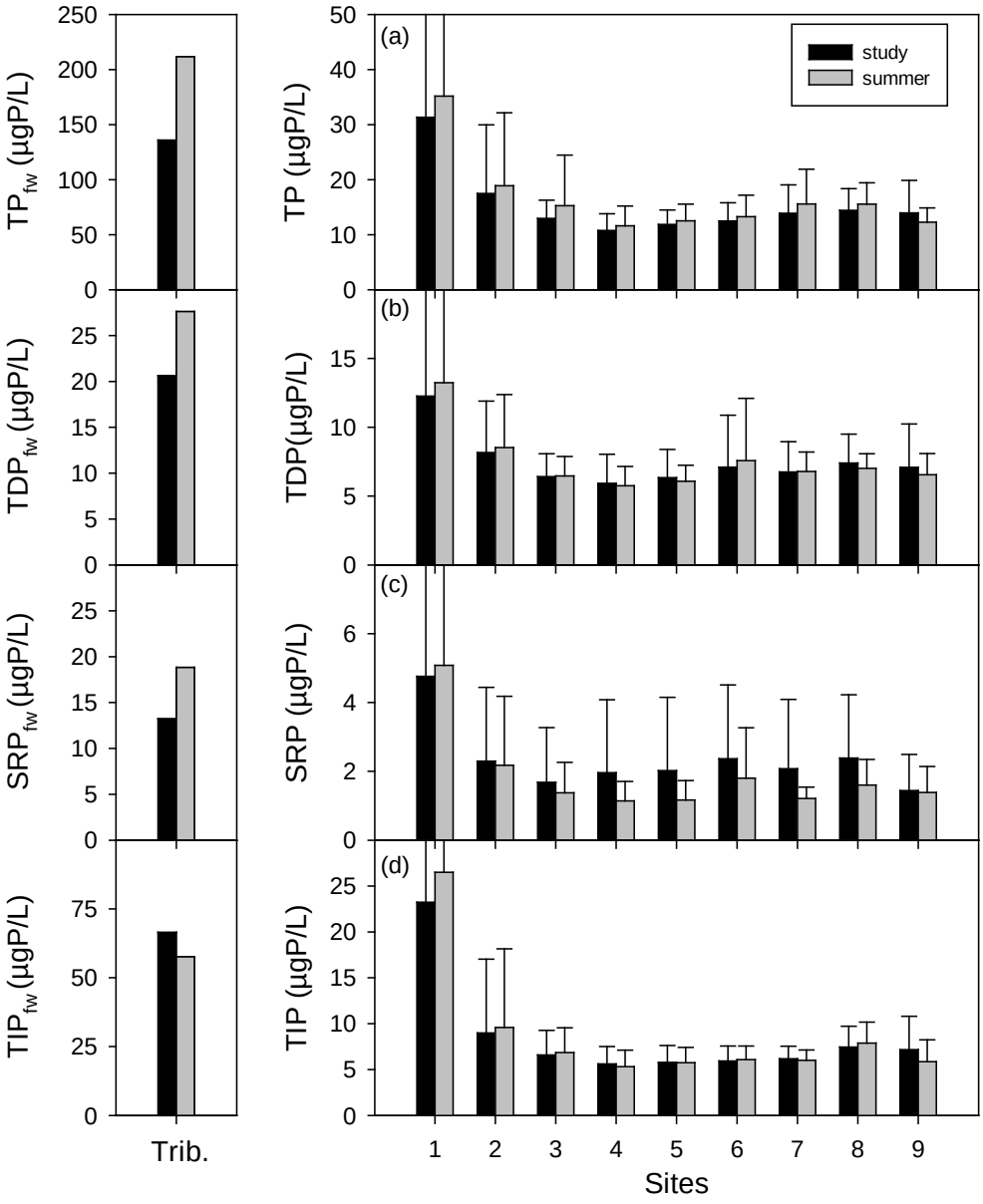

Figure 5-30. Spatial patterns for Cayuga Lake as average values at nine sites for two intervals in 2013, the entire study and summer (Jun-Sept.): (a) TP, (b) TDP,(c) SRP, and (d) TIP. Flow weighted concentrations for the four USGS gaged streams are presented (on the left) for comparison to in-lake concentrations. Temporal variability represented by one standard deviation bar.

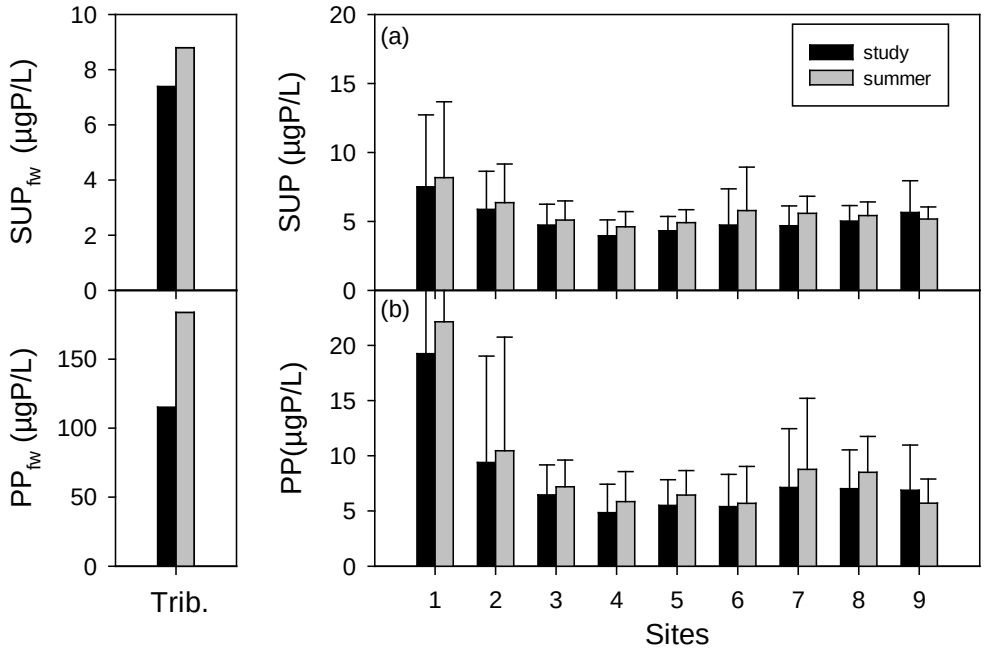

Figure 5-31. Spatial patterns for Cayuga Lake as average values at nine sites for two intervals in 2013, the entire study and summer (Jun-Sept.): (a) SUP, and (b) PP. Flow weighted concentrations for the four USGS gaged streams are presented (on the left) for comparison to in-lake concentrations. Temporal variability represented by one standard deviation bar.

Table 5-3. Average concentrations and contributions of P fractions to TP for entire study and summer for Cayuga Lake in 2013, for site 1, site 2, site 3 and the average of sites 4-8.

Component	Sites															
	1				2				3				4-8 avg.			
	season		summer		season		summer		season		summer		season		summer	
	µgP/L	%	µgP/L	%	µgP/L	%	µgP/L	%	µgP/L	%	µgP/L	%	µgP/L	%	µgP/L	%
SRP	4.8	15	5.1	14	2.3	13	2.2	12	1.7	13	1.4	10	2.2	17	1.4	10
SUP	7.5	24	8.2	23	5.9	34	6.4	34	4.8	37	5.1	37	4.5	36	5.3	38
PP	19.3	61	22.2	63	9.4	54	10.5	55	6.5	50	7.2	52	6.0	47	7.1	51

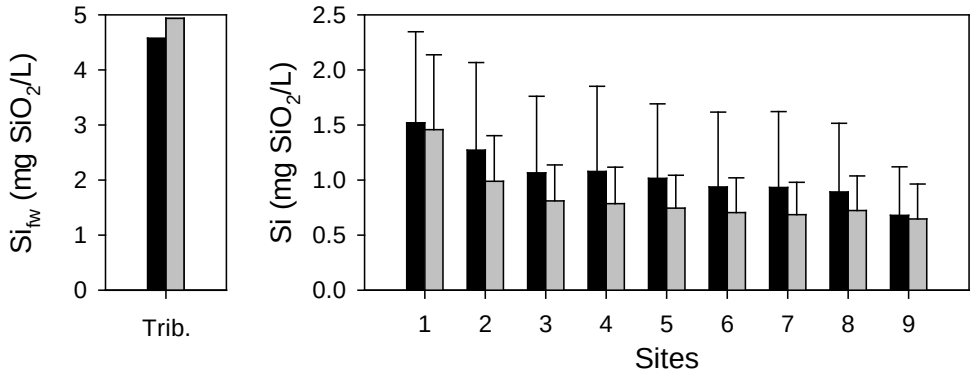

Figure 5-32. Spatial patterns for Cayuga Lake as average values at nine sites for two intervals in 2013, the entire study and summer (Jun-Sept.) for Si. Flow weighted concentrations for the four USGS gaged streams are presented (on the left) for comparison to in-lake concentrations. Temporal variability represented by one standard deviation bar.

Nitrogen (N) is another critical nutrient for supporting primary production, and in certain systems is the limiting nutrient (Wetzel 2001). Spatial distributions of four forms of N measured in Cayuga Lake in 2013 are presented, ammonia (total, t-NH_3: Figure 5-33a), the combination of nitrate and nitrite (NO_X; Figure 5-33b), total dissolved N (TDN; Figure 5-33c), and total N (TN; Figure 5-33d). Nitrate (NO_3^-) generally dominates NO_X (Wetzel 2001). Two of these forms can be taken up by algae to support growth, t-NH_3 and NO_3^-; t-NH_3 is generally favored for energetic reasons. However, t-NH_3 concentrations were relatively low in Cayuga Lake (Figure 5-33a), at levels that utilization of NO_3^- would be expected (Wetzel 2001). The flow weighted t-NH_3 concentrations of the tributaries were similar to those of the lake, except the high concentrations at site 1, that probably reflect local inputs from the two WWTPs. Strong spatial differences were not observed among the other sites. Concentrations of NO_X remained much higher in the lake, and on average approached 1000 µgN/L (1 mgN/L; Figure 5-33b). These concentrations substantially exceed levels considered limiting to algae growth (Reynolds 2006). These high lake concentrations reflect the effects of the high levels in the tributary inputs (Figure 5-33b), associated in large part with agricultural inputs (Haith et al. 2012). Lake concentrations of TDN demonstrated a similar spatial uniformity (Figure 5-33c) to that observed for NO_X (Figure 5-33b), with an average of ~1250 µN/L. The level of dissolved organic N (DON) can be estimated by subtraction of the

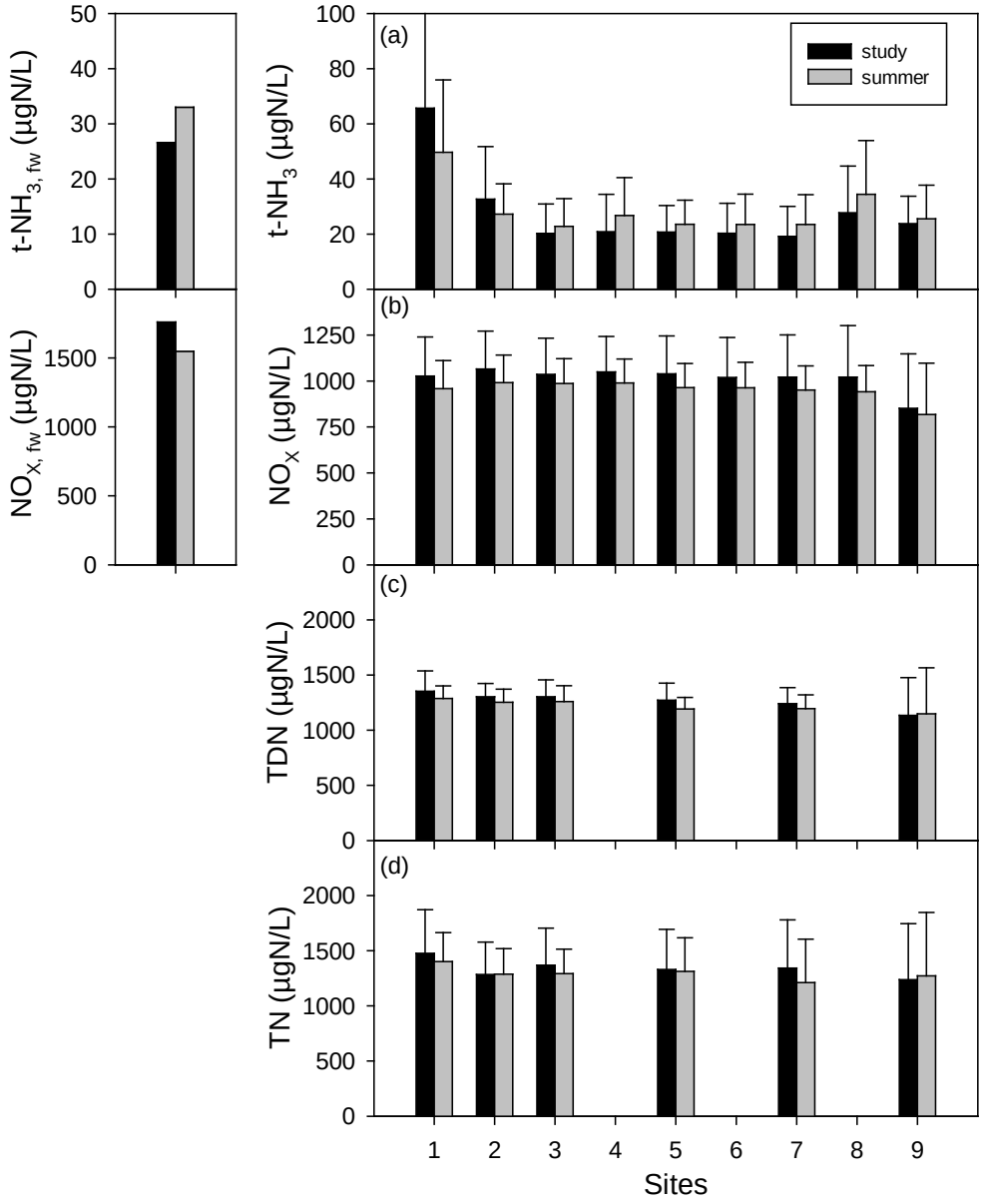

Figure 5-33. Spatial patterns for Cayuga Lake as average values at nine sites for two intervals in 2013, the entire study and summer (Jun-Sept.): (a) t-NH_3, (b) NO_X, (c) TDN, and (d) TN. Flow weighted concentrations for the four USGS gaged streams are presented (on the left) for comparison to in-lake concentrations. Temporal variability represented by one standard deviation bar.

sum of NO_X and t-NH_3 from TDN (DON = TDN-(NO_X + t-NH_3)). Accordingly, DON was, on average, about 250 µgN/L. Levels of TN were generally greater than TDN by only a relatively small margin, but more variable (Figure 5-33d), making estimates of particulate N based on the residual calculation (= TN-TDN) unreliable.

Organic carbon is important to lake metabolism (Wetzel 2001). The labile portion of the dissolved organic C (DOC) pool supports heterotrophic activity by aquatic bacteria. This form of metabolism can exceed primary production in certain lakes, a situation described as net heterotrophy (Hanson et al. 2003). Tributary fw DOC concentrations were roughly 5 to 6 mg C/L, about 2-fold higher than lake levels (Figure 5-34a), depicting the functioning of the lake as a sink, consistent with the utilization of the labile fraction of the external load by heterotrophs within the lake. Average concentrations of DOC were slightly greater at site 1 proximate to the tributary inflows; otherwise levels were relatively uniform throughout the upper waters of the lake, with only minor temporal variability. Particulate organic C is used as a metric of biomass (Wetzel 2001), though organic detritus may also contribute. The higher POC concentrations, on average, at the shelf sites (Figure 5-34b), and the particularly high levels observed irregularly at site 1, were consistent with detrital C contributions from the tributaries. This position was further supported by the absence of higher chlorophyll *a* (Chl-*a*) concentrations at those sites compared to pelagic areas (Figure 5-34c). Temporal variations in POC (Figure 5-34b) were relatively much greater than for DOC, though similar to Chl-*a* (Figure 5-34c). Despite the local inputs of P, and the higher concentrations of bioavailable dissolved forms (Figure 5-30b and c), locally higher levels of Chl-*a* were not manifested for the shelf (Figure 5-34c). Average Chl-*a* concentrations were less than 5 µg/L at all sites, and the values were distinctly lower at site 9. This lack of a longitudinal differences between the shelf and pelagic sites represents a strong contrast to the spatial patterns observed for various constituents that are received from the southern tributaries in elevated concentrations.

Spatial patterns of metrics of sediment and turbidity are represented for four related parameters, total suspended solids (TSS; Figure 5-35), fixed (or inorganic) suspended solids (FSS; Figure 5-35b), volatile (organic) suspended solids (VSS; Figure 5-35c), and turbidity (Tn; Figure 5-35d). TSS and Tn are generally found to be positively correlated. Generally fw tributary levels were about an order of magnitude greater than average shelf values, and even greater margins prevailed based on comparisons with pelagic sites. Levels on the shelf and at site 9, another shallow area, were substantially greater than in pelagic waters (Figure 5-35 a, b and d), except for VSS (Figure 5-35c) for which only the site 1 values were substantially greater. Concentrations in pelagic waters were, on average relatively uniform. TSS levels in the tributaries were dominated by FSS (> 90%, on average). In contrast, VSS levels (Figure 5-35c) were greater than FSS concentrations, on average, at the pelagic sites. The lake is a major sink for TSS (sediment), and associated Tn.

The spatial distributions of site average conditions for 2013 are presented for the three widely used trophic state metrics together, TP (Figure 5-36a), Chl-*a* (Figure 5-36b), and SD

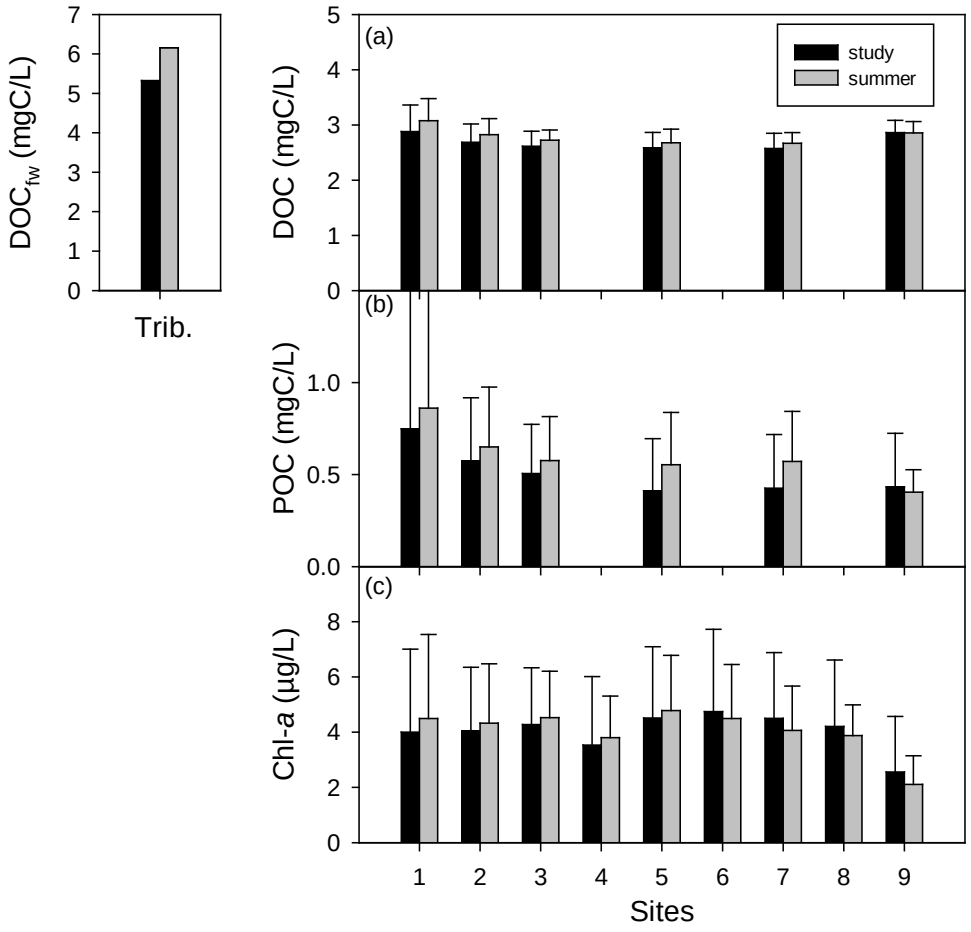

Figure 5-34. Spatial patterns for Cayuga Lake as average values at nine sites for two intervals in 2013, the entire study and summer (Jun-Sept.): (a) DOC, (b) POC, and (c) Chl-*a*. Flow weighted concentrations for the four USGS gaged streams are presented (on the left) for comparison to in-lake concentrations. Temporal variability represented by one standard deviation bar.

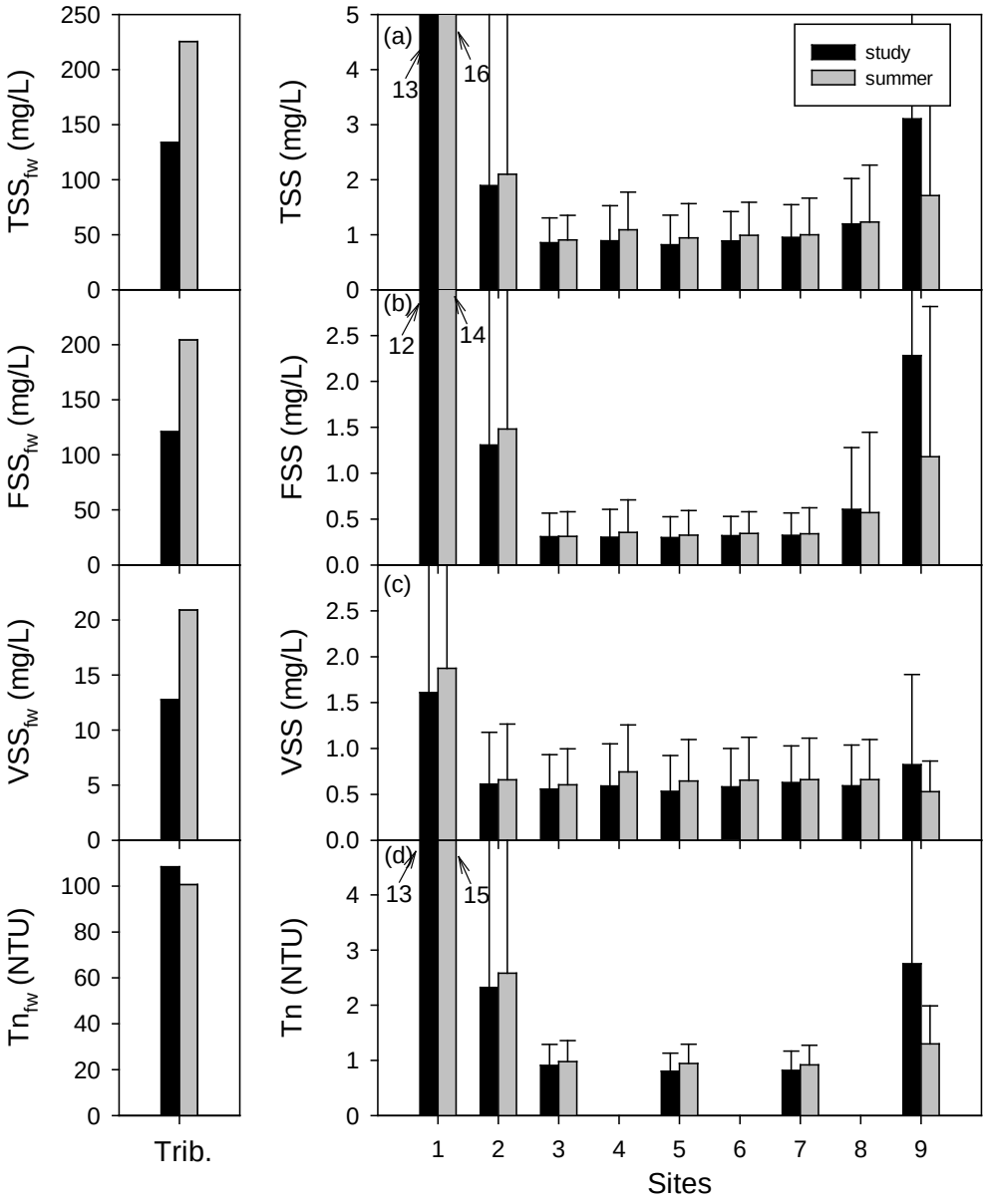

Figure 5-35 Spatial patterns for Cayuga Lake as average values at nine sites for two intervals in 2013, the entire study and summer (Jun-Sept.): (a) TSS, (b) FSS, (c) VSS, and (d) Tn. Flow weighted concentrations for the four USGS gaged streams are presented (on the left) for comparison to in-lake concentrations. Temporal variability represented by one standard deviation bar.

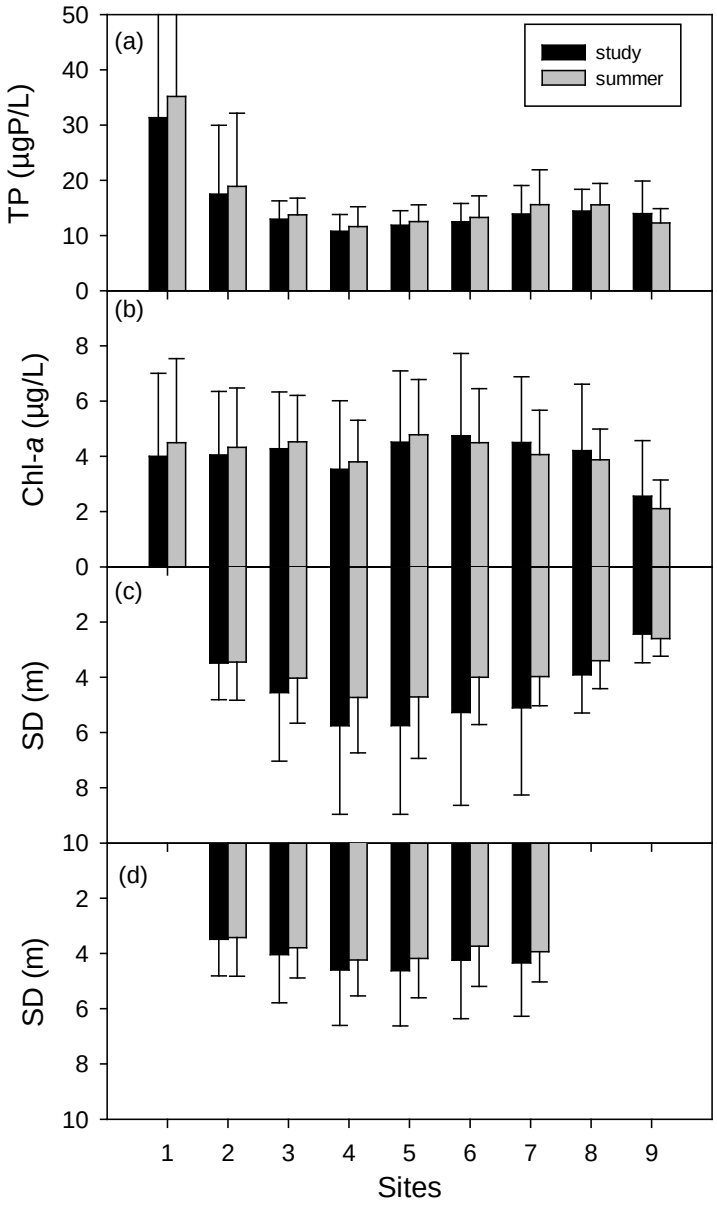

Figure 5-36. Spatial patterns for Cayuga Lake as average values at nine sites for two intervals in 2013, the entire study and summer (Jun-Sept.): (a) TP, (b) Chl-*a*, (c) SD, and (d) SD for all sites only for days when the SD at site 2 was not on the bottom (3 days dropped). Temporal variability represented by one standard deviation bar.

(Figure 5-36c). Each of these have been presented previously. These appear again here to provide a more complete representation of the various trophic state indicators, and to identify the extent of consistency amongst the three patterns. Unifying consistent indications of degraded eutrophication – based conditions on the shelf are not manifested. While TP concentrations are distinctly higher (Figure 5-36a) and SD values lower (Figure 5-36c) on the shelf, Chl-*a* levels are not significantly different on the shelf relative to pelagic sites (Figure 5-36b). A more direct and fair comparison of shelf SD to other sites is presented (Figure 5-36d) for which observations on days the disk was seen on the bottom at site 2 were deleted from the populations of observations for the other sites. This adjustment did not alter the basic observation that SD was lower on the shelf. The lack of higher Chl-*a* levels on the shelf relative to pelagic waters is a recurring feature for the lake that has been reported previously (Effler et al. 2010). The high flushing rate of the shelf relative to phytoplankton growth rates has been identified as contributing to this lack of locally higher phytoplankton biomass (Effler et al. 2010). Moreover, elevated concentrations of inorganic P-containing particles received from the local tributary inputs have been identified as contributing to both high TP and low SD on the shelf, that compromises these parameters as indicators of trophic state. These effects are exacerbated following runoff events because of the elevated amount of inorganic sediment delivered by the tributaries during these high flow intervals (see Section 3.6.1.5 and 3.6.1.6; Effler et al. 2014, Effler and Peng 2014).

5.2.3. Temporal Patterns

Temporal patterns are presented for multiple sites to evaluate, and describe structures, in the context of model needs, and to identify those patterns that offer opportunities to support model testing. The time-series of daily average flow rates of Fall Creek, the single largest tributary, with the longest record of gaged measurements (since 1925), that is a good indicator of the dynamics of total tributary flow (Effler et al. 1989), is presented with each of the water quality parameter time-series. This provides tributary hydrology, and associated constituent loading, context to the lake patterns.

A recurring theme of the following descriptions of temporal patterns for many of the water quality parameters, particularly those related to sediment, are the strong dynamics for conditions on the shelf coupled to runoff events. These dynamics reflect the transient conditions that prevail on the shelf, intermediate between the lotic (tributary) and lentic (pelagic areas of the lake) environments. The perturbations of runoff events were generally manifested in measurements on the shelf, but were attenuated in the much larger volume of the lake's pelagic waters. Simple dilution effects contribute to this attenuation, as well as multiple biogeochemical processes that operate on a constituent-specific basis at various rates. Two sets of time series are presented for each constituent: (1) the average of sites 1 and 2, the shelf sites, compared with site 3, and (2) site 3 compared with the average of sites 4 through 8. The first of these represents the shelf versus the nearest pelagic site, with generally paired observations and increased frequency in summer. The second time-series compares site 3 with pelagic water conditions through the remainder of the lake, monitored less frequently (bi-weekly) in summer.

Concentrations of TP on the shelf (average of site 1 and 2) were usually higher than at pelagic sites 3 (Figure 5-37b), but particularly during the high runoff months of July and August (Figure 5-37a). Concentrations tended to converge for the shelf and this pelagic sites only during lower flow intervals (e.g., late August – October). In contrast, the temporal patterns of TP concentrations within the upper waters converged for the various pelagic sites (Figure 5-37c). Concentrations generally increased in pelagic waters starting in June and decreased in September. The seasonal peak was about 16 µgP/L. Concentrations of TDP were also systematically higher on the shelf compared with pelagic site 3, particularly following runoff events (Figure 5-37d), from the increased loads and concentration of TDP delivered by the local tributaries. TDP concentration patterns for the pelagic sites were similar (Figure 5-37e). An increase was observed in early July, coincident with a major runoff event, though a similar response was not observed for the larger event of early August (Figure 5-37a and e). Decreases in TDP occurred lake-wide in May.

The timing of the differences in SRP concentrations between the shelf and pelagic site 3 (Figure 5-38b) were similar to those reported above for TP (Figure 5-37b) and TDP (Figure 5-37d), with shelf concentrations exceeding pelagic area levels by a wide margin following runoff events. Convergence of concentrations for these areas was observed only during relatively dry intervals. Lake-wide decreases were observed from late April through mid-May (Figure 5-38b and c). Similar patterns of SRP were observed throughout the pelagic waters (multiple sites). Concentrations in these portions of the lake often were ≤ 1 µP/L from June through October. Timing features of divergence of TIP concentrations for the shelf and pelagic site 3 were similar (Figure 5-38d) to those reported above for the other measured forms of P (Figure 5-37b and d, Figure 5-38b). Patterns were similar for the various pelagic sites demonstrating generally progressive increases over the June (~ 5 µgP/L) through early September interval (Figure 5-38e).

The character of the differences between the shelf and site 3 for the calculated forms of P, SUP (=TDP – SRP; Figure 5-39b) and PP (= TP – TDP; Figure 5-39d) was similar to that for the measured forms above. Runoff events (Figure 5-39a) clearly caused increases in both forms of P. Again approximate convergences of concentrations amongst the pelagic sites were observed for these two calculated forms of P (Figure 5-39c and e). The SUP temporal patterns for the pelagic waters (Figure 5-39c) had interesting contrasting features to that of SRP (Figure 5-38c). SUP increased progressively through mid-July, coincident with increased tributary flow, including the major early July event (Figure 5-39a). A major increase occurred in late July, followed by a generally progressive increase through August, perhaps related to the largest runoff event of the year in early August. In contrast, a broad peak (~10 µgP/L) in PP occurred in pelagic waters over the summer (Figure 5-39e), a pattern that was similar to that for TP (Figure 5-37c).

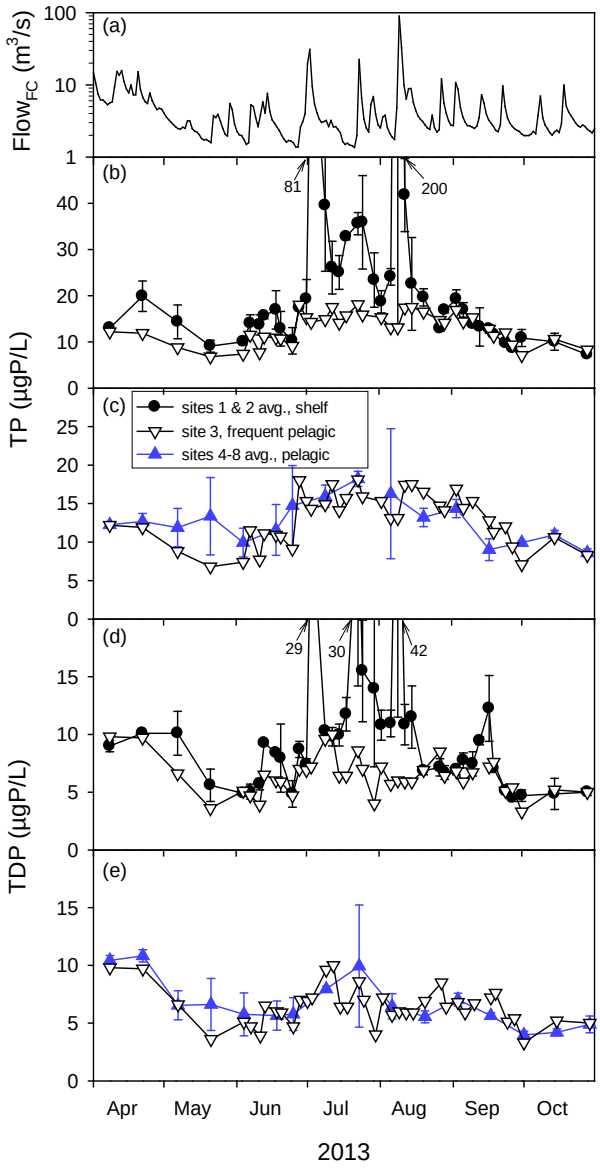

Figure 5-37. Temporal patterns for Cayuga Lake, 2013: (a) daily USGS flows in Fall Creek, (b) TP, as the average of sites 1 & 2 and at site 3, the frequently sampled pelagic site, (c) TP at site 3 and the average of sites 4-8, (d) TDP, as the average of sites 1 & 2 and at site 3, and (e) TDP at site 3 and the average of sites 4-8. Spatial variability is represented by range bars in (b) and (d), and one standard deviation bar in the in (c) and (e).

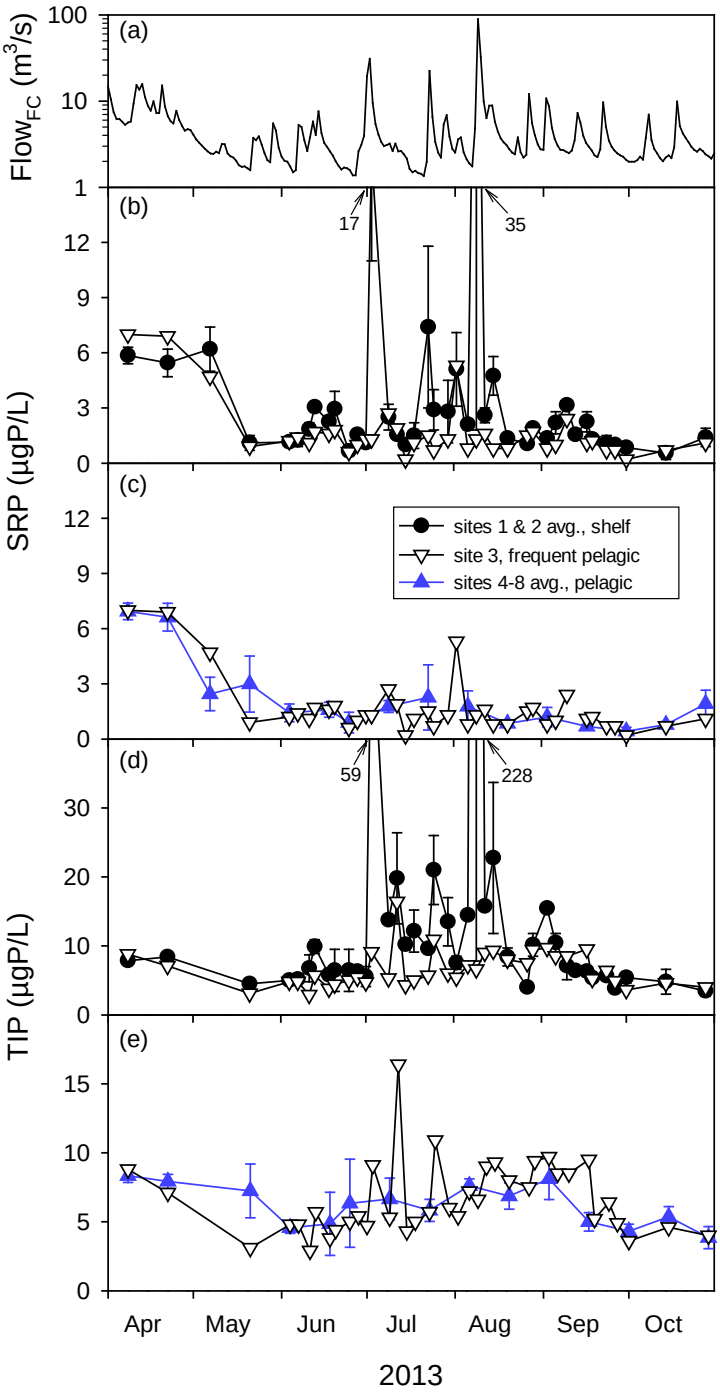

Figure 5-38. Temporal patterns for Cayuga Lake, 2013: (a) daily USGS flows in Fall Creek, (b) SRP, as the average of sites 1 & 2 and at site 3, the frequently sampled pelagic site, (c) SRP at site 3 and the average of sites 4-8, (d) TIP, as the average of sites 1 & 2 and at site 3, and (e) TIP at site 3 and the average of sites 4-8. Spatial variability is represented by range bars in (b) and (d), and one standard deviation bar in (c) and (e).

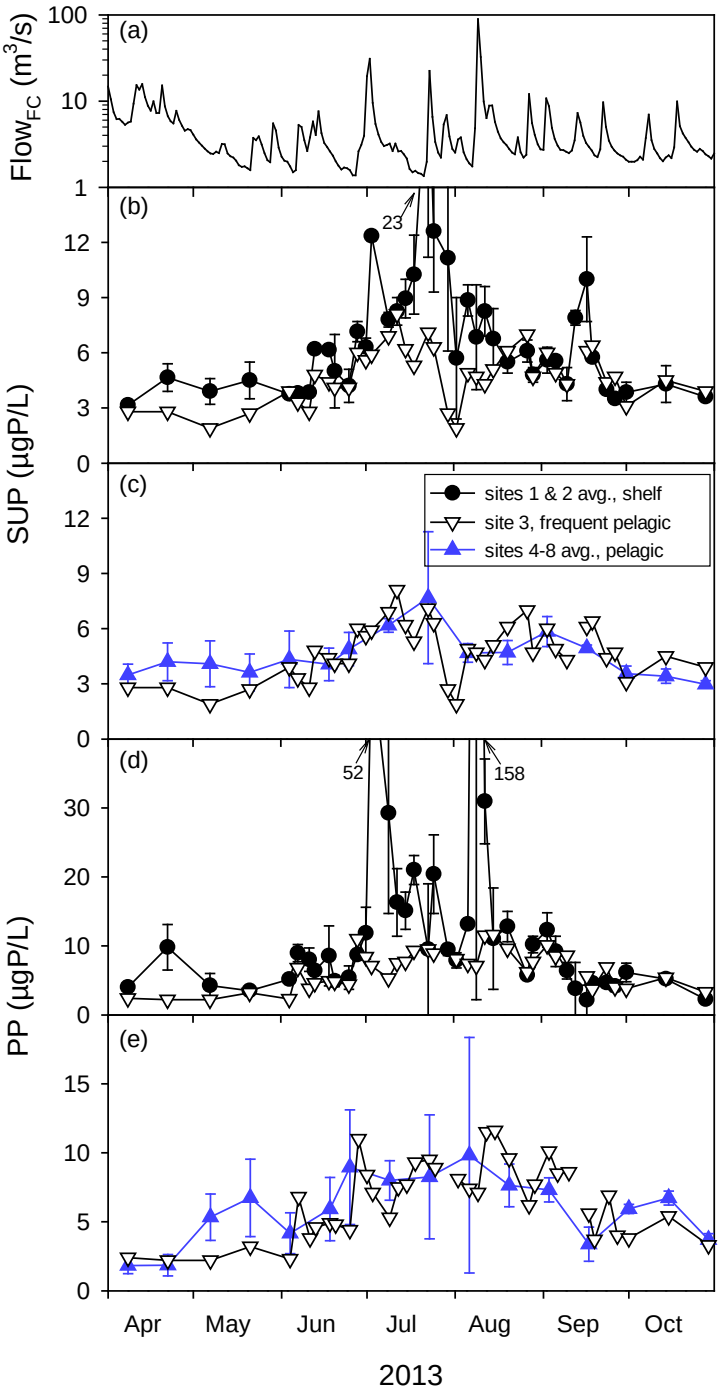

Figure 5-39. Temporal patterns for Cayuga Lake, 2013: (a) daily USGS flows in Fall Creek, (b) SUP, as the average of sites 1 & 2 and at site 3, the frequently sampled pelagic site, (c) SUP at site 3 and the average of sites 4-8, (d) PP, as the average of sites 1 & 2 and at site 3, and (e) PP at site 3 and the average of sites 4-8. Spatial variability is represented by range bars in (b) and (d), and one standard deviation bar in (c) and (e).

Temporal patterns of Si (Figure 5-40b and c) differed substantially from those for forms of P. First, the differences between the shelf and site 3 were relatively small (Figure 5-40b), consistent with the smaller differences between tributary and lake concentrations (Figure 5-32), though shelf concentrations were often lower. A distinct temporal pattern was manifested for pelagic waters, depletion from ~2.5 mg SiO_2/L in April to ~0.5 mg SiO_2/L in June, followed by an increase to more than 1 mg SiO_2/L in August, with a subsequent decrease to mid-October (Figure 5-40c). This pattern is qualitatively consistent with the timing of contributions of diatoms to the phytoplankton community (Section 5.4.1.3.1).

Temporal patterns for the two forms of N available to support algae growth are presented (Figure 5-41b-e). Concentrations of t-NH_3 were irregularly substantially greater on the shelf, particularly in spring (Figure 5-41b). These conditions were likely associated with inputs from WWTPs, as tributary concentrations were similar to the lake (Figure 5-33a). Irregular variations were observed for pelagic waters (Figure 5-41c). However, these are not deemed as particularly important, due to the much higher (30 to100 – fold) concentrations of NO_X that prevailed (Figure 5-41d and e). Temporal patterns were generally uniform lake-wide. Progressive decreases were observed from April through mid-July, with concentrations remaining relatively unchanged thereafter. The decrease is likely a signature of phytoplankton uptake. The subsequent leveling-off may reflect the compensating effect of coincident increases in external loading from multiple runoff events (Figure 5-41a). Temporal patterns in TDN (Figure 5-42b and c) and TN (Figure 5-42d and e) had features similar to NO_X, the dominant form of N and its dissolved pool in this lake.

Concentrations of DOC on the shelf were modestly higher than at pelagic site 3 (Figure 5-43b) during intervals of elevated stream flow (Figure 5-43a). These small differences are consistent with the modest differences in tributary and lake concentrations that prevailed (Figure 5-34). DOC temporal patterns for the various pelagic sites tracked each other (Figure 5-43c). DOC increased from an initial concentration of ~2 mgC/L to ~3 mgC/L by July, and remained largely unchanged thereafter. POC concentrations were higher on the shelf than at pelagic site 3 after runoff events (Figure 5-43d), indicating local allochthonous contributions. The largest of these signatures was a POC concentration of 3.7 mgC/L after the largest runoff event of early August. Temporal patterns of POC were similar for the pelagic sites, though the higher monitoring frequency for site 3 supported increased resolution of structure. POC peaks were observed in pelagic waters in early June, late July, and lake August (Figure 5-43e).

Noteworthy differences in temporal patterns of Chl-*a* between the shelf and pelagic site 3 occurred in several instances (Figure 5-44b). However, unlike the parameters considered above, concentrations of Chl-*a* on the shelf were more often lower than at pelagic site 3. Allochthonous (external) sources of this algal pigment are generally negligible compared to autochthonous (internal) production. Differences in patterns amongst the pelagic sites were

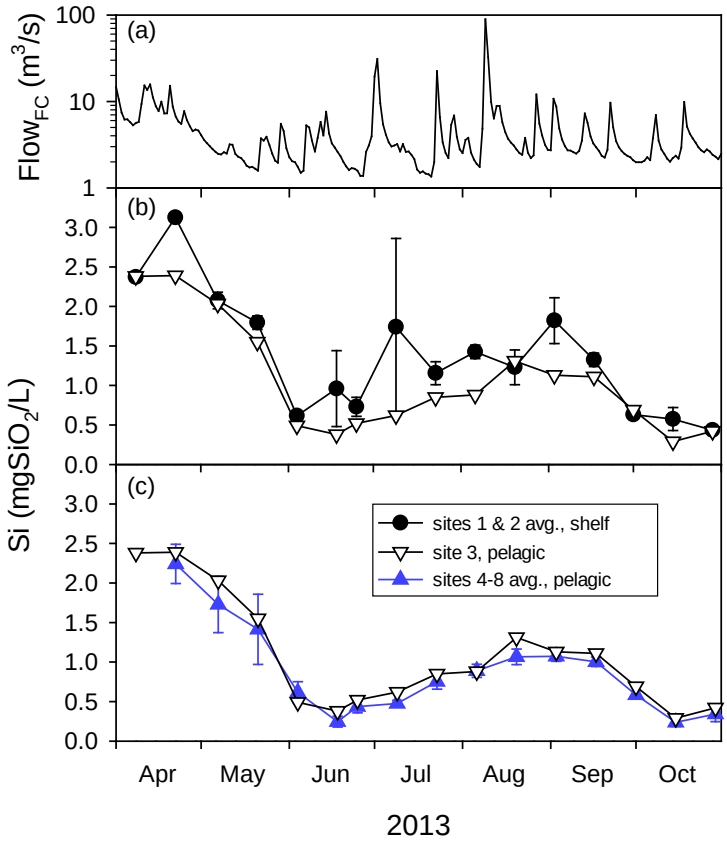

Figure 5-40. Temporal patterns for Cayuga Lake, 2013: (a) daily USGS flows in Fall Creek, (b) Si, as the average of sites 1 & 2 and at site 3, and (c) Si at site 3 and the average of sites 4-8. Spatial variability is represented by range bars in (b) and one standard deviation bar in (c).

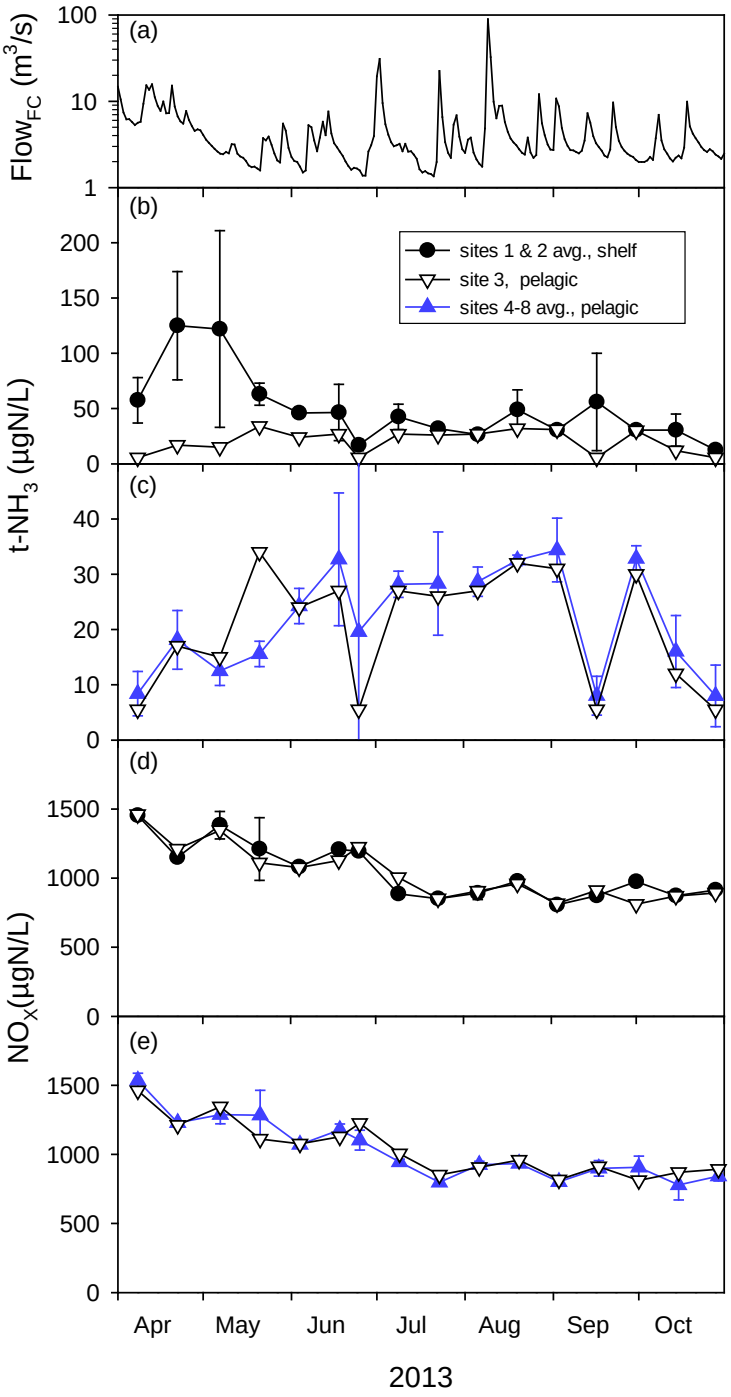

Figure 5-41. Temporal patterns for Cayuga Lake, 2013: (a) daily USGS flows in Fall Creek, (b) t-NH_3, as the average of sites 1 & 2 and at site 3, (c) t-NH_3 at site 3 and the average of sites 4-8, (d) NO_X as the average of sites 1 & 2 and at site 3, and (e) NO_X at site 3 and the average of sites 4-8. Spatial variability is represented range bars in (b) and (d), and one standard deviation bar in (c) and (e).

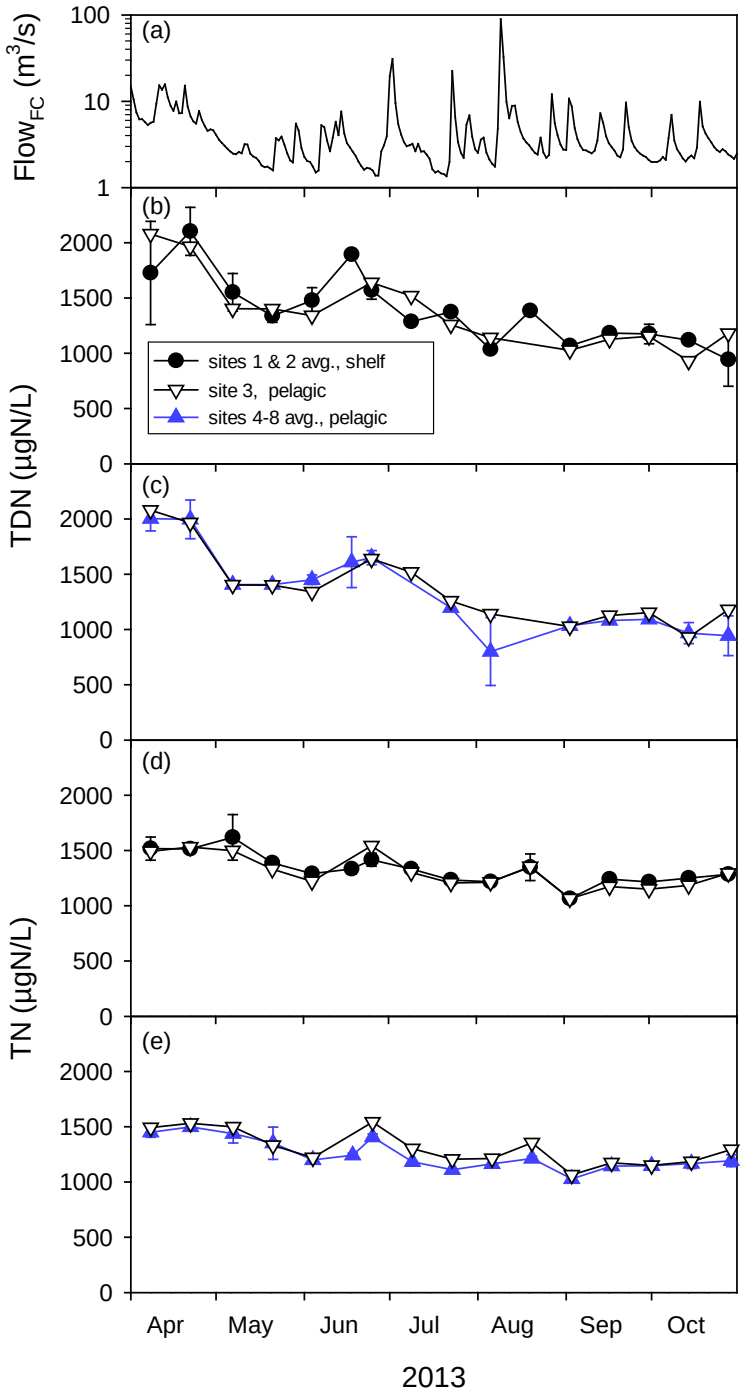

Figure 5-42. Temporal patterns for Cayuga Lake, 2013: (a) daily USGS flows in Fall Creek, (b) TDN, as the average of sites 1 & 2 and at site 3, (c) TDN at site 3 and the average of sites 4-8, (d) TN, as the average of sites 1 & 2 and at site 3, and (e) TN at site 3 and the average of sites 4-8. Spatial variability is represented by range bars in (b) and (d), and one standard deviation bar in (c) and (e).

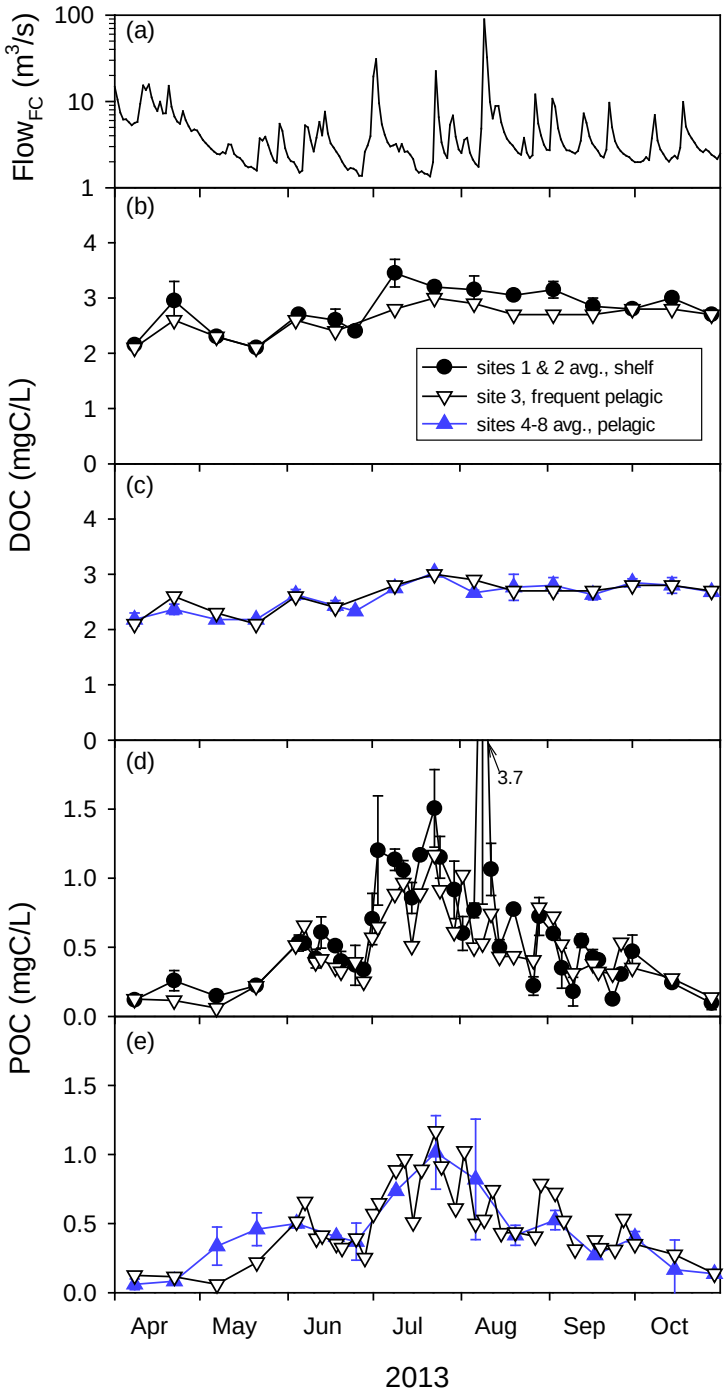

Figure 5-43. Temporal patterns for Cayuga Lake, 2013: (a) daily USGS flows in Fall Creek, (b) DOC, as the average of sites 1 & 2 and at site 3, the frequently sampled pelagic site, (c) DOC at site 3 and the average of sites 4-8, (d) POC, as the average of sites 1 & 2 and at site 3, and (e) POC at site 3 and the average of sites 4-8. Spatial variability is represented by range bars in (b) and (d), and one standard deviation bar in (c) and (e).

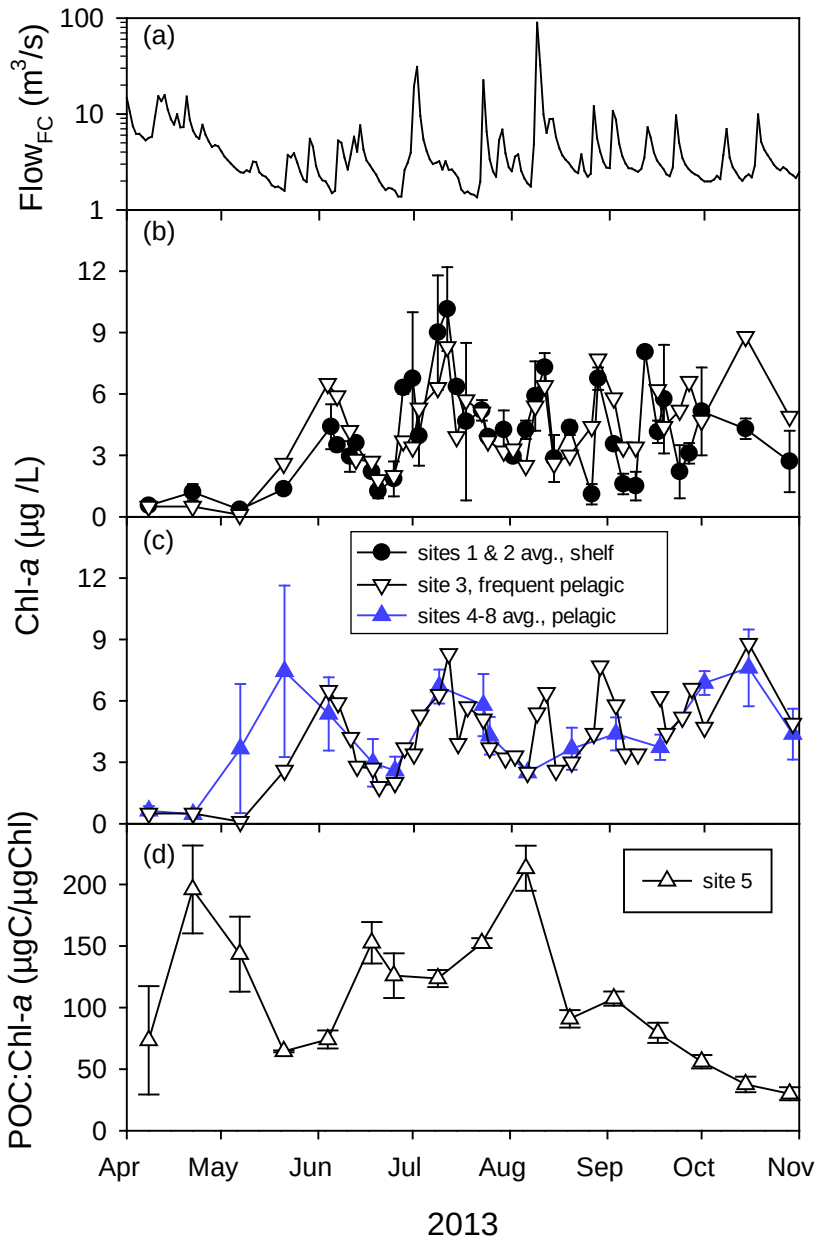

Figure 5-44. Temporal patterns for Cayuga Lake, 2013: (a) daily USGS flows in Fall Creek, (b) Chl-*a*, as the average of sites 1 & 2 and at site 3, (c) Chl-*a* at site 3 and the average of sites 4-8, and (d) POC:Chl-*a* ratio for site 5. Spatial variability represented by range bars in (b), and one standard deviation bar in (c).

minor except in May (Figure 5-44c). According to the most frequent pelagic measurements at site 3, there were peaks in early June, early July, early and late August and mid-October.

POC and Chl-*a* represent two alternate metrics of phytoplankton biomass (Wetzel 2001). The ratio of POC:Chl-*a* is widely considered in stoichiometric analyses and mathematical modeling of phytoplankton growth (Chapra 1997). The time series of this ratio is presented for pelagic site 5. Strong temporal variations in this ratio are reported (Figure 5-44d), with peaks in April, mid-June, and early August. The range, average value, and coefficient of variation of the ratio were 30-213 µgC/µg Chl-*a*, 108 µgC/µg Chl-*a* and14% respectively. This variability indicates that the selection of the metric of phytoplankton biomass is a potentially important feature for a P-eutrophication modeling initiative for the lake.

Comparisons of temporal patterns for the shelf and pelagic site 3 for suspended solids and Tn utilized a common log y-axis to accommodate the very high observations on the shelf following runoff events (Figure 5-45a), particularly in early July and early August. The peak observations were roughly two orders of magnitude higher than for the pelagic site 3 for both TSS (Figure 5-45b) and Tn (Figure 5-45d). Outside of these two events TSS and Tn on the shelf were usually higher, though by a smaller margin. These systematic differences between the shelf and pelagic site 3 reflect the enriched sediment content of the stream inputs delivered to the shelf, that become more extreme during runoff events (Section 3.6.1.5). Linear axes are used instead in comparison of patterns for the pelagic sites (Figure 5-45c and e). Suspended solids concentrations become more uncertain for typical lacustrine conditions (e.g., Table 5.2) because of the low levels that typically prevail. TSS concentrations remained ≤ 2 mg/L for the pelagic sites, with peaks in early June, late July, mid-August, and early September (Figure 5-45c). TSS patterns demonstrated a significant ($p < 0.001$) positive correlation (r^2=0.41) with Tn. The maximum Tn at site 3 in mid-August was ~ 2NTU.

The pattern for FSS on the shelf (Figure 5-46b) was very similar to that for TSS (Figure 5-47b, r^2= 0.27), reflecting the dominance of the FSS component in the tributaries (Section 3.6.1.5). These shelf FSS levels were much greater than measured for pelagic site 3, as well as the other pelagic sites. Pelagic concentrations of FSS remained <1.2 mg/L (Figure 5-46c). Concentrations of VSS were higher on the shelf following runoff events (Figure 5-46b), because VSS (organic material) makes only a modest contribution to TSS in local tributary inputs. The temporal patterns for VSS at the pelagic sites (Figure 5-46e) was significantly ($p<0.0001$) correlated (r^2 = 0.61) with POC pattern (Figure 5-43e). The maximum VSS at site 3 was in late July, ~ 2 mg/L.

Previously presented time series comparing conditions on the shelf to pelagic site 3 for the trophic state metrics of TP (Figure 5-47b), Chl-*a* (Figure 5-47c), and SD (Figure 5-47d) are grouped together for comparative purposes. Average values for the summer and the entire study also appear. Particularly TP, but also SD, shelf patterns depict a conspicuous degradation of much higher TP and lower SD on the shelf coupled to high runoff events. However, no coupled

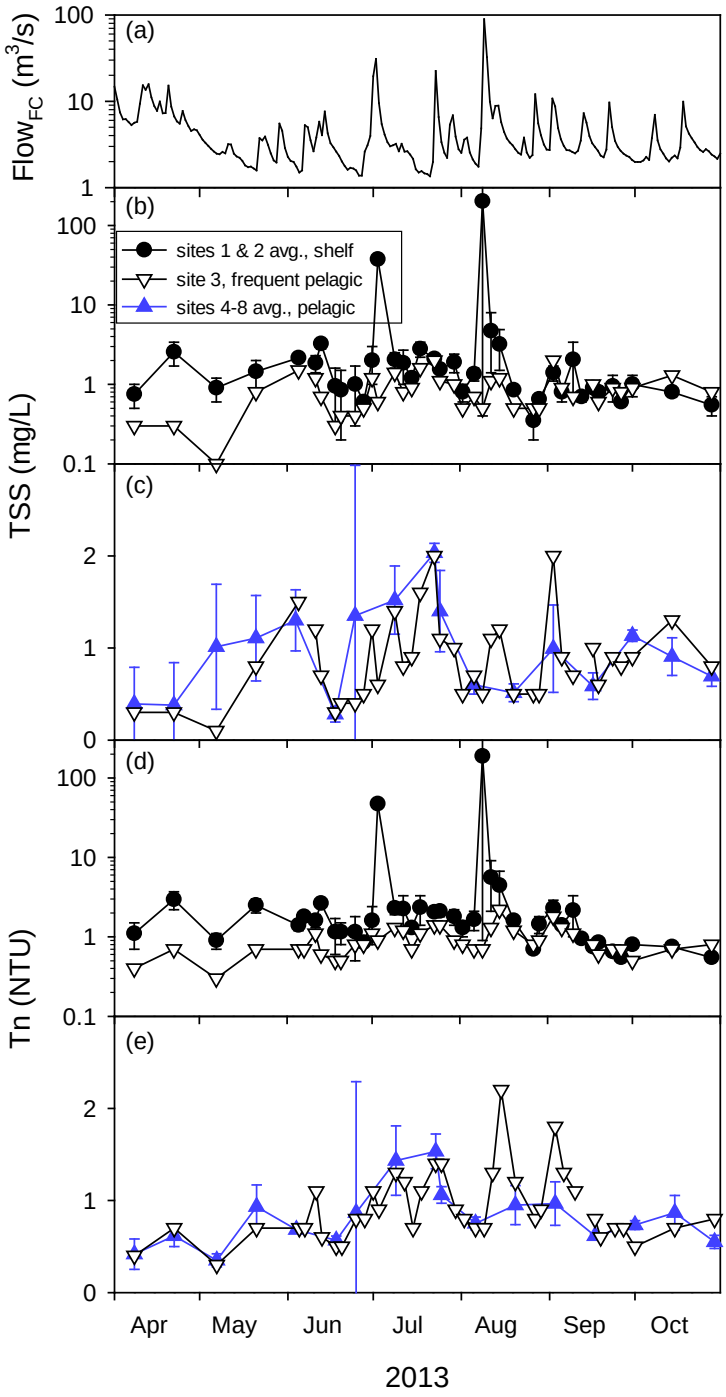

Figure 5-45. Temporal patterns for Cayuga Lake, 2013: (a) daily USGS flows in Fall Creek, (b) TSS, as the average of sites 1 & 2 and at site 3, the frequently sampled pelagic site, and (c) TSS at site 3 and the average of sites 4-8, (d) Tn as the average of sites 1 & 2 and at site 3, and (e) Tn at site 3 and the average of sites 4-8. Spatial variability represented by range bars in (b) and (d), and one standard deviation bar in (c) and (e).

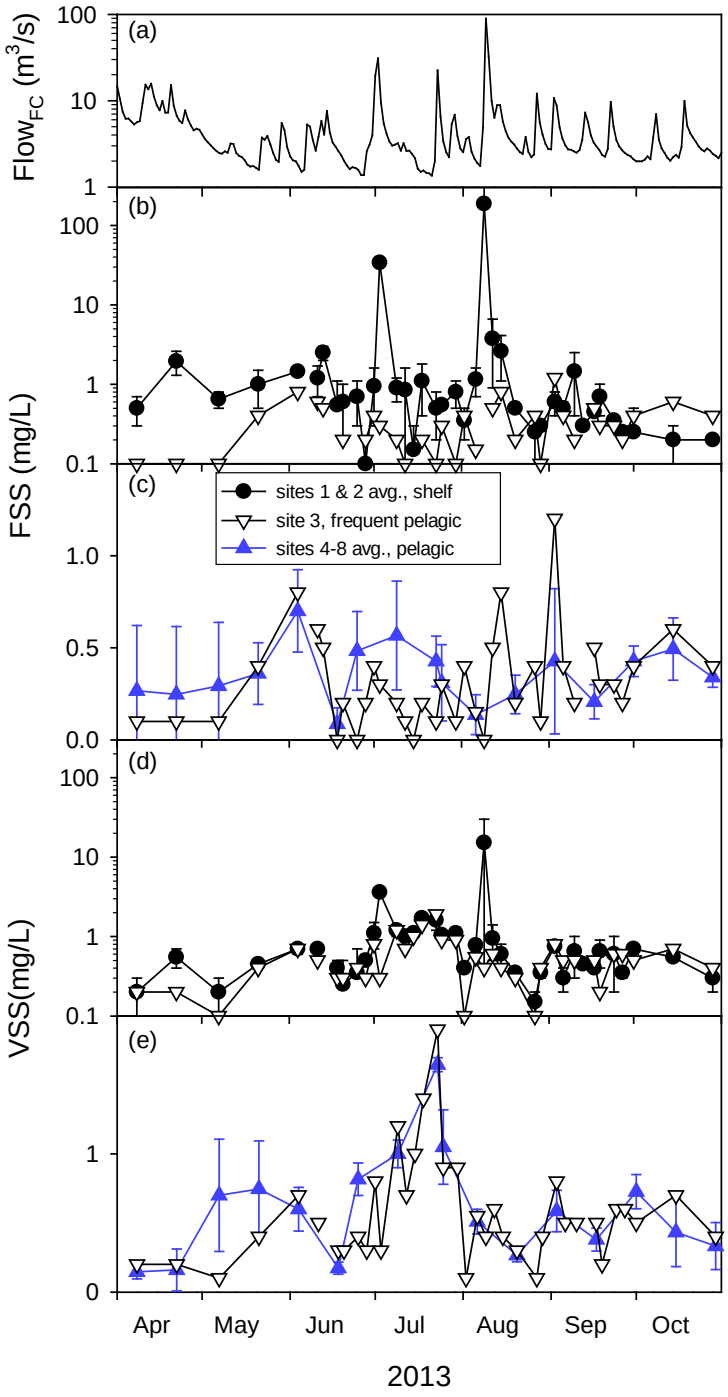

Figure 5-46. Temporal patterns for Cayuga Lake, 2013: (a) daily USGS flows in Fall Creek, (b) FSS, as the average of sites 1 & 2 and at site 3, the frequently sampled pelagic site, and (c) FSS at site 3 and the average of sites 4-8, (d) VSS, as the average of sites 1 & 2 and at site 3, and (e) VSS at site 3 and the average of sites 4-8. Spatial variability represented by range bars in (b) and (d), and one standard deviation bar in (c) and (e).

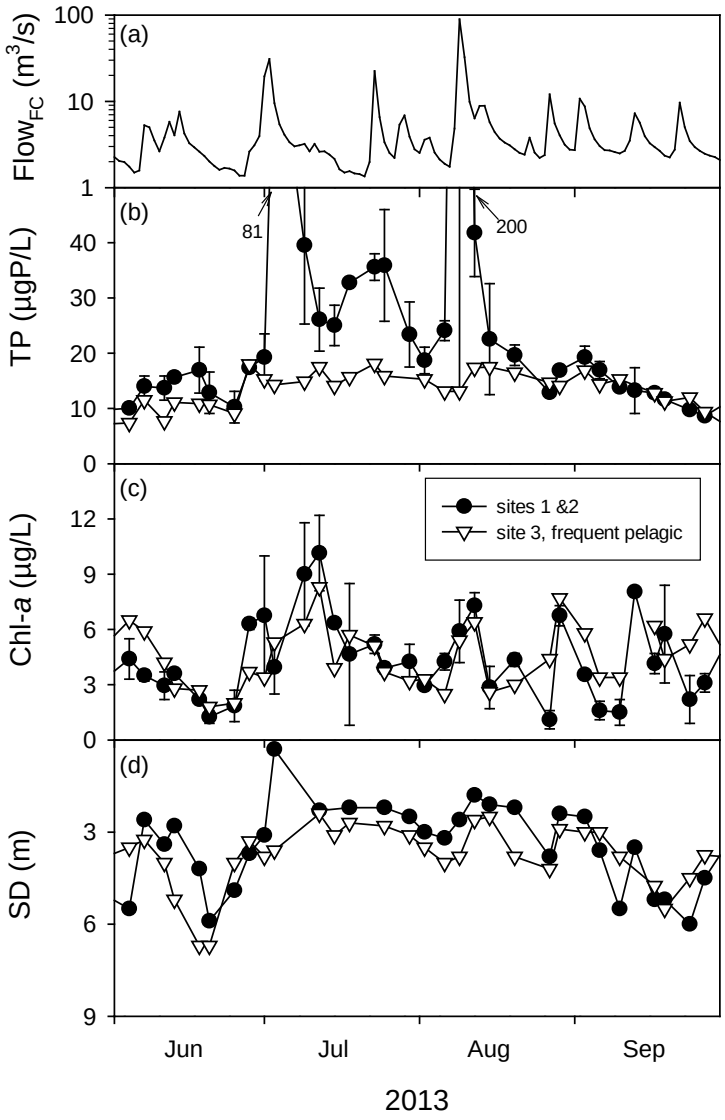

Figure 5-47. Temporal patterns for flow and trophic state indicators in Cayuga Lake, 2013: (a) daily USGS flows in Fall Creek, (b) TP, as the average of sites 1 & 2 and at site 3, the frequently sample pelagic site, (c) Chl-*a* at the average of sites 1 & 2 and site 3, and (d) SD at site 2 and site 3. Spatial variability represented by range bars in (b), and (c).

effects on Chl-*a* were observed. Rather, Chl-*a* levels on the shelf corresponded closely to those measured throughout the pelagic areas of the lake, indicating the dominance of lake-wide processes. The shelf versus pelagic area differences in TP and SD can be explained primarily by the effects of local inputs of inorganic particles (Effler and Peng 2014, Effler et al. 2014).

Depth – time contours are presented for selected parameters for the 0 to 20 m depth interval for site 5 observations to provide a more vertically robust representation. These are supported by observations form four depths over that vertical interval, 0, 5, 10 and 20 m. The dynamics of the lower boundary of the epilimnion are presented for reference, as this feature of stratification affects the patterns in some cases. This boundary was positioned between the sampling depths of 10 and 20m for much of the study interval (Figure 5-49a; e.g., May through August).

Decreases in TP were observed in the surface waters in late May, with increases in July and August, and decreases again in September and late October (Figure 5-48b). Concentrations below the epilimnion remained lower by comparison. The timing of increases in the epilimnion were roughly coincident with the intervals of greatest tributary inputs. Temporally progressive depletion of SRP over the April – May interval was observed throughout this depth range (Figure 5-48c). Increases in SUP occurred in the upper 10 m though mid-July and again in August (Figure 5-48d), timing that was likely linked to that of the external loads for SUP, driven by runoff events. Peaks of PP were greatest in the near-surface waters, but with similar timing (July and August Figure 5-48e) identified above for TP and SUP. A mostly temporally progressive decrease in NO_X was evident through the 0 to 20 m depth interval from April to mid-July, with concentrations remaining largely unchanged through those depths thereafter (Figure 5-49). DOC increased in the upper 10 m stating in mid-July (Figure 5-50) likely in response to the early July runoff event. The affected depth interval deepened in August as the epilimnion deepened with a substantial change in DOC concentration, likely in response to the early August runoff event. The increases in POC were mostly confined to the upper 10 m (Figure 5-50b).

Multiple signatures are manifested for the dynamics of SRP when the entire water column (0 to 120 m) is considered (Figure 5-51), instead of just the epilimnetic depths (e.g., 0 to 20 m, Figure 5-48c). The depth interval of depleted SRP levels for the mid-May through October period extends substantially below productive depths (e.g., 1% light level), to a depth of ~50 m. SRP concentrations increased progressively in the near-bottom layers starting with the onset of stratification, with a maximum at the bottom of ~18 µgP/L. This pattern indicates a net imbalance of sources exceeding sinks of SRP in those near-bottom layers. However, these concentrations do not approach levels observed where anoxia develops in a hypolimnion seasonally, consistent with the well oxygenated conditions that are maintained throughout the hypolimnion of Cayuga Lake (Figure 5-52). Quagga mussel metabolism (e.g., excretion) has received some attention as a possible explanation, as these invaders are found throughout the full range of depths (Watkins et al. 2012). Quagga mussel densities are substantially greater within

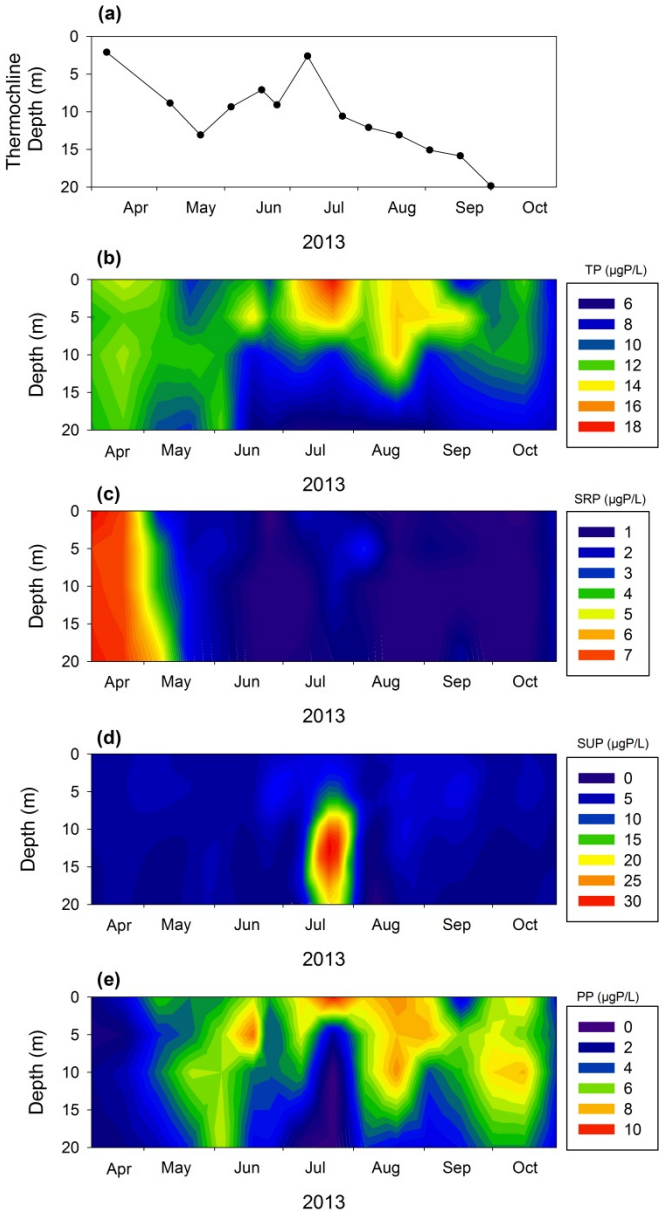

Figure 5-48. Observed (a) thermocline depth in Cayuga Lake 2013 based on Seabird temperature profiles at station 5. Temporal contours for phosphorus in the upper waters (0-20 m) at site 5 in Cayuga Lake, 2013: (b) TP, and (c) SRP (d) SUP and (e) PP.

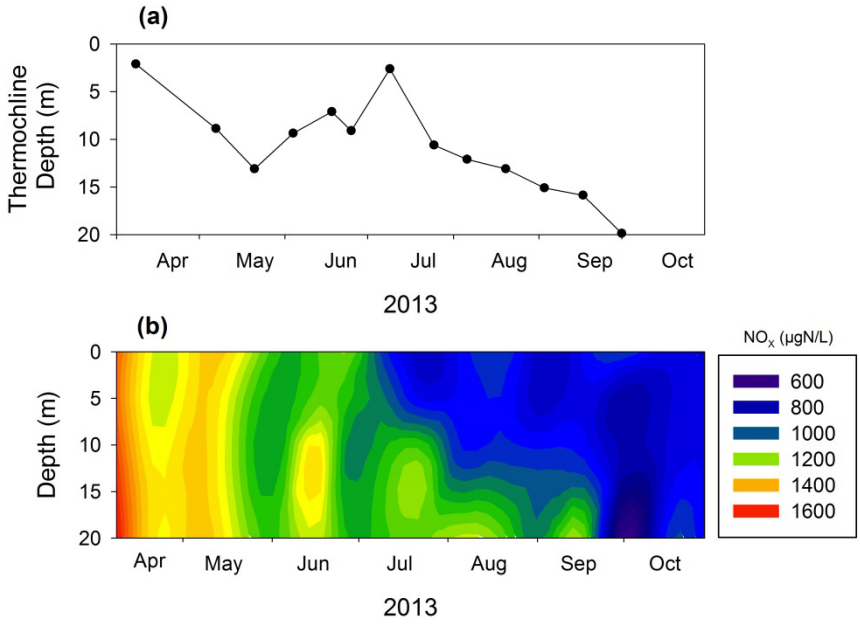

Figure 5-49. Observed (a) thermocline depth in Cayuga Lake 2013 based on Seabird temperature profiles at station 5. Temporal contours for (b) NO_X in the upper waters (0-20 m) at site 5 in Cayuga Lake, 2013.

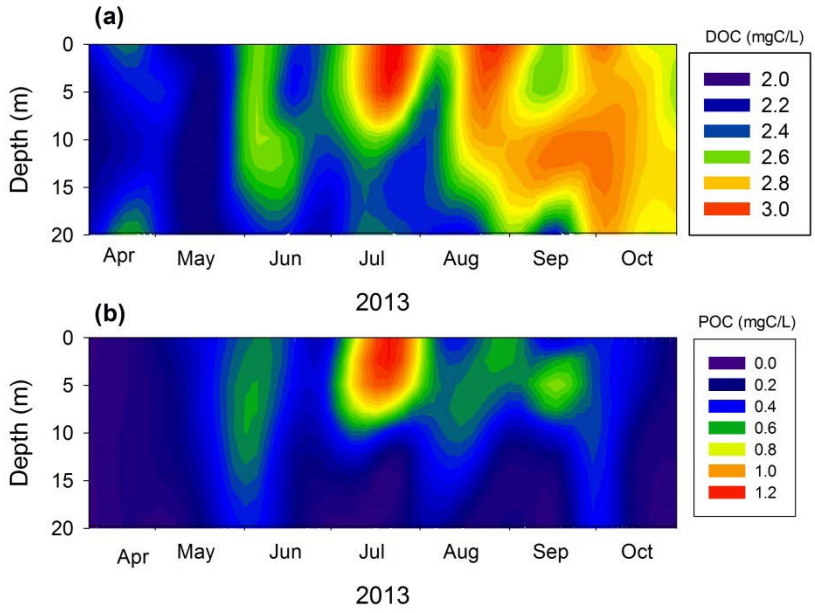

Figure 5-50. Temporal contours for carbon in the upper waters (0-20 m) at site 5 in Cayuga Lake, 2013: (a) DOC, and (b) POC.

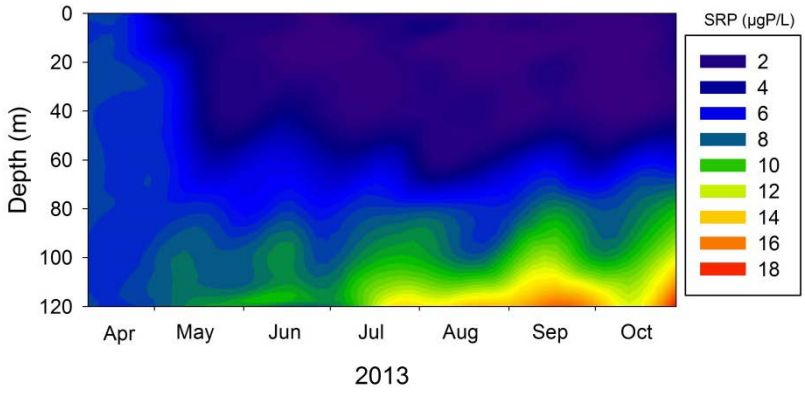

Figure 5-51. Depth-time contours for SRP for the full water column at site 5 in Cayuga Lake, 2013.

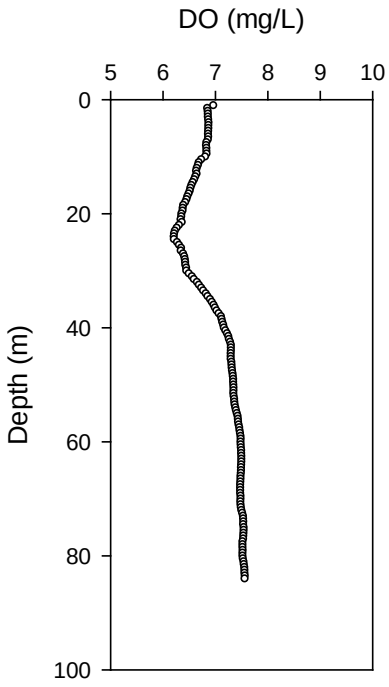

Figure 5-52. DO profile measured at Myers Point in Cayuga Lake on October 8, 2006 by the Cornell Biological Field Station.

metalimnetic and upper hypolimnetic depths (see Section 5.4.2.3.1). Preliminary applications of the validated transport model for the lake (see Section 6) indicated very little transfer from these enriched depths to the upper productive depths occurs during stratification. Enrichment of productive layers would be limited to the subsequent turnover interval. The drivers for the overall depth-time structure of SRP remain to be fully resolved, as well the associated implications for the lake's overall metabolism.

5.2.4. Summary

The generally good precision demonstrated for laboratory analyses of lake samples collected in triplicate throughout the April – October study interval supports the representativeness of the patterns resolved in time and spare based on laboratory measurements. Spatial patterns for the upper waters were resolved on a time – averaged basis for two intervals, the entire study period of 2013 and the June – September interval. These average values were presented for each of the nine lake sites. Flow – weighted concentrations for the four monitored gauge tributaries were included for constituents for which these were available, to provide a tributary versus lake context. For most parameters a gradient in concentrations was observed, according to tributaries >site 1 (shelf) > site 2 (shelf) > pelagic sites. Particularly noteworthy exceptions were Chl-*a* and NO_X, for which no significant differences between the shelf and pelagic sites were observed. In general, reasonably spatially uniform conditions were observed at the pelagic sites. The gradient was particularly strong for particulate metrics, including PP, TSS, FSS and Tn. However, it was also observed for all the measured forms of P (e.g., TP, TDP, SRP), as well as the calculated forms. The TP guidance value of a summer average concentration of 20 µg/L was exceeded at site 1 and approached at site 2. FSS dominated TSS in the tributaries and on the shelf (on average), but not in pelagic waters.

A recurring theme for temporal patterns for many water quality parameters, including the forms of P and metrics of sediment, were the strong dynamics on the shelf, positively linked to runoff events. These transient shelf conditions were intermediate between those of the lotic (stream) systems and lentic environment (e.g., pelagic waters). Time series for each constituent were presented with comparisons of (1) the average of sites 1 and 2 with site 3, and (2) site 3 compared with the average of the other pelagic sites (4-8). The greatest differences between the shelf and pelagic conditions were observed following the major runoff events of summer. Conditions approached convergence for these areas during dry weather. Differences between the various pelagic sites were generally minor. A number of noteworthy patterns were resolved for pelagic sites, including: (1) a decrease in SRP in spring, (2) an increase in SUP in June and July, (3) an increase in PP in summer, (4) a progressive depletion of Si over the spring to early summer interval, (5) a progressive depletion of NO_X over the April to early July interval, (6) a peak in POC in July, (7) multiple Chl-*a* peaks, (8) wide variations in the POC: Chl-*a* ratio, (9) depleted depths of SRP extending through the metalimnion, and (10) a progressive increase in SRP in near bottom waters through late summer and early fall.

5.3. Evaluation of Relationships and Potential Trends

5.3.1. Different Measures of Chlorophyll *a*

The laboratory fluorometric method adopted as the primary protocol for chlorophyll *a* (Chl-*a*) measurements in this study is widely used. The spectrophotometric method made on a subset of samples (split samples) had been used for the LSC monitoring program, starting in 1998. It is less often used now, because of its lower sensitivity, that requires substantially more sample volume (~10-fold) to compensate for this short-coming. The change for the 2013 study was based in part on this shortcoming, and to be consistent with the contemporary prevalence of the fluorometric method. A strong linear relationship ($r^2 = 0.89$) prevailed between the two methods for the spilt samples of this study (Figure 5-53a). The average % difference of the paired measurements was 14% (Figure 5-53a). This near equivalence supports the position that no adjustments are necessary in comparing the 2013 observations to the earlier LSC data sets, or in addressing this parameter in the modeling analyses.

The laboratory Chl-*a* data for the upper waters are compared to paired (same day of sample collection) field epilimnetic (upper 3 m of observations not considered to avoid the artifact of photoinhibition) fluorometric measurements. While linearity was generally indicated, and the best fit linear regression slope approached 1.0, the relationship was decidedly weaker ($r^2 = 0.50$; Figure 5-53b) than that between two different laboratory methods. These observations are consistent with those for many lacustrine systems; field measurements are only a rough indicator of the concentration of this pigment, following proper extraction, in the laboratory. The ease of the field measurements is the primary advantage, enabling rapid, vertically detailed, representations.

Broad use of field Chl-*a*_f measurement capabilities has enabled the identification of the deep chlorophyll maximum (DCM) phenomenon, where a distinct maximum is manifested in stratified layers. At first this was interpreted as a localization of primary production and phytoplankton growth in these layers. However, photoadaptation by various phytoplankton, resulting in increased cellular content of this pigment to compensate for relatively low light levels (Reynolds 2006), is also known to contribute to the DCM phenomenon (Fennel and Boss 2003). Paired vertical patterns of biomass would address the extent to which the DCM is indicative of phytoplankton growth. Various investigators have adopted $\boldsymbol{c}_{660}$_f as an indicator of biomass and considered paired Chl-*a*_f and $\boldsymbol{c}_{660}$_f profiles in the context of the cases of photoadaptation versus biomass/growth peak as responsible for the DCM signature (Fennel and

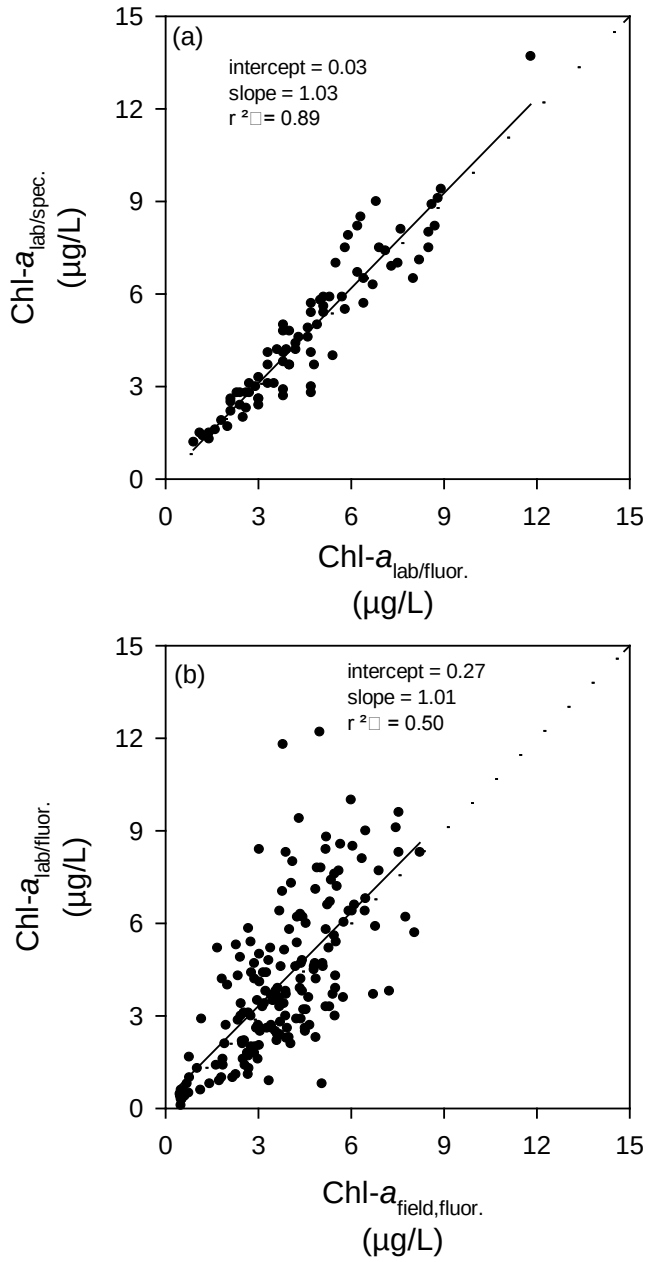

Figure 5-53. Evaluation of the relationships between different metrics of chlorophyll *a* (Chl-*a*) in Cayuga Lake from 2013 monitoring: (a) spectrophotometric laboratory measurements of Chl-*a* versus fluorometric laboratory measurements of Chl-*a* sites 1-3, 5, 7-9, and (b) fluorometric laboratory measurements of Chl-*a* versus field fluorometric (Chl-*a*_f) measurements sites 1-9. Associated linear least-squares regression statics presented.

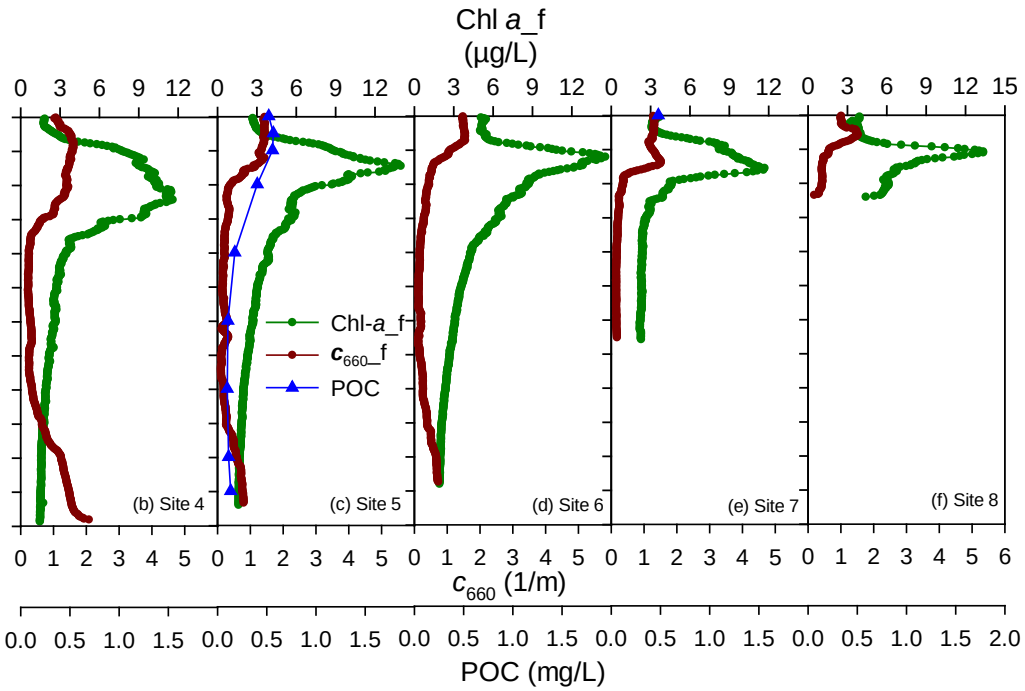

Figure 5-54. Vertical profiles of Chl-*a*_f, and $\boldsymbol{c}_{660\_f}$, at pelagic sites in Cayuga Lake on June 4, 2013: (a) site 3, (b) site 4, (c) site 5, POC profile included, (d) site 6, (e) site 7, and site 8.

Boss 2003). The responsible driver for the strongest DCM signature (Figure 5-54) of the study period (June 4, 2013) is considered here. Very distinctive Chl-*a*_f peaks in metalimnetic layers were manifested on this date throughout the pelagic portion of the lake (Figure 5-54a-f). Differences in vertical details along the axis of the lake (e.g., broad peak at southern site 3 versus narrower at the northern sites) were likely attributable to attendant seiche activity. The vertical patterns of $\boldsymbol{c}_{660}$_f had substantially different shapes. Relatively minor vertical variations in $\boldsymbol{c}_{660}$_f were observed over the same depth interval. It is noteworthy that the vertical patterns of POC, an alternate metric of biomass, closely tracked that for the $\boldsymbol{c}_{660}$_f at site 5 (Figure 5-54c). These differences in the vertical details of the Chl-*a*_f and $\boldsymbol{c}_{660}$_f profiles support the position that the DCM in Cayuga Lake on this date was primarily due to photoadaptation. Other days with the DCM had similar features, supporting photoadaptation. However, these signatures have been generally recurring, based on measurements made in other years at site 3 as part of the monitoring for LSC (Appendix C-1). Accordingly, this feature is not considered a valid indicator of localized phytoplankton growth in the lake.

5.3.2. Chlorophyll *a* versus Particulate Organic Carbon

Chlorophyll *a* (Chl-*a*) and particulate organic carbon (POC) are both used as metrics of phytoplankton biomass (Chapra 1997). Chl-*a* is by far the more commonly used measure of biomass. The extent to which these are interchangeable, and the potential advantage of one over the other, are of interest to P-eutrophication modeling issues, and for Cayuga Lake specifically. The relationship between POC and Chl-*a* was poor on the shelf (Figure 5-55a) and the pelagic waters (Figure 5-55b). The higher slope, from linear least-squares regression fits, for the shelf may reflect the effect of contributions from terrigenous POC inputs, particularly during runoff events. These poor relationships are consistent with the strong variations in the POC:Chl-*a* ratio presented for the study period for site 5 (Figure 5-44d).

These two biomass metrics were evaluated as predictors of other trophic state indicators. POC was a better predictor of 1/SD (Figure 5-56a) than Chl-*a* (Figure 5-56b). POC explained 47% of the variations in 1/SD in the pelagic waters compared with 15% for Chl-*a*, according to linear least-squares regression. Similarly, POC was a better predictor of particulate P (PP) than Chl-*a* in pelagic waters, explaining 45% of the variations in PP (Figure 5-56c), compared with 18% (Figure 5-56d), according to linear least squares regression

5.3.3. Secchi Depth, Particulate Phosphorus, and Beam Attenuation Coefficient

The relationship between Secchi depth (SD) and particulate phosphorus (PP) was evaluated for both the shelf (Figure 5-57a) and pelagic sites (Figure 5-57b). The effects of both organic (phytoplankton, detritus) and inorganic (clay minerals, and perhaps calcite) particles influence both SD (Effler and Peng 2014) and PP (Effler et al. 2014) measurements. Accordingly, it is not unreasonable to expect these relationships to be somewhat stronger than between Chl-*a* and these metrics, and perhaps POC and these parameters. The relationship was stronger on the shelf than in pelagic waters (Figure 5-57a and b), but largely associated with the effect of some particularly high values observed on the shelf. The relationship for the pelagic site was somewhat stronger (r^2 = 0.35) than 1/SD versus Chl-*a* (Figure 5-56b) and P versus Chl-*a* (Figure 5-56d) relationships, but the margin was modest. The relationships based on POC, instead of Chl-*a* (Figure 5-56a and c), were stronger than the 1/SD-PP relationships. These differences suggest variability in particle stoichiometry in pelagic waters for the lake in the order Chl-*a* > PP > POC.

The beam attenuation coefficient ($\boldsymbol{c}_{660}$_f) has been widely used to estimate POC in oceanographic studies (Fennel and Boss 2003). Rather strong linear relationships were also observed between POC and $\boldsymbol{c}_{660}$_f in the pelagic waters of Cayuga Lake in 2013 (Figure 5-58). Similar relationships were observed for the upper waters at all pelagic sites (Figure 5-58a) and

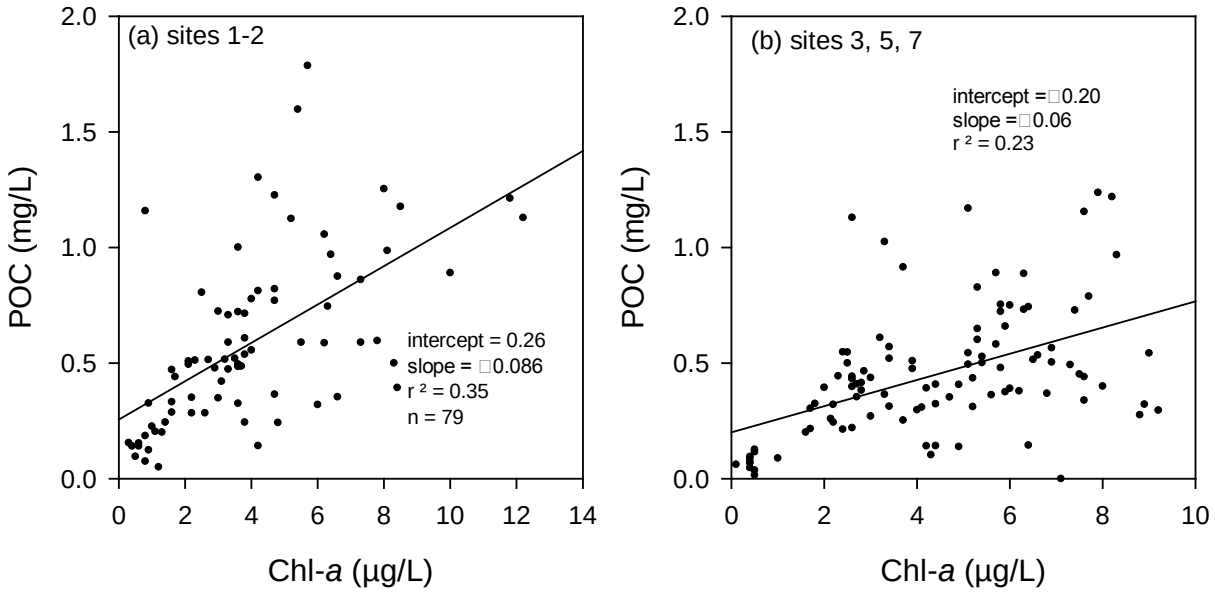

Figure 5-55. Evaluation of the relationships between POC and Chl-*a* in Cayuga Lake in 2013: (a) shelf sites 1 and 2, and (b) pelagic sites 3, 5, and 7. The associated linear least-squares regression statistics are presented.

at all sampled depths at site 5 (Figure 5-58b). Variations in $\boldsymbol{c}_{660}$_f explained ≥ 75% of the variability in POC in both cases, according to linear least-squares regression. The slopes of the best fit relationships were similar, and the y-intercepts approached zero (Figure 5-58a and b). $\boldsymbol{c}_{660}$_f was also a good predictor of 1/SD (Figure 5-59). Differences in $\boldsymbol{c}_{660}$_f explained 74% of the variations in 1/SD in pelagic waters in 2013, according to linear least-squares regression. Strong 1/SD - $\boldsymbol{c}_{660}$_f relationships are widely observed in lakes (Davies-Colley et al. 2003).

5.3.4. Long-term Trends

Long-term data sets collected by LSC monitoring program are considered here in the context of trophic state metrics in the effort to identify and characterize potential trends. The trophic state metrics of TP (Figure 5-60a), Chl-*a* (Figure 5-60b), and SD (Figure 5-60c) are evaluated for that entire record, 1998-2012 for pelagic site 3 and compared to shelf sites. The shelf sites are represented by the average of sites 1 and 2 for TP (Figure 5-60a) and Chl-*a* (Figure 5-60b), but only for site 2 for SD (Figure 5-60c; SD depth > water depth at site 1 for a number of sampling dates). The selection of the shelf sites are consistent with the monitoring program of 2013 (Figure 5-47). However, more shelf sites were included as part of the LSC monitoring program.

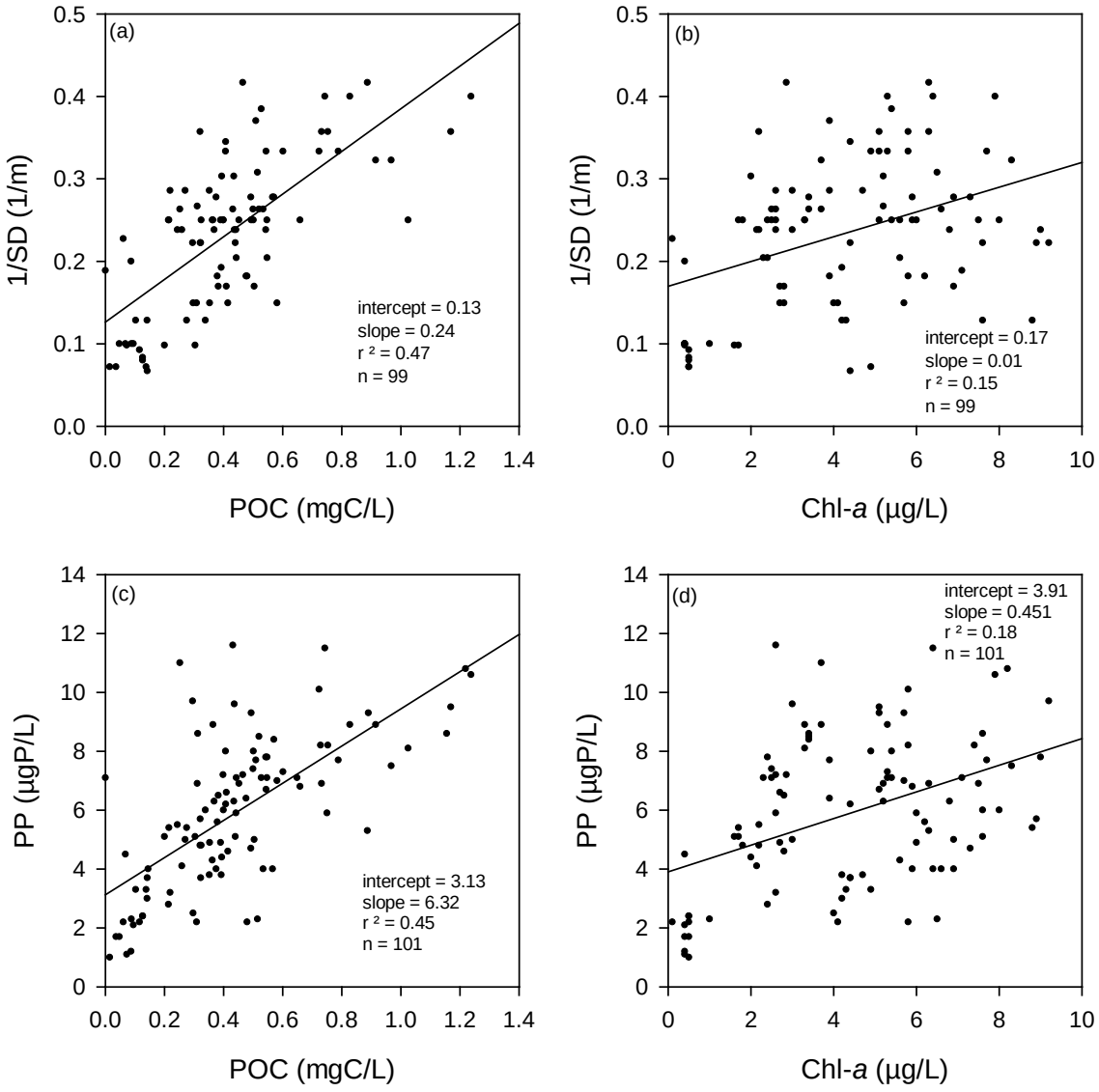

Figure 5-56. Evaluation of the relationships between trophic state, PP, and phytoplankton biomass metrics in Cayuga Lake in 2013: (a) 1/SD versus POC, (b) 1/SD versus Chl-*a*, (c) PP versus POC, and (d) PP versus Chl-*a*. The associated linear least-squares regression statistics are presented.

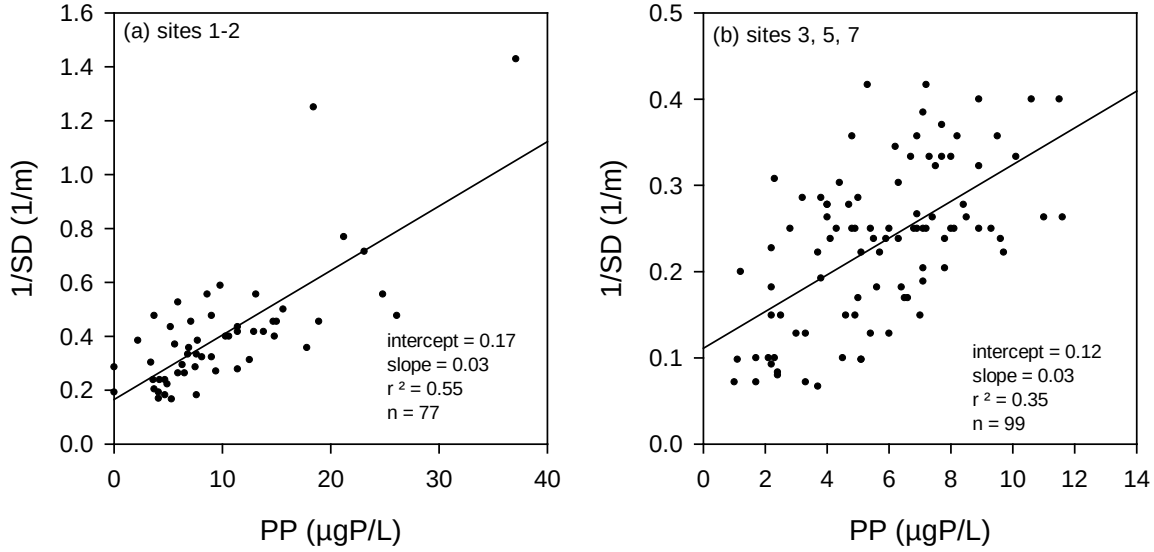

Figure 5-57. Evaluation of the relationships between 1/SD and PP in Cayuga Lake in 2013: (a) shelf sites 1and 2, and (b) pelagic sites 3, 5, and 7. The associated linear least-squares regression statistics are presented.

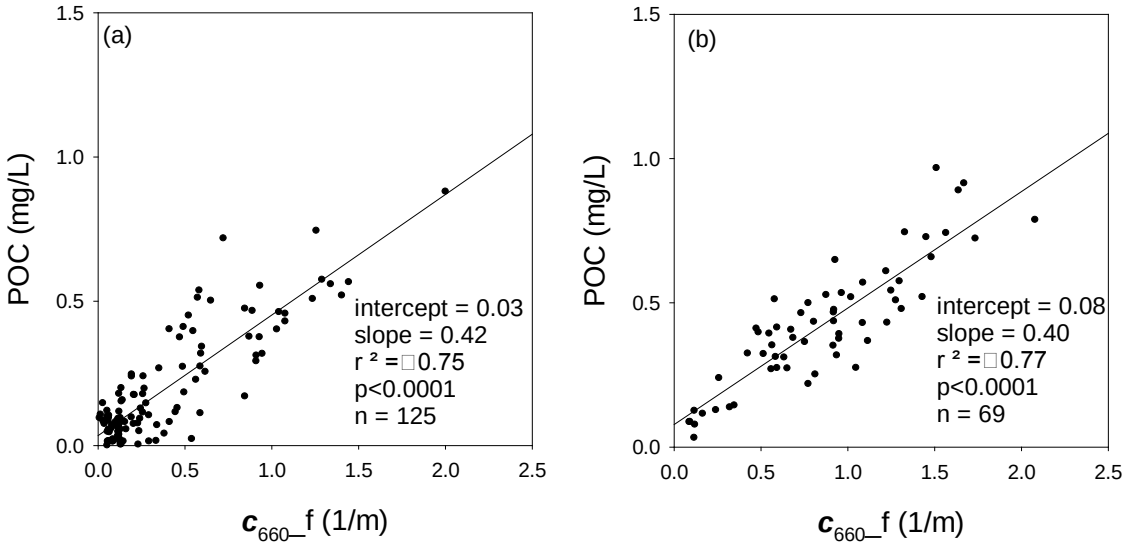

Figure 5-58. Evaluation of the relationship between POC and c_{660_f} in Cayuga Lake in 2013 (a) upper waters at pelagic sites 3, 5, and 7, and (b) profiles at site 5 (0 – 100 m). The associated linear least-squares regression statistics are presented.

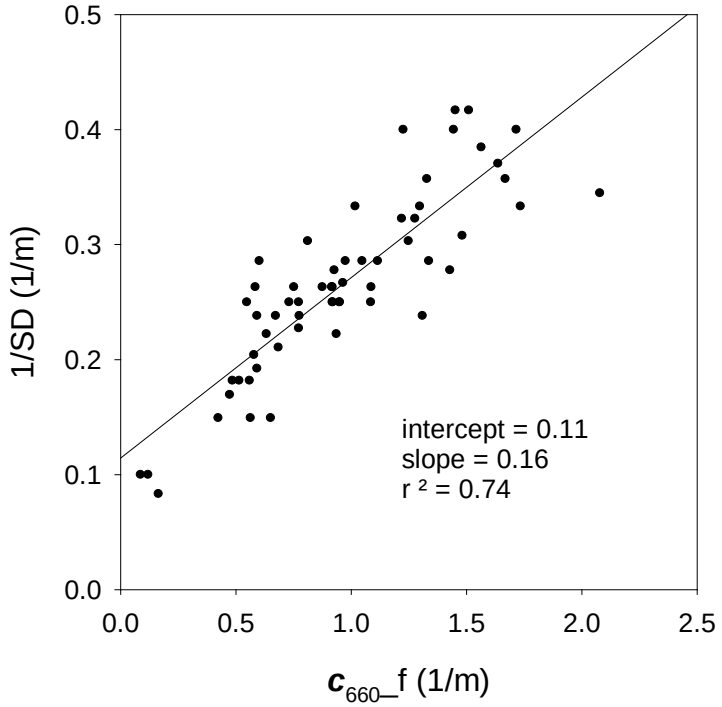

Figure 5-59. Evaluation of the relationship between 1/SD and c_{660}_f for the upper waters of pelagic sites 3, 5, and 7 in Cayuga Lake in 2013. The associated linear least-squares regression statistics are presented.

Thus depending on the "averaging" protocol adopted for the various sites, modest differences from historic shelf values and the shelf values presented here could occur. The values presented are summer averages (June – September), to be consistent with the regulatory context of the analysis. In general, the observations of 2013 have been recurring over this record. TP has been higher on the shelf and SD lower. However, differences in Chl-*a* between these portions of the lake have been minor by comparison. Thus there have been inconsistencies between the three metrics of trophic state with respect to these areas. The differences in TP between the pelagic site 3 and the shelf were the smallest in the last three years (Figure 5-60a), but divergence was again substantial in 2013. Chl-*a* was slightly lower on the shelf in five of the last six years compared to site 3.

Annual average concentrations of forms of P in the LSC discharge are presented for the period of operation of the facility (Figure 5-61). Concentrations of forms of P in the LSC discharge reflected hypolimnetic conditions (intake located at depth of 73 m). Apparent coincident increase in TP (Figure 5-61a), TDP (Figure 5-61b), and SRP (Figure 5-61c) occurred in 2004. Over a longer interval, PP appears to have decreased (Figure 5-61d), while SUP seems to have remained largely unchanged (Figure 5-61e). Three different trend analyses were performed for these data sets, regression analysis over the entire 14 year record, the seasonal Kendall analysis, and the T-test (Table 5-4). Significant increases in TDP and SRP, and a decrease in PP, were found by regression analysis (Table 5-4). These were also supported by the Seasonal Kendall analysis. By specifying a demarcation in the record between 2003 and 2004, the increases in TP, TDP and SRP were found to be significant (Table 5-4). Essentially, the increase in TP and TDP were driven by those in SRP. The cause(s) for these changes remains unestablished, though it has been hypothesized that it reflects the effects of an expanding quagga mussel population.

We considered pelagic (site 3) epilimnetic TP concentrations for the 1998-2012 period for three different averaging intervals, April – October (Figure 5-62a), April – May (Figure 5-62b), and June – September (Figure 5-62c; summer average). The averages are presented with ± 1 standard deviation bars. Two test were conducted, a regression analysis for the 15 year period and a t-test. The t-test was conducted for two different demarcations between 2003 and 2004 (as per LSC P) and 2005-2006 (from inspection). No significant trend was found (Table 5-5). The same analyses were conducted for SRP for the upper waters of pelagic site 3. Superficially, differences in average values between years were apparent for all three seasonal intervals considered (Figure 5-63a–c). Mostly progressive increase in the averages were apparent over the 2002-2007 interval for the April – October (Figure 5-63b) intervals, through the temporal variability within these intervals of each year was large. However, the only significant change identified was the increase in SRP for the April – May interval ($p = 0.01$), using the demarcation of between 2003 and 2004 (Table 5-6), the same one used for LSC.

Long-term trend analyses of spring turnover lake SRP and summer average Chl-*a* concentrations have been conducted by D. Bouldin (see power point presentation of 2014) using

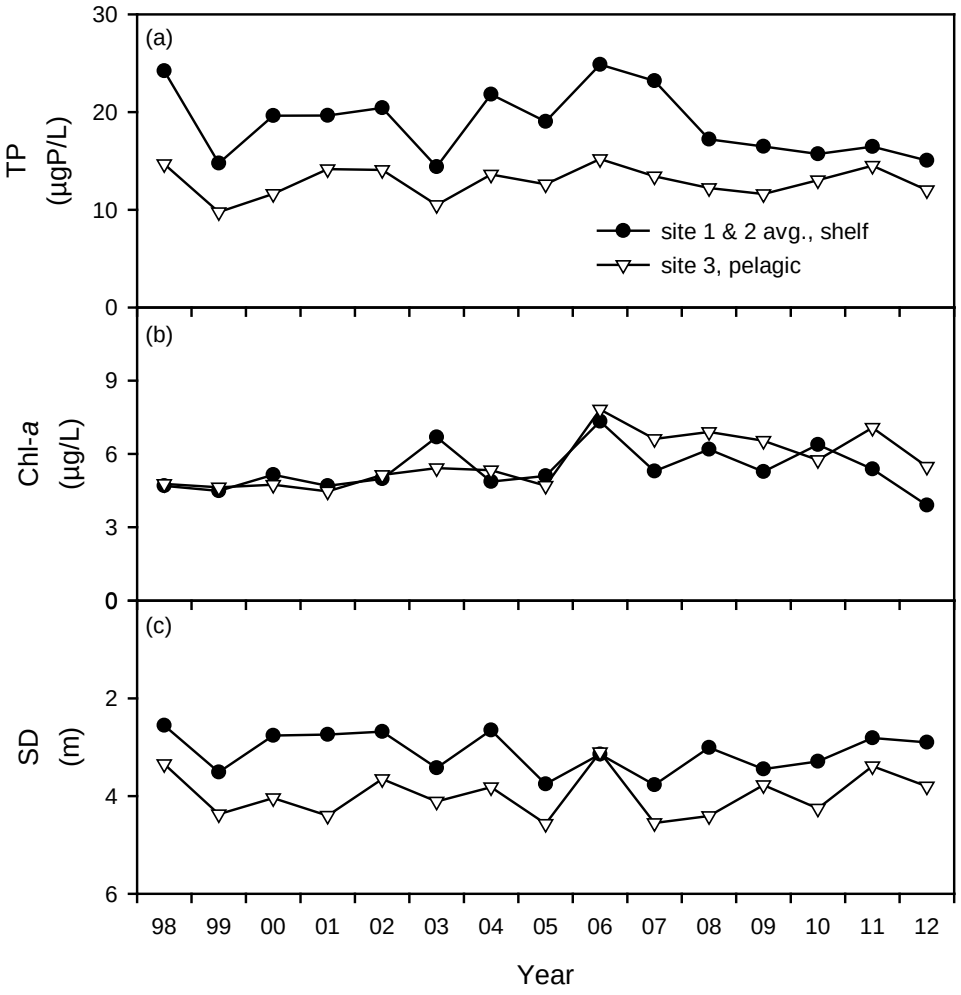

Figure 5-60. Comparison of the time series of summer average trophic state metrics in Cayuga Lake for the shelf and pelagic site 3 for the period 1998-2012: (a) TP, (b) Chl-*a*, and (c) SD.

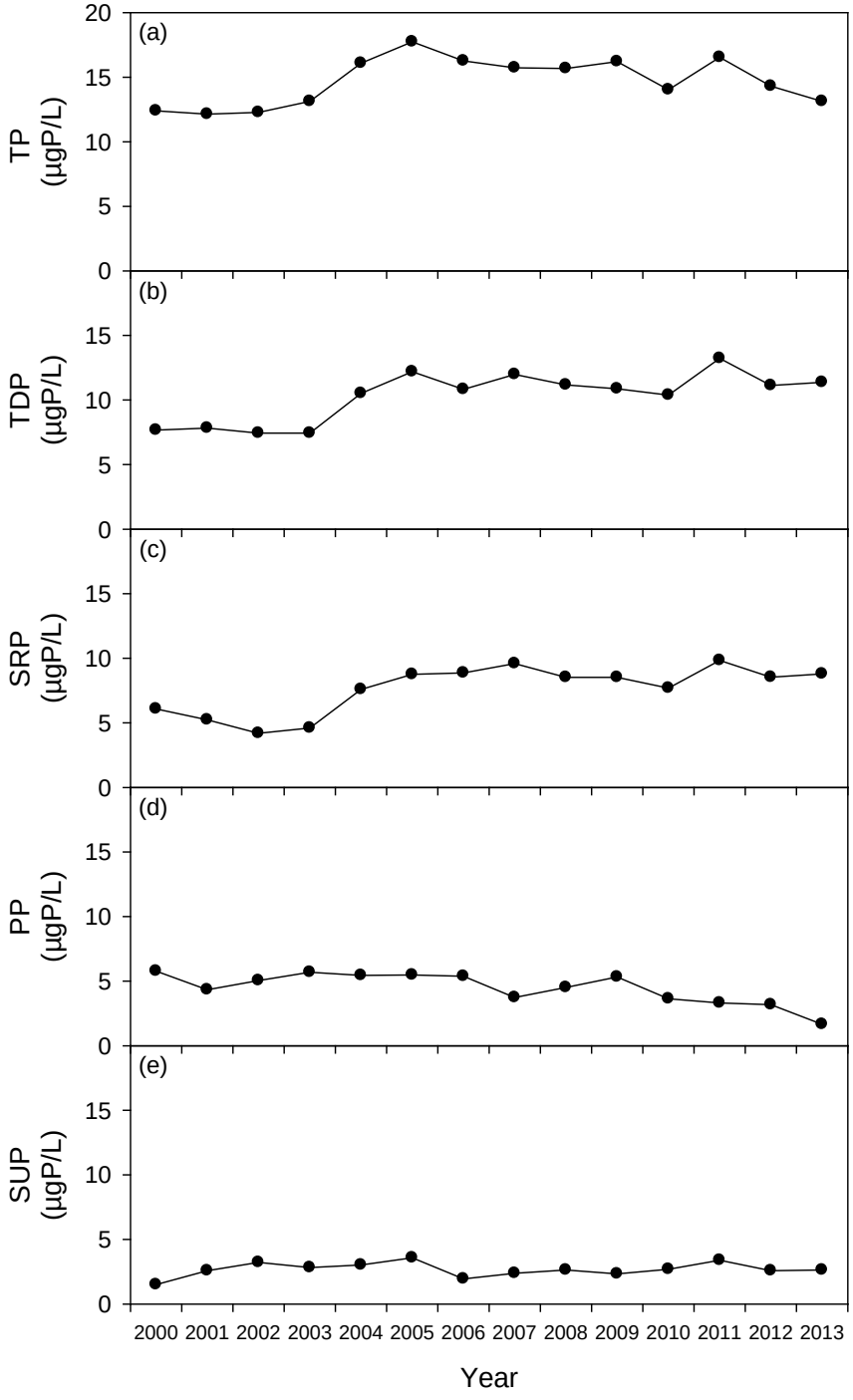

Figure 5-61. Time series of annual average concentrations of forms of P in the LSC discharge to Cayuga Lake over the period 2000-2013 (a) TP, (b) TDP, (c) SRP, (d) PP, (e) SUP.

Table 5-4. Summary of statistical analyses (n = 3) of changes in concentrations of TP, TDP, SRP, PP, SUP annual average 1998-2013 for the LSC effluent.

Parameter	Regression[1]				Seasonal Kendall[2]				t-test[3]		
	direction	magnitude (µg/L/yr)	n	p-value	direction	magnitude (µg/L/yr)	n	p-value	2000-2003 (n = 4) avg. (µgP/L)	2004-2013 (n = 10) avg. (µgP/L)	p-value
TP	increasing	0.159	14	0.2088	increasing	0.153	671	0.2595	**12.5**	**15.6**	**<0.001**
TDP	**increasing**	**0.345**	**14**	**0.0018**	**increasing**	**0.350**	**671**	**0.0024**	**7.6**	**11.4**	**<0.001**
SRP	**increasing**	**0.327**	**14**	**0.0025**	**increasing**	**0.310**	**674**	**0.0075**	**5.0**	**8.7**	**<0.001**
PP	**decreasing**	**0.223**	**14**	**0.0014**	**decreasing**	**-0.215**	**653**	**0.0026**	5.2	4.2	0.153
SUP	increasing	0.0208	14	0.5881	increasing	0.033	656	0.225	2.5	2.7	0.586

[1] regression based on yearly average of 14 years of data 2000-2013.
[2] Seasonal Kendall based on all the data for all 14 years.
[3] t-test based on comparing the average of 2000-2003 to the average of 2004-2013.

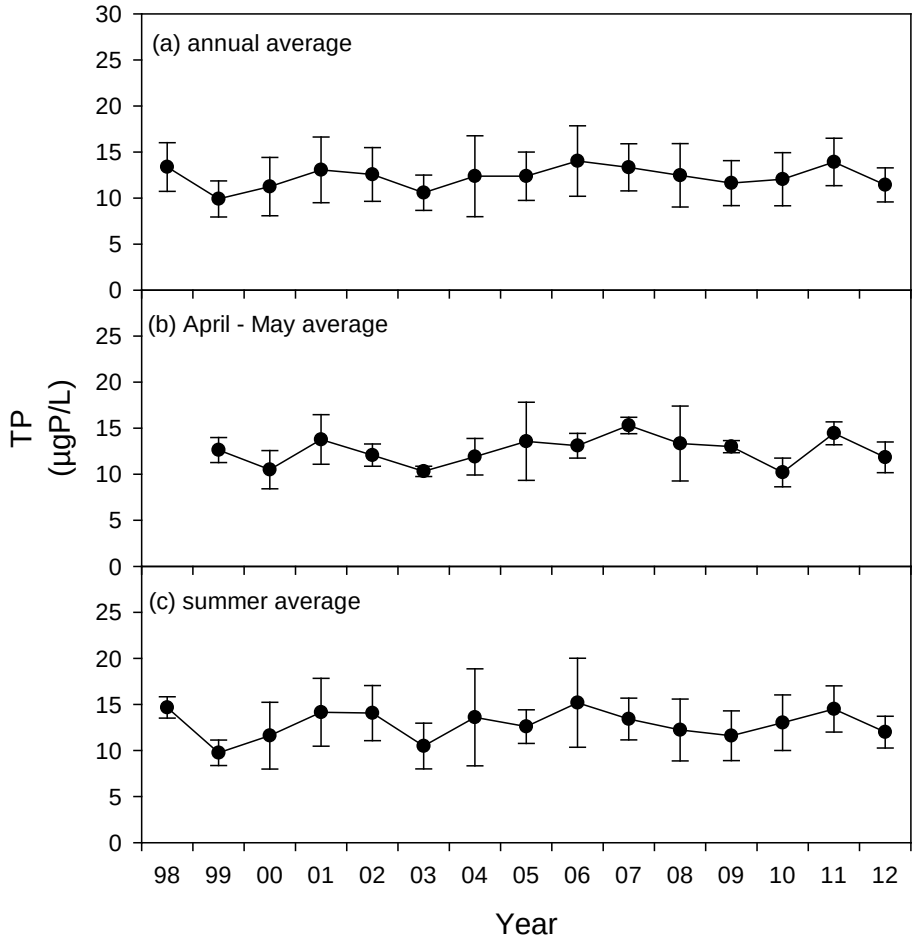

Figure 5-62. Time series of average TP concentrations in Cayuga Lake at pelagic site 3 for the 1998-2012 period for three time intervals: (a) April – October, (b) April – May, and (c) June – September (summer). Vertical bars are ± one standard deviation, as a metric of temporal variability.

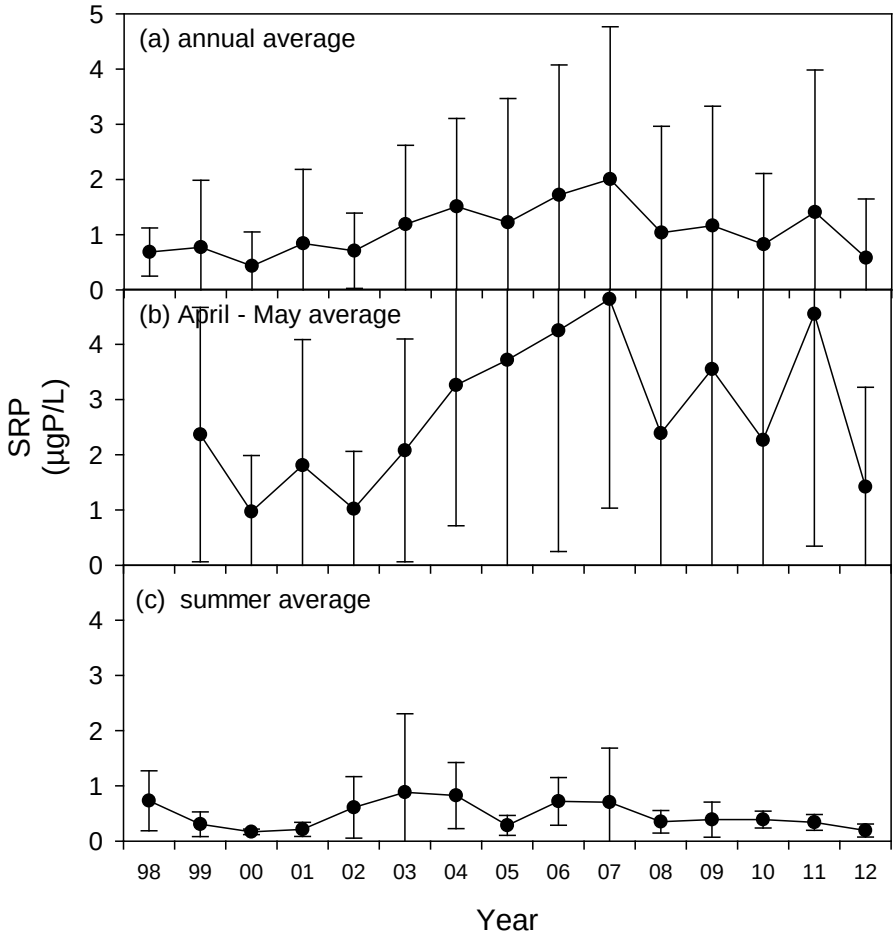

Figure 5-63. Time series of average SRP concentrations in Cayuga Lake at pelagic site 3 for the 1998-2012 period for three time intervals: (a) April – October, (b) April – May, and (c) June – September (summer). Vertical bars are ± one standard deviation, as a metric of temporal variability.

Table 5-5. Summary of statistical analyses (n = 2) of changes in concentrations of TP for three seasonal intervals of the period 1998-2012 at pelagic site 3. The t-tests were run over two different demarcation intervals.

Time Period	Regression[1]				t-test[2]			t-test[3]		
	direction	magnitude (µg/L/yr)	n	p-value	2000-2003 (n = 4) avg. (µgP/L)	2004-2012 (n = 9) avg. (µgP/L)	p-value	2000-2005 (n = 6) avg. (µgP/L)	2006-2012 (n = 7) avg. (µgP/L)	p-value
annual average	increasing	0.0556	15	0.4517	11.9	12.6	0.233	12.0	12.7	0.265
spring	increasing	0.0706	15	0.5102	11.7	13	0.187	12.0	13.0	0.278
summer	increasing	0.0307	15	0.7585	12.6	13.1	0.523	12.8	13.1	0.631

[1] regression based on yearly average of 15 years of data 1998-2012.
[2] t-test based on comparing the average of 2000-2003 to the average of 2004-2012.
[3] t-test based on comparing the average of 2000-2005 to the average of 2006-2012.

Table 5-6. Summary of statistical analyses (n = 2) of changes in concentrations of SRP for three seasonal intervals of the period 1998-2012 at pelagic site 3. The t-tests were run over two different demarcation intervals.

Time Period	Regression[1]				t-test[2]			t-test[3]		
	direction	magnitude (µg/L/yr)	n	p-value	2000-2003 (n = 4) avg. (µgP/L)	2004-2012 (n = 9) avg. (µgP/L)	p-value	2000-2005 (n = 6) avg. (µgP/L)	2006-2012 (n = 7) avg. (µgP/L)	p-value
annual average	increasing	0.0326	15	0.2339	0.792	1.27	0.078	0.98	1.25	0.320
spring	increasing	0.1223	15	0.1223	**1.47**	**3.36**	**0.01**	2.14	3.32	0.114
summer	decreasing	0.01067	15	0.4870	0.47	0.47	0.99	0.497	0.441	0.704

[1] regression based on yearly average of 15 years of data 1998-2012.
[2] t-test based on comparing the average of 2000-2003 to the average of 2004-2012.
[3] t-test based on comparing the average of 2000-2005 to the average of 2006-2012.

estimates of molybdate reactive P loads from Fall Creek as the driver. The Fall Creek load estiamtes were used as a proxy of the total load from the entire watershed. These stream inputs, averaged over the previous six years were found to be significantly correlated with spring lake SRP and summer average Chl-*a*. The interannual variations in stream loads were attributed to natural variations in stream flow (i.e., no systematic shifts in stream P concentrations).

The potential for long-term trends in Chl-*a* was considered for both the shelf and pelagic site 3, again utilizing three statistical approaches, regression over the entire period, the seasonal Kendall test, and the T-test. Two different demarcations intervals over the period were considered, 2003 - 2004, and 2005 – 2006. No significant trends were identified for the shelf sites. However, some statistically significant changes were identified for site 3. Again three time intervals were considered, April – October (Figure 5-64a), April – May (Figure 5-64), and June – September (Figure 5-64c). Regression analyses indicated significant increasing trends for the April – October and June- September intervals (Table 5-7). However, no significant trends were indicated by the seasonal Kendall test, while significant increases were indicated by t-tests that adopted a demarcation between 2005 and 2006.for all three intervals. Note that this demarcation, selected from visual inspection, did not correspond to those selected for LSC P. Considered as a whole, the evidence is weak that there has been a significant increase in Chl-*a* in the pelagic waters of Cayuga Lake over the LSC monitoring period. The well-known sources of variability of Chl-*a* that are uncoupled from trophic state, such as dependence on species composition of phytoplankton and ambient environmental conditions (Reynolds 2006), further compromises the position that noteworthy changes have occurred.

Finally, we evaluated whether there has been a significant change in SD in pelagic waters over the same period, addressing the same time intervals using the same statistical approaches. The time series of summer average SD values at site 3 for the LSC monitoring record is presented in Figure 5-65. No significant trends were identified in this SD record.

5.3.5. Apparent Retention Factors

Retention factors were estimated according to the ratio of the difference in the external load and export form the lake, divided by the external load. These were calculated for several constituents (Table 5-8). The external loads are those developed and presented in Section 3 for the entire April through October period. The estimates of export are based on epilimnetic concentrations of the constituents and estimates of outflow, developed from an overall flow budget for the lake. These retention factors are described as apparent as only a portion of the annual cycle was addressed and changes in lake content over the interval were not considered.

This simple analysis indicates the lake acts as a sink for all of these constituents, including for the four forms of P, NO_X, DOC and Si. Deposition and incorporation of constituents into the lake sediments is a manifestation of the lake's sink function. Particularly large fractions of retention are indicated for TP, SRP, DOC and Si.

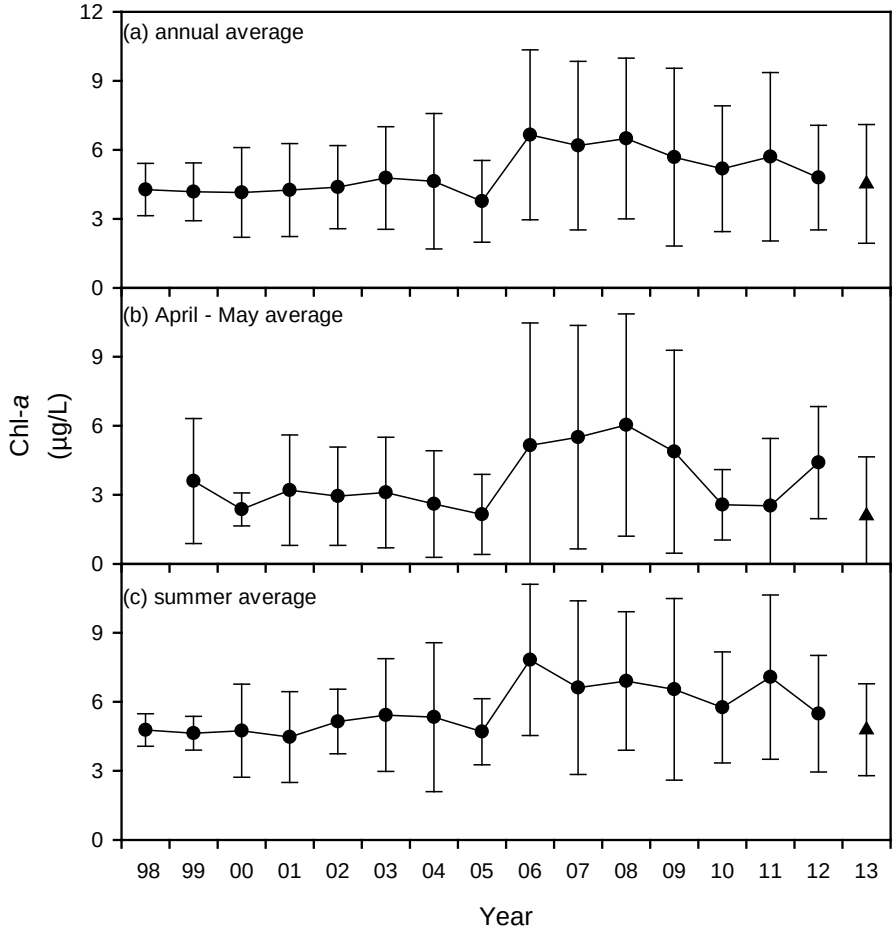

Figure 5-64. Time series of average Chl-*a* concentrations in Cayuga Lake at pelagic site 3 for the 1998-2013 period for three time intervals: (a) April – October, (b) April – May, and (c) June – September (summer). Vertical bars are ± one standard deviation, as a metric of temporal variability.

Table 5-7. Summary of statistical analyses (n=2) of changes in concentrations of TP for three seasonal intervals of the period 1998-2012 at pelagic site 3. The t-tests were run over two different demarcation periods.

Time Period	Regression[1]				Seasonal Kendall[2]				t-test[3]		
	direction	magnitude	n	p-value	direction	magnitude	n	p-value	2000-2003 (n=4) avg. (µgP/L)	2004-2013 (n = 10) avg. (µgP/L)	p-value
annual average	+	**0.124**	**15**	**0.017**	+	0.163	14	0.205	4.4	5.5	0.054
spring	+	0.102	15	0.251	+	0.098	14	0.244	3.0	4.4	0.487
summer	+	**0.154**	**15**	**0.0079**	+	0.0853	14	0.269	**4.9**	**6.6**	**<0.001**

Time Period	t-test[3]		
	2000-2005 (n = 6) avg. (µgP/L)	2006-2012 (n = 7) avg. (µgP/L)	p-value
annual average	**4.3**	**5.8**	**<0.001**
spring	**2.7**	**4.4**	**0.015**
summer	**4.9**	**6.2**	**0.031**

[1] regression based on yearly average of 15 years of data 1998-2012.
[2] Seasonal Kendall based on all the data for all 14 years.
[3] t-test based on comparing the average of 2000-2003 to the average of 2004-2012
[4] t-test based on comparing the average of 2000-2005 to the average of 2006-2012

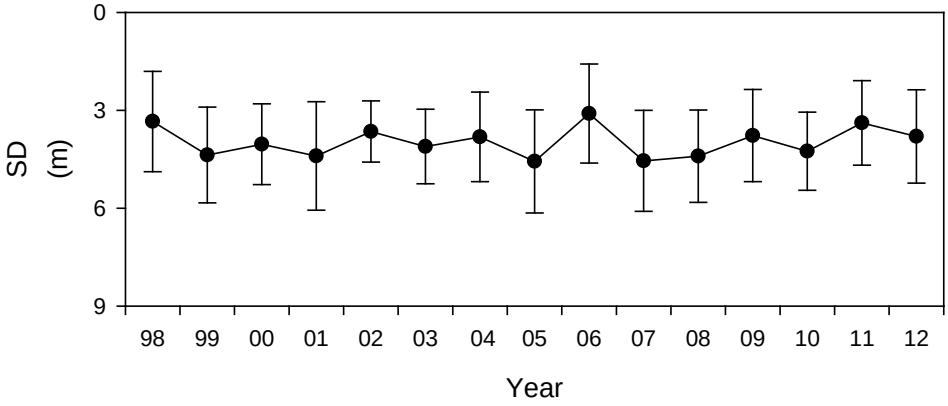

Figure 5-65. Time series of average SD for the June – September (summer) interval in Cayuga Lake at pelagic site 3 for the 1998-2013 period. Vertical bars are ± one standard deviation, as a metric of temporal variability.

Table 5-8. Retention factors for selected constituents in Cayuga Lake for the interval of April – October 2013.

Constituent	Load (MT)	Export (MT)	Retention Factor
TP	55	7	0.87
TDP	9.7	4.4	0.54
SRP	5.6	1.5	0.73
SUP	4.1	3.0	0.26
NO_X	822	608	0.26
DOC	2258	345	0.85
Si*	1505	81	0.95

* Jun. – Oct. interval

5.3.6. Summary

The distributions of the two most widely used metrics of phytoplankton biomass, Chl-*a* and POC, in Cayuga Lake were considered, including relative to each other and other water quality metrics. A change in the laboratory protocol was made as part of the 2013 study to conform to the methodology now most widely used. Split samples for the two protocols demonstrated good convergence. While the field fluorometric measurements of Chl-*a* (Chl-*a*_f) have diagnostic value, these are more uncertain and can yield vertical patterns, such as the deep chlorophyll maximum (DCM), that can be mis-interpreted. The DCM observed from in situ profiles on certain days in 2013 was not indicative of subsurface peaks in phytoplankton biomass, but instead apparently was an indication of the widely encountered photoadaptation to low light levels.

The relationship between Chl-*a* and POC was weak in Cayuga Lake; a related manifestation was strong temporal variations in POC:Chl-*a* ratio. POC was a better predictor of SD and PP in the lake than Chl-*a*. A strong relationship between POC and $\boldsymbol{c}_{660}$_f was observed in the pelagic waters of the lake, as well as between 1/SD and $\boldsymbol{c}_{660}$_f.

Data from the LSC monitoring program (1998-2012) were reviewed and analyzed in an effort to identify changes or trends over that period. Higher TP and lower SD on the shelf compared with pelagic conditions (site 3), based on summer average values, have been recurring in each case. However, that lack of noteworthy differences in summer average Chl-*a* values between these areas was also recurring over that same period. Increases in SRP, and thereby TDP and TP, were noted in the LSC discharge starting in 2004, that reflects a corresponding change in the hypolimnion. Three different statistical tests were conducted to test for significance of these changes. Significant increases in TDP and SRP and decreases in PP were found. Using the same statistical tests, no significant changes in SD or TP were observed for the pelagic site on a summer average basis. Similarly, no trends were found for Chl-*a* on the shelf. However, a significant increase in pelagic summer average Chl-*a* was identified according to certain tests. The statistics representing this change were not particularly strong. This, together with the well-known sources of variability in Chl-*a* that are uncoupled from trophic state, suggests the evidence is weak that a noteworthy change in phytoplankton biomass levels has occurred.

5.4. Biology

5.4.1. Cayuga Lake Plankton

5.4.1.1. Introduction

Phytoplankton production and biomass in lakes in the north temperate zone is typically limited by a combination of phosphorus availability and seasonally intense zooplankton grazing (Wetzel 2001). Cayuga Lake is typical of this group (Schaffner and Oglesby 1978). Because

phosphorus-enriched lakes frequently exhibit high concentrations of phytoplankton, and because blooms of cyanobacteria are characteristic of highly enriched lakes, that determining the seasonal density of these groups is relevant to investigations of lake trophic state.

Even in lakes highly enriched with phosphorus, phytoplankton biomass may not always be high. This is the case when the abundance of grazing zooplankton is high, especially members of the genus *Daphnia* (Lampert 2011; Miner et al. 2012). Species in this group are capable of driving phytoplankton densities very low when grazing rate exceeds phytoplankton growth rate. Grazer control of phytoplankton biomass is typically a seasonal phenomenon restricted to a period in late Spring called the "clear-water phase" (Lampert et al. 1986; Hairston et al. 2005). Grazer limitation of algal biomass can occur even in highly enriched lake ecosystems. As a result, knowing the seasonal pattern of zooplankton densities and taxonomic identity can be a critical seasonal determinant of water quality.

5.4.1.2. Methods

5.4.1.2.1. Phytoplankton

Phytoplankton samples were collected on 7 dates between 22 April and 2 September 2013 at 5 stations (Sites 1, 3, 5, 7 and 9) along the length of Cayuga Lake. Sites 1 and 9 are located on the south and north shallow shelf portions of the lake basin so samples were only collected from a single depth stratum (3-0 m integrated tube sample: epilimnion). At the other three sites, water was collected separately from the epilimnion (10-0 m) and hypolimnion (60 m). Single samples were collected on each date at each site, except Site-5 where duplicate samples were collected on each date and depth to determine sampling method repeatability. All samples were preserved with Lugol's solution, concentrated in a settling chamber and counted under an inverted microscope using the Utermöhl method. Cells were identified to the lowest taxonomic category possible within the constraints of the method – most often to species or genus, but always to Division. Representative cells of each taxon were measured so that cell densities could be converted to biovolume, where biovolume is a measure of taxon-specific biomass. Because most phytoplankton cells are effectively neutrally buoyant, cell volumes can be converted to biomass by assuming they have the specific gravity of water (i.e., 1 g/mL). In this report, phytoplankton densities are reported as biovolumes (μm^3 of cell volume/mL of lake water).

5.4.1.2.2. Zooplankton

Zooplankton samples were collected on 16 dates between 8 April and 29 October at five stations (Sites 1, 3, 5, 7 and 9) using a 75 µm-mesh, half-meter diameter, Puget Sound closing net pulled slowly though a specified vertical portion of the water column while the boat was stationary. The volume sampled was calculated as that of the cylinder traversed by the net. As was the case with phytoplankton sampling, epilimnetic samples (10-0 m) were collected at all sites and separate hypolimnetic samples (60-40 m) were collected at Sites 3, 5, and 7. Single samples were collected on each date, site and depth except at Site-5 where duplicate samples

were obtained from both depths on each date to determine sampling method repeatability. Samples were preserved in 70% ethanol and a subsample was counted in a Bogorov-Litt plankton tray using a dissecting microscope. Taxa were identified to species whenever possible, otherwise to genus. The lengths of representative individuals of each taxon were measured for each sample and animal densities were converted to biomass densities using published length-weight regression equations.

5.4.1.2.3. Quality Control

Duplicate samples were collected on each date at Site 5 as a way of estimating the replicability of plankton data. For total phytoplankton biovolume, the mean coefficient of variation (CV= [standard deviation/mean], expressed as a percentage for n=2 samples) was 23% with a min-max range for individual sampling dates of 3% to 41%. For the individual phytoplankton taxonomic categories illustrated in Figure 5-67, the mean CV was 70% with a range of 25% to 134%. For total zooplankton biomass, the mean CV was 32% with a range of 0.02% to 96%, and for the individual zooplankton taxonomic categories illustrated in Figure 5-70, the mean CV was 50% with a range of 0.2% to 141%.

5.4.1.3. Results

5.4.1.3.1. Phytoplankton

Seasonal dynamics of the phytoplankton in Cayuga Lake were similar at all sites with a spring diatom bloom developing in May and ending in mid-June (Figure 5-66 and 5-67). Total phytoplankton biovolume was greatest during this diatom bloom (and most marked mid-lake at Sites 3, 5 and 7) and was substantially lower the rest of the year at all sites (Figure 5-66). Cyanobacteria were present at Sites 3 and 5 (very scarce at all other sites) from July through early September, but were less than 10% of total phytoplankton biovolume at Site 3 and reached a maximum of 23% on 9 July at Site 5 (Figure 5-67). Total phytoplankton biovolume was low lake-wide from mid-June through early September (the final date for which phytoplankton samples were counted for all five sites. Counts for Sites 1, 5 and 9 on three dates in October show that filamentous cyanobacteria remained present but in relatively low density on 1 October and 15 October, but was essential gone by 29 October. Other features of phytoplankton seasonal succession show the May-June diatom bloom preceded by a mixture of cryptophytes and dinoflagellates, and succeeded in June and July by cryptophytes, chrysophytes, and chlorophytes and then in July and August by cyanobacteria and dinoflagellates (Figure 5-67).

Phytoplankton biovolume is a measure of phytoplankton biomass that is independent of other measures such as chlorophyll-*a* (Chl-*a*) and particulate organic carbon (POC). Regressions of biovolume against these two other measures for Cayuga surface waters on all dates and sites for which biovolume was determined (Figure 5-68) shows a statistically significant positive, but

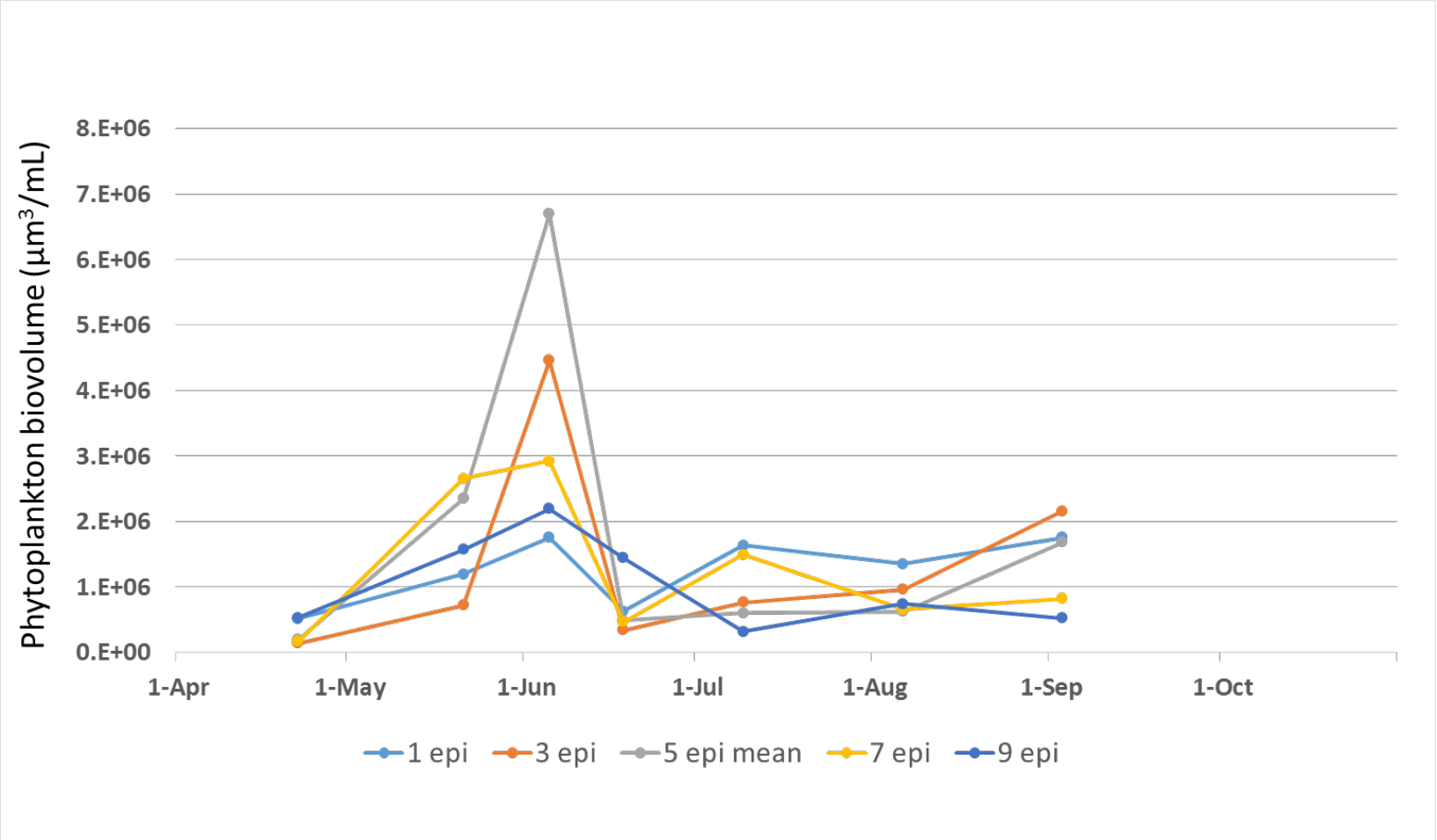

Figure 5-66. The total phytoplankton biovolume concentrations of for the epilimnion (0-10 m) of five sampling sites along the main south (Site 1) to north (Site 9) axis of Cayuga Lake in 2013.

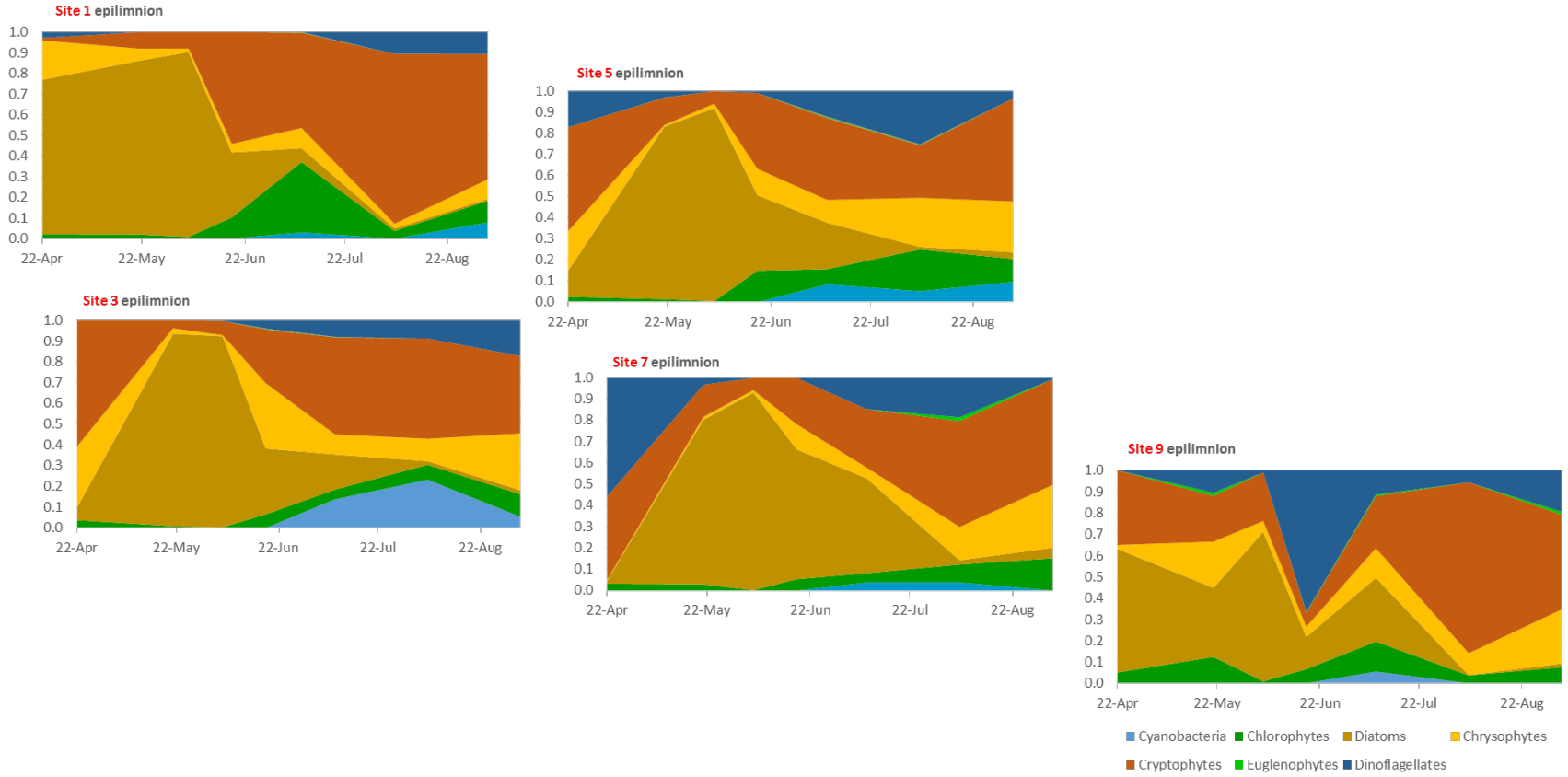

Figure 5-67. Fractional composition by biovolume of major phytoplankton taxa in Cayuga Lake epilimnion 2013.

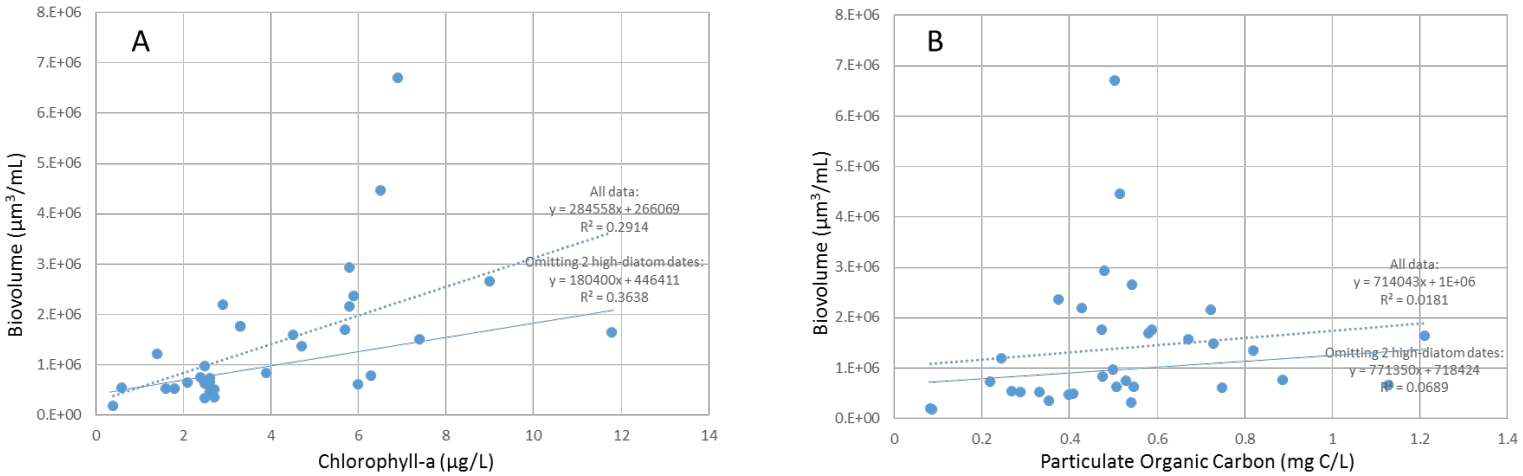

Figure 5-68. Relationships between different measures of phytoplankton biomass in Cayuga Lake 2013 from integrated 0-10m samples five stations: (a) total biovolumes calculated from cell counts and measures of cell dimensions versus chlorophyll *a*, (b) Biovolume versus particulate organic carbon.

not especially strong positive relationship for Chl-*a* (r^2= 0.29, $p < 0.001$) and no significant relationship with POC (r^2 = 0.02). During the June diatom bloom, biovolume was much higher compared with either Chl-*a* or POC, presumably because much of the cell volume is comprised of silicate-rich cell wall structures. Removing the two most extreme of these points from the regression did not, however, substantially improve the relationships (Chl-*a*: r^2= 0.36, $p < 0.001$, POC r^2= 0.07, not significant).

One particularly clear pattern in the data is the relationship between dissolved silicate epilimnion concentration and diatoms densities at each of the three central-lake sites (Sites 3, 5 and 7; Figure 5-69). The dynamics are especially interesting because diatoms make up the great majority of the phytoplankton in late spring, and in autumn (phytoplankton was counted on October dates only for Site 5). As diatom densities increase in these two time periods, they took up silicate to make their siliceous cell walls. Dissolved silicate concentrations fell as a result which appears to have resulted in a subsequent decline in diatom growth rates presumably due to limitation by silica availability. Because the siliceous cell walls are much denser than water, they sink and transport silica to the lake bottom, stripping it from the water column (Schelske et al. 1983). Once the diatoms declined, silicate concentrations rose slowly over the summer resupplied by stream inflows from the watershed. Diatoms then bloomed again in fall (Site 5 data), again causing a decline in silicate concentration. This pattern traces a classic consumer-resource cycle.

5.4.1.3.2. Zooplankton

Crustacean and rotifer zooplankton densities in the epilimnion were low until mid-June when the markedly increased at all sites except Site 9 (the north-end shelf) where the biomass increase was delayed until late June (Figure 5-70). Total zooplankton biomass then declined in August and remained relatively low until the end of the sampling period in late-October (an exception is a spike in densities at Site-1 – the south self: cf. Figures 5-70 and 5-71). The zooplankton was comprised primarily by copepods extending from winter to April, followed by dominance by rotifers in May and early June, and then a major increase in cladocerans in mid-to-late June (Figure 5-71). The major phytoplankton-grazing taxon, *Daphnia* (in Cayuga Lake, represented solely by the small-bodied species, *D. retrocurva*) did not become a notable component of the cladoceran assemblage until July. Hypolimnetic zooplankton were dominated by copepods with only minor reflection seen of the epilimnion seasonal succession (not illustrated).

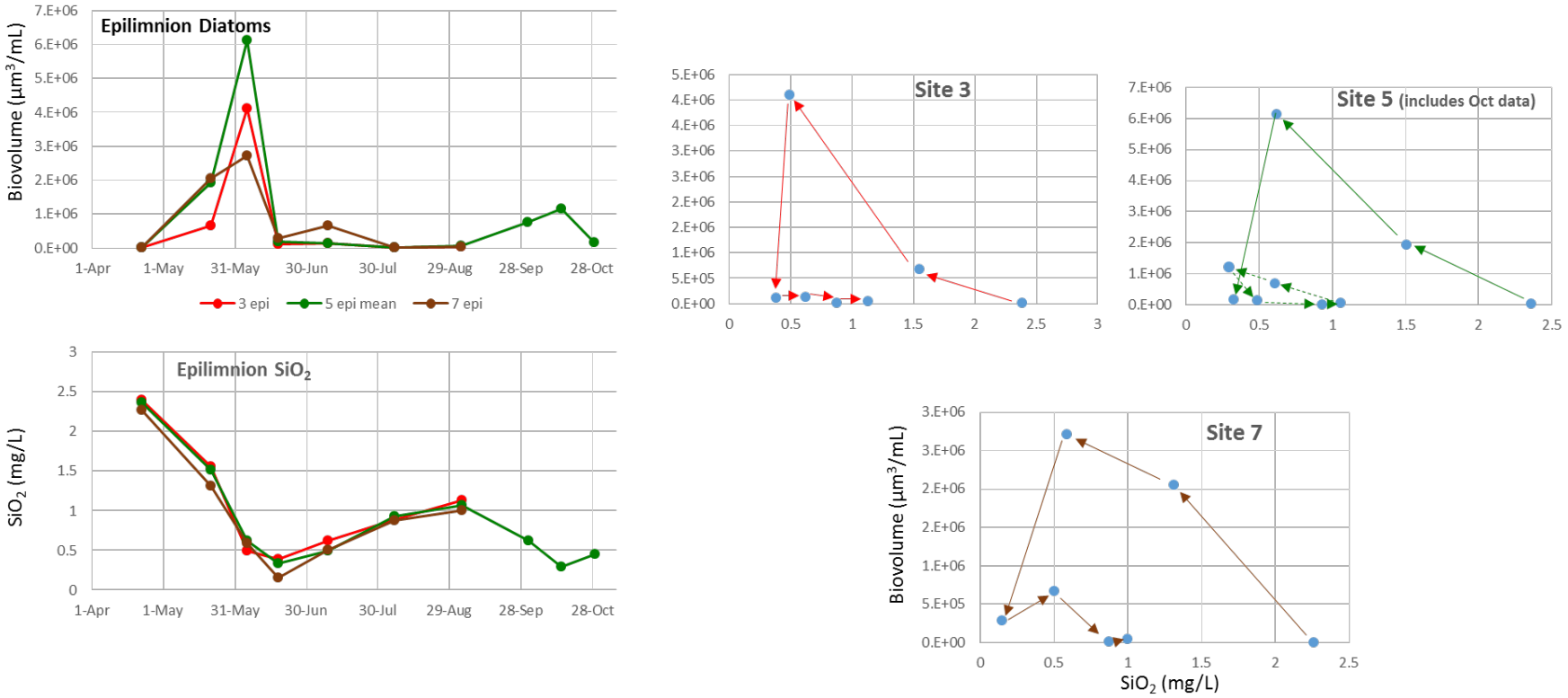

Figure 5-69. The relationship between epilimnetic diatom biomass densities and silicate concentrations at the three central Cayuga Lake sites counted for phytoplankton. The two graphs on the left show seasonal cycling in both metrics at sites 3, 5 and 7. The three phase-plane graphs on the right show, at each sampling site, consumer (diatom) – resource (silicate) cycling with diatom density changes following changes in silicate concentration.

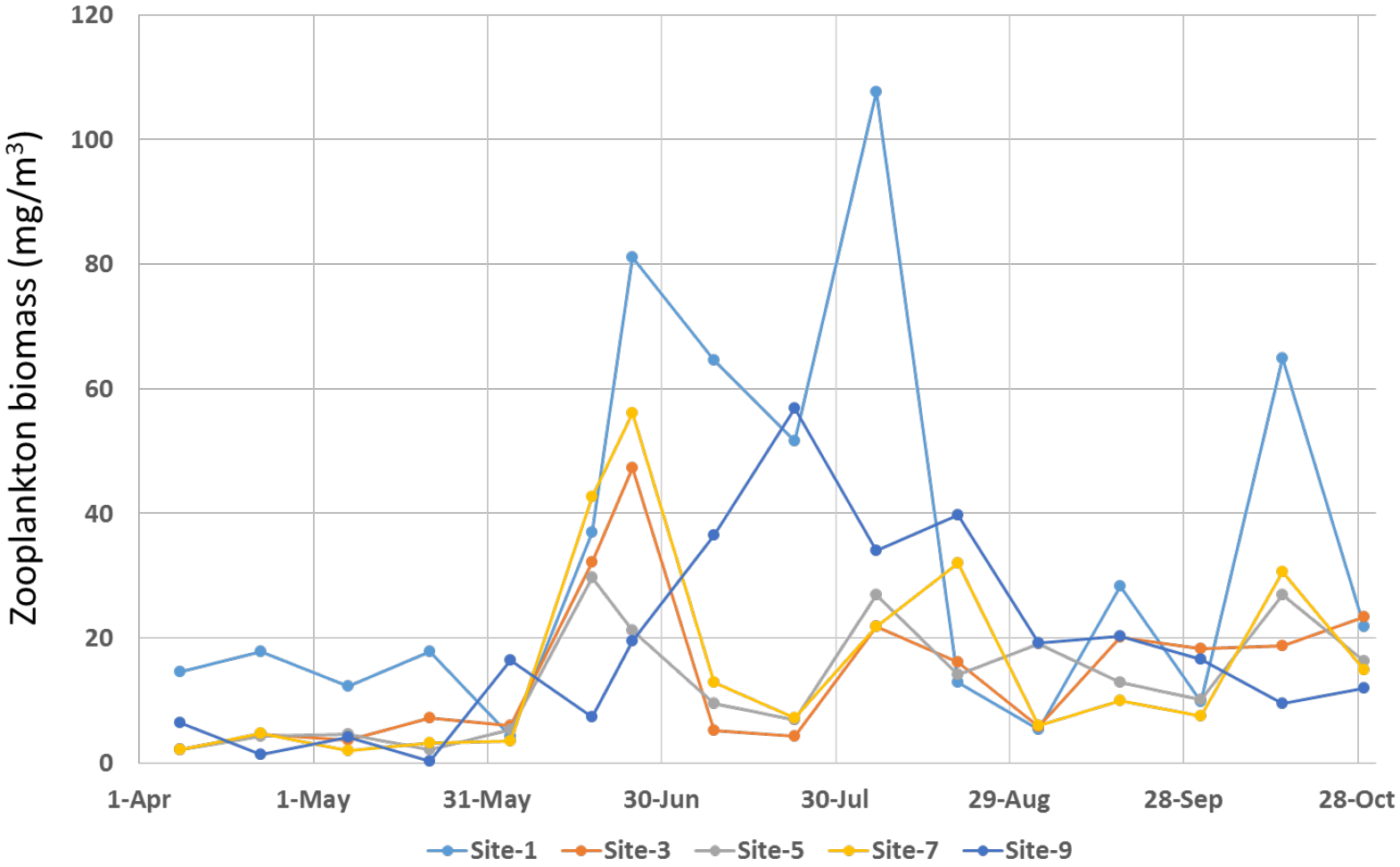

Figure 5-70. The total zooplankton biomass concentrations of for the epilimnion (0-10 m) of five sampling sites along the main south (Site 1) to north (Site 9) axis of Cayuga Lake in 2013.

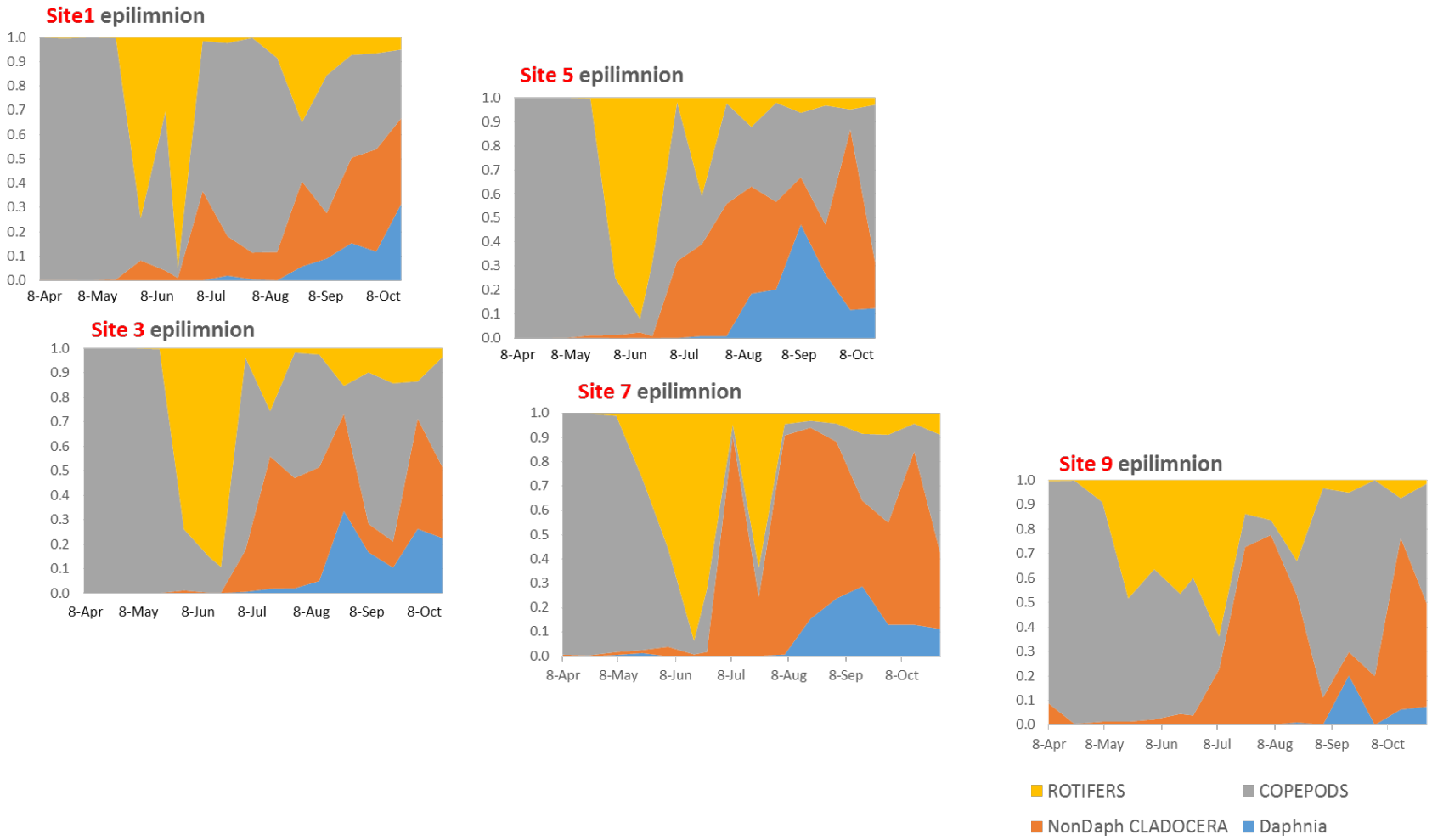

Figure 5-71. Fractional composition by biomass of major zooplankton taxa in Cayuga Lake epilimnion 2013.

5.4.1.3.3. Phytoplankton – Zooplankton Dynamics

The most striking feature of the combined picture of phytoplankton and zooplankton (Figure 5-72) is the decline in phytoplankton density at the end of the diatom bloom in mid-June accompanied by the marked increase in zooplankton density at the same time. Because diatoms are generally a high-quality food for grazing zooplankton, it seems very likely that the dense diatoms in early June fed the zooplankton, resulting in their increase in population size, which then in turn led to the decline in diatoms as the zooplankton grazed them down. One way to test this interpretation will be to calculate zooplankton birth rates based on their clutch sizes and egg development times.

5.4.1.4. Summary and Primary Findings

The seasonal abundances of phytoplankton and zooplankton in Cayuga Lake in 2013 were unremarkable and in many ways consistent with the general Plankton Ecology Group (PEG) model description of lake plankton dynamics (Sommer et al. 1986, Sommer et al. 2012). The diatom bloom is typical of large lakes with a turbulent epilimnion that keeps these heavy silica-rich cells suspended. The termination of the spring bloom by a combination of silica limitation of phytoplankton and an increase in grazing zooplankton is also typical of north-temperate zone lakes in general, as is the mixed summer phytoplankton assemblage of chlorophytes, chrysophytes, and cryptophytes, followed as the lake continues to warm by cyanobacteria and dinoflagellates, although none of these groups became very abundant. Cyanobacteria did not become sufficiently dense to form nuisance blooms or floating scums.

1. Phytoplankton biovolume density was moderate to low at all sites and dates, except at two sites during an early June diatom bloom.

2. Cyanobacteria biovolume density was low at all sites throughout the sampling period. Cyanobacteria made up a maximum of 14-23% of the phytoplankton biovolume at a single site in July and August 2013.

3. A mid-June decline in diatom densities coincides with a marked increase in the biomass density of grazing zooplankton and a shift in dominance from copepods and rotifers to cladocerans. Initially these cladocerans were comprised of primarily of *Bosmina*. The invasive predatory cladoceran, *Cercopagis*, also increased at this time.

4. Daphnia, the major grazing cladoceran taxon in many lakes, was only a notable component of zooplankton biomass from July-October and was comprised entirely of D. retrocurva, a small species with low feeding rate. Maxiumum Daphnia density.

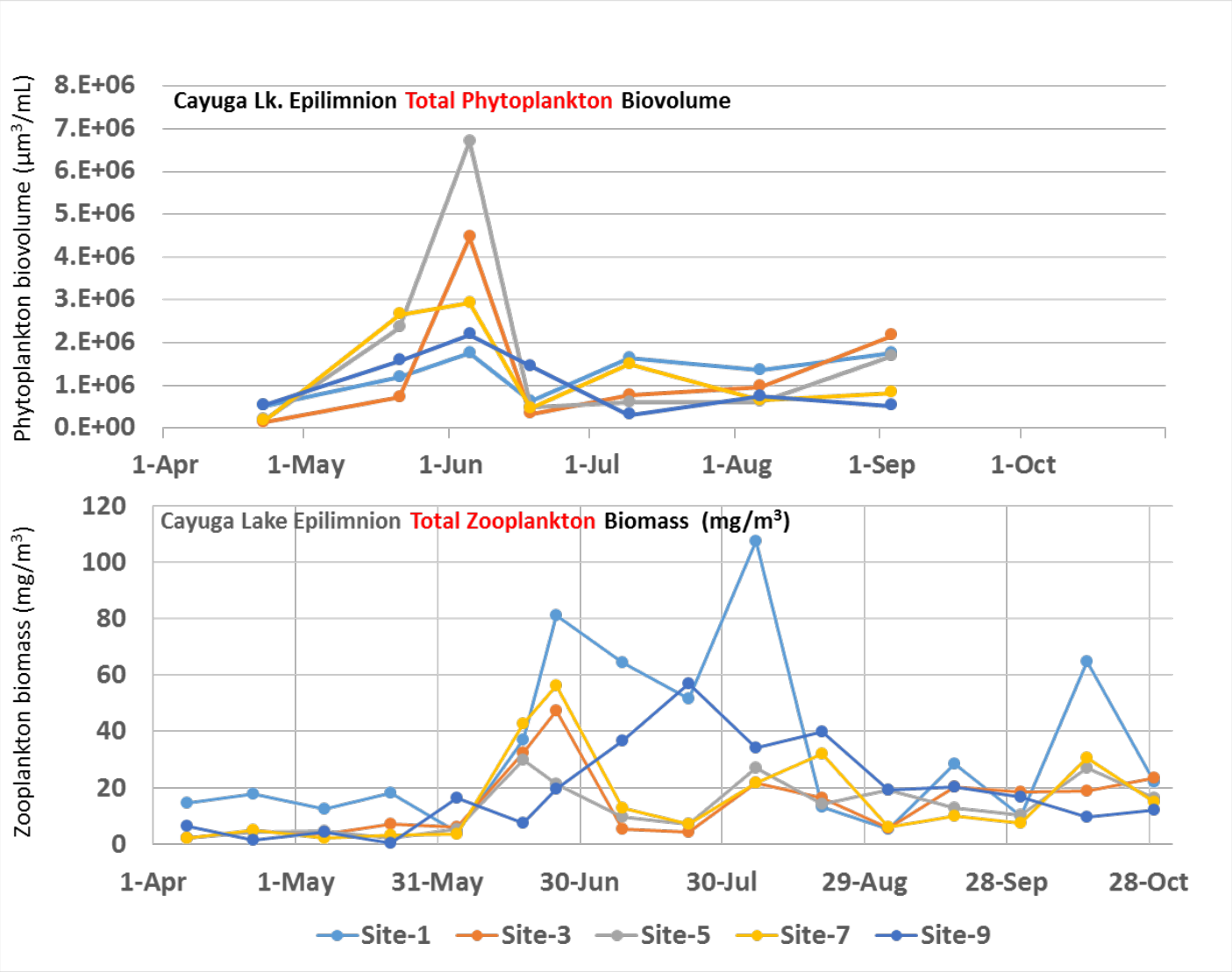

Figure 5-72. Comparison of the seasonal dynamics of total phytoplankton (top) and total zooplankton (bottom) for the epilimnion (0-10 m) of five sampling sites along the main south (Site 1) to north (Site 9) axis of Cayuga Lake in 2013.

did not exceed 20% of zooplankton biomass except on one date in September at a single site when epilimnion abundance reached 6.2 µg/L (8.8 *D. retrocurva*/L).

5.4.2. Mussels

5.4.2.1. Introduction

Cornell University has monitored hypolimnetic soluble reactive phosphorus (SRP) weekly since the year 2000 as part of their Lake Source Cooling program (Cornell University, 2012). Water is sampled at the intake of the system at a depth of 73 m. The time-series of SRP of the intake indicates an increase of nearly 4 µg/L after 2004 (Figure 5-61). A strong seasonal signal tracks a build-up of phosphorus in the hypolimnion during the stratified season, followed by a sharp decrease at the end of the year after mixing due to fall turnover. This seasonal pattern is consistent with a phosphorus source within the hypolimnion that is not being utilized by phytoplankton.

Inland waters receive phosphorus loading from external (watershed) and internal (bottom sediment) sources. Internal loading is known to be important in shallow productive lakes that experience summer anoxia (Sondergaard et al. 2003). Phosphorus binds tightly with iron oxyhydroxides absorbed on the surfaces of sediment particles, but is released into the water column at low oxygen conditions. This process is less important in deep lakes such as Cayuga Lake having a maximum depth of 133 meters. Cool hypolimnia of deep lakes are well oxygenated throughout the summer so that phosphorus released within deeper sediments is trapped at the sediment surface. Therefore, for deep lakes, watershed sources of phosphorus are generally thought to be more important than sediments.

Over long time scales, phosphorus added by watershed loading is considered to be at balance with phosphorus burial in sediments. Increased watershed loading could shift this balance and lead to eutrophication. Thus, internal cycling processes such as bacterial decomposition and excretion by organisms are not considered to be adding additional phosphorus, instead they regenerate phosphorus from particulate to dissolved forms. Invasive species such as nonindigenous dreissenid mussels can quickly attain high biomass, displacing native communities for space and food. Quagga mussels (*Dreissena rostriformis bugensis*) are tolerant of soft substrates, coldwater temperatures, and low food supply, and are thus well positioned to build up biomass levels that have never been attained by any native benthic organism in profundal habitats. Phosphorus excretion by dreissenids is lower than that of other benthic macroinvertebrates and zooplankton (Sereda and Hudson 2011). Excretion by dreissenid mussels in shallow habitats of lakes has been identified as a phosphorus source enhancing growth of the nuisance algae *Cladophora* (Ozersky et al. 2009).

Although outside the objective of this paper, our quantification of invasive mussel populations is also essential for understanding trends in trophic state tracked by parameters such as chlorophyll *a* and water clarity. Dreissenid mussel grazing is a recognized force that

decreases Chl-*a* (45% on average) and increases water clarity (1 m) across a wide range of invaded freshwater systems (Higgins and VanderZanden 2010). Invasive mussels quickly attain large standing stocks, and their efficient filter feeding can clear an entire water body in less than a day, exceeding phytoplankton growth. Their role as an ecosystem engineer has been described as "benthification", where nutrients and carbon are transferred from pelagic to benthic pools (Mayer et al. 2014). When tracking the changing trophic state of an important natural resource such as the Finger Lakes, the potential role of dreissenids cannot be ignored.

The primary objective of this paper is to take a first step in evaluating the potential significance of mussel excretion in Cayuga Lake. We outline a simple model of an isolated hypolimnion receiving a continuous internal load of phosphorus from benthic mussels living along its slopes that is thoroughly mixed and escapes utilization by phytoplankton below the photic zone. Clearly the hydrodynamics of Cayuga Lake are much more complex and include both limiting benthic boundary layers and dynamic seiches. Later manuscripts will discuss the incorporation of our mussel population estimates within a more sophisticated two-dimensional hydrodynamic model of Cayuga Lake (Gelda et al. 2015).

5.4.2.2. Methods

5.4.2.2.1. Benthic Survey and Lab Processing

Cayuga Lake is the longest of eleven north-south oriented lakes in central New York known as the Finger Lakes. It is a long (61 km), narrow (3 km) lake up to 133 m deep. Our survey design was based on east-west transects centered by eleven mid-lake sites along the axis of the lake (Figure 5-73, Table 5-9). Transects were positioned perpendicular to the steep slope. Several sites on the western and eastern slopes were chosen in the field to provide a range of depths. Transects on the shallow northern and southern ends of the lake required fewer sites. Sampling was conducted in September-October 2013.

A petite Ponar benthic grab (sample area 0.023 m^2) was used to collect triplicate samples at each of 98 sites (Table 5-9). Each sediment sample was sieved through a 500 μm mesh, with all benthic organisms and detritus preserved in 90% ethanol. In the lab, subsampling was done on some occasions if more than 200 mussels were within a sample. Mussels were sorted and identified to species. Wet weight (including shells, in g) was measured for each species in each sample. Shells > 5 mm were laid out on a white background and photographed with a cm scale. Images were processed using ImageJ (http://imagej.nih.gov/ij/) that outlines each shell as an ellipse and automatically counts and outputs resulting major axis lengths. Shells < 5 mm were counted but not photographed and sized.

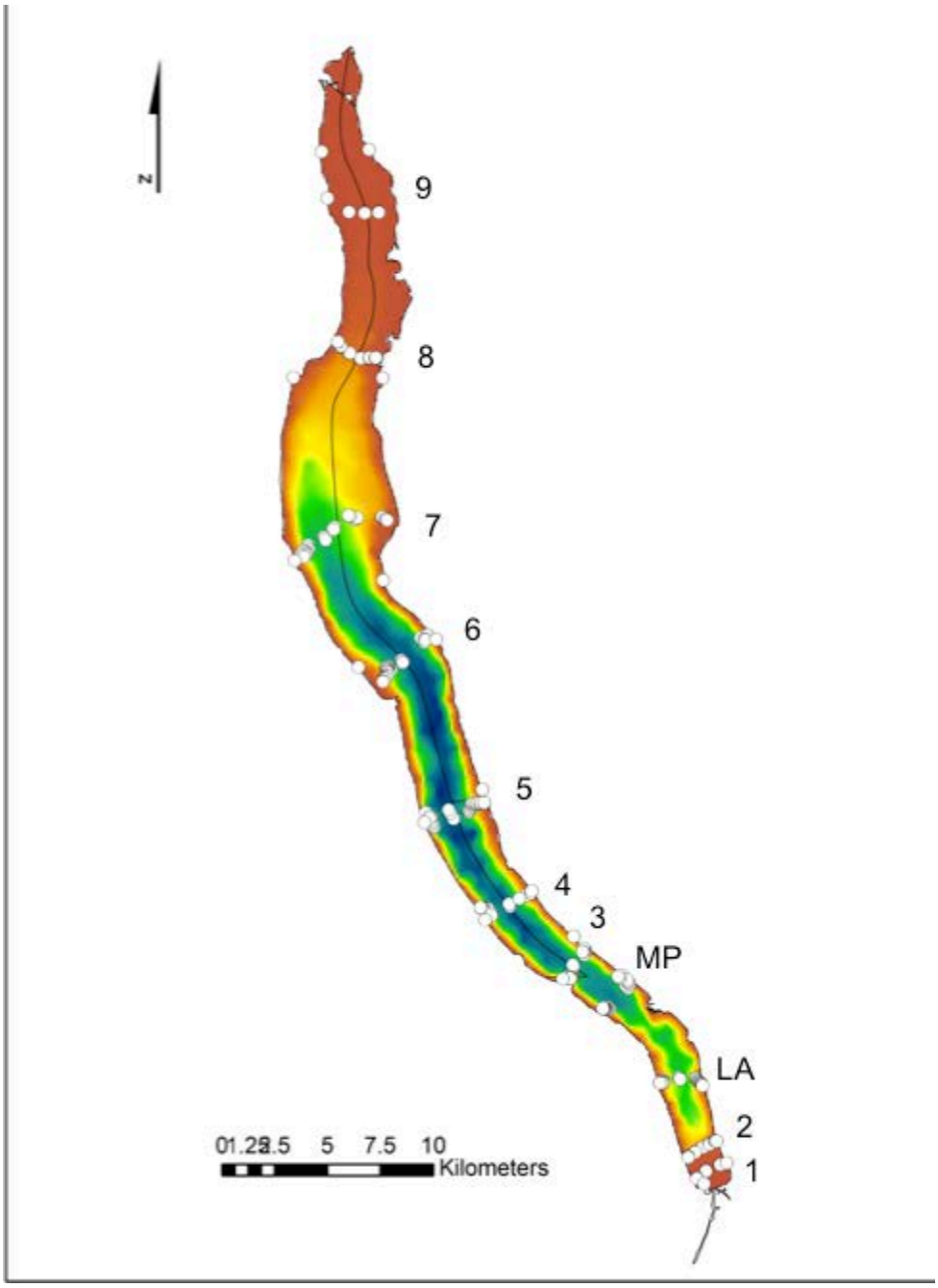

Figure 5-73. Map of benthic survey sites in 2013 superimposed on a bathymetric map of Cayuga Lake. Numbers 1-9 correspond to midlake sites established by sampling program. MP (Myers Point) and LA (Lansing) transects were added between stations 2 and 3. Sites were selected in the field along the western and eastern slopes.

Table 5-9. Location of sampling sites in Cayuga Lake for dreissenid mussels in 2013. (M = mid-lake station for each transect).

transect	No.	Site Name	Latitude	depth	comment
1 01M002 (2 m)	2	1E003	42.468	3	east
	3-4	1W001, 1W001A.2	42.468	1, 1	west
2 02M008 (8 m)	6-7	2E009, 2E010	42.4771	9, 10	east
	8-9	2W004, 2W007	42.4771	4, 7	west
Lansing LAM090 (90 m)	11-14	LAE015, LAE025, LAE045, LAE065	42.5073	15, 25, 45, 65	east
	15-17	LAW015, LAW030, LAW055	42.5073	15, 30, 55	west
Myers Point MPM115 (115 m)	19-23	MPE025, MPE045, MPE060, MPE075, MPE090	42.537	25, 45, 60, 75, 90	east
	24-27	MPW030, MPW055, MPW065, MPW090	42.537	30, 55, 65, 90	west
3 3M110 (110 m)	29-32	3E020, 3E045, 3E070, 3E090	42.5543	20, 45, 70, 90	east
	33-38	3W001, 3W030, 3W040, 3W055, 3W075, 3W095	42.5543	1, 30, 40, 55, 75, 95	west
4 4M125 (125 m)	40-45	4E001, 4E010, 4E025, 4E045, 4E070, 4E085	42.579	1, 10, 25, 45, 70, 85	east
	46-50	4W001, 4W025, 4W045, 4W065, 4W090,	42.579	1, 25, 45, 65, 90	west
5 5M120 (120 m)	52-58	5E001, 5E010, 5E025, 5E035, 5E045, 5E065, 5E085	42.6191	1, 10, 25, 35, 45, 65, 85	east
	59-63	5W001, 5W020, 5W040, 5W065, 5W090	42.6191	1, 20, 40, 65, 90	west
6 6M120 (120 m)	65-69	6E001, 6E015, 6E030, 6E060, 6E085	42.684	1, 15, 30, 60, 85	east
	70-77	6W001, 6W010, 6W020, 6W035, 6W050, 6W065, 6W080, 6W090	42.684	1, 10, 20, 35, 50, 65, 80, 90	west
7 7M075 (75 m)	79-83	7E001, 7E010, 7E025, 7E040, 7E060	42.74	1, 10, 25, 40, 60	east
	84-89	7W001, 7W025, 7W045, 7W060, 7W080, 7W090	42.74	1, 25, 45, 60, 80, 90	west
8 8M010 (10 m)	91-92	8E001, 8E005	42.8122	1, 5	east
	93-95	8W005, 8W010, 8W020	42.8122	5, 10, 20	west
9 9M003 (3 m)	97	9E003	42.8745	3	east
	98	9W002	42.8745	2	west

Shell lengths were converted to dry weight biomass (shell-free) using length-weight relationships developed for each species in Lake Michigan by Nalepa et al. (2010). These relationships follow the form DW = EXP(a*LN(L)+b), with dry weight (DW) in mg and length (L) in mm. The value of a and b selected for quagga mussels were 3.143 and -6.535, and for zebra mussels are 2.651 and -5.226. These are very close to our unpublished relationships based on measurements of mussels from Cayuga Lake. Shells < 5 mm were assigned a length of 2.5 mm that yielded a dry weight biomass of 0.026 mg for quagga mussels and 0.061 mg for zebra mussels. Density, wet weight (including shells) and dry weight (not including shells) were compiled for each sample and normalized to the sample area using any subsampling factor and dividing by the area sampled. Tables of individual length measurements are linked to field sampling and laboratory analysis information tables in a relational database that can be queried to output these compilations.

5.4.2.2.2. Phosphorus Excretion Measurements

Dreissenid mussel excretion rates reported in the literature have been reviewed in Bootsma and Liao (2014). We also measured excretion of SRP directly by Cayuga Lake mussels. Live quagga mussels were collected from three depths (25, 50, and 80 m) on the eastern slope off of Myers Point near Lansing, NY. Mussels were sorted in the field- approximately 60 individuals (3 replicates of 20 mussels each) were needed for the 50 and 80 m treatments and 180 individuals needed for the 25 m treatments (three temperature treatments and three replicates). Each treatment's mussels had an average length that ranged from 17-19 mm. 20 Liters of mid-lake surface lake water was collected in a single acid washed carboy. Lake water was filtered using a 0.45 micron membrane filter and filtrate was transferred to a second acid washed carboy. This water represents a low soluble reactive phosphorus (SRP) water used as the baseline for the excretion study. 300 ml of this water was added to several acid washed glass jars. Five jars were chosen as "initial" values and 150 ml of water from each was put into an acid washed glass sample bottle. Twenty mussels were rinsed in deionized water and then added to three replicate treatment jars. One jar with no mussels was used as a control. After ten hours, 150 ml of water was removed from each jar and filtered with a 0.45 micron filter mounted on a syringe. Filtrate was put into an acid washed glass sample bottle. Water was measured for soluble reactive phosphorus using standard methods by UFI (Upstate Freshwater Institute 2013). Each set of twenty mussels were photographed and measured for length using the program Image J. Shell-free dry weight mussel biomass was calculated using length-weight equations. The specific excretion rate (micromoles of phosphorus per g dry weight mussels per hour) was calculated using the increase of phosphorus (concentration increase times water volume to yield micromoles of phosphorus), the dry weight biomass of the mussels (g), and the duration of the experiment (hrs).

5.4.2.2.3. Simple Hypolimnion Model

An areal excretion rate (micromoles of phosphorus per m^2 of substrate per hour) was calculated by combining the benthic survey results (g shell free dry weight of mussels per m^2) with the literature-based or experimentally determined specific excretion rates. This was done for each 10 m depth interval below 20 m (assumed metalimnion depth) and then multiplied by the known substrate area (in m^2) for each depth interval and the time period of stratification (100 days). The total micromoles of phosphorus excreted by the benthos (20-130 m) was converted to micrograms (multiplied by 31) and then divided by the total volume of the hypolimnion (in liters). This final step yields the SRP concentration increase (μg/L) expected from the excretion by the observed mussel biomass. This calculation was done using three specific excretion rates- 1) the average rate in the literature (0.33 μmol P/g DW/hr, in Bootsma and Liao 2014), 2) a rate based on our laboratory measurements at 4°C, and 3) a rate that varies with temperature following our lab measurements. The variable rate follows thermal gradients with depth.

5.4.2.3. Results

5.4.2.3.1. Benthic Survey

Quagga mussels were collected in 96% of the 279 samples throughout all depths of Cayuga Lake. Zebra mussels were found in only 24% of the samples, and were most common in only the shallowest samples. Out of 26,117 quagga mussels counted, 32% were juveniles smaller than 5 mm (Figure 5-74). Similarly, 26% of the 1, 326 zebra mussels were smaller than 5 mm. Most quagga mussels larger than 5 mm were from 6 to 15 mm and reached maximum size of 30 mm. Few zebra mussels exceeded 15 mm. As indicated by the length-weight relationships (Figure 5-75), small individuals, although abundant, contribute very little to the overall biomass. Mussel density was poorly correlated to both wet and dry biomass. Wet (with shell) and dry (without shell) biomass indicies were strongly correlated (r^2=0.89, WW:DW ratio 38.5). Grazing and excretion rates are size dependent and therefore require the incorporation of biomass in rate estimates.

Our focus on the hypolimnion led us to follow the abundance of quagga mussels for deeper transects only (omitting transects 1-2 and 8-9 and zebra mussel biomass). Quagga mussel biomass decreased continually from levels near 95 g/m^2 at shallow depths (< 20 m) to levels less than 10 g/m^2 deeper than 80 m (Figure 5-76). The high variability seen at shallow depth intervals is characteristic of patchily distributed mussel beds. Variation in the trend of mussel biomass with depth from south to north also contribute to this variation (Figure 5-77). For example, quagga mussel biomass at the southern end of the lake near Myers Point (Myers Point and Transect 3) is much higher at depths of 40-60 m relative to other transects. Note that zebra mussels are represented as white circles in this figure and it is clear that they are shallowly distributed and make up very little of the overall mussel biomass. High quagga mussel biomass values at shallow depths reflect both more numerous mussels as well as larger mussels (Figure 5-78). Size is variable (averaging 7 to 17 mm for mussels > 5 mm) but peaks at 20 m depth.

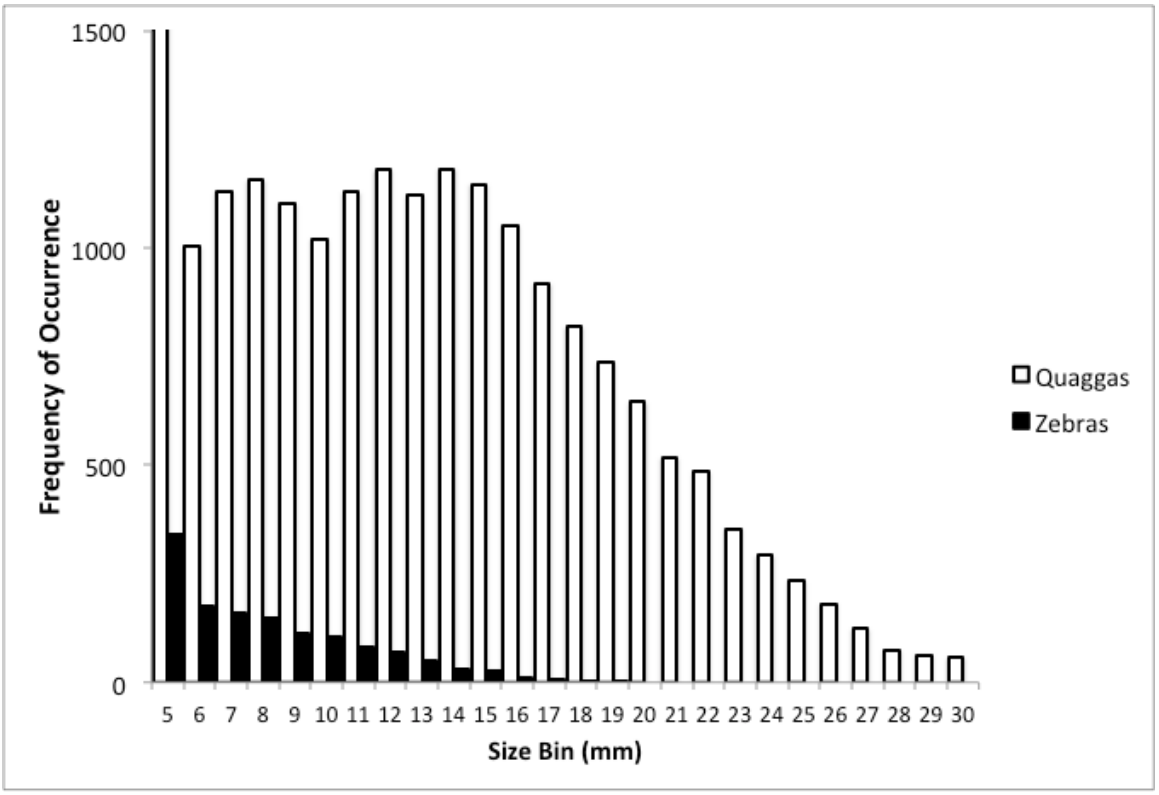

Figure 5-74. Size distribution histogram of quagga (white bars) and zebra mussels (filled bars). 5 mm size bin represents all individuals smaller than 5 mm and for quagga mussels is off scale at 8,333 individuals.

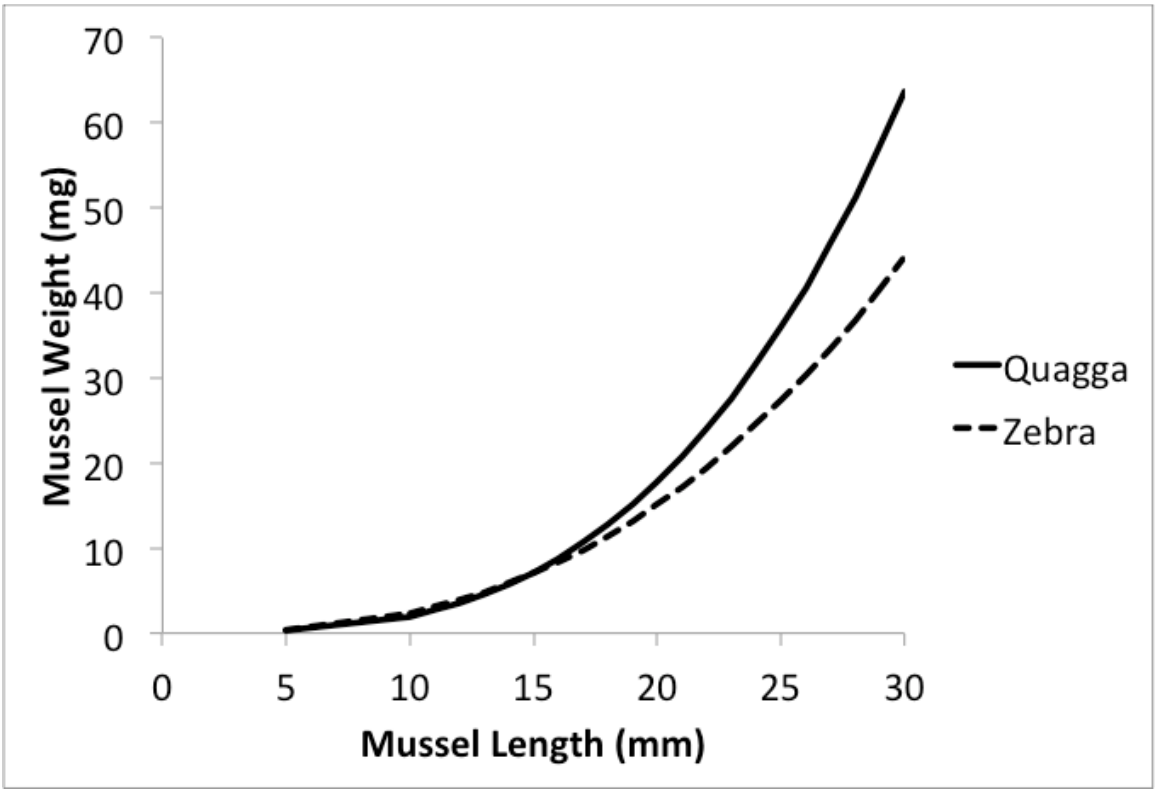

Figure 5-75. Relationships for each mussel species relating mussel length (in mm) to mussel dry weight (in mg, without shells). Source of values used are Nalepa et al. (2010) that is very similar to unpublished measurements of Cayuga mussels.

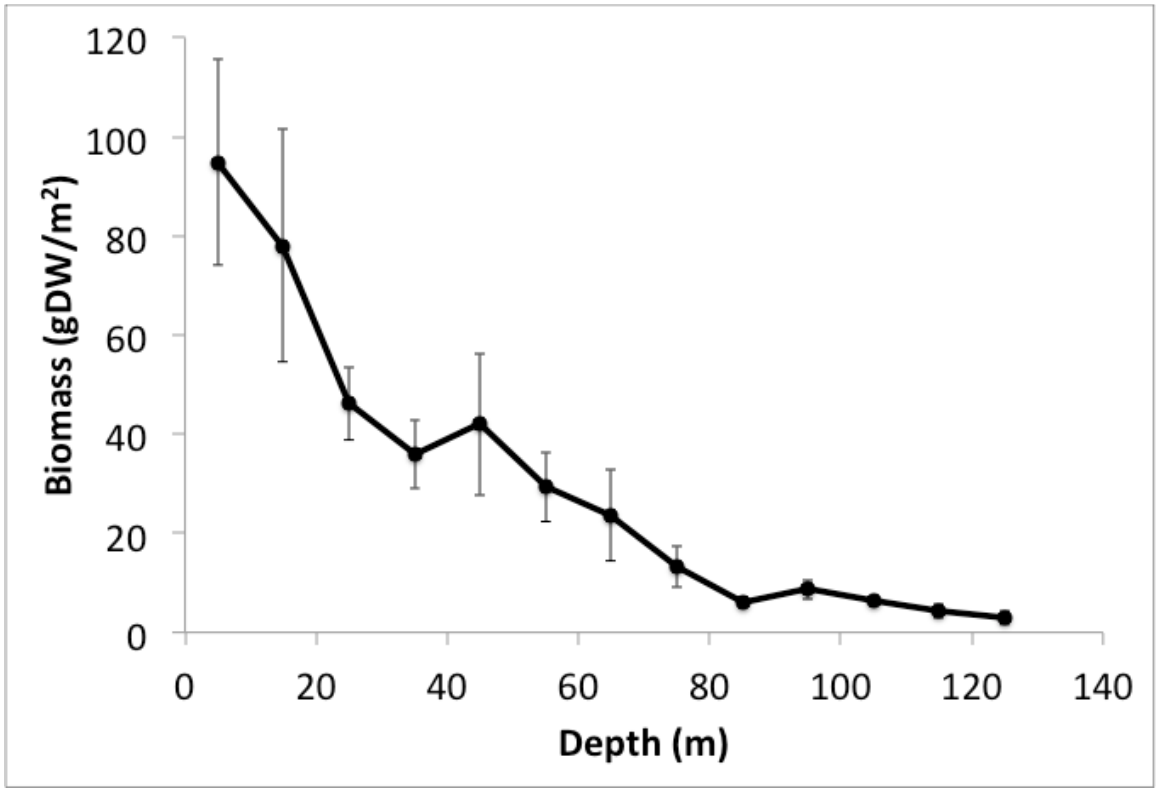

Figure 5-76. Quagga mussel biomass (dry weight) trends with depth. Line represents the overall average for each depth interval (10 m resolution). Error bars represent 1 SE.

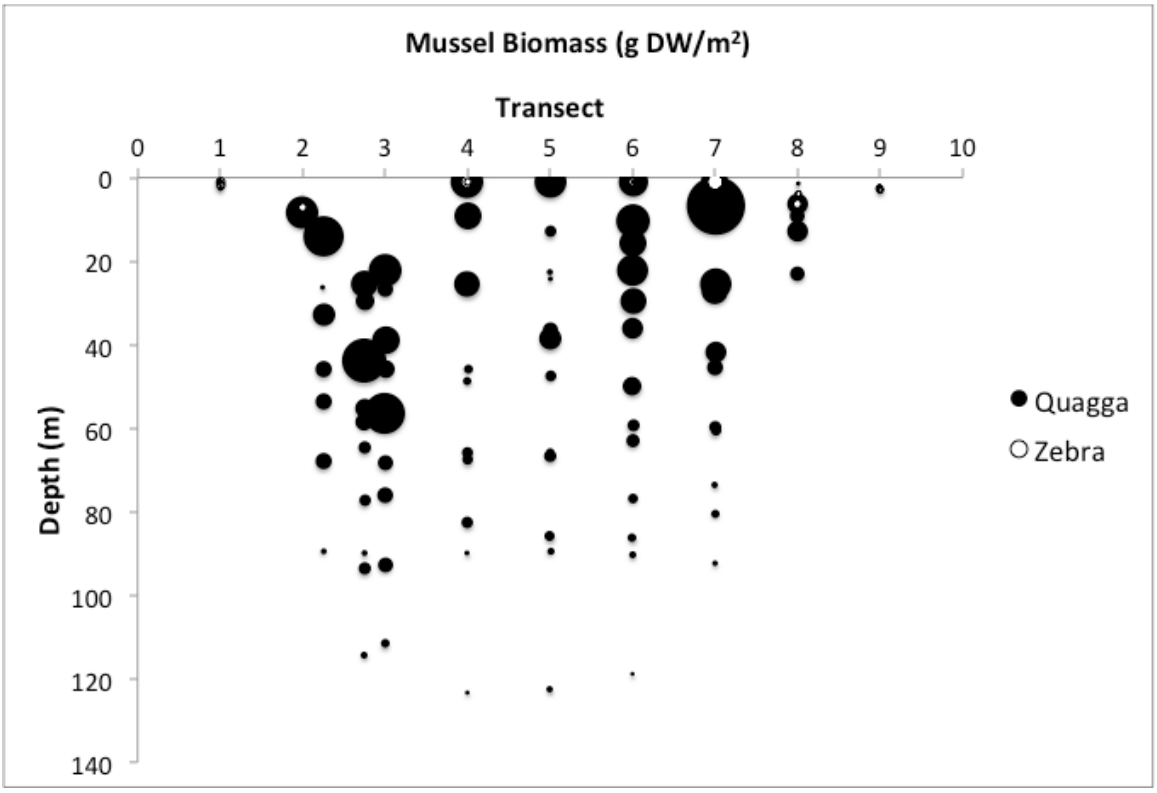

Figure 5-77. Distribution of biomass with depth along each transect from the south end (1) to the north end (9). Size of dot is related to mussel biomass. Zebra mussels (white fill) are very small with a shallow distribution.

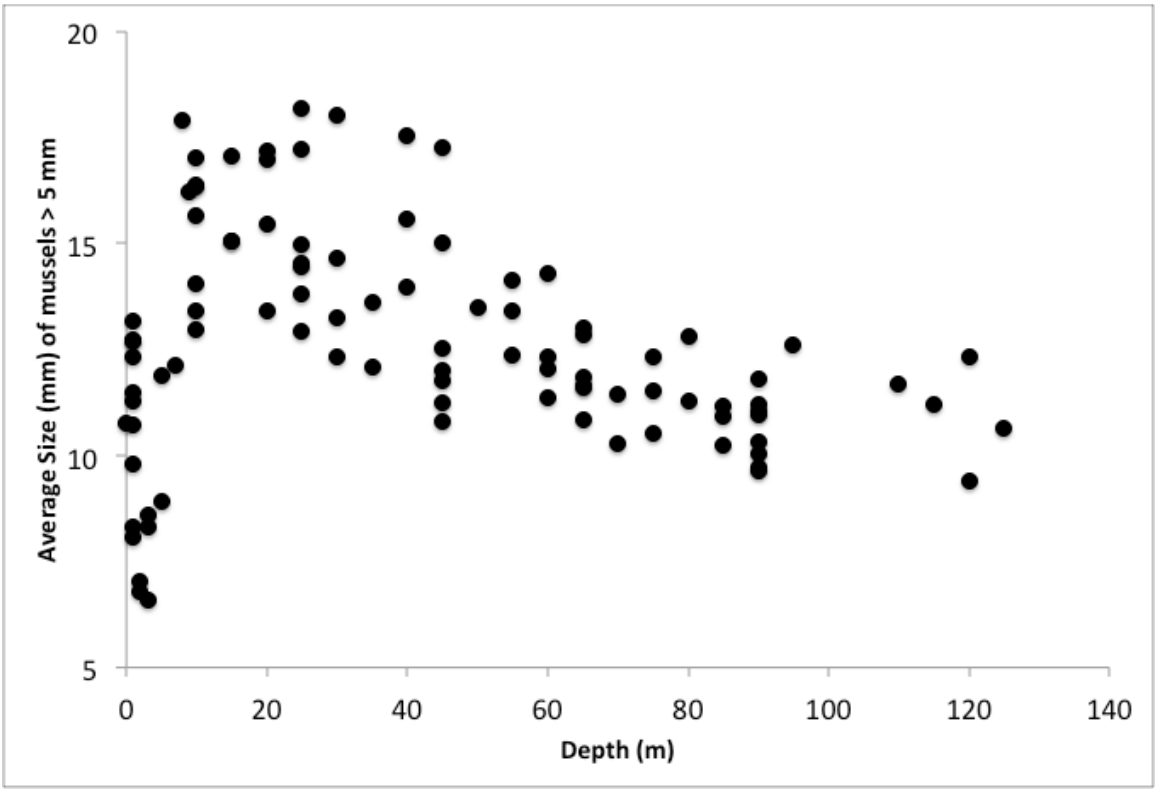

Figure 5-78. Average size of quagga mussels for benthic sites (omitting individuals < 5 mm).

Populations within this depth interval also include very few mussels < 5 mm compared to other depths where small mussels comprise 30-50% of the population.

5.4.2.3.2. Excretion Rate Measurements

Measured excretion rates (µmol P/g DW/hr) were normalized to the dry weight biomass of the 20 quagga mussels in each replicate. The excretion rates at 4°C temperatures typical of the hypolimnion (n=9) averaged 0.07 µmol P/g DW/hr. The 50 m population had the highest excretion rate at this temperature (0.11 µmol P/g DW/hr), significantly higher than the rate of the deep population (0.04 µmol P/g DW/hr, p-value 0.0156; Figure 5-79). The temperature treatments for the shallow (25 m) mussel population demonstrated a nearly linear increase in excretion rate with temperature, from 0.06 µmol P/g DW/hr at 4°C, 0.14 at 12°C, and 0.26 at 20°C. The high temperature treatment was significantly higher than the low temperature treatment (p-value 0.0012) but not the intermediate treatment.

5.4.2.3.3. Calculation for Hypolimnion

For estimating phosphorus loading to the hypolimnion, we use three estimates of mussel excretion- the average in the literature (0.33 µmol P/g DW/hr), our average measured value at hypolimnetic temperatures (0.07 µmol P/g DW/hr; Figure 5-80), and a rate that varies with temperature so that shallower populations (20-50 m) in warmer water have higher excretion rates (0.10-0.14 µmol P/g DW/hr) than deeper populations (0.06 µmol P/g DW/hr). Table 5-10 follows the calculation for the uniform experimental rate. This calculation yields predictions that hypolimnetic phosphorus concentrations would increase by 7.5 µg/L for the average literature rate, 1.6 µg/L for the hypolimnetic measured rate, and 2.1 µg/L for the temperature dependent rate due to mussel excretion during a 100-day period.

5.4.2.4. Discussion

For both before and after dreissenid mussel invasion, decreasing benthic biomass with depth has been a common pattern in deep lakes due to low food supply in profundal habitats. The photic zone generates particles that decrease in abundance as they sink and remineralize. In Lake Michigan, benthic biomass peaks at intermediate depths (30-50 m), and although originally composed of the native amphipod *Diporeia*, is now dominated by quagga mussels (Nalepa 1989 and Nalepa et al. 2010). While the overall pattern of biomass with depth is the same in Lake Michigan, the most stunning aspect of the quagga mussel expansion has been the dramatic increase in benthic biomass from 8 to near 50 g DW/m^2 that occurred between 2003 and 2008. Cayuga Lake, similar in its native and exotic benthic fauna, has experienced a similar increase in benthic biomass. Highest quagga mussel biomass in Cayuga Lake was at shallow (0 to 20 m) depths, whereas lower benthic biomass nearshore in Lake Michigan has been attributed to high temperature variability and substrate instability.

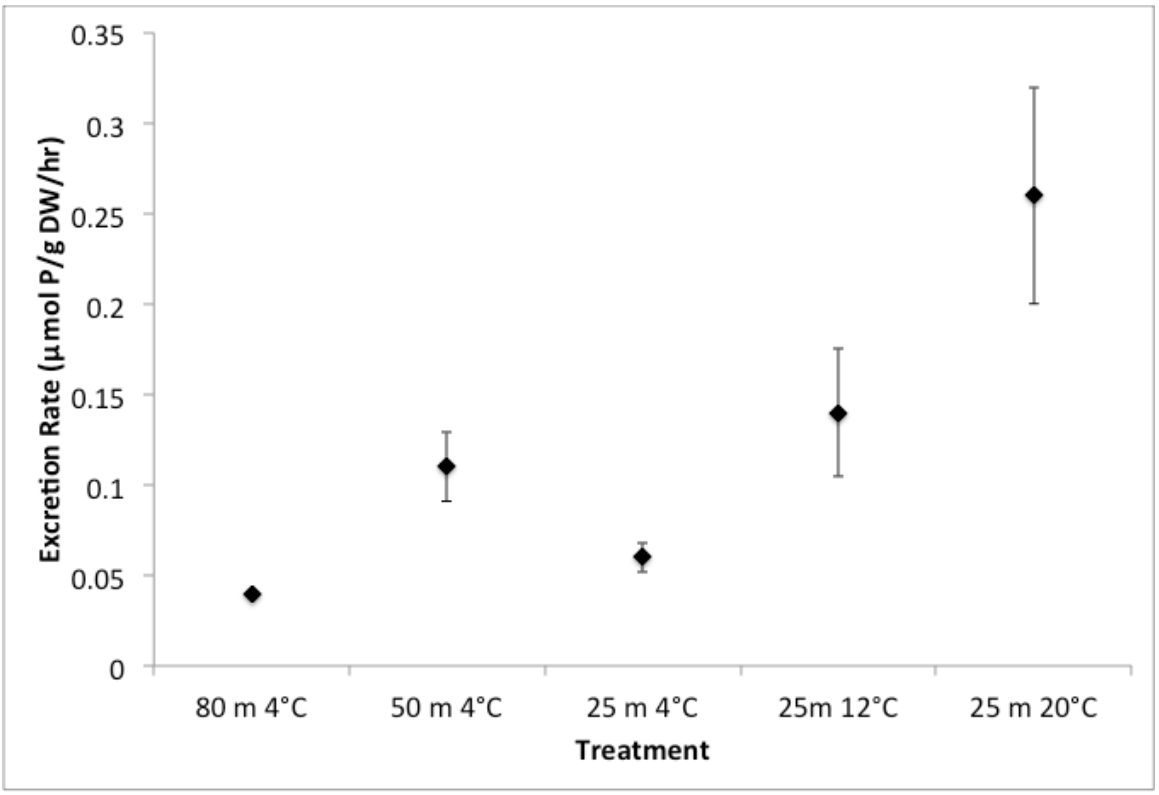

Figure 5-79. Phosphorus (SRP) excretion rates measured over a 10-hour period and normalized to the dry weight biomass of the 20 mussels of each triplicate. Depth indicates source of Cayuga Lake (Myers Point) mussels and temperature indicates temperature mussels maintained at during experiment. Error bars are 1 SE for triplicate measurements. Average of excretion rates in literature is 0.33 (+/- 0.18) µmol P/g DW/hr (Bootsma and Liao 2014).

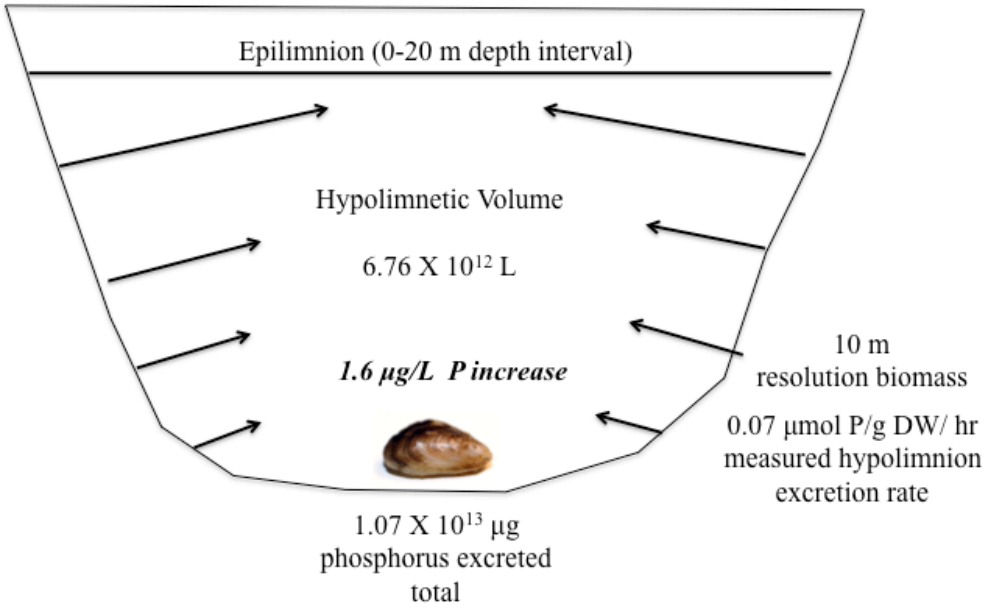

Figure 5-80. Schematic of a closed hypolimnion for Cayuga Lake. Mussel phosphorus excretion was estimated from mussel biomass following literature or experimental based rates for a 100 day period of stratification. The concentration increase was calculated by dividing the mussel phosphorus excretion by the volume of the hypolimnion (see Table 5-10 for calculation). Note the size of the arrows reflect the decrease in biomass with depth and is not to scale.

Table 5-10. Calculation of mussel loading by excretion to hypolimnion (below 20 m).

Depth Interval	Mussel Biomass g DW/m^2	Benthic Area km^2	Water Volume x 10^{12} L	Excretion Rate µmol/g DW/ hr	Excreted P µg P/100 days
0-10 m	94.8	47.4	1.4357		
10-20 m	78.0	12.7	1.1834		
20-30 m	46.2	8.0	1.0802	0.07	**1.92424E+12**
30-40 m	36.0	10.1	0.9896	0.07	**1.89473E+12**
40-50 m	42.0	12.0	0.8787	0.07	**2.62435E+12**
50-60 m	29.4	8.3	0.7773	0.07	**1.27156E+12**
60-70 m	23.6	7.8	0.6964	0.07	**9.59691E+11**
70-80 m	13.2	7.1	0.6220	0.07	**4.89171E+11**
80-90 m	6.0	8.0	0.5468	0.07	**2.5185E+11**
90-100 m	8.7	8.4	0.4648	0.07	**3.79573E+11**
100-110 m	6.5	8.4	0.3805	0.07	**2.84357E+11**
110-120 m	4.4	17.9	0.2442	0.07	**4.07454E+11**
120-130 m	2.9	16.1	0.0798	0.07	**2.47289E+11**
			6.7603E+12		**1.07343E+13**
				P Increase (ug/L)	**1.59**

Although quagga mussel biomass is highest at shallow depths in Cayuga Lake, we do not consider the excretion of these mussels in our calculation since phosphorus released by these mussels goes into the epilimnion where it is available to phytoplankton. We instead focus on populations below 20 m that could influence hypolimnion concentrations. Mussel biomass within the 20-50 m depth interval in Cayuga Lake is near 40 g DW/m^2 and therefore a likely source. Our three estimates of SRP mussel release are on the same order of magnitude and bracket the 4 μg/L increase observed in the hypolimnion. This suggests that mussel excretion likely plays a significant role in phosphorus cycling even despite the vast volumes of water represented by the hypolimnion of a deep lake. The average excretion rates in the literature yield an increase nearly twice that observed. Consistent with these rates being high, when they are applied to the two dimensional W-2 hydrodynamic model of Cayuga Lake, vertical phosphorus profiles increase to unrealistic values. Note that most of the studies in the literature were done at higher temperatures (15-23°C), so the lower rates we measured may be more appropriate for a hypolimnion estimate.

Note our simple model of the hypolimnion assumes complete mixing of a hypolimnion isolated from the surface layer. This approach ignores the effects of benthic boundary layers that limit transport of dreissenid food and excretion products and seiches that mix along the metalimnion. These physical processes are considered within hydrodynamic models. The vertical distribution of quagga mussels has an important effect on phosphorus generation and dissipation in these models. Our calculations estimate that the large biomass of quagga mussels inhabiting substrates between 20 and 50 m (27% of hypolimnion substrate surface) would generate nearly 74% of the phosphorus increase even without considering temperature effects on excretion rate. This depth interval lines up with seiche activity, which could break up the benthic boundary layer and have the dual effect of ensuring food supply to benthic mussels and also dispersing mussel generated phosphorus into the water column. However, this newly generated phosphorus is closer to the metalimnion and photic zone and thus much more subject to mixing into the epilimnion and being utilized by phytoplankton.

Our observations confirm that quagga mussels have largely replaced zebra mussels, a pattern evident as early as 2006 (Watkins et al. 2012). Quagga mussels in Cayuga Lake occur in the deepest profundal habitats of the lake and have reached biomass levels on the steep slopes comparable to those seen in the Great Lakes (e.g., Ontario and Michigan) in the early 2000s (Watkins et al. 2007, Nalepa et al. 2010). Zebra mussels still have a presence in shallow habitats along the immediate shoreline and at the extreme southern and northern end of the lake, but their biomass is minimal in comparison with quagga mussels. Mussel biomass (both zebra and quagga) is low at the southern end of Cayuga Lake and therefore impacts from grazing and excretion are likely minimal in this area of concern. Quagga mussels (with some zebra mussels) are very abundant in shallow habitats bordering the deep basin and likely impact phytoplankton through grazing and phosphorus supply. Less abundant but still significant quagga mussel

biomass inhabiting the 20 to 50 m depth interval could supply a large portion of the phosphorus increase seen in the hypolimnion.

5.4.2.5. Summary

Long-term monitoring detected a doubling (nearly 4 μg/L increase) in the concentration of soluble reactive phosphorus (SRP) within the hypolimnion of Cayuga Lake, NY after 2004. Increased levels of phosphorus raises concern of eutrophication of this high quality water resource. This increase occurred despite large reductions in municipal point source loading and few changes in watershed landuse and development trends. We hypothesize that excretion by expanding nonindigenous dreissenid mussels (*Dreissena polymorpha* (zebra mussels) and *Dreissena rostriformis bugensis* (quagga mussels)) could have contributed to the observed SRP increase in the hypolimnion. Toward testing this hypothesis, we quantified the density and biomass of dreissenid mussels in an extensive benthic survey in September-October, 2013. Ninety eight sites along eleven east-west transects were sampled in triplicate using a petite Ponar benthic sampler. Biomass was directly measured as wet weight (including shells) and also estimated as shell-free dry weight using measured length and standard length-weight equations. Quagga mussels were collected at all depths and 96.1% of the samples, while zebra mussels were generally collected only at shallow depths (<10 m) and 24.4% of the samples. Quagga mussels were more abundant than zebra mussels at most sites except for the shallow (< 5 m) southern and northern ends of the lake. Overall, dreissenid biomass (shell free dry weight) decreased with depth from levels of 95 g/m^2 to less than 10 g/m^2 deeper than 80 m. Applying literature-based and our experimental excretion rates to our lakewide biomass estimate support our hypothesis that mussel excretion has made a large contribution to the phosphorus increase in the hypolimnion (1.6 to 7.5 μg/L increase). Although historical data are limited, the timing of mussel expansion in Cayuga Lake is also consistent with the hypolimnetic SRP increase after 2004.

This page intenstionally left blank.

Section 6. Hydrothermal/ Transport Modeling

A model is a theoretical construct that assigns numerical values to parameters and relates external inputs or forcing conditions to system variable responses (Thomann and Mueller 1987, Chapra 1997). An open-source two-dimensional hydrothermal/transport model (submodel of CE-QUAL-W2; W2 hereafter; Cole and Wells 2013) was chosen for this Cayuga Lake project. W2 is a dynamic, laterally averaged, two-dimensional (2-D) model. The model is based on the finite-difference solution of laterally averaged fluid motion and mass transport. The basic equations of the model that describe horizontal momentum, hydrostatic pressure, free water surface elevation, continuity, density dependencies, and constituent transport, have been presented in the user manual (Cole and Wells 2013).

The setup, testing, and application of W2 model for Cayuga Lake, NY is documented in a manuscript that has been submitted to *Inland Waters* for review and publication (please see the link below to the full manuscript). Model testing was based on comparisons of model predictions with measured (1) fixed-frequency vertical temperature profiles for ten years, (2) signatures of oscillations in stratified layers and intrusions of hypolimnetic waters into surface layers (upwelling events) from high frequency temperature measurements, and (3) signatures of tributary entry to both upper and stratified layers from a passive tracer. The applicability of the model for other lacustrine systems, and its appropriateness to support an overall water quality model for Cayuga Lake, were considered. The validated model was applied to describe and quantify features of transport that have implications with respect to water quality modeling, including residence time of stream inputs, transport and fate of inflowing streams, and exchange between the hypolimnion and epilimnion

Below is a link to a pdf of the draft manuscript on Cayuga Lake hydrothermal modeling. This manuscript is currently being submitted for review.

Testing and application of a two-dimensional hydrothermal/transport model for a long, deep and narrow lake with moderate Rossby number

Rakesh K Gelda[1,*], Alexandra T. King[2], Steven W. Effler[1], Seth A. Schweitzer[2] and Edwin A. Cowen[2]
[1] *Upstate Freshwater Institute, P.O. Box 506, Syracuse, NY, 13214, USA*
[2] *DeFrees Hydraulics Laboratory, School of Civil and Environmental Engineering, Cornell University, Ithaca, NY, 14853-3501, USA*
[*] *Corresponding author email: RKGelda@upstatefreshwater.org*
Submitted to Inland Waters 17 October 2014

Abstract

Setup, testing, and application of a two-dimensional longitudinal-vertical hydrothermal/transport model (the transport submodel of CE-QUAL-W2) is documented for Cayuga Lake, New York, where the Rossby radius is on the order of the lake's width. The model is supported by long-term monitoring of meteorological and hydrologic drivers and calibrated and validated using in-lake temperature measurements made at multiple temporal and spatial scales over sixteen years. Measurements included (1) temperature profiles at multiple lake sites for ten years, (2) near-surface temperatures at one end of the lake for sixteen years, including irregular occurrences of upwelling events, (3) timing and magnitude of seiche activity at multiple depths for two years, and (4) transport of a conservative passive tracer. The model demonstrates excellent temporal stability, maintaining good performance in uninterrupted simulations over a period of fifteen years. Performance is better when modeling is supported by on-lake versus land-based meteorological measurements. The validated model is applied, through numeric tracer experiments, to evaluate various features of transport of interest to water quality issues for the lake, including (1) residence times of stream inputs within the entire lake and a smaller region defined bathymetrically as a shallow shelf, (2) transport and fate of negatively buoyant streams, and (3) the extent of transport from the hypolimnion to the epilimnion. This hydrothermal/transport model is appropriate to serve as the transport submodel for a forthcoming water quality model for this lake and for other high aspect (length to width) ratio lacustrine systems for which the internal Rossby number is order one or greater.

Key words: thermal stratification, transport, two-dimensional, model, calibration, validation, seiche, Rossby number, lake

Introduction

Temperature is a fundamental regulator of the physical character of water and thereby the ecology and quality of surface waters, as it structures biological communities and affects the rates of biochemical processes (Wetzel 2001). Seasonal thermal stratification is ubiquitous in deep temperate lakes and reservoirs and an important regulator of transport processes (Imboden 2004). The critical dependence of lake metabolism and related metrics of water quality on stratification and associated transport regimes has been widely acknowledged (e.g., Lam and Schertzer 1987, Wetzel 2001, Imboden 2004). Features of stratification and transport regimes that specifically mediate cycling of material, metabolic rates, hypolimnetic oxygen resources, and other signatures of water quality include (1) temperatures of the stratified layers, (2) vertical dimensions of the layers, (3) duration of stratification, (4) transport and fate of inflows, and (5) magnitude and timing of transport processes acting in multiple dimensions (Powell and Jassby 1974, Fischer and Smith 1983, Lam and Schertzer 1987, Imberger 1994, Imboden 2004, Rueda and Cowen 2005a, 2005b, Rueda et al. 2006, O'Donnell et al. 2010, Owens et al. 2013).

Water motion and features of stratification in lakes and reservoirs depend on a number of factors, including basin morphometry, setting, hydrology, and meteorological conditions (Csanady 1973, Imboden 1990, Imberger 1994, Imboden 2004). Internal seiches (successive oscillations of stratified layers) are particularly prominent features of water motion in long narrow (high aspect ratio) lakes (Hunkins and Fliegel 1973, Lemmin and Mortimer 1986, Ivey and Nokes 1989), promoting turbulence and thus vertical transport (Gloor et al. 1994, MacIntyre and Jellison 2001, Wüest and Lorke 2003). Substantial year-to-year variations in stratification and transport occur in response to natural

Click here to load hydrothermal modeling manuscript

Additional hydrothermal modeling details and results are provided in Appendix D-1. Details on the methodology used to transform off-site meteorological data to on-site data can be found in Appendix D-2.

This page intentionally left blank

Section 7. Approach Consideration for Phase 2 Water Quality Modeling

7.1. Background

The primary water quality issue of concern that is being addressed by this study of Cayuga Lake is the potential for phosphorus (P) – driven cultural eutrophication problems in the southern end of the lake. Indeed, much of the tributary inflow (~ 40%) and associated constituent loading, as well as multiple point sources, enter this southern portion of the lake, described as the shelf. This localization of inflows at one end is similar to conditions that prevail in many reservoirs. Multiple common metrics of water quality are degraded on the shelf relative to conditions further north in deeper pelagic portions of the lake, at multiple time scales. The shelf is presently listed for multiple water quality issues by the NYSDEC, including (1) phosphorus (the focus of this study), and (2) sediment. The phosphorus listing is intended to protect against cultural eutrophication, and was apparently guided by the irregular exceedances of the state's guidance value (summer average TP concentration of 20 µg/L). The metric and limit for the sediment issue has not been stated. Based on material presented in earlier sections, and addressed again in this section, the sediment and P issues cannot be separated in the context of addressing P levels in this lake.

The required product of this Cayuga Lake study is a credible, successfully tested, mechanistic P-eutrophication model for the lake, with the capability of lake-wide simulations. The model will be appropriate to support management deliberations common to the TMDL process. The model will be capable of supporting a focus on the southern shelf area, acknowledging that lake-wide simulations are necessary to support such a local focus and are of interest relative to management of the invaluable resource of the entire lake. The model will be a quantitative tool with which to evaluate water resource alternatives. The modeling initiative will serve to resolve drivers/processes responsible for prevailing conditions relative to the P-eutrophication and sediment conditions. The overall modeling initiative features the linkage of watershed and lake models. The lake model will be made up of multiple sub-models that will be described subsequently.

The attributes needed in the lake model to address the P-eutrophication issue(s) are considered in the following text, in the context of limnological analyses of the 2013 data set and earlier monitoring data. Specifically, we address model needs related to (1) temporal scales to be resolved, (2) spatial scales to be resolved, (3) processes to be represented, (4) model state variables (parameters to be predicted), and (5) model drivers. Certain graphics will be presented again here that appeared in earlier sections to support logic patterns related to model needs. The sub-models that will make up the overall water quality model will be identified, and described, to varied levels of specificity.

7.2. Guidance from the Disconnect in Trophic State Metrics, Shelf versus Pelagic Waters

A conspicuous disconnect in the patterns of the three trophic state metrics (the concentrations of TP and Chl-*a*, and Secchi depth) has emerged in the limnological analysis of the 2013 data set (the most comprehensive) as well as in the entire LSC monitoring record. Degraded conditions on the shelf relative to pelagic waters has been documented for TP and SD, but not for Chl-*a*. On a summer average basis TP concentrations on the shelf have been higher (Figure 7-1a, Figure 7-2a) and SD has been lower (Figure 7-1c and Figure 7-2c). In sharp contrast (the "disconnect") Chl-*a* concentrations have been nearly equal, and in some recent years slightly lower on the shelf (Figure 7-1b and Figure 7-2b). Effective simulation of this disconnect is a primary target for the modeling initiative.

Much of the disconnect is associated with intervals of strong divergences between the shelf and pelagic areas that are temporally linked to runoff events (Figure 7-3). The top panel of stacked plots illustrating this point is the hydrograph for Fall Creek, representing that stream's flow at a time step of 1 day. Flow conditions in this stream, the single largest with the longest record of flow measurements, are generally considered representative for other inflows (note the logarithmic Y-axis, Figure 7-3a). Note that much higher TP concentrations (Figure 7-3b) and lower SD values (Figure 7-3c) generally followed the three largest runoff events. The degradation in these two trophic state metrics on the shelf following high flow intervals are primarily associated with high concentrations of minerogenic particles (Figure 7-4) delivered by the local tributaries during the high stream flow intervals. Concentrations of this inorganic sediment increase greatly in these tributaries as the flow rate increases, as illustrated for Fall Creek (Figure 7-5). Two metrics of minerogenic particle concentrations are used to portray these dynamics for the study period of 2013, FSS (Figure 7-4b), and PAV_m (the projected area of minerogenic particles per unit volume; Figure 7-4c). Note the logarithmic Y-axis, to accommodate the major changes that occur in response to runoff events. Though signatures of increases are apparent after the events even in pelagic waters (site 3), those measured on the shelf are much greater. The PAV_m metric is more sensitive and certain compared to FSS for the common range of lacustrine conditions. Moreover, PAV_m is a more powerful metric to represent the effects of these particles on P (Effler et al. 2014) and SD (Effler and Peng 2014) levels. Simulation of the patterns of PAV_m in time and space in the lake will be undertaken as part of the water quality modeling initiative to represent these interactions.

A stoichiometric approach has been developed to quantify the contribution of P associated with minerogenic particles to the particulate P (PP), and thereby the total P (TP), pool. Accordingly, PP is partitioned into two pools

Eq. 7-1. $$PP = PP_m + PP_o$$

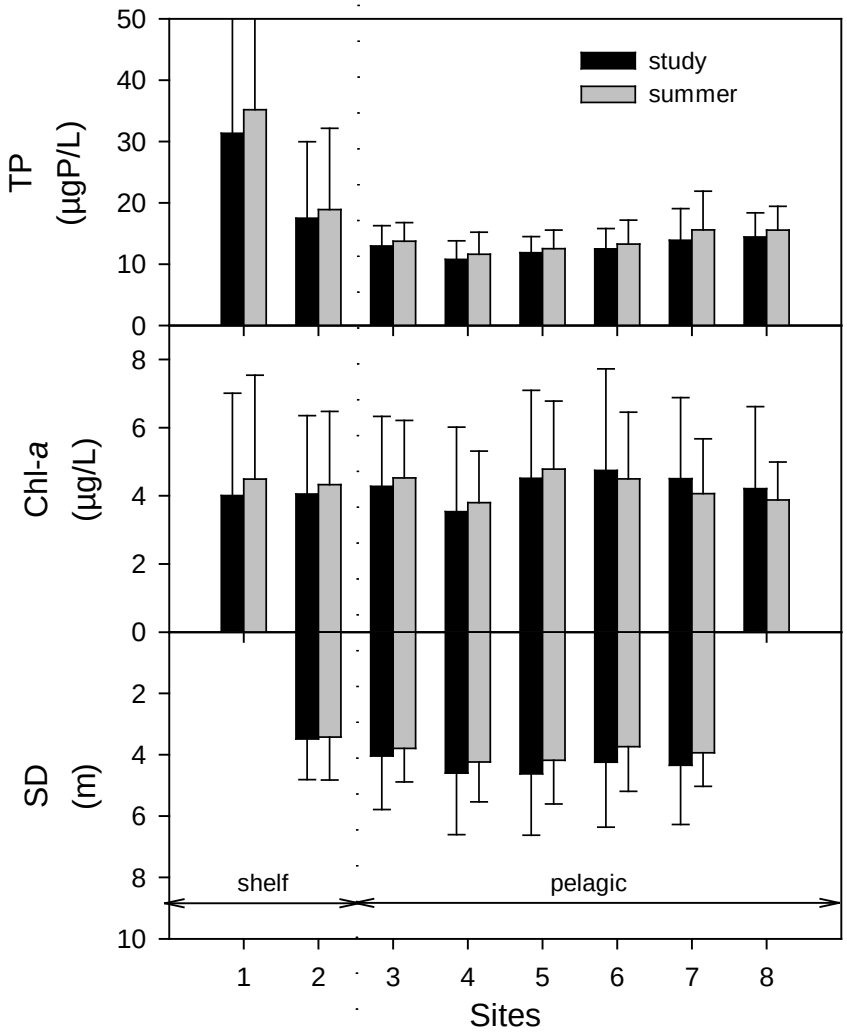

Figure 7-1. Spatial patterns for Cayuga Lake as average values at eight sites for two intervals in 2013, the entire study and summer (Jun-Sept.): (a) TP, (b) Chl-*a*, and (c) SD for all sites only for days when the SD at site 2 was not on the bottom (3 days dropped). Temporal variability is represented by one standard deviation bar.

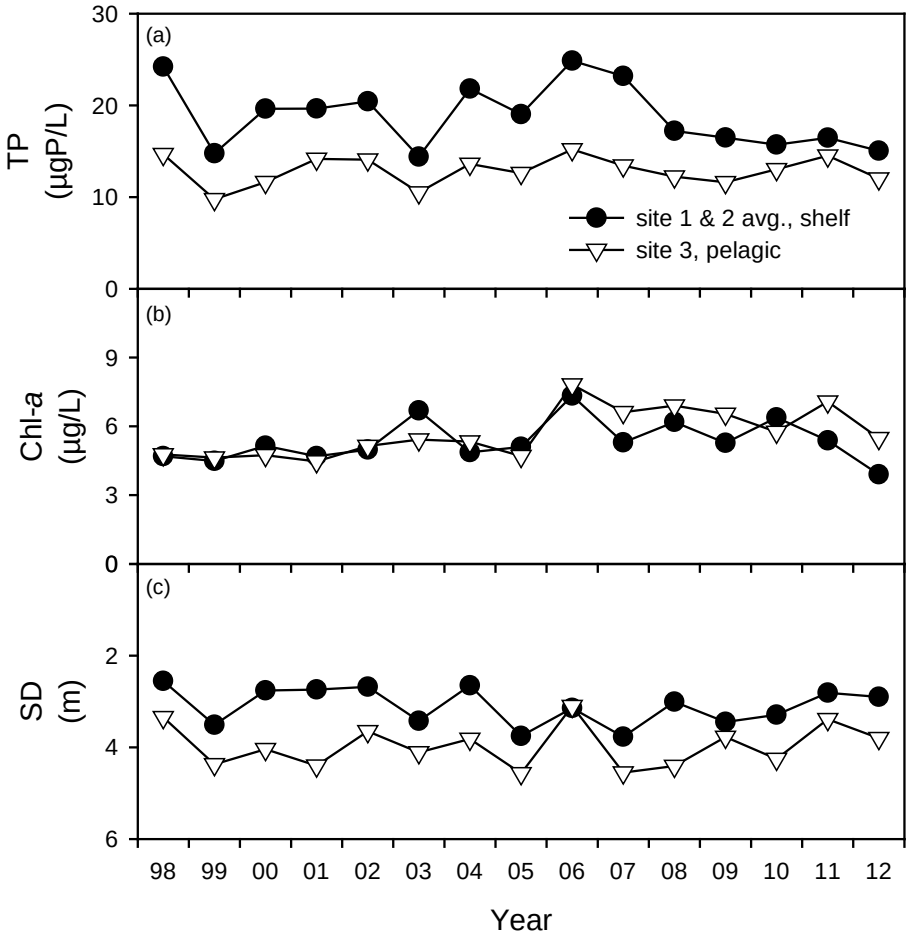

Figure 7-2. Long-term trends for the upper waters of Cayuga Lake for the 1998 – 2012 period at site 3 (a) TP, (b) Chl-*a*, and (c) SD.

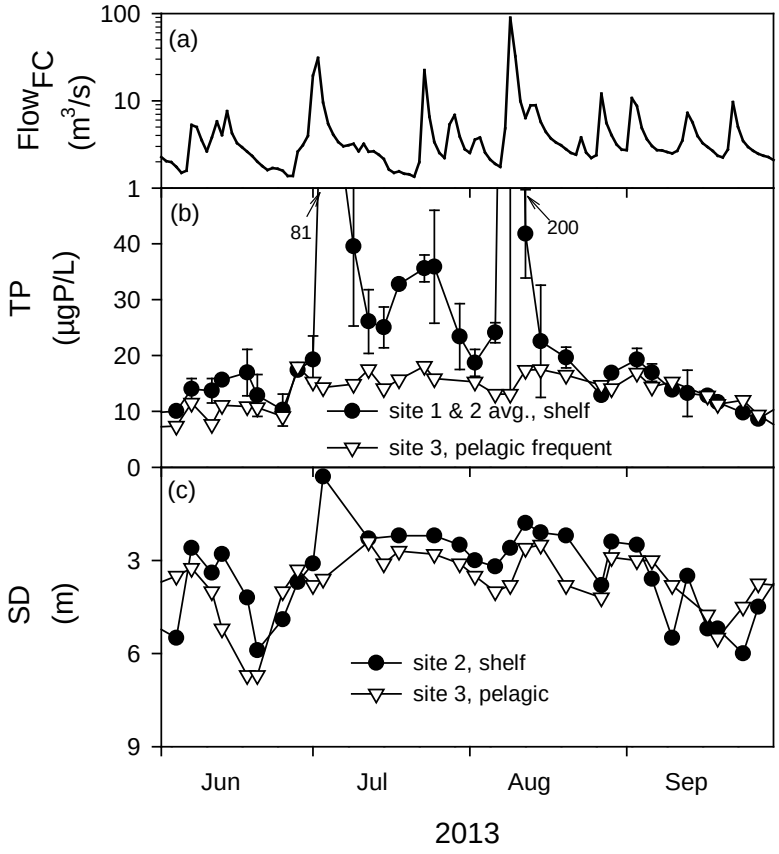

Figure 7-3. Temporal patterns for flow and trophic state indicators in Cayuga Lake, 2013: (a) daily USGS flows in Fall Creek, (b) TP, as the average of sites 1 & 2 and at site 3, the frequently sampled pelagic site, and (c) SD at site 2 and site 3. Spatial variability on the shelf is represented by range bars in (b).

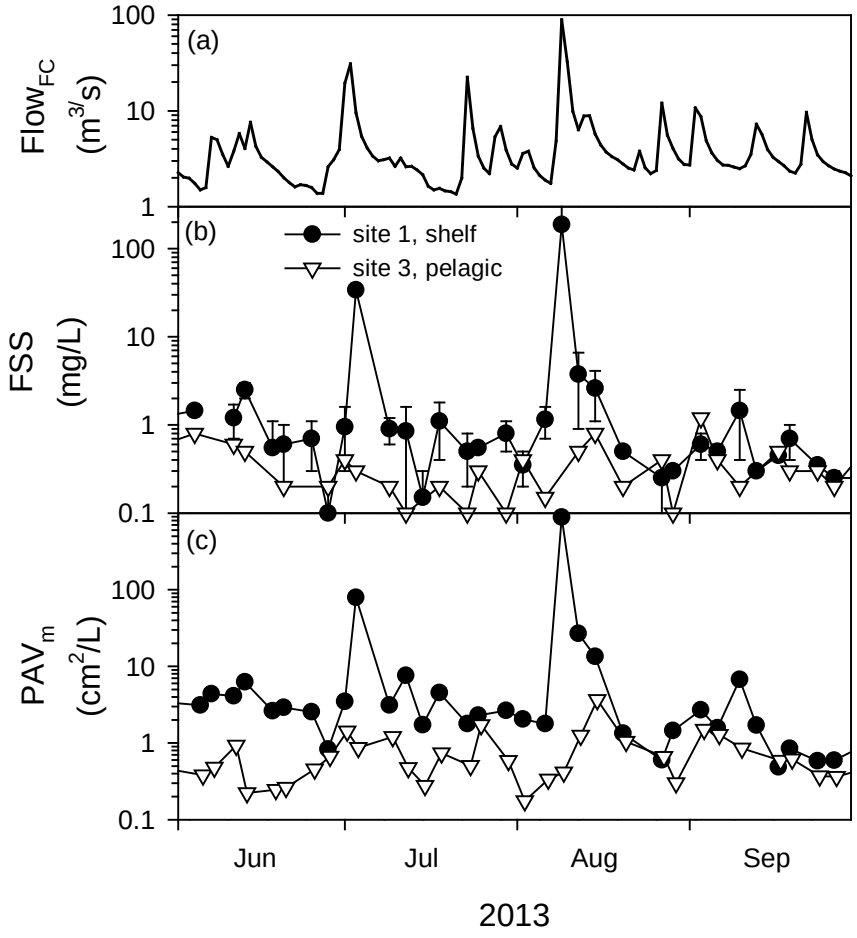

Figure 7-4. Temporal patterns for Cayuga Lake, 2013: (a) daily USGS flows in Fall Creek, (b) FSS, as the average of sites 1 & 2 and at site 3, the frequently sampled pelagic site, and (c) PAV at sites 1 and site 3. Spatial variability on the shelf represented by range bars in (b).

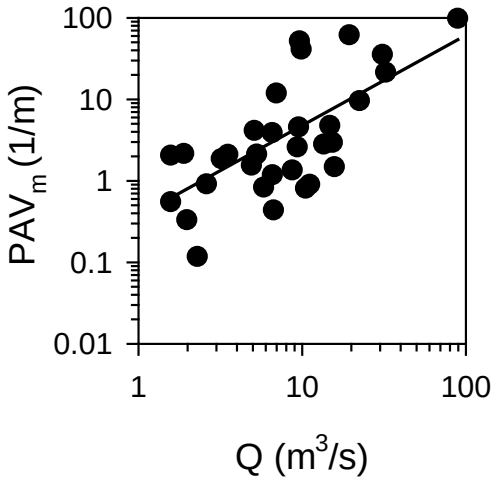

Figure 7-5. Evaluation of the relationship between PAV_m and flow in Fall Creek in 2013.

where PP_m and PP_o correspond to components associated with minerogenic and organic (i.e., includes phytoplankton) particles, respectively. Using appropriate stoichiometric coefficients, this summation can be described by

Eq. 7-2. $$PP = (PP_m{:}PAV_m) \bullet PAV_m + (PP_o{:}\text{Chl-}a) \bullet \text{Chl-}a$$

First estimates of the two stoichiometric ratios for the lake were presented by Effler et al. (2014). These ratio values may be modified with ongoing analyses. The water quality model's prediction of PAV_m and Chl-*a* will support partitioning of PP according to PP_m and PP_o. Based on PP, PAV_m and Chl-*a* observations and the coefficients presented by Effler et al. (2014), the partitioning of the observed summer average TP concentrations of 2013 for sites 1, 2 and 3 is presented (Figure 7-6). The contributions of PP_m to TP on the shelf are shown to be substantial. This capability will also be provided by the model.

The next step in the logic pattern that separated the PP_m component from the simulation of phytoplankton growth and as an indicator of trophic state, was supported by the results of a bioavailability bioassay conducted on shelf water following the major late June runoff event of 2013. The bioavailability fraction of PP from that sample was very low (0.03), establishing that there is a disconnect between such a measurement (and extending to TP) and the trophic state issue. This observation is not supportive of the inclusion of post-runoff event TP observations for assessment of trophic state status, nor of summer average values of TP for the shelf that include such observations to assess status relative to NYSDEC's guidance value.

A quantitative framework, consistent with optical theory, is also available that will describe the effect of minerogenic particles in causing the disconnect between phytoplankton biomass and water clarity (e.g., Secchi depth). SD is controlled primarily by the magnitude of light scattering, as quantified by the particulate light scattering coefficient (b_p). These are inversely related, as described by

Eq. 7-3. $$SD^{-1} \alpha\ b_p$$

The magnitude of b_p can be partitioned according to the contributions of minerogenic (b_m) and organic (e.g., phytoplankton; b_o) particles, as described by

Eq. 7-4. $$b_p = b_m + b_o$$

SD is a reasonable metric of trophic state where b_o dominates. As minerogenic particle content becomes elevated b_m increases, causing lower SD, consistent with the character of the disconnect reported for the shelf versus pelagic conditions and the observed elevated PAV_m values on the shelf (Effler and Peng 2014). Often simple empirical relationships between Chl-*a* and SD, as well as between Chl-*a* and the light attenuation coefficient, have been used in water quality models. However, such relationships have been observed to be poor in Cayuga Lake, in

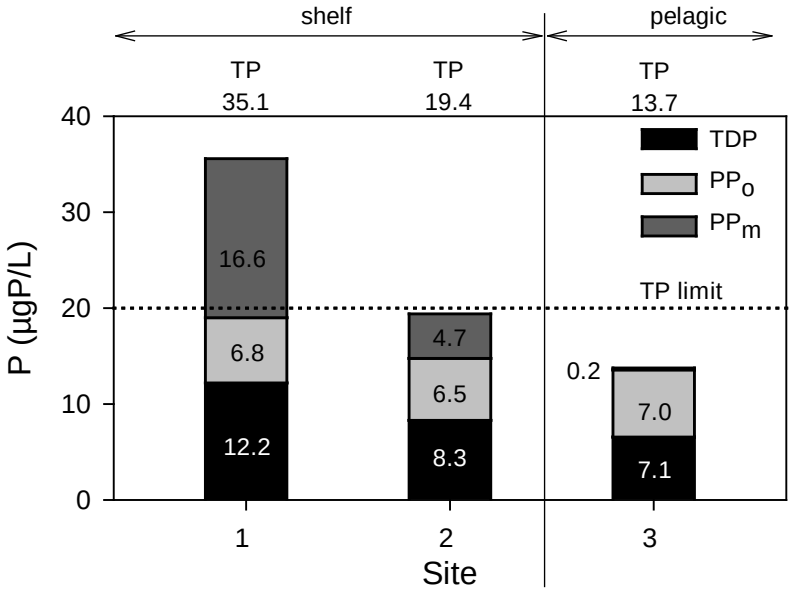

Figure 7-6. Summer average measured concentrations of TP and TDP in 2013, with estimated partitioning of PP (= TP – TDP) according to contributions of PP_o and PP_m.

part because of the temporal and spatial variations in minerogenic particle levels (i.e., b_m; Effler and Peng 2014). A mechanistic optics submodel will be embedded in the overall water quality model that will provide better performance, in part by simulating the dynamics and spatial patterns of PAV_m, and thereby b_m.

The effect of minerogenic particle inputs from local tributaries, that causes increases in TP concentrations (as PP_m) and decreases in SD (as b_m increases), are responsible, in part, for the disconnect between the shelf and pelagic waters. However, there is a second important component of this disconnect. The metric of biomass, Chl-*a* remains nearly equivalent in pelagic waters and the shelf despite the greater nutrient-based growth potential that often prevails on the shelf. This growth potential is appropriately represented by soluble reactive P (SRP), which is completely bioavailable (Prestigiacomo et al. 2015), rather than by TP. SRP concentrations are often higher on the shelf than in pelagic waters, particularly following major runoff events (Figure 7-7a and b). Despite these major divergences in SRP levels, temporal patterns of Chl-*a* remain roughly spatially uniform throughout the upper waters of the lake, including the shelf (Figure 7-7c). This similarity leads to the position that phytoplankton conditions on the shelf essentially represent lake-wide conditions. The question remains, why aren't locally higher biomass conditions observed on the shelf where locally higher SRP concentrations often prevail. Moreover, these conditions have been recurring for the shelf, even before local point source inputs were substantially reduced through treatment upgrades. These features will be an important target of the water quality model testing. There are at least three factors that contribute to this lack of increased phytoplankton biomass on the shelf relative to pelagic waters (1) short residence times for local external inputs on the shelf (i.e., rapid flushing), (2) a dilution effect from the external inputs (e.g., no Chl-*a* content in the inflows), (3) reduced light availability (e.g., high values of the light attenuation coefficient) on the shelf, particularly following runoff events. Each of these effects will be well quantified in the water quality model.

7.3. Guidance from Lake-wide Signatures

There are a number of important signatures that emerged from the detailed lake-wide and tributary monitoring of 2013 that provide guidance relative to model needs, opportunities and challenges to support effective representation in the water quality model. For example, NO_X (dominated by NO_3^-) demonstrated lake wide progressive decreases in the upper waters through mid-summer and then leveled off (Figure 7-8a). NO_3^- is the dominant form of nitrogen (N) used to support phytoplankton needs for N in Cayuga Lake, as t-NH_3 remained much lower, approaching detection levels (external input concentrations were also low). Moreover, despite the observed seasonal depletion, the concentrations of NO_X remained well above levels considered potentially limiting to phytoplankton growth. This will support a kinetic simplification in describing nutrient limitation of phytoplankton growth in the lake. Moreover, the temporal signature for NO_X (Figure 7-8a) represents an opportunity to assess the temporal

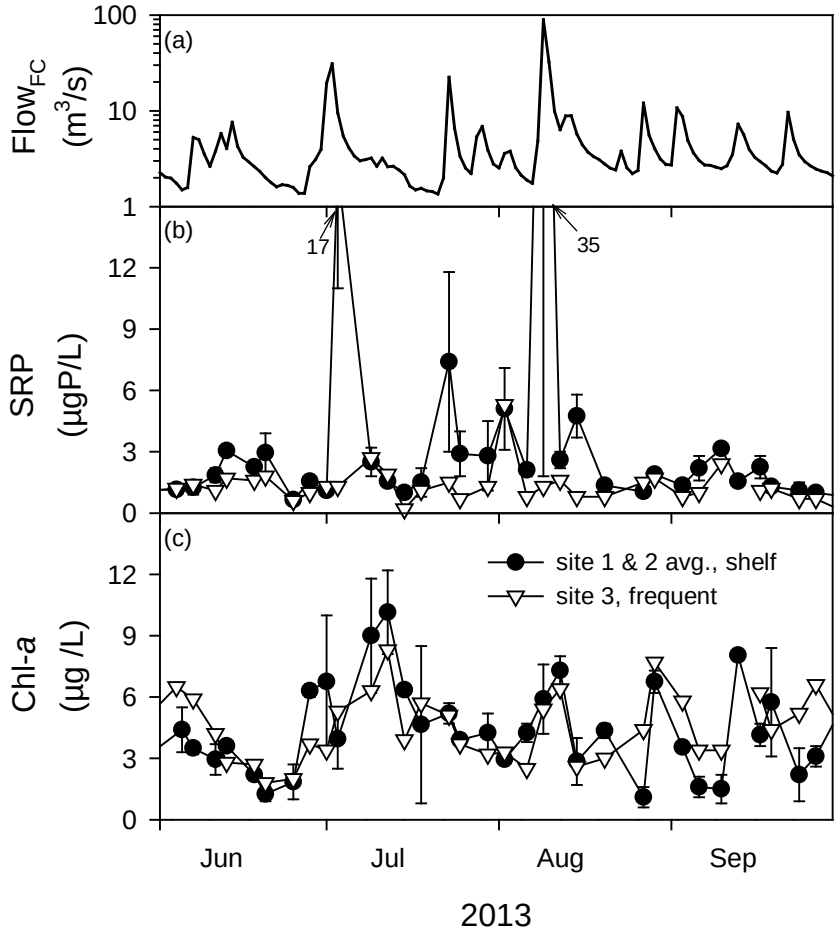

Figure 7-7. Temporal patterns for Cayuga Lake, 2013: (a) daily USGS flows in Fall Creek, (b) SRP, as the average of sites 1 & 2 and at site 3, and (b) Chl-*a* as the average of sites 1 & 2 and at site 3. Spatial variability on the shelf is represented by range bars in (b) and (c).

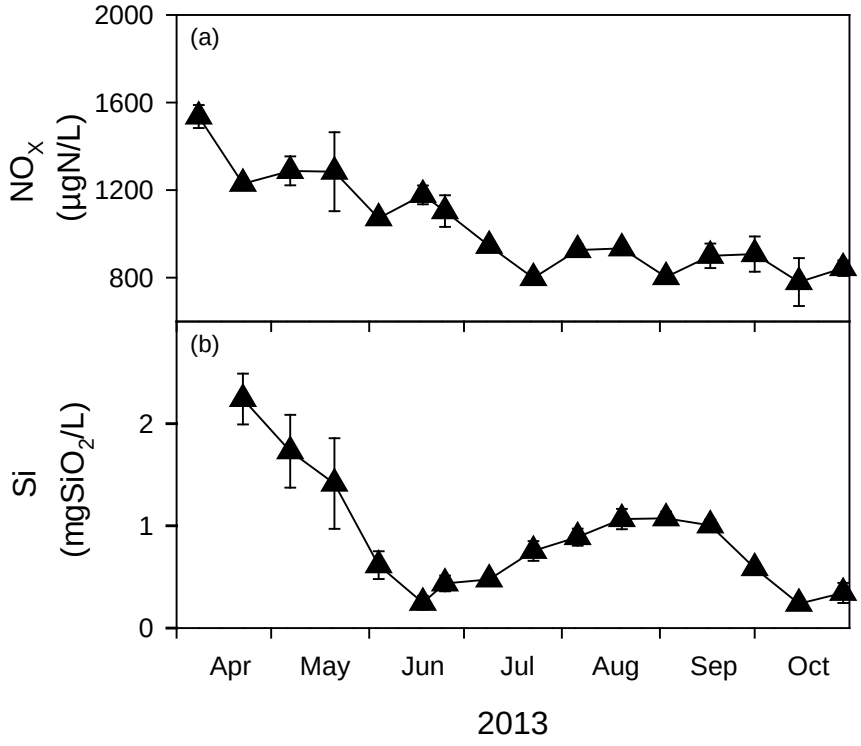

Figure 7-8. Temporal patterns for the average of the upper waters of the pelagic sites (average of 4-8) in Cayuga Lake, 2013: (a) NO_X and (c) Si. Spatial variability represented by one standard deviation bar.

trajectory of the epilimnetic N sinks (e.g., phytoplankton) through calibration, by accommodating the well-defined external inputs. This likely can be best done as a separate modeling exercise using the transport submodel framework and driving simulations with the detailed external loading estimates. The difference between a conservative behavior assumption simulation and the observations will be a measure of the net sink effect for NOx. Sink kinetics that result in a reasonable match with observations may contribute insights in representing processes in the overall water quality model.

Another conspicuous signature was the temporal trajectory of Si in the lake's upper waters (Figure 7-8b). Its features in 2013 were consistent with those of the lake's diatom community. The strong depletion of Si over the April to mid-June interval was coincident with a diatom bloom. This signature may be valuable in supporting the calibration of a phytoplankton model that partitions the community according to functional groups. This is not presently deemed to be a primary modeling goal (e.g., secondary).

A detailed survey conducted in 2013 established a dense population of the exotic bivalve, the quagga mussel (zebra mussel also present but lower levels, in upper waters), is present in Cayuga Lake. Though the densest populations are in the upper 20 m, these mussels are found throughout all depths (Figure 7-9a). Dense populations are known to impart impacts that can be substantial, associated with their metabolic activities of non-selective grazing, excretion and respiration (Nalepa and Schloesser 2014). Increases in these populations in deep layers may be responsible for the significant increase in SRP concentrations observed in the LSC facility starting in about 2004. Given the dense populations that prevail in the lake and the potential for substantial impact as quantified by the mass-based metabolic fluxes reported in the literature (Nalepa and Schloesser 2014), it is deemed necessary to accommodate their potential impact in the lake-wide water quality model. However, preliminary analyses, utilizing the tested transport submodel, suggest there presently is an inconsistency – use of typical laboratory excretion flux values for SRP over-predict observed levels in stratified layers by a wide margin (Figure 7-9b). It appears that the potential effects of mussel metabolism on the lake's water column (e.g., open waters) is less than indicated by fluxes derived from laboratory experiments. A process(es) apparently acts to diminish the effective fluxes on a water column basis. Recent studies suggest this diminishment has a hydrodynamic basis; e.g., the formation of a boundary layer during low ambient mixing conditions (Boegman et al. 2008a, Boegman et al. 2008b), that limits the effects on open waters.

There appears to be an issue related to indicators or metrics of phytoplankton biomass. The most widely measured, and thereby adopted, is Chl-*a*. It also serves as one of the three most common metrics of trophic state, along with TP and SD (Chapra 1997). The other most common metric of phytoplankton biomass, though less often measured, is the concentration of POC (Chapra 1997). The time series of Chl-*a* (Figure 7-10a) and POC (Figure 7-10b) are compared for site 5, a pelagic location, for which triplicate samples were analyzed. The uncertainty in the observations is represented by ± 1 standard deviation, based on the results for the triplicate

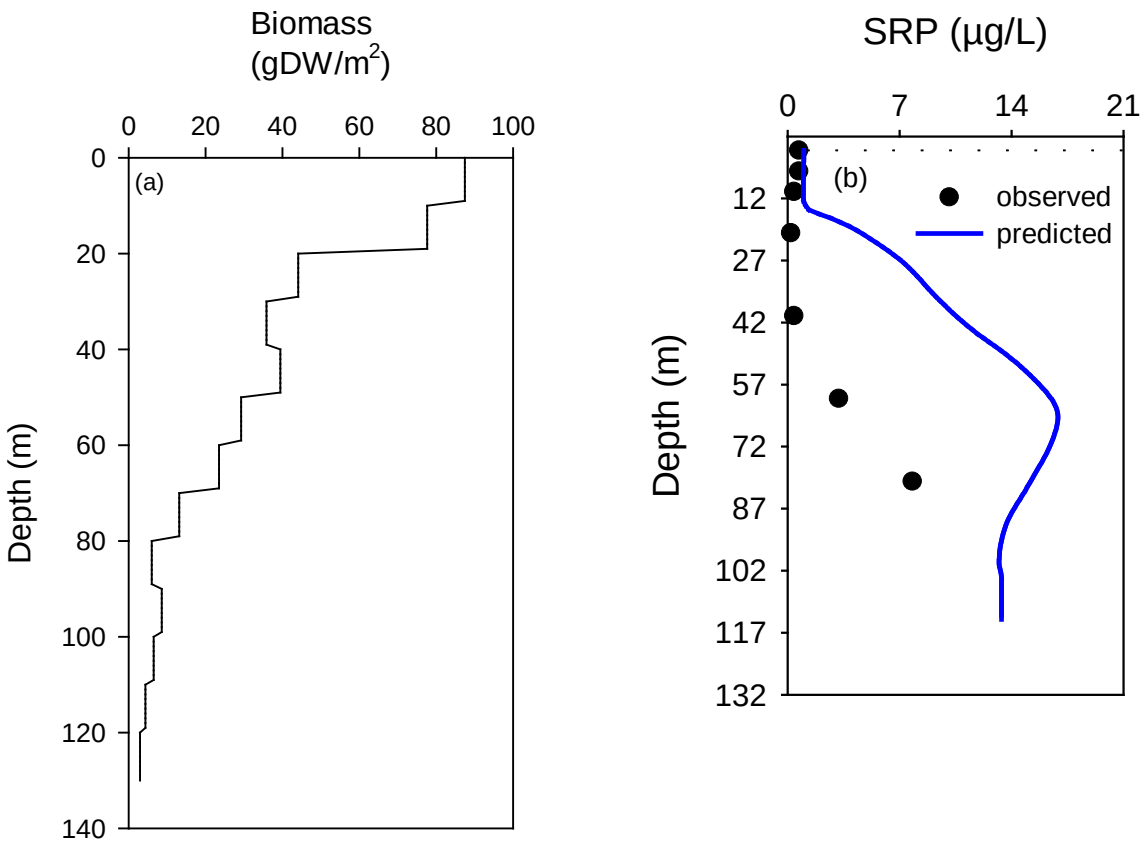

Figure 7-9. Vertical profiles in Cayuga Lake in 2013 (a) intergrated (lake-wide) estimated mussel areal biomass (mass/area), based on comprehensive survey, and (b) observed and predicted (prelimninary) SRP concentrations for October 15 at site 3.

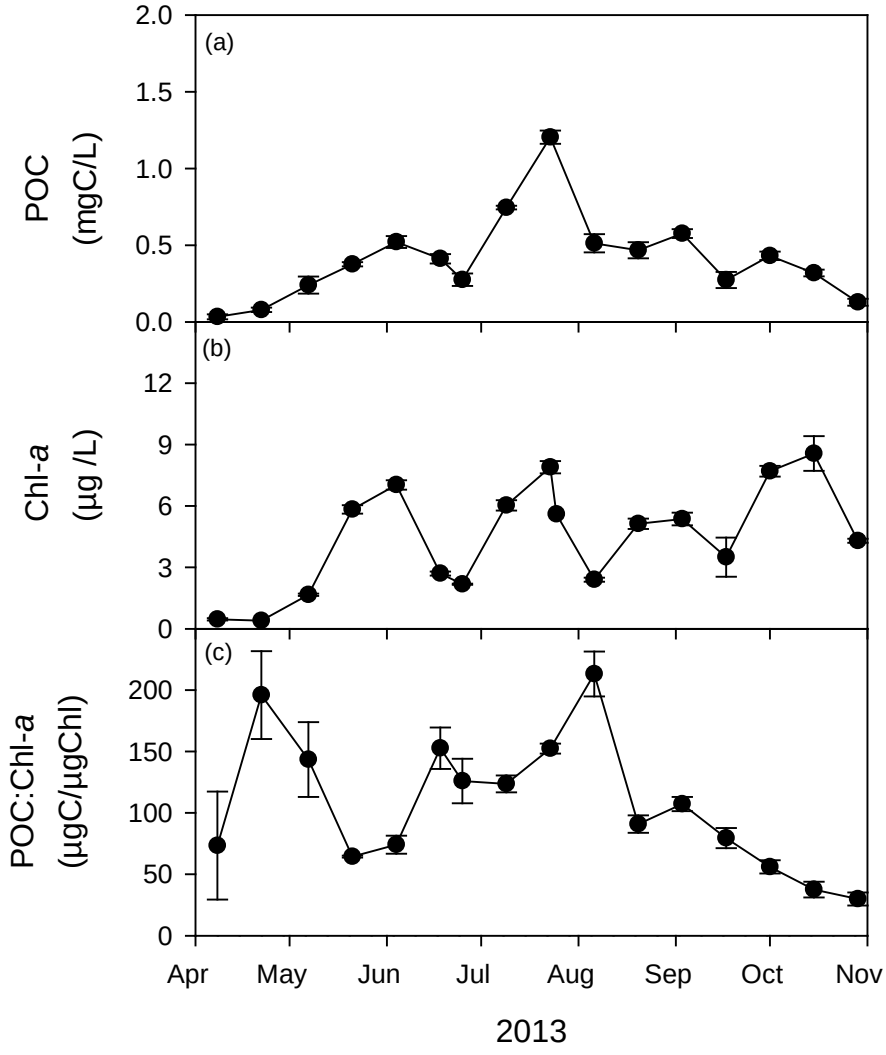

Figure 7-10. Temporal patterns for triplicate measurements at site 5 for Cayuga Lake, 2013: (a) POC, (b) Chl-*a*, and (c) POC:Chl-*a* ratio. Sample variability represented one standard deviation bar.

samples. In general, this uncertainty was small relative to the temporal dynamics observed for both Chl-*a* (Figure 7-10a) and POC (Figure 7-10b), supporting the patterns as representative for these parameters. However, the temporal patterns for these two metrics of phytoplankton biomass were decidedly different. There were several well defined peaks for Chl-*a*, in early June, early July, early August, late August, and October (Figure 7-10a). There was a single peak in POC in late July, with other variations that were generally small in magnitude (Figure 7-10b) compared with those for Chl-*a*. A temporally uniform POC:Chl-*a* ratio would result from similar patterns in these two biomass metrics. Instead this ratio demonstrated strong temporal variations (Figure 7-10c), with values that ranged from about 30-213 µgC/µg Chl-*a*. Without a strong relationship between an environmental driver(s) and these dynamics, the observed divergences for these two metrics are problematic with respect to efforts to use them as approximately interchangeable measures of biomass. Accordingly, it raises the issue which of the two will be the primary metric of phytoplankton biomass to be simulated in the water quality model.

To some extent, this decision has been embedded in the framework of contemporary mechanistic P-eutrophication water quality models. Most of these have adopted organic material or organic C (e.g., POC) as the primary metric of phytoplankton (e.g., Robson 2014). There is some system-specific support for this choice based on the comparative performance of these two measures in explaining variations in light scattering. It should be noted that light scattering is linearly dependent on the projected area of particles (Bowers and Braithwaite 2012, Effler et al. 2013). It seems likely that POC would be more tightly linked to this feature of geometry than Chl-*a*, a measure of pigment content. Indeed, a stronger relationship was observed between the estimated scattering coefficient for organic particles, b_o (represented by the residual, $b_p - b_m$; where b_p and b_m are the bulk particulate and estimated minerogenic component, respectively), and POC (Figure 7-11a), than for Chl-*a* (Figure 7-11b), based as the 2013 lake data set.

The primary metric of phytoplankton biomass to be targeted in the Cayuga Lake P-eutrophication model will be POC. The initial time resolution goal will be seasonal, typical of such initiatives. However, it is important to acknowledge that it is not uncommon to accept more temporally coarse performance (e.g., summer average as acceptable), that may be unavoidable. Chl-*a* will be only a secondary target of the initiative, at a coarse time scale of summer average, and perhaps study average. Recall this is not inconsistent with the known dependence of Chl-*a* on species composition, as well as ambient light and other environmental conditions (Reynolds 2006). Indeed, the POC:Chl-*a* ratio has been reported to be dependent on not only light availability but nutrient status (Chalup and Laws 1990, Laws and Chalup 1990, Hecky et al. 1993). Model frameworks have been proposed to describe the variations in this stoichiometry (Laws and Chalup 1990, Chapra 1997), however, clear success of such initiatives for lacustrine systems has yet to be demonstrated.

As part of the process of estimating external constituent loading rates to the lake based on the intensive 2013 sampling program, relationships with environmental drivers (primarily stream

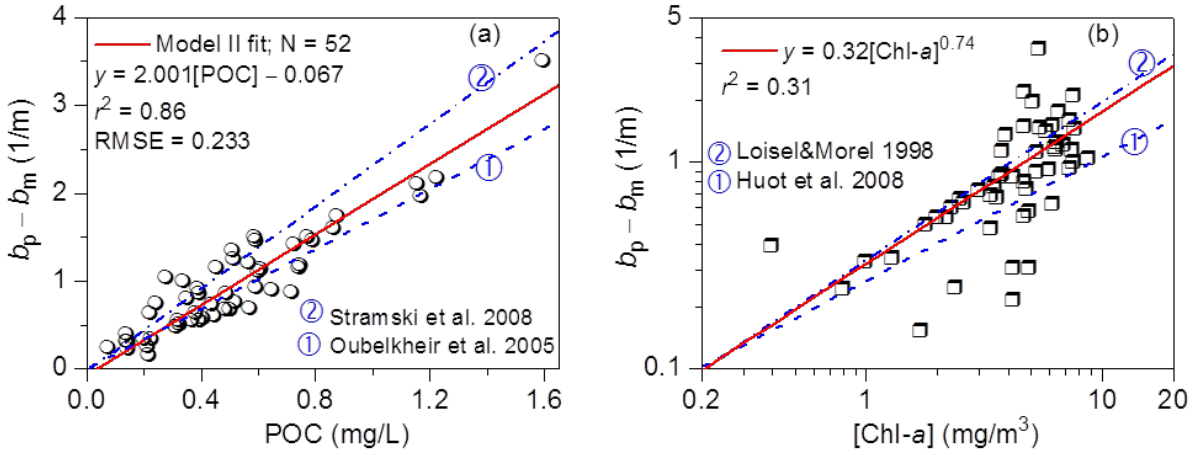

Figure 7-11. Relationships between $b_p - b_m$ (= b_o) and surrogates of phytoplankton biomass in Cayuga Lake in 2013, relative to these reported in the literature: (a) POC, and (b) Chl-*a*.

Q) were developed. Those developed for bioavailable forms of P (Prestigiacomo et al. 2015) are particularly critical to the P-eutrophication modeling initiative for Cayuga Lake. The inclusion of the quantification of the bioavailability of the important inputs (BAP_L) will represent a key feature of the credibility for the modeling initiative. Only about 25% of the total P load was found to be bioavailable (Prestigiacomo et al. 2015). While the bioavailability concept is being integrated into more such initiatives (e.g., Effler et al. 2012), most models continue to use P loading estimates that do not represent the incomplete bioavailability of PP and SUP. In other words, the P loads are false high relative to their potential to support plant growth. Such systematic errors in P loading estimates inevitably lead to compensating misrepresentation of source and/or sink processes for P as part of model calibration.

A second crucial feature of the P loading estimates for Cayuga Lake was the evaluation of interannual variations in BAP_L's. These were estimated based on application of the concentration – driver relationships for the various forms of P developed in 2013 for the longer-term records of stream Q for the 2000 to 2012 period (Prestigiacomo et al. 2015). The position that major shifts in these relationships had not occurred over that period was supported by the lack of substantial changes in the TP-Q dependence reported based on annual monitoring (Community Science Institute) since 2002. The interannual variations in total BAP_L using these empirical relationships were large relative to the total tributary BAP_L estimate of 2013, and of course even more so when compared to the individual source estimates for Salmon Creek and the summed point sources (Figure 7-12). It is appropriate to consider the potential benefits of a systematic reduction in any external source(s) in the context of these variations in BAP_L that are attributable to natural variations in drivers (particularly Q). Such variability will act to mask the effects of reductions in individual inputs. It will be important to predict interannual variations in

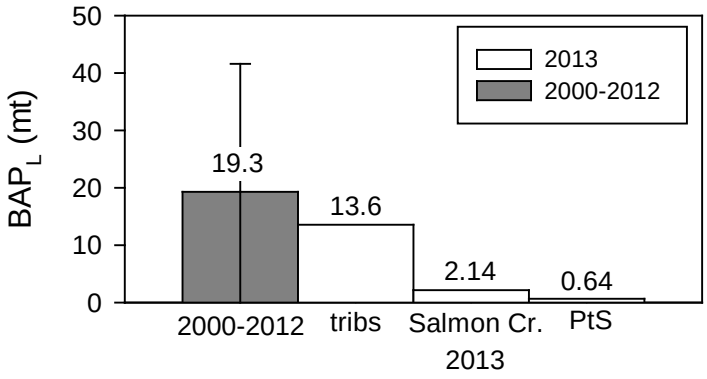

Figure 7-12. Comparisons of estimates of summed tributary BAP_L for the April – October interval for the period 2000-2012 (with ± standard deviation limits as a metric of temporal variations), to 2013 estimates. 2013 estimates are for summed tributaries (tribs), Salmon Creek, and summed point sources (PtS).

lake quality in response to such variations and compare the responses to those predicted for management alternatives. Such long-term simulation approaches provide a probabilistic context to support management deliberations.

7.4. Model Needs

The modeling initiative for the P-eutrophication model for Cayuga Lake will adopt the modeling philosophy of parsimony, making it only as complex as necessary to address the issue, with credibility. The model structure and capabilities must also be consistent with the needs and options for management consideration. This philosophy and the management issue(s) identified are manifested in multiple choices made in model structure and approaches. Selected cases are considered here related to the representation of lake-wide processes (Figure 7-13).

A robust representation of the dynamics of the thermal stratification/transport regimes is deemed important for this modeling initiative, which can predict not only temperature (T) dynamics, but also transport in the longitudinal and vertical dimensions. In particular, transport between the shelf and pelagic waters, and from stratified layers to the productive epilimnion must be appropriately represented. Those features will be simulated with W2/T, a two dimensional hydrothermal/transport model, as demonstrated and documented in Section 4 of this

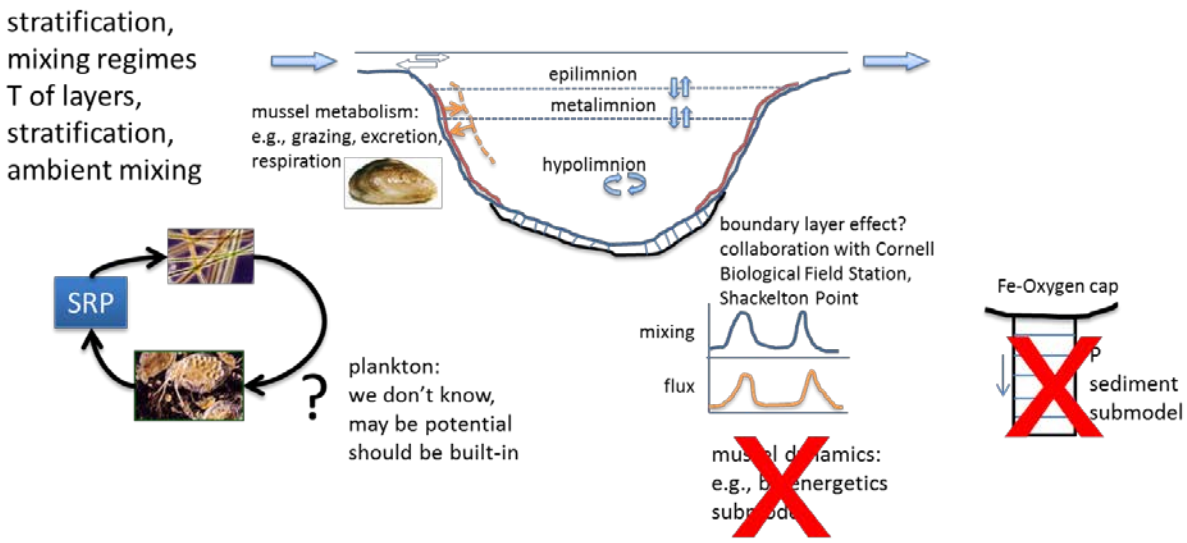

Figure 7-13. Selective representation of potential processes to be represented in the Cayuga Lake P-eutrophication model, with eliminations for excessive complexity illustrated.

report. This model is a parsimonious choice to serve as the hydrothermal/transport submodel of the overall P-eutrophication model. A more complex three-dimensional model would provide a more complete representation of the hydrodynamics of the lake. However, such a model would have disadvantages for this initiative that make it an inappropriate choice, including (1) large computation demands, and (2) the need for re-initialization for simulations of extended intervals (common over-mixing problem). These issues would be particularly problematic for long-term (multiple years) simulations that have been deemed to be important for this modeling initiative.

While a nutrient-phytoplankton growth submodel(s) is certainly required, the effects of zooplankton grazing do not necessarily have to be represented. The results of surveys of the zooplankton community for 2013 suggest a relatively low level of grazing pressure on the phytoplankton community. In particular, the efficient grazers, large *Daphnia*, were essentially absent. Their species can have major impacts on phytoplankton biomass levels. When present in substantial population densities these zooplankton can nearly eliminate edible phytoplankton, causing high SD values, a condition described as the clear water phase (Lampert et al. 1986). A

zooplankton grazing effect capability will likely be included in the Cayuga Lake model, though whether activation of this interaction will be necessary has yet to be decided. This will emerge from ongoing analyses and feedback from model testing efforts.

The potential fluxes associated with the documented mussel population densities reported here dictate that their effects be appropriately represented in the model (Figure 7-13). Our primary focus will be representing these metabolic effects on a lake-wide basis. The prevailing over-prediction of SRP levels in stratified layers has led to speculation on the operation of a hydrodynamic process(es), a boundary layer effect (Boegmann et al. 2008a, b), that limits lake-wide impacts except during interval of elevated ambient mixing. This modeling initiative will consider a similar approach, and other alternatives, to provide a reasonable representation of the lake-wide effects of mussel metabolism (Figure 7-13). However, this initiative will not undertake an effort to simulate long-term dynamics in the responsible resident mussel population, an added level of complexity that is deemed too uncertain to pursue at this time. Another example of complexity that will be avoided in this initiative is a mechanistic sediment diagenesis model (Figure 7-13). This decision is supported by the well-oxygenated conditions that extend to the lake bottom in pelagic portions of the lake that prevents the mobilization of substantial quantities of SRP, that instead is widely observed in lakes with seasonal anoxia (Chapra 1997).

A number of features that will be required to address the contrasting water quality signatures of the shelf versus pelagic portions of the lake emerged in the above description of the "disconnect" in trophic state metrics for these areas. The model must consider related water quality conditions over a broad range of time scales, extending from days through multiple years. The lower portion of this range will support resolution of the short-term effects of runoff events that impart conspicuous water quality signatures (Figure 7-3, 7-4 and 7-7). These, together with seasonal (weeks to months) simulations will support averaged representations of water quality metrics adopted by regulators, such as summer (June-Sept.) average values (Figure 7-1), in evaluating management options. Yet longer time scales, such as multiple years, enable representation of the effects of natural interannual variations in drivers (e.g., stream flow and associated P loading), that provide invaluable context for managers to consider the relative benefits of management options (Gelda and Effler 2008).

The detailed spatial patterns of trophic state metrics and related parameters resolved in the 2013 monitoring program establish the spatial resolution needs of the P-eutrophication model to address the identified "disconnect" issue (Section 5.2.2, Figure 5-36; Section 5.2.3, Figure 5-47). The "disconnect" issue is primarily longitudinal, the differences in water quality that occur from the entry of multiple inputs to the shelf, extending across the shelf, and between the shelf and pelagic waters. The two-dimensional hydrothermal/transport model (Gelda et al. 2015; Section 6), W2/T, provides an appropriate framework to represent the primary longitudinal features of these water quality patterns, that are most strongly manifested following runoff events. The longitudinal segmentation featured by this successfully tested model (Gelda et al. 2015; Section

6) will provide robust spatial resolution, with a total of 48 segments. The 10 segments on the shelf will allow representation of longitudinal gradients in that area, that are manifested particularly following runoff events. This longitudinal segmentation will also support testing of the model's ability to predict the near uniformity of water quality conditions observed in the pelagic portions of the lake. The entire water column of this deep lake must be represented, because all of the lake's layers influence the cycling of P and thereby primary production. The two dimensional model provides a robust representation of physical processes, including the mixing and seasonal stratification regimes (Gelda et al. 2015; Section 6).

The constituents and characteristics to be predicted by the water quality model are described as the model's state variables. The overall water quality (P-eutrophication) model will have a robust array of model state variables (Table 7-1), that together will address the issues identified here for Cayuga Lake targeted by this study. This listing is presently described as tentative, as modest changes may be made as the modeling progresses. The state variables have been partitioned according to those that will be directly simulated ("state variables"; Table 7-1) and those that will be calculated from directly simulated variables (derived state variables, Table 7-2). Multiple forms of P will be predicted, including particulate and dissolved fractions, that are partitioned according to labile (subject to reactions/transformations) and refractory (not subject to reactions/transformations), and organic vs inorganic, components. Phytoplankton biomass and organic carbon (C) will also be simulated, with multiple forms of C (dissolved versus particulate, labile versus refractory) predicted. Chl-*a* will be derived from the simulated phytoplankton biomass (ALG) times the Chl-*a*:ALG ratio. The remaining two primary trophic state metrics TP and SD will be derived. TP will be derived by summing all the simulated dissolved and particulate forms of phosphorus. SD will be predicted by the optics submodel. Multiple metrics of sediment will be simulated, including PAV_m, Tn, TSS, and FSS (Table 7-1 and Table 7-2). Optical metrics, including Tn and K_0(PAR) (the attenuation coefficient for scalar PAR) will be predicted by the optics submodel. Likely additions to the list of model state variables are NO_X and Si. Both had distinctive depletion signatures in the pelagic waters of the lake (Section 5.2.3, Figure 5-42 and Figure 5-40 respectively).

The signatures resolved from the 2013 monitoring data set, as well as the LSC monitoring program support the identification of targets for the model testing, a number related to the "disconnect". Some of these targets include:

1. differences in concentration of multiple forms of P between the shelf and pelagic waters, over a range of time scales (e.g., runoff events to summer average)
2. differences in the levels of sediments, according to multiple metrics, between the shelf and pelagic waters, over a range of time scales (e.g., runoff events to summer average)
3. differences in SD between the shelf and pelagic waters and the role of sediment versus phytoplankton biomass

Table 7-1. Tentative list of state variable names and abbreviations.

Pool	Name	Abbreviation
carbon	labile dissolved organic carbon	LDOC
	refractory dissolved organic carbon	RDOC
	labile particulate organic carbon	LPOC
	refractory particulate organic carbon	RPOC
	algal biomass	ALG
phosphorus	soluble reactive phosphorus	SRP
	labile soluble unreactive phosphorus	LSUP
	refractory soluble unreactive phosphorus	RSUP
	labile particulate organic phosphorus	LPOP
	refractory particulate organic phosphorus	RPOP
	labile particulate inorganic phosphorus	LPIP
	refractory particulate inorganic phosphorus	RPIP
optics/ particles	turbidity in size class i	Tn_i
	PAV in size class i	$PAV_{m,i}$
	Secchi disc	SD
	scalar attenuation coefficient for PAR	K_0(PAR)
	downwelling irradiance	E_d

Table 7-2. Tentative list of derived state variable names, abbreviations and components.

Pool	Name	Abbreviation	Components
carbon	dissolved organic carbon	DOC	= LDOC + RDOC
	particulate organic carbon	POC	= LPOC + RPOC
	total organic carbon	TOC	= DOC + POC
algal biomass	total chlorophyll *a*	Chl-*a*	=ALG · Chl-*a*/ POC:
phosphorus	soluble unreactive phosphorus	SUP	=LSUP + RSUP
	particulate organic phosphorus	POP	=LPOP + RPOP
	particulate inorganic phosphorus	PIP	=LPIP + RPIP
	total dissolve phosphorus	TDP	=SRP + SUP
	particulate phosphorus	PP	=POP + PIP
	total phosphorus	TP	=TDP + PP
optics particles	total turbidity	Tn	$= \sum_{i=1}^{N} Tn_i$
	total PAV	PAV_m	$= \sum_{i=1}^{N} PAV_{m,i}$
	total suspended solids	TSS	empirical relationship with Tn
	total inorganic suspended solids	FSS	empirical relationship with Tn

4. representation of the effects of mussel metabolism on common water quality metrics in the pelagic waters
5. patterns of phytoplankton biomass in pelagic waters (e.g., and thereby the shelf) at multiple times scales (seasonal to summer average) for POC, and summer average values for Chl-*a*.

7.5. Water Quality Model for Cayuga Lake

7.5.1. Model Drivers

The primary drivers for the model fall into one of three types (1) hydrologic, (2) meteorological, and (3) constituent loading (Table 7-3). Several of the major tributaries that enter the lake (Section 3) are presently continuously gaged by the United States Geological Survey (USGS; Table 7-3). The longest record is for Fall Creek (since 1925). Lake surface elevation is also monitored by the USGS. Estimates of overall tributary inflow and lake level are embedded in the overall hydrologic budget that will be maintained within the model. Meteorological measurements are critical to drive the hydrothermal/transport submodel. Incident light is utilized in the phytoplankton growth submodel. These measurements are available from a proximate location on Cornell campus (hourly since 1987), and from a site on the lake at its southern end (15 min. intervals) since 2011 (Table 7-3).

Constituent loads will be available in two forms (1) estimates based on a combination of observed concentrations, and those estimated from Q measurements, as described by concentration - Q relationships (Section 3), and (2) predictions from the tested watershed/landuse model. The first form will utilize the FLUX32 software that provides the estimates at a daily time step. This temporal resolution is generally consistent with the goal(s) of P-eutrophication models, and will likely be adequate to address the short-term issues of the shelf related to runoff events. Yet shorter time resolution can be adopted for the external load estimates, if it is found to be necessary. Loading estimates for years without regular tributary monitoring of concentrations will depend primarily on the concentration – Q relationship developed from the 2013 data set (the most intensive available), but will also be informed from longer-term monitoring. Accordingly, these loading estimates are limited to the period of Q gaging. The second form of loading inputs to the water quality model, output from the watershed/landuse model, represents a linkage of the models that is attractive for evaluating landuse management alternatives. Empirical relationships will be developed and applied as necessary to make the watershed/landuse model output consistent with the input needs of the water quality model.

Table 7-3. Primary model drivers.

Driver Type	Location	Availability	Notes
meteorological	piling cluster (Cornell University)	10/27/2011-12/31/2013	10 minute frequency; missing data (T_{air} and T_{dew} 1/3/2013 – 5/13/2013 filled in from Ithaca Airport
	Game Farm Road (Cornell University)	1987-2013	Hourly frequency; missing data (0.8% days) were filled in from Ithaca Airport data
hydrological	Fall Creek	flow record 1925-present	Temperature record 9/21/2011-11/18/2011; 5/13/2013 -11/1/2013
	Cayuga Inlet	flow record 1937-9/30/2011; 6/1/2012-present	5/9/2013-11/13/2013
	Salmon Creek	flow record 2006 - present	limited during 2013
	Six Mile Creek	flow record 1995 - present	limited during 2013
	Taughannock Creek	Pro-rated according to Fall Creek flow/watershed area	--
	ungaged inflows	Pro-rated according to Fall Creek flow/watershed area	--
constituent loading	Fall Creek	2013	GWLF/ empirical model 2000-2012
	Cayuga Inlet	2013	GWLF/ empirical model 2000-2012
	Salmon Creek	2013	GWLF/ empirical model 2000-2012
	Six Mile Creek	2013	GWLF/ empirical model 2000-2012
	Taughannock Creek	2013	GWLF/ empirical model 2000-2012
	ungaged inflows	2013	GWLF/ empirical model 2000-2012

7.5.2. Submodels of the Water Quality Model

7.5.2.1. Hydrothermal/Transport Submodel

The two-dimensional hydrothermal/transport model, W2/T, has been set-up, rigorously tested, and preliminarily applied for Cayuga Lake, as described in Section 6 (Gelda et al. 2015) of this report. This model serves as the transport submodel of the water quality model, CE-QUAL-W2, a public access model developed by the U.S. Army Corp. This model will serve as the transport submodel of the Cayuga Lake P-eutrophication model. The two-dimensional model simulates the thermal stratification regime and mixing/transport processes in the vertical and longitudinal dimensions. The model was calibrated for the conditions of 2013, and validated for the 1998- 2012 period through continuous simulations.

The time and space features of W/T2 are consistent with the water quality issues identified for Cayuga Lake (Section 6), and particularly to resolve the effects of runoff events and the differences between the shelf and pelagic areas. The model is capable of representing various complexities of transport processes that may be noteworthy with regards to the water quality issues of the lake, including the residence time of local tributary inputs on the shelf, the seasonal plunging of tributaries, and vertical transport from the hypolimnion to the productive epilimnion (Gelda et al. 2015).

7.5.2.2. Minerogenic Particle Submodel

As described in Section 5 and the peer-reviewed literature, minerogenic particles delivered to Cayuga Lake from its watershed play an important role in metrics of water quality in the lake, including phosphorus, turbidity, clarity and light penetration. The key model state variable is the projected area of minerogenic particles per unit volume (PAV_m). The modeling approach is similar to that developed and successfully tested and applied for turbidity (Tn) in the New York City water supply reservoirs (Gelda and Effler 2007, Gelda et al. 2009, Gelda et al. 2012, Gelda et al. 2013). PAV_m will be partitioned into the contributions of multiple size classes. Four size classes have been adopted in data analyses presented here (Section 5), though other segmentation schemes may be adopted to represent the associated behavior responsible for temporal patterns observed following external inputs (Figure 7-14).

External loads of PAV_m will be received for the same size classes, as specified by measurements for the calibration year of 2013, and based on PAV_m – Q relationships (Figure 7-14) for days without observations in 2013, as well as for model validation years. The size

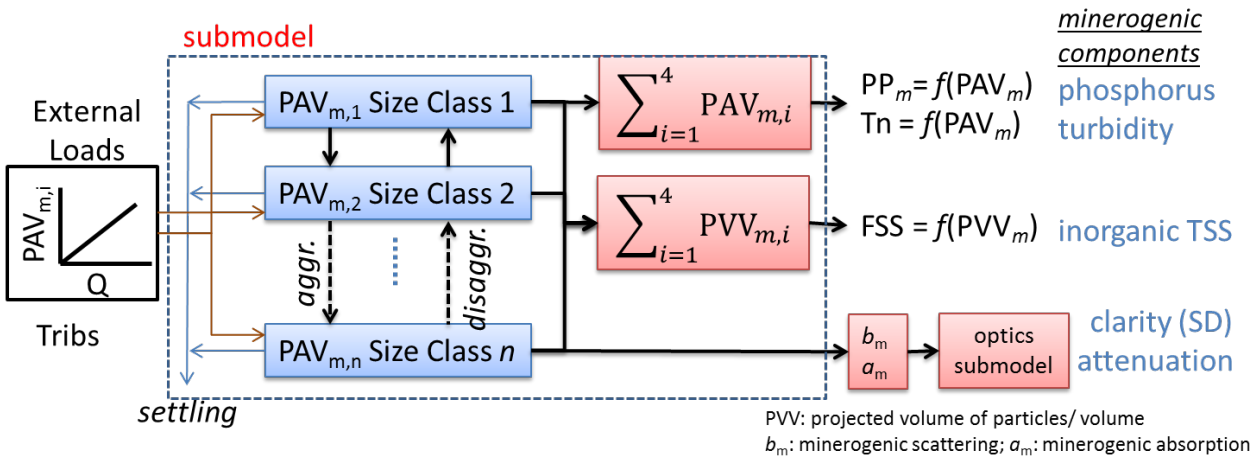

Figure 7-14. Conceptual diagram for a minerogenic particle submodel.

classes will be subjected to size – dependent settling losses (Stokes' Law) and conversions to other size classes associated with aggregation/disaggregation processes (Figure 7-14). The aggregation/disaggregation processes will likely be represented by a "net" aggregation that will be quantified through calibration of the submodel to track observations of in-lake patterns. Predictions of PAV_m in time and space will be the summation of the contributions for the different size classes. Predictions of particle volumes of minerogenic particles per unit volume (PVV_m) will be calculated from the PAV_m size class values (Figure 7-14) assuming a particle geometry (initially spherical, but may be platelets). Predictions of PAV_m can support predictions of (Figure 7-14) (1) the minerogenic component of PP (PP_m), (2) the minerogenic component of Tn (Tn/m), and (3) levels the absorption (a_m) and scattering (b_m) coefficients for minerogenic particles, that serve as inputs to the optics submodel (described subsequently). The predictions of PVV_m could serve to support predictions of inorganic (fixed) suspended solids (FSS). The submodel will be integrated into the overall water quality model.

7.5.2.3. Optics Submodel

Predictive capabilities are required for the optical metrics of water clarity, as represented by Secchi depth (SD), and the attenuation coefficient for scalar irradiance (K_0(PAR)). SD is a primary tropic state and water quality metric of concern for lacustrine systems, including Cayuga Lake. K_0(PAR) is important as it specifies the light available at various depths to support photosynthesis and phytoplankton growth. Empirical relationships between each of these metrics and Chl-*a*, as a measure of phytoplankton biomass, have been widely adopted as part of the P-eutrophication modeling. However, in Cayuga Lake, as well as many other lakes, this is inadequate (e.g., performs poorly) because other substances contribute importantly to these

optics conditions, and these do not necessarily covary with phytoplankton. Alternately, a mechanistic framework, one that is consistent with optical theory, is adopted.

A theoretically sound mechanistic framework is described in the schematic of Figure 7-15 (see Table 7-4 for definition of symbols). Accordingly (moving left to right), the constituents that influence the optical measures of concern (SD and K_0(PAR)), described as apparent optical properties (AOPs) are described as the optically active constituents (OACs). The OACs are mostly state variables of the water quality model, or can be independently specified. These include measures of phytoplankton biomass (Chl-*a* or POC) and minerogenic particles (PAV_m or FSS (ISPM)). Associated components of the absorption (*a*) and scattering (*b*) coefficients, both described as inherent optical properties (IOPs), are estimated according to OAC – specific coefficients (cross-sections; Figure 7-15). The desired AOPs are predicted from IOPs using well – established equations (radiative transfer expressions; Figure 7-15). Most of the elements of the model have been developed and successfully tested for Cayuga Lake (Effler et al. 2015b), including (1) development of cross-sections, (2) closure of the summation of absorbing components with overall absorption, and (3) closure IOPs and AOPs through application of the radiative transfer equations. Testing of the overall submodel will be conducted. The submodel will be integrated into the overall water quality model (Figure 7-16).

7.5.2.4. Phosphorus Submodel

A robust representation of the overall P pool and cycle is required to address the various issues identified here for Cayuga Lake (Figure 7-17). This will include multiple dissolved forms; SRP, and both labile (LSUP) and unreactive SUP (RSUP). Particulate (PP) forms will include both organic (POP) and inorganic (PIP) forms and partitioning between labile and recalcitrant components. A robust array of source and sink processes will be represented (Figure 7-17), including: (1) uptake of SRP to support phytoplankton growth, (2) adsorption and desorption of SRP from PIP, (3) hydrolysis of POP to form dissolved species, (4) mineralization/hydrolysis of SUP to form SRP, and (5) deposition of particulate forms.

The details of the framework for the submodel and specification of values of kinetic coefficients that quantify the various processes will be guided by established public domain models (e.g., CE-QUAL-W2, Lake2K), UFI's P-eutrophication model applied to New York City's reservoirs, as well as recent reviews of related models (Arhonditsis and Brett 2004, Arhonditisis et al. 2006, Robson 2014). Cycling of P associated with the metabolism of biological communities will also be considered, including dreissend mussels and zooplankton. Data analyses will support decisions regarding the need for inclusion of these pathways. The minerogenic particle submodel will support simulations of the refractory PIP (RPIP; Figure 7-17). The concentration of TP will be predicted as the summation of the individual forms.

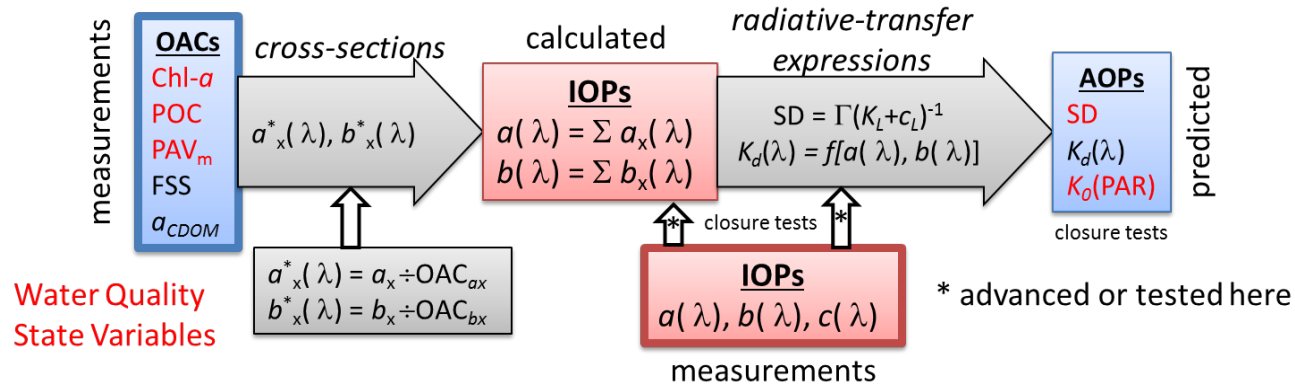

Figure 7-15. Conceptual diagram for an optics submodel.

Table 7-4. Specifications of symbols in the optics submodel.

Symbol	Specifications
OACs	optically active constituents
Chl-*a*	chlorophyll *a* concentration
POC	particulate organic carbon concentration
PAV_m	projected area of minerogenic particles concentration
FSS	inorganic suspended particulate material concentration (ISPM)
a_{CDOM}	absorption coefficient for CDOM
OAC_{ax}	OAC for a_x
OAC_{bx}	OAC for b_x
IOPs	inherent optical properties
$a(\lambda)$	spectral absorption coefficient
$b(\lambda)$	spectral scattering coefficient
$c(\lambda)$	spectral beam attenuation coefficient
$a_x^*(\lambda)$	spectral absorption cross-section for component
$b_x^*(\lambda)$	spectral scattering cross-section for component
a_x	absorption coefficient for component x
b_x	scattering coefficient for component x
c_L	beam attenuation illuminance coefficient
AOPs	apparent optical properties
SD	Secchi depth
$K_d(\lambda)$	spectral downwelling attenuation coefficient
K_0(PAR)	scalar attenuation coefficient for PAR
Γ	coefficient for SD radiative transfer function
K_L	downwelling attenuation illuminance coefficient

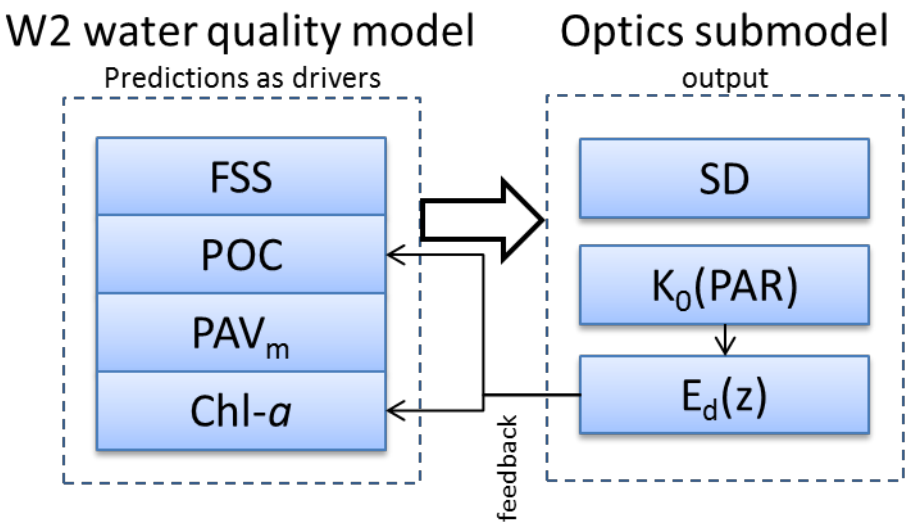

Figure 7-16. Conceptual diagram for optics submodel linkage with W-2 water quality submodel.

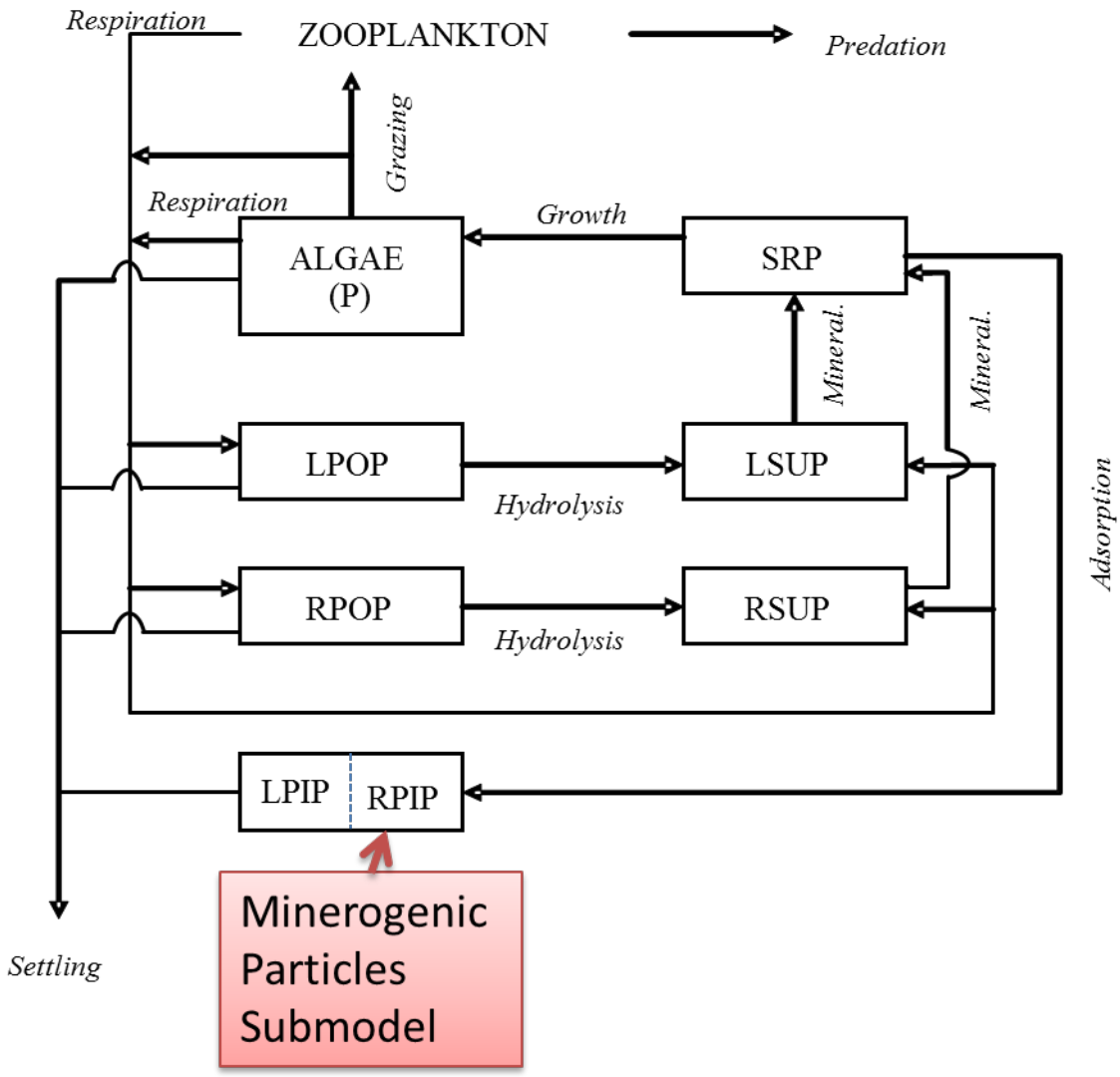

Figure 7-17. Conceptual diagram for a phosphorus submodel.

7.5.2.5. Phytoplankton Growth/Biomass Submodel

Prediction of phytoplankton biomass is a primary goal of the P-eutrophication modeling initiative. The predictions will be made with a mechanistic phytoplankton growth/biomass submodel (Figure 7-18). The primary metric of phytoplankton biomass will be POC; prediction of Chl-*a* will be a secondary goal, at a longer time-scale of seasonal average. The quantitative details of the framework will draw upon other models, including the public domain CE-QUAL-W2 and Lake2k, UFI's P-eutrophication model applied to New York City's reservoirs, as well as recent reviews of related models (Arhonditsis and Brett 2004, Arhonditisis et al. 2006, Robson 2014). This will include representations of the phytoplankton community, kinetic expressions, and values of various coefficients.

The dynamics of phytoplankton biomass dynamics will reflect the dynamics of the source (growth) and sink (respiration, settling, and grazing) processes (Figure 7-18). Grazing will reflect the effects of dreissenid mussels and potentially zooplankton (if found to be noteworthy). The effects of their ambient drivers of phytoplankton growth will be quantitatively represented in the model, including (1) temperature, (2) light availability, and (3) nutrients (Figure 7-18). Phosphorus (P) is the primary nutrient to be considered. Nitrogen (N) and silica (Si) will be secondary. Si will need to be considered if the diatom group is to be differentiated in the simulations. Partitioning of the phytoplankton community according to multiple groups has not been established as a modeling goal, but may emerge as the analysis progresses.

7.6. Summary

The presentation and analyses of monitoring information for Cayuga Lake, particularly the detailed data set collected in 2013 as part of this study (Phase 1), have provided invaluable insights to guide Phase 2 of this study. In Phase 2 a mechanistic P-eutrophication model will be developed tested and preliminarily applied to address the potential cultural eutrophication issue for the lake, with particular focus on the shelf. It has been made clear that the P and sediment issues cannot be separated for this system.

The character of the conspicuous "disconnect" in the three common trophic state metrics (the concentration of TP and Chl-*a*, and Secchi depth) that has emerged in the limnological analyses established model attributes that will be necessary to adequacy address these features. The disconnect refers to the lack of significant differences in Chl-*a* between the shelf and pelagic waters of the lake, despite clearly degraded TP (higher) and SD (lower) conditions on the shelf. The disconnect has two primary elements (1) the greater contributions of minerogenic particles to TP and SD level on the shelf from local tributary inputs, and (2) the absence of locally greater phytoplankton growth on the shelf despite higher concentrations of immediately bioavailable forms of P. The first element requires a robust treatment of minerogenic particles in the model. The second element requires attributes that appropriately represents the effects of the short residence time of tributary inflows on the shelf, the more limited availability of light on the shelf,

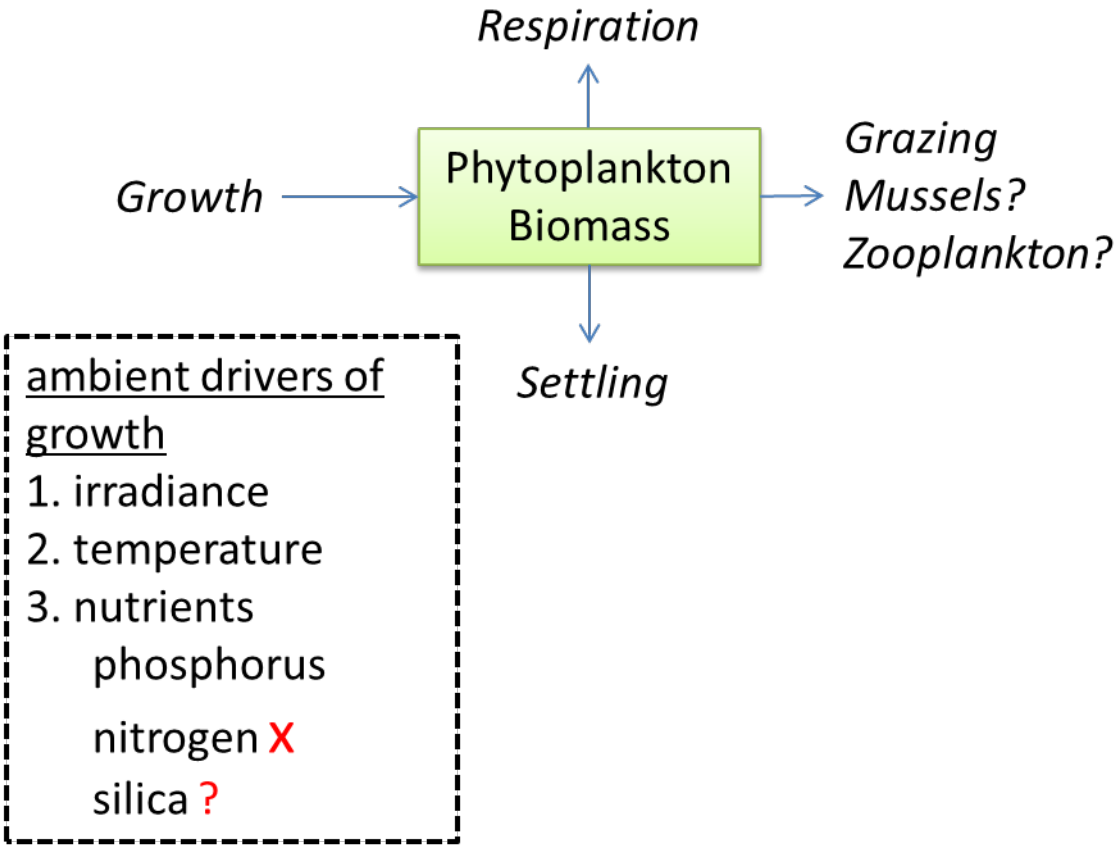

Figure 7-18. Conceptual diagram for a phytoplankton growth/biomass submodel.

and the diluting effect on local phytoplankton biomass concentrations from tributary inputs. Given that the Chl-*a* patterns for the shelf generally track lake-wide pelagic conditions, there are several nutrient and phytoplankton biomass signatures that were identified for pelagic waters that will be valuable in testing the P-eutrophication model.

Modeling activities in Phase 2 will embrace the principle of parsimony, accordingly there will be an effort to avoid overly complex components and submodels that can be accompanied by greater uncertainty and excessive computational demands. Robust temporal and spatial scales will be represented to address the primary signatures resolved in monitoring related to the project goals. Short-term patterns in response to runoff events, that are primary drivers of the shelf versus pelagic waters differences, need to be resolved, as well as the seasonality in phytoplankton growth manifested lake-wide, and the potential effects of year-to-year differences in runoff. Spatial structure must resolve longitudinal differences on the shelf, between the shelf and pelagic waters, and lake-wide mixing and the effects of the thermal stratification regime. The two-dimensional model (W2/T) and the adopted segmentation scheme, will provide a robust representation of these features. Drivers for the water quality model will include (a) local meteorological data, (2) hydrologic data for primary tributaries, and (3) loading rate estimates for multiple constituents, as described in this report.

A tentative listing of model state variables (n~30) has been presented that establishes the water quality model to be developed and tested in Phase 2 will have robust predictive capabilities. The overall water quality model will be composed of several submodels, that include: (1) the two-dimensional hydrothermal/transport submodel, (2) a minerogenic particle submodel, (3) an optics submodel, (4) a phosphorus submodel, and (5) a phytoplankton growth/biomass submodel. Conceptual models depicting structural features are presented for each in this report, that reflect insights and results of analyses derived from the Phase 1 work.

Section 8. References

Archibald, J. A., B. P. Buchanan, D. R. Fuka, C. B Georgakakos, S. W. Lyon and M. T. Walter. 2014. A simple, regionally parameterized model for predicting nonpoint source areas in the Northeastern US. Journal of Hydrology: Regional Studies (in review).

Arhonditsis, G. B., B. A. Adams-VanHarn, L. Nielsen, C. A. Stow and K. H. Reckhow. 2006. Evaluation of the current state of mechanistic aquatic biogeochemical modeling: citation analysis and future perspectives. Environ. Sci. Technol. 40:6547-6554.

Arhonditsis, G. B. and M. T. Brett. 2004. Evaluation of the current state of mechanistic aquatic biogeochemical modeling. Marine Ecology Progress Series 271:13-26.

Auer, M. T., K. A. Tomasoski, M. J. Babiera, M. Needham, S. W. Effler, E. M. Owens and J. M. Hansen. 1998. Phosphorus bioavailability and P-cycling in Cannonsville Reservoir. Lake and Reserv. Manage. 14:278-289.

Baker, D. B., R. Confesor, D. E. Ewing, L. T. Johnson, J. W. Kramer and B. J. Merryfield. 2014. Phosphorus loading to Lake Erie from the Maumee, Sandusky and Cuyahoga rivers: The importance of bioavailability. J. Great Lakes Res. 40:502-517.

Bloesch, J. 1995. Mechanisms, measurement and importance of sediment resuspension in lakes. Mar. Freshwat. Res. 46:295-304.

Boegman, L., M. R. Loewen, P. F. Hamblin and D. A. Culver. 2008a. Vertical mixing and weak stratification over zebra mussel colonies in western Lake Erie. Limnol. Oceanogr. 53:1093.

Boegman, L., M. R. Loewen, D. A. Culver, P. F. Hamblin and M. N. Charlton. 2008b. Spatial-dynamic modeling of algal biomass in Lake Erie: Relative impacts of dreissenid mussels and nutrient loads. J. Environ. Eng. 134:456-468.

Bootsma, H. A. and Q. Liao. 2014. Nutrient cycling by Dreissenid mussels: Controlling factors and ecosystem response (Chapter 35). P. -775. In: T. F. Nalepa and D. W. Schloesser (eds). Quagga and Zebra Mussels: Biology, Impacts, and Control, Second Edition. CRC Press Taylor & Francis Group, Boca Raton, FL.

Boström, B., G. Persson and B. Broberg. 1988. Bioavailability of different phosphorus forms in freshwater systems. Hydrobiologia 170:133-155.

Bowers, D. G. and K. M. Braithwaite. 2012. Evidence that satellites sense the cross-sectional area of suspended particles in shelf seas and estuaries better than their mass. Geo-Mar Lett 32:165-171.

Brady, N. C. and R. R. Weil. 1999. The nature and properties of soils. Prentice Hall, New Jersey. 881 p.

Chalup, M.S., E.A. Laws. 1990. A test of the assumptions and predictions of recent microalgal growth models with marine phytoplankton *Pavlova lutheri*. Limnol. Oceanogr. 35:583-596.

Chapra, S. C. 1997. Surface water-quality modeling. McGraw-Hill, New York. 844 p.

Clesceri, L. S., A. E. Greenberg and A. D. Eaton. 1998. Standard methods for the examination of water and wastewater, 20th ed. American Public Health Association, American Water Works Association, Water Environment Federation, Washington, D.C.

Cole, T. M. and S. A. Wells. 2013. CE-QUAL-W2: A Two-Dimensional, Laterally Averaged, Hydrodynamic and Water Quality Model, Version 3.71. Department of Civil and Environmental Engineering, Portland State University, Portland, Oregon.

Cooke, G. D., E. B. Welch, S. A. Peterson and S. A. Nichols. 2005. Restoration and management of lakes and reservoirs. Taylor and Francis, CRC Press, Boca Raton, FL.

Cornell University. 2012. Cayuga Lake Water Quality Monitoring Related to the LSC Facility: 2012. Cornell University, Ithaca, NY.

Correll, D. L. 1998. The role of phosphorus in the eutrophication of receiving waters: a review. J. Environ. Qual. 27:261-266.

Davies-Colley, R. J., W. N. Vant and D. G. Smith. 2003. Colour and Clarity of Natural Waters: Science and Management of Optical Water Quality. Blackburn Press, Caldwell, New Jersey. 310 p.

Defew, L. H., L. May and K. V. Heal. 2013. Uncertainties in estimated phosphorus loads as a function of different sampling frequencies and common calculation methods. Mar. Freshwat. Res. 64:373-386.

DePinto, J. V., T. C. Young and S. C. Martin. 1981. Algal-available phosphorus in suspended sediments from lower Great Lakes tributaries. J. Great Lakes Res. 7:311-325.

Dolan, D. M., A. K. Yui and R. D. Geist. 1981. Evaluation of river load estimation methods for total phosphorus. J. Great Lakes Res. 7:207-214.

Easton, Z. M., D. R. Fuka, M. T. Walter, D. M. Cowan, E. M. Schneiderman and T. S. Steenhuis. 2008. Re-conceptualizing the Soil and Water Assessment Tool (SWAT) model to predict saturation excess runoff from variable source areas. Journal of Hydrology 348:279-291.

Effler, A. J. P., F. Peng, S. W. Effler, C. M. Strait, M. G. Perkins and K. L. Schulz. 2015a. Light absorption by phytoplankton and minerogenic particles in Cayuga Lake, New York. Inland Waters (in review).

Effler, A. J. P., C. M. Strait, S. W. Effler, D. M. O'Donnell and K. L. Schulz. 2015b. Towards optical theory-based models for diffuse attenuation coefficients and Secchi depth. Inland Waters (in review).

Effler, S. W. 1985. Attenuation versus transparency. J. Environ. Eng. 111:448-459.

Effler, S. W., M. T. Auer and N. A. Johnson. 1989. Modeling Cl concentration in Cayuga Lake, USA. Water, Air, Soil Pollut. 44:347-362.

Effler, S. W., M. T. Auer, F. Peng, M. G. Perkins, S. M. O'Donnell, A. R. Prestigiacomo, D. A. Matthews, P. A. DePetro, R. S. Lambert and N. M. Minott. 2012. Factors diminishing the effectiveness of phosphorus loading from municipal waste effluent: Critical information for TMDL analyses. Wat. Environ. Res. 84:254-264.

Effler, S. W., D. A. Matthews, M. G. Perkins, D. L. Johnson, F. Peng, M. R. Penn and M. T. Auer. 2002. Patterns and impacts of inorganic tripton in Cayuga Lake. Hydrobiol. 482:137-150.

Effler, S. W. and F. Peng. 2014. Long-term study of minerogenic particle optics in Cayuga Lake, New York. Limnol. Oceanogr. 59:325-339.

Effler, S. W., F. Peng, D. M. O'Donnell and C. M. Strait. 2013. The backscattering coefficient and its components in the Great Lakes: A review and synthesis. J. Great Lakes Res. 39:108-122.

Effler, S. W., A. R. Prestigiacomo, D. A. Matthews, R. K. Gelda, F. Peng, E. A. Cowen and S. A. Schweitzer. 2010. Tripton, trophic state metrics, and near-shore versus pelagic zone responses to external loads in Cayuga Lake, New York. Fund. Appl. Limnol. 178:1-15.

Effler, S. W., A. R. Prestigiacomo, F. Peng, R. K. Gelda and D. A. Matthews. 2014. Partitioning the contributions of minerogenic particles and bioseston to particulate phosphorus and turbidity. Inland Waters 2:179-192.

Ekholm, P. and K. Krogerus. 2003. Determining algal-available phosphorus of differing origin: routine phosphorus analyses versus algal assays. Hydrobiologia 492:29-42.

Ellison, M. E. and M. T. Brett. 2006. Particulate phosphorus bioavailability as a function of stream flow and land cover. Wat. Res. 40:1258-1268.

Fennel, K. and E. Boss. 2003. Surface maxima of phytoplankton and chlorophyll: Steady-state solutions from a simple model. Limnol. Oceanogr. 48:1521-1534.

Fischer, G., F. Nachtergaele, S. Prieler, H. T. Van Velthuizen, L. Verelst and D. Wiberg. 2008. Global agro-ecological zones assessment for agriculture (GAEZ 2008). IIASA, Laxenburg, Austria and FAO, Rome, Italy.

FLUX32. 2013. Load Estimation Software (version 3.31) [software]. US Army Corp. of Engineers. Retrieved from http://el.erdc.usace.army.mil.

Fry, J. A., G. Xian, S. Jin, J. A. Dewitz, C. G. Homer, Y. A. N. G. LIMIN, C. A. Barnes, N. D. Herold and J. D. Wickham. 2011. Completion of the 2006 national land cover database for the conterminous United States. Photogram Eng Remote Sensing 77:858-864.

Fuka, D. R., M. T. Walter, C. MacAlister, T. S. Steenhuis and Z. M. Easton. 2014. SWATmodel: A Multi-Operating System, Multi-Platform SWAT Model Package in R. J Am Water Resour Assoc 50:1349-1353.

Gelda, R. K. and S. W. Effler. 2007. Testing and application of a two-dimensional hydrothermal model for a water supply reservoir: Implications of sedimentation. J. Environ. Eng. Sci. 6:73-84.

Gelda, R. K. and S. W. Effler. 2008. Probabilistic model for temperature and turbidity in a reservoir withdrawal. Lake and Reserv. Manage. 24:219-230.

Gelda, R. K., S. W. Effler and F. Peng. 2012. Modeling turbidity and the effects of alum application for a water supply reservoir. J. Environ. Eng. 138:38-47.

Gelda, R. K., S. W. Effler, F. Peng, E. M. Owens and D. C. Pierson. 2009. Turbidity model for Ashokan Reservoir, New York: Case Study. J. Environ. Eng. 135:885-895.

Gelda, R. K., S. W. Effler, A. R. Prestigiacomo, F. Peng, A. J. P. Effler, B. A. Wagner, M. G. Perkins, D. M. O'Donnell, S. M. O'Donnell and D. C. Pierson. 2013. Characterizations and modeling of turbidity in a water supply reservoir following an extreme runoff event. Inland Waters 3: 377-390.

Gelda, R. K., Alexandra T. King, S. W. Effler, S. A. Schweitzer and E. A. Cowen. 2015. Testing and application of a two-dimensional hydrothermal/transport model for a long, deep and narrow lake with moderate Rossby number. Inland Waters (in review).

Gesch, D. 2007. The national elevation dataset. P. 99-118. In: D. Maune (ed). Digital elevation model technologies and applications: the DEM users manual, 2nd edition. American Society for Photogrammetry and Remote Sensing, Bethesda, Maryland.

Gesch, D., M. Oimoen, S. Greenlee, C. Nelson, M. Steuck and D. Tyler. 2002. The national elevation dataset. Photogram Eng Remote Sensing 68:5-32.

Gloor, M., A. Wuest and M. Munnich. 1994. Benthic boundary mixing and resuspension induced by internal seiches. Hydrobiologia 284:59-68.

Hairston, N. G., Jr., C. M. Kearns, L. P. Demma and S. W. Effler. 2005. Species-specific Daphnia Phenotypes: A history of industrial pollution and pelagic ecosystem response. Ecol. 86:1669-1678.

Haith, D. A., N. Hollingshead, M. L. Bell, S. W. Kreszewski and S. J. Morey. 2009. Estimation of nutrient and sediment loads to Cayuga Lake using the GWLF watershed model. Department of Biological and Environmental Engineering, Cornell University, Ithaca, NY, and The Cayuga Lake Watershed Network, Wells College, Aurora, NY, 67 p.

Haith, D. A., N. Hollingshead, M. L. Bell, S. W. Kreszewski and S. J. Morey. 2012. Nutrient Loads to Cayuga Lake, New York: Watershed Modeling on a Budget. Journal of Water Resources Planning and Management 138:571-580.

Hanson, P. C., D. L. Bade, S. R. Carpenter and T. K. Kratz. 2003. Lake metabolism: Relationships with dissolved organic carbon and phosphorus. Limnol. Oceanogr. 48:1112-1119.

Hecky, R. E., P. Campbell, and L. L. Hendzel. 1993. The stoichiometry of carbon, nitrogen and phosphorus in particulate matter of lakes and oceans. Limnol. Oceanogr. 38: 709-724.

Hergert, G. W., D. R. Bouldin, S. D. Klausner and P. J. Zwerman. 1981. Phosphorus concentration-water flow interactions in tile effluent rom manured land. J. Environ. Qual. 10:338-344.

Higgins, S. N. and M. J. Vander Zanden. 2010. What a difference a species makes: a meta-analysis of dreissenid mussel impacts on freshwater ecosystems. Ecol. Monogr. 80:179-196.

Hutchinson, G. E. 1973. Eutrophication: the scientific background of a contemporary practical problem. Am. Sci. 61:269-279.

Johnes, P. J. 2007. Uncertainties in annual riverine phosphorus load estimation: impact of load estimation methodology, sampling frequency, baseflow index and catchment population density. Journal of Hydrology 332:241-258.

Johnson, A. H., D. R. Bouldin, E. A. Goyette and A. M. Hedges. 1976a. Nitrate dynamics in Fall Creek, New York. Journal of Environmental Quality 5:386-391.

Johnson, A. H., D. R. Bouldin, E. A. Goyette and A. M. Hedges. 1976b. Phosphorus loss by stream transport from a rural watershed: quantities, processes, and sources. Journal of Environmental Quality 5:148-157.

Kirk, J. T. O. 2011. Light and Photosynthesis in Aquatic Ecosystems, 3rd ed. Cambridge University Press, New York, NY. 662 p.

Lambert, R. S. 2012. Great Lakes tributary phosphorus bioavailability. M.S. Thesis. Civil and Environmental Engineering, Michigan Technological University, Houghton, MI.

Lampert, W., W. Fleckner, H. Rai and B. E. Taylor. 1986. Phytoplankton control by grazing zooplankton:A study on the spring clear-water phase. Limnol. Oceanogr. 31:478-490.

Lampert, W. 2011. Daphnia: development of a model organism in ecology and evolution. In: O. Kinne (ed). Excellence in Ecology, Book 21. Oldendorf/Luhe: International Ecology Institute

Laws, E. A. and M. S. Chalup. 1990. A microbial growth model. Limnol. Oceanogr. 35:597-608.

Likens, G. E. 1974a. The runoff of water and nutrients from watersheds tributary to Cayuga Lake, New York. Technical Report No. 81. Cornell University Water Resources and Marine Sciences Center, Cornell University, Ithaca, NY. 124 p.

Likens, G. E. 1974b. Water quality and nutrient budgets for Cayuga Lake, New York. Technical Report No. 82. Cornell University Water Resources and Marine Sciences Center, Cornell University, Ithaca, NY. 91 p.

Loisel, H. and A. Morel. 1998. Light scattering and chlorophyll concentration in case 1 waters: A reexamination. Limnol. Oceanogr. 43:847-858.

Longabucco, P. and M. R. Rafferty. 1998. Analysis of material loading to Cannonsville Reservoir: advantages of event-based sampling. Lake and Reserv. Manage. 14:197-212.

Lyon, S. W., M. R. McHale, M. T. Walter and T. S. Steenhuis. 2006. The impact of runoff generation mechanisms on the location of critical source areas. Journal of the American Water Resource Association 42:793-804.

Mayer, C. M., L. E. Burlakova, P. Eklov, D. Fitzgerald, A. Y. Karatayev, S. A. Ludsin, S. Millard, E. L. Mills, A. P. Ostapenya, L. G. Rudstam, B. Zhu and T. V. Zhukova. 2014. Benthification of freshwater lakes, Exotic mussels turning ecosystems upside down (Chapter 36). P. 575-585. In: T. F. Nalepa and D. W. Schloesser (eds). Quagga and Zebra Mussels: Biology, Impacts, and Control, Second Edition. CRC Press Taylor & Francis Group, Boca Raton, FL.

Menne, M. J., I. Durre, S. Korzeniewski, K. McNeal, Y. X. Thomas, S. Anthony, R. Ray, R. S. Vose, B. E. Gleason and T. G. Houston. 2012. Global historical climatology network-daily database (GHCN-Daily), Version 3. NOAA National Climatic Data Center.

Miner, B. E., L. De Meester, M. E. Pfrender, W. Lampert and N. G. Hairston. 2012. Linking genes to communities and ecosystems: Daphnia as an ecogenomic model. Proceedings of the Royal Society B: Biological Sciences 279:1873-1882.

Nalepa, T. F. and D. W. Schloesser. 2014. Quagga and Zebra Mussels: Biology, Impacts, and Control, Second Edition. CRC Press Taylor & Francis Group, Boca Raton, FL. 775 p.

Nalepa, T. F. 1989. Estimates of macroinvertebrate biomass in Lake Michigan. J. Great Lakes Res. 15:437-443.

Nalepa, T. F., D. L. Fanslow and G. A. Lang. 2009. Transformation of the offshore benthic community in Lake Michigan: recent shift from the native amphipod Diporeia spp. to the invasive mussel Dreissena rostriformis bugensis. Freshwat. Biol. 54:466-479.

Nalepa, T. F., D. L. Fanslow and S. A. Pothoven. 2010. Recent changes in density, biomass, recruitment, size structure, and nutritional state of Dreissena populations in southern Lake Michigan. J. Great Lakes Res. 36:5-19.

Nash, J. E. and J. V. Sutcliffe. 1970. River flow forecasting through conceptual models. Part I a discussion of principles. Journal of Hydrology 10:282-290.

National Center for Atmospheric Research (NCAR). 2014. The climate data guide: Climate forcast system reanalysis (CFSR).

Neter, J., M. H. Kutner, C. J. Nachtsheim and W. Wasserman. 1996. Applied Linear Regression Models. McGraw-Hill, 720 p.

Nietsch, S. L., J. G. Arnold, J. R. Kiniry and J. R. Williams. 2011. Soil and water assessment tool theoretical documentation, Version 2009. Texas Water Resource Institute, College Station, TX.

Oglesby, R. T. 1978. The limnology of Cayuga Lake. P. 2-121. In: J. A. Bloomfield (ed). Lakes of New York State, Volume I, Ecology of Finger Lakes. Academic Press, New York.

Ozersky, T., S. Y. Malkin, D. R. Barton and R. E. Hecky. 2009. Dreissenid phosphorus excretion can sustain C. glomerata growth along a portion of Lake Ontario shoreline. J. Great Lakes Res. 35:321-328.

Peng, F. and S. W. Effler. 2007. Suspended minerogenic particles in a reservoir: light scattering features from individual particle analysis. Limnol. Oceanogr. 52:204-216.

Peng, F. and S. W. Effler. 2011. Characterizations of the light-scattering attributes of mineral particles in Lake Ontario and the effects of whiting. J. Great Lakes Res. 37:672-682.

Peng, F. and S. W. Effler. 2012. Mass-specific scattering coefficient for natural minerogenic particle populations: particle size distribution effect and closure analyses. Appl. Opt. 51:2236-2249.

Peng, F., S. W. Effler, D. M. O'Donnell, A. D. Weidemann and M. T. Auer. 2009. Characterization of minerogenic particles in support of modeling light scattering in Lake Superior through a two-component approach. Limnol. Oceanogr. 54:1369-1381.

Prestigiacomo, A. R., S. W. Effler, D. A. Matthews, Martin T. Auer, Benjamin E. Downer, Anika Kuczynski and M. Todd Walter. 2015. Apportionment of bioavailable phosphorus loads entering Cayuga Lake, New York. J. Am. Wat. Resour. Assoc. (in internal review).

Prestigiacomo, A. R., S. W. Effler, D. M. O'Donnell, J. M. Hassett, E. M. Michelanko, Z. Lee and A. D. Weidemann. 2007. Turbidity and suspended solids levels and loads in a sediment enriched stream: implications for impacted lotic and lentic ecosystems. Lake and Reserv. Manage. 23:231-244.

Pritchett, W. L. and R. F. Fisher. 1987. Properties and Management of Forest Soils. Wiley, New York, 494 p.

Raymond, P. and J. Saiers. 2010. Event controlled DOC export from forested watersheds. Biogeochemistry 100:197-209.

Reynolds, C. 2006. The Ecology of Phytoplankton. Cambridge University Press, Cambridge, MA. 436 p.

Reynolds, C. S. and P. S. Davies. 2001. Sources and bioavailability of phosphorus fractions in freshwaters: a British perspective. Biological reviews of the Cambridge Philosophical Society 76:27-64.

Richards, R. P. and J. Holloway. 1987. Monte Carlo studies of sampling strategies for estimating tributary loads. Wat. Resour. Res. 23:1939-1948.

Robson, B. J. 2014. State of the art in modelling of phosphorus in aquatic systems: Review, criticisms and commentary. Environ. Model. Softw. (in press):

Rueda, F., E. Moreno-Ostos and J. Armengol. 2006. The residence time of river water in reservoirs. Ecol. Model. 191:260-274.

Schaffner, W. R. and R. T. Oglesby. 1978. Phosphorus loadings to lake and some of their responses. Part 1. A new calculation of phosphorus loadings and its applications to 13 New York lakes. Limnology and Oceanography 23:120-134.

Schelske, C. L., E. F. Stoermer, D. J. Conley, J. A. Robbins and R. M. Glover. 1983. Early Eutrophication in the Lower Great Lakes. Science 222:320-322.

Sereda, J. M. and J. J. Hudson. 2011. Empirical models for predicting the excretion of nutrients (N and P) by aquatic metazoans: taxonomic differences in rates and element ratios. Freshwat. Biol. 56:250-263.

Sommer, U., M. Gliwicz, W. Lampert and A. Duncan. 1986. The PEG-model of seasonal succession of planktonic events in fresh waters. Arch. Hydrobiol. 106:433-471.

Sommer, U., R. Adrian, L. De Senerpont Domis, J. J. Elser, U. Gaedke, B. Ibelings, E. Jeppesen, M. Lürling, J. C. Molinero and W. M. Mooij. 2012. Beyond the Plankton Ecology Group (PEG) model: mechanisms driving plankton succession. Annual Review of Ecology, Evolution, and Systematics 43:429-448.

Sondergaard, M., E. Jeppesen, T. L. Lauridsen, C. Skov, E. H. Van Nes, R. Roijackers, E. Lammens and R. Portielje. 2007. Lake restoration: success, failures and long-term effects. Journal of Applied Ecology 44:1095-1105.

Søndergaard, M., J. P. Jensen and E. Jeppesen. 2003. Role of sediment and internal loading of phosphorus in shallow lakes. Hydrobiologia 506:135-145.

StatSoft. 2003. STATISTICA (data analysis software system), version 6. www.statsoft.com.

Swift, T. J., P. L. Joaquim, S. G. Schladow, E. R. John, D. J. Alan and R. G. Charles. 2006. Water clarity modeling in Lake Tahoe: Linking suspended matter characteristics to Secchi depth. Aquat. Sci. 68:1-15.

Thomann, R. V. and J. A. Mueller. 1987. Principles of surface water quality modeling and control. Harper & Row Publishers, NY.

Upstate Freshwater Institute. 2012. Environmental Testing Field Methods Manual. UFI-CD-022. revision 2. Syracuse, NY, 126 pp.

Upstate Freshwater Institute. 2013. Quality Assurance Project Plan for Phase 1: Monitoring and Modeling Support for a Phosphorus/Eutrophication Model for Cayuga Lake. Submitted to the New York State Department of Environmental Conservations, Albany, New York. Upstate Freshwater Institute, Syracuse, NY. 25 p.

USEPA (United States Environmental Protection Agency). 1991. Guidance for water quality-based decisions: The TMDL process. EPA 440-4-91-001. Office of Water, Washington, DC.

Vanderploeg, H. A., J. R. Liebig, T. F. Nalepa, G. L. Fahnenstiel and S. A. Pothoven. 2010. Dreissena and the disappearance of the spring phytoplankton bloom in Lake Michigan. J. Great Lakes Res. 36:50-59.

Veith, T. L., A. N. Sharpley and J. G. Arnold. 2008. Modeling a small northeastern watershed with detailed, field-level data. Transactions of the American Society of Agricultural and Biological Engineers 51:471-483.

Vogel, R. M., J. R. Stedinger and R. P. Hooper. 2003. Discharge indices for water quality loads. Wat. Resour. Res. 39:1273.

Vollenweider, R. A. 1976. Advances in defining critical loading levels for phosphorus in lake eutrophication. Mem. Ist. Ital. Idrobiol. 33:53-83.

Walker, W. W. 1995. FLUX: Stream load computations Version 4.5. Environmental Laboratory, USACE Waterways Experiment Station, Vicksburg, MS.

Walter, M. T., M. F. Walter, E. S. Brooks, T. S. Steenhuis, J. Boll and K. Weiler. 2000. Hydrologically sensitive areas: Variable source area hydrology implications for water quality risk assessment. Journal of Soil and Water Conservation 55:277-284.

Watkins, J. M., R. Dermott, S. J. Lozano, E. L. Mills, L. G. Rudstam and J. V. Scharold. 2007. Evidence for remote effects of dreissenid mussels on the amphipod Diporeia: Analysis of Lake Ontario benthic surveys, 1972-2003. J. Great Lakes Res. 33:642-657.

Watkins, J. M., L. G. Rudstam, E. L. Mills and M. A. Teece. 2012. Coexistence of the native benthic amphipod Diporeia spp. and exotic dreissenid mussels in the New York Finger Lakes. J. Great Lakes Res. 38:226-235.

Wetzel, R. G. 2001. Limnology: lake and reservoir ecosystems. Academic Press, New York.

Yaksich, S. M. and F. H. Verhoff. 1983. Sampling strategy for river pollutant transport. J. Environ. Eng. 109:219-231.

Young, T. C., J. V. DePinto, S. E. Flint, S. M. Switzenbaum and J. K. Edzwald. 1982. Algal availability of phosphorus in municipal wastewater. J. Water Pollut. Control Fed. 54:1505-1516.

Young, T. C., J. V. DePinto, S. C. Martin and J. S. Bonner. 1985. Algal-available particulate phosphorus in the Great Lake basin. J. Great Lakes Res. 11:434-446.